

A Classical Treatment of the Quadratic Zeeman

Effect in Atomic Hydrogen.

by

Maher Abdul-Hakim Abdul-Hafez Al-Laithy

Thesis submitted for the degree of

DOCTOR OF PHILOSOPHY

in

The Faculty of Science of the *University of London*

Department of Mathematics

Royal Holloway and Bedford New College

April, 1988



ProQuest Number: 10090147

All rights reserved

INFORMATION TO ALL USERS

The quality of this reproduction is dependent upon the quality of the copy submitted.

In the unlikely event that the author did not send a complete manuscript and there are missing pages, these will be noted. Also, if material had to be removed, a note will indicate the deletion.



ProQuest 10090147

Published by ProQuest LLC(2016). Copyright of the Dissertation is held by the Author.

All rights reserved.

This work is protected against unauthorized copying under Title 17, United States Code.
Microform Edition © ProQuest LLC.

ProQuest LLC
789 East Eisenhower Parkway
P.O. Box 1346
Ann Arbor, MI 48106-1346

ABSTRACT

The classical Hamiltonian describing the hydrogen atom in the presence of a static magnetic field of arbitrary strength for arbitrary angular momentum is derived. For this Hamiltonian the transition from the regular to the chaotic motion is observed by means of the Poincare mappings.

Two different classes of non-planar periodic orbits are traced in both regular and irregular regions. The bifurcations and variation of the periodic motion with the change of the total energy parameter throughout the regular regime and into the chaotic regime are given together with the relevant frequencies. For both classes the stability/instability of the periodic orbits is studied by calculating the linearization matrix in the neighbourhood of the corresponding fixed points of the Poincare mappings. In one class, the class of orbits that approach very close to the nucleus, we have surprisingly found that a set of periodic orbits bifurcate from the same periodic orbit along the field at various values of the energy. These values are determined numerically. A repeated pattern of stability and instability of these orbits exists over decreasing intervals of energy until the escape energy is approached. All these periodic orbits are unstable beyond the ionization limit. On the other hand we have found that the bifurcation of the second class of orbits is, generally, generic.

Three sets of the energy separation lines due to three types of periodic motions are given when $B = 60$ kG with $m = 0$. Other sets of lines are given for $B = 42$ kG with $m = 0$, $m = -1$ and $m = -2$. Many of these lines coincide with the spectral lines obtained experimentally by A. Holle *et al* (1986).

The energy spacing $0.64 \hbar\omega_c$ near the ionisation limit, which has been found recently in the experiments of Holle *et al* (1986) is due to one of the non-planar orbits. Other new predicted spacings arising from other orbits have been seen in high resolution experiments on atoms in external fields (Main *et al* 1986).

I am indebted to Dr. D. Richards whose advice and comments enrich this thesis, and thank Professor M.V. Berry, Dr. R.S. MacKay, Dr. P. G. Mahony and Dr. K. Taylor for useful discussions.

I also thank Dr. L. Morgan, Mr. J. Anderson, Mr. P. Taylor and Mr. L. Nades in the RBNO (University of London) Computer Centre for their help.

I appreciate the patience of my wife and children throughout the years of doing this research. Finally, I take this opportunity to express my gratitude to the Egyptian Government for a studentship and the U.K. Government for an O.R.S. Grant.

Acknowledgements

I should like to express my thanks to both Dr. C. Farmer and Professor M.R.C. McDowell who supervised this work. They sought every opportunity to help and encourage me.

I am indebted to Dr. D. Richards whose advice and comments enrich this thesis, and thank Professor M.V. Berry, Dr. R.S. MacKay, Dr. P. O'Mahony and Dr. K. Taylor for useful discussions.

I also thank Dr. L. Morgan, Mr. J. Anderson, Mr. P. Taylor and Mr. L. Nodes in the RHBNC (*University of London*) Computer Centre for their help.

I appreciate the patience of my wife and children throughout the years of doing this research. Finally, I take this opportunity to express my gratitude to the Egyptian Government for a studentship and the U.K. Government for an O.R.S. Grant.

4.2.3 Poincaré fixed point	CONTENTS	37
4.3 Linear stability in area-preserving maps.		38
4.3.1 Linearization of map.	CHAPTER (1)	38
4.3.2 The residue.	Introduction	1
4.3.3 The Poincaré-Birkhoff theorem and the microcosmic structure under	CHAPTER (2)	43
4.3.4 Complex dynamics, hyperbolic points and chaotic motion.	Hamiltonian Dynamics	44
2.1 Equivalent forms of the equations of motion.		11
2.2 Canonical transformations.		15
2.3 Volume preservation of phase flow.		16
2.4 The extended phase space.		18
2.5 Canonical transformations in the extended phase space.		20
2.6 Generalized time transformation.		20
CHAPTER (3)		
Regular and irregular motion (I)		
3.1 Integrable systems and invariant tori.		22
3.2 Resonant and non-resonant tori.		25
3.3 Canonical perturbation theorem.		26
3.4 The KAM theorem.		28
CHAPTER (4)		
Regular and irregular motion (II)		
4.1 The surface of section.		31
4.2.1 The twist mapping.		34
4.2.2 Perturbed twist mapping.		36

4.2.3 Poincaré fixed point theorem.	37
4.3 Linear stability in area-preserving maps.	38
4.3.1 Linearization of an area-preserving map.	38
4.3.2 The residue.	42
4.3.3 The Poincare-Birkhoff theorem and the microcosmic structure under perturbations.	43
4.3.4 Complexity of structure around hyperbolic points and chaotic motion.	44
4.3.5 Poincaré index.	51
4.3.6 Fixed point bifurcations.	52
4.3.7 Renormalization.	55
4.4. Ergodicity.	56

CHAPTER (5)

Mathematical formulation of the problem	62
---	----

CHAPTER (6)

Regularization

6.1 First regularization: non-Hamiltonian system.	70
6.2 Second regularization: Hamiltonian system.	75

CHAPTER (7)

Surface of section calculation of the quadratic Zeeman Hamiltonian

7.1 More visible surfaces of section.	82
7.2 The surface of section for the quadratic Zeeman potential.	85
7.3 Numerical methods and computation.	92

CHAPTER (8)

Planar orbits

122

CHAPTER (9)

Non-planar orbits

9.1	Periodic orbits of class CI.	129
9.2	Periodic orbits of class CII.	133
9.3	Change of the periodic orbits with the energy parameter.	138

CHAPTER (10)

Stability of periodic orbits

10.1	Liapunove characteristic exponents.	156
10.2	The characteristic exponents of a Hamiltonian system.	158
10.3	Linearization of a map (calculating the characteristic exponents of periodic orbits).	161
10.4	Stability of the periodic orbits in the classes CI and CII.	167
10.4.1	Stability of the periodic orbits in the class CI.	167
10.4.2	Stability of the periodic orbits in the class CII.	169
10.4.3	The dependence of the angles of emission of the periodic orbits of class CII on E .	171
10.4.4	Clarification of the stable-unstable sequence of the orbit OZ .	174

CHAPTER (1)

CHAPTER (11)

Semi-classical quantization and
comparison with experiments

11.1	Semiclassical quantization.	195
11.2	Quantization of periodic orbits in the quadratic - Zeeman problem.	201
11.3	Comparison with experiments.	207

CHAPTER (12)

Conclusions

	Appendix.	241
	References.	244

CHAPTER (1)

Introduction

The first attempt at studying the effect of external magnetic fields on atoms was made by Faraday when he placed a sodium flame in a strong magnetic field to determine whether any change would be produced in the wavelength or frequency of its spectral lines. Because the spectroscope he used had not sufficient resolving power he was not able to observe any effect. In 1896 P. Zeeman, using apparatus of greater resolving power, observed that the spectral lines of atoms were split into components. Since then the study of the behaviour of atoms in the presence of magnetic fields has become a subject of interest to the spectroscopists.

Lorentz (1897) developed the classical theory of the motion of an electron undergoing simple harmonic motion in the presence of a superimposed magnetic field. The Lorentz explanation of the Zeeman effect is based on the idea that monochromatic light is emitted by an electron revolving in a circular orbit at an angular velocity, ω , which is related to the frequency ν of the light by the relation $\omega = 2\pi\nu$ and that the radiation is produced by the acceleration of the charge : when the magnetic field is switched on, the radial equation of motion is

$$m_e r \omega_0^2 + \frac{e}{c} B r \omega_1 = m_e r \omega_1^2, \quad (1.1)$$

where the second term is the radial Lorentz force due to the application of a magnetic field of flux density B . ω_0 and ω_1 are, respectively, the angular frequencies before and after the application of the magnetic field. Provided that

$$\left(\frac{eB}{m_e c}\right)^2 \ll 4\omega_0^2, \quad (1.2)$$

i.e. the cyclotron frequency is negligible in comparison with $2\omega_0$,
the solution of (1.1) for ω_1 gives

$$\omega_{1,2} \simeq \omega_0 \pm \frac{eB}{2m_e c}, \quad (1.3)$$

or

$$\nu_{1,2} \simeq \nu_0 \pm \frac{eB}{4\pi m_e c}. \quad (1.4)$$

The quantity $\frac{eB}{4m_e c}$ ($= \frac{\omega_c}{4}$) is called the normal Zeeman separation and ω_c is the cyclotron frequency, associated with a magnetic field of flux density B . Also the importance of (1.4), though deduced through a simplified classical assumption, is that it is the correct equation for determining the value $\frac{e}{m_e}$ from experiments involving the singlet lines which are emitted by atoms in states of zero spin angular momentum ($S = 0$) so that the total and the orbital angular momentum are equal ($L = J$). Atoms of elements in the second group of the periodic table, for example, Mg or Ca, possess such states.

Although Lorentz theory predicted that all spectral lines would show 'normal' Lorentz triplet splitting, many lines were found which showed more complicated (anomalous) splittings. These were explained by the work of Lande (1923) on multiplet structure and the discovery by Uhlenbeck and Goudsmit (1925) of the spin and magnetic moment of the electron. The splitting of a spectral line into components in the presence of a (small) magnetic field became known as the anomalous Zeeman effect.

The quantum theory of the Zeeman effect was developed by many workers. Jenkins and Segre (1939) studied the quadratic Zeeman effect. They observed the principal series lines of sodium and potassium in absorption at a field of 27 kG. The quadratic Zeeman effect was observed for $12 \leq n \leq 20$ and the line shifts were proportional to n^4 in agreement with perturbation theory. For higher values of n

however the shifts were larger than those predicted by perturbation theory. Garton and Tomkins (1969) performed an experiment on the photoionisation of strontium and barium in the presence of an external magnetic field. They found a new series of equally spaced resonances above the ionisation threshold in both strontium and barium with a spacing of $1.5 \hbar \omega_c$ where ω_c is the cyclotron frequency appropriate to the field. This evenly spaced line sequence and other sequences of that order have been compared with the so-called Landau spectrum of a free electron in a magnetic field, where the level spacing is $\hbar \omega_c$. These structures have therefore become known as quasi-Landau levels and have been attributed to the competition between the Coulomb and magnetic fields.

In the past few years there has been a great deal of interest in the study of atoms in the presence of strong magnetic fields both from the intrinsic importance and in view of possible plasma and astrophysical applications. A broad review of the subject can be obtained from the proceedings of the 1982 CNRS colloquium (D.Delande, C.Chardonnet, F. Biraben and J.C. Gay) and also from Garstang (1977).

Most theoretical work has focused on the prototype system of atomic hydrogen. The importance of hydrogen or Hydrogen-like atoms lies in the fact that the problem, in these cases, is one of the simplest Hamiltonians realizable in the laboratory giving rise to irregular motion. However, there is a difficulty of dealing with atoms in external fields which arises from the simultaneous presence of separate forces of different symmetry. We have the Coulomb potential which has O_4 symmetry; for the unperturbed system the component equations of the Schrodinger equation for θ and ϕ do not contain the energy \mathcal{E} , which is determined entirely by the value of n , the principal quantum

number. For each $n \geq 1$ there are several values of the orbital quantum number l and the magnetic quantum number m . So we have degenerate states. It should be noted that the appearance of degeneracy in two out of three quantum numbers for a problem in spherical coordinates *occurs in* the hydrogen problem, being a peculiarity of the $\frac{1}{r}$ ^{and r^2} potential laws. Together with the Coulomb interaction we have a cylindrically symmetric interaction between the electron and the magnetic field.

The potential may be regarded as consisting of two terms: first the Coulomb potential, $-\frac{1}{r}$, and second, the diamagnetic potential, proportional to $r^2 \sin^2 \theta$, where θ is the angle between the magnetic field axis and the electron position.

In atomic units the ratio of the quadratic term in B , the magnetic field, to the linear term in B is of order $\simeq B \times 10^{-5}$, where B is expressed in kG. The term linear in B , compared with the Coulomb potential energy is of order $\simeq B \times 10^{-5}$ for the ground state. *The linear term has no n -dependence, but the quadratic term, when it can be still treated as a perturbation produces energy shifts proportional to n^4 (Garstang 1977).*

If the linear term is considered alone, choosing the z -direction to coincide with that of \mathbf{B} , the Hamiltonian with $\mathbf{B} = 0$ is altered by the addition of $H_1 = \omega_L M_z$ where $\omega_L = \frac{eB}{2\mu c}$ is the Larmor frequency and M_z is the z -component of the angular momentum. Therefore the existing energy levels, with their $(2l+1)$ -fold degeneracy are split into $(2l+1)$ components that are equally spaced, with energies given by

$$E = -\frac{\mu Z^2 e^4}{2\hbar^2 n^2} + \hbar\omega_L m. \quad (1.5)$$

According to the allowed selection rules that the magnetic quantum number m changes by zero or unity, the single line representing a transition with $B = 0$ splits into three lines. This is the *normal Zeeman effect*. Thus when the Coulomb potential is dominant, the

bound state problem can be solved by perturbation theory and the energy eigenvalues are the usual Coulomb levels with paramagnetic and diamagnetic perturbations. The quadratic term can become very important if the magnetic field is very intense; it is believed that fields as large as 10^9 kG may exist on the surface of neutron stars, and this would radically alter the structure of atoms (Cohen *et al*, 1970). The quadratic term will also be important when we consider the macroscopic motion of an electron in an external field.

For a very strong magnetic field the electron orbital radius is large, the Coulomb interaction is a small perturbation and the energy levels approach the usual Landau levels (Landau and Lifshitz 1977). If, however, the magnetic field is so strong that the Coulomb potential may be neglected, this strong field (with its linear and quadratic terms taken into consideration) causes a shift, from the free particle lines, which is twice the normal Zeeman shift (i.e. $2\omega_L \hbar$) for large positive magnetic quantum numbers (Gasiorowicz, 1974). In this case the maximum radius of the orbit, as determined by the peaking of the radial probability distribution, equals r_n (or corresponds to) the classical value. The problem in this case gives a beautiful illustration of the correspondence principle.

The least understood regime is where the Coulomb and the magnetic interaction exert a comparable influence on the electron motion. With those two forces of different symmetries and comparable strengths, perturbation treatment is impossible. While the *weak field* states are well understood (Solov'ev 1982), the region where $\Delta\mathcal{E}_{n,n\pm 1} \simeq \hbar\omega_c$ is not. As n increases we find l -mixing within a given n and then levels belonging to different n mix (n -mixing). This regime is called the *strong field mixing regime* (Rau(1979)) and has recently

been given a special interest by many workers both experimentally and theoretically and we are in turn focusing on it.

The basic method is to represent the Hamiltonian operator in some complete basis which should provide a rapid convergence of the eigenvalues so that the error can be controlled in spite of the necessary truncations. The hydrogen basis could be completed by adding the continuum hydrogenic functions but this leads to divergence difficulties in calculating the matrix elements. Clark and Taylor (1980,1981) obtained a solution to this problem. At a field strength of 47 kG they used an approach similar to the one used by Edmonds (1973) for higher magnetic fields ($B \simeq 10^4$ kG). The Schrodinger equation is

$$\left(-\frac{1}{2}\nabla^2 - \frac{1}{r} + \frac{1}{2}\beta^2 r^2 \sin^2 \theta\right)\psi = \mathcal{E}\psi, \quad (1.6)$$

where $\beta = \omega_L$. The linear term βM_z does not appear in (1.6) since it is a constant energy shift and plays no significant role in the dynamics (Clark and Taylor (1981)). The method was to expand the wave function ψ in a basis of Sturmian radial functions $S_{nl}^{(\xi)}(\hat{r})$

$$\psi(\mathbf{r}) = \sum_{n,l} r^{-1} \psi_{nl} S_{nl}^{(\xi)}(r) Y_{lm}(\hat{r}), \quad (1.7)$$

where $S_{nl}^{(\xi)}(r)$ are given by

$$S_{nl}^{(\xi)} = \left(\frac{(n-l-1)!}{2(n+l)!}\right)^{-\frac{1}{2}} (\xi r)^{l+1} L_{n-l-1}^{2l+1}(\xi r) e^{-\frac{\xi r}{2}}, \quad (1.8)$$

with L being the associated Laguerre functions and ξ is a parameter whose value is to be determined by the requirements of convergence. A rapid convergence of the highly excited levels in a laboratory field strength (for example 50 kG) was achieved. Thus the use of the complete basis of Sturmian functions proves to be suitable in cases of laboratory as well as of astrophysical interest.

Close to and above the ionisation threshold ($E = 0$) most treatments are based on Edmonds (1970), who recognized that the particular orbits round the nucleus in the plane perpendicular to the field are important because of the agreement with the experimental data (results) available then.* This $z = 0$ plane problem could be tackled semi-classically. This treatment (Edmonds 1970, Starace 1973, Rau 1979 and O'Connell (1974)) gives a correct account of the spacing of the quasi-Landau resonances observed in the alkaline earths (Garton and Tomkins 1969).

To give specific and quantitative criteria: the different regimes, discussed above, can be classified by comparison with the spacing between the unperturbed Coulomb levels $2Ry/n^3$. We have (Gay, 1984)

- (1) inter- l -mixing when the diamagnetic perturbation term of the Hamiltonian is much smaller than $2Ry/n^3$, i.e. $H_D \sim \frac{e^2 B^2}{8 m_e} a_0 n^4 \ll \frac{2Ry}{n^3}$.
- (2) inter- n -mixing when they are comparable, i.e. $H_D \sim \frac{2Ry}{n^3}$.
- (3) strong field mixing regime when the magnetic interaction is competing with the electrostatic interaction of comparable strength so that Landau and atomic radii are approximately equal ($\frac{2Ry}{n^3} \sim \hbar\omega_c$).
- (4) the Landau regime when $2Ry/n^3$ is much smaller than the Landau spacing $\hbar\omega_c$.

Since we are in the region of high principal quantum number for the unperturbed system where the quantum solutions are prohibitively expensive, the question arises as to what extent the principal features of the problem can be accounted for by a purely classical treatment.

* The experiments are concerned with absorption spectra so that, exciting from the ground state, only those states having significant overlap with this state will appear.

But it is well known that specific systems, particularly those of interest to atomic physics, are so complex that a computational approach has so far been the most fruitful. The system we are dealing with is but one of these specific examples.

Edmonds and Pullen (1980) attempted a classical explanation and gave a macroscopic description of the motion, through studying surfaces of section, for the zero angular momentum case only, by examining the surfaces of sections. They also attribute the $1.5 \hbar \omega_c$ spacing near the ionization limit to planar orbits in the $z = 0$ plane. Further investigations were made by Robnik (1981) and by Delos *et al* (1984) but their work, using different approaches, is applied to strong magnetic fields.

We have generalized Edmonds and Pullen's method to arbitrary angular momentum, located periodic orbits and given a serious answer to the question of their stability. Some of the well known (generic and non-generic) types of bifurcation of periodic orbits are found. A new pattern of bifurcation of periodic orbits, in autonomous Hamiltonian systems, has been discovered. We have calculated new energy spacings associated with some of these periodic orbits. These spacings are confirmed by recent photoionization experiments.

This thesis comprises twelve chapters. In chapter (2) we give an introduction to Hamiltonian dynamics: canonical transformations, properties of phase flow, the extended phase space and the generalized time regularization technique, are all explained.

In chapter (3) perturbed integrable systems are explained with reference to the KAM theorem. Chapter (4) gives a comprehensive

account of surfaces of section, twisting maps and properties of area-preserving maps.

The classical Hamiltonian, for the quadratic Zeeman problem, and Hamilton's equations of motion are derived in dimensionless forms, in both spherical and cylindrical coordinates (chapter (5)).

In order to avoid numerical difficulties as we compute the phase space trajectories, we achieved (in chapter (6)) two kinds of regularization, one by a canonical transformation and the other by a non-canonical one.

Chapter (7) includes a description of the regular and irregular motion and shows, by investigating the surfaces of section, the transition from the regular regime to the chaotic regime in the cases $0 \leq |m| \leq 3$ with laboratory magnetic field strengths. (Al-Laithy *et al* (1985)). An explanation of the numerical and the computational methods used are also given.

The planar motions (in the xy -plane) perpendicular to the magnetic field \mathbf{B} are described in chapter (8).

In chapter (9) we explain how the non-planar periodic orbits are located and classification of them is given.

The bifurcations of these orbits are followed, for the different classes, with respect to variations in the energy parameter.

The stability of periodic orbits in Hamiltonian systems, through the Liapunov characteristic exponents, is explained. The calculation of

these exponents, by linearization of the corresponding Poincaré map, is explained. An application of this method to the periodic orbits in the quadratic Zeeman potential is given. Non-generic bifurcations, in addition to the period doubling bifurcation, of these orbits are found (chapter (10)).

Various semiclassical quantization rules are explained in chapter (11). Quantization is achieved for some of the periodic orbits and new level spacings are predicted. The predicted spectra, due to these periodic motions, are calculated for several field strengths and compared with recent observations (Holle *et al* (1986)). The conclusions are summarized in a final chapter.

$$\ddot{X} = F(X, \dot{X}, t), \quad (2.1.1)$$

where the function $F: R^N \times R^N \times R \rightarrow R^N$ is determined experimentally and its form constitutes the definition of the system.

Under certain smoothness conditions on the function F the existence and uniqueness theorems apply in the sense that F and the initial conditions $X(t_0)$ and $\dot{X}(t_0)$ uniquely determine the motion. The image of the mapping, γ , is called a trajectory or a curve in R^N .

If there exists a function $\mathcal{H}(X)$ such that $F = -\frac{\partial \mathcal{H}}{\partial X}$, the motion is conservative and equation (2.1.1) takes the form $\ddot{X} + \frac{\partial \mathcal{H}}{\partial X} = 0$.

Now let y be a vector in the N -dimensional coordinate space R^N and

$$y = ((t, \gamma) : y = \gamma(t), t_0 \leq t \leq t_1)$$

be the set of all curves joining the two points (t_0, γ_0) and (t_1, γ_1) in

CHAPTER (2)

Hamiltonian dynamics

(2.1) Equivalent forms of the equations of motion.

The general motion of a system of s points (with unit masses) in the three-dimensional Euclidian space R^3 defines a mapping χ of the time axis into the configuration space of the points, i.e. $\chi : R \rightarrow R^N$ where $N = 3s$.

Newton's principle of determinacy states that the initial state of a mechanical system (i.e. its initial position $\mathbf{X}(t_0)$ and initial velocity $\dot{\mathbf{X}}(t_0)$) determines all its motion. The acceleration $\ddot{\mathbf{X}}(t)$ is given by Newton's equation

$$\ddot{\mathbf{X}} = \mathbf{F}(\mathbf{X}, \dot{\mathbf{X}}, t), \quad (2.1.1)$$

where the function $\mathbf{F} : R^N \times R^N \times R \rightarrow R^N$ is determined experimentally and its form constitutes the definition of the system.

Under certain smoothness conditions on the function \mathbf{F} the existence and uniqueness theorems apply in the sense that \mathbf{F} and the initial conditions $\mathbf{X}(t_0)$ and $\dot{\mathbf{X}}(t_0)$ uniquely determine the motion. The image of the mapping, \mathbf{X} , is called a trajectory or a curve in R^N .

If there exists a function $U(\mathbf{X})$ such that $\mathbf{F} = -\frac{\partial U}{\partial \mathbf{X}}$, the motion is conservative and equation (2.1.1) takes the form $\ddot{\mathbf{X}} + \frac{\partial U}{\partial \mathbf{X}} = 0$.

Now let \mathbf{y} be a vector in the N -dimensional coordinate space R^N and

$$\gamma = \{(t, \mathbf{y}) : \mathbf{y} = \mathbf{y}(t), t_0 \leq t \leq t_1\}$$

be the set of all curves joining the two points (t_0, \mathbf{y}_0) and (t_1, \mathbf{y}_1) in

R^{N+1} . An extremal of a differentiable functional $\Phi(\gamma)$ is defined as a curve γ such that $\delta\Phi(\gamma, h) = 0$ for all curve variations h ($|h| < \epsilon \ll 1$). A theorem in the calculus of variations (Shilov 1974 and Arnold 1978) states that a curve in γ is an extremal of the functional

$$\Phi(\gamma) = \int_{t_0}^{t_1} L(y, \dot{y}, t) dt$$

i.e.

$$\delta\Phi = \delta \int_{t_0}^{t_1} L dt = 0, \quad (2.1.2)$$

if and only if the Euler-Lagrange equation $\frac{d}{dt}(\frac{\partial L}{\partial \dot{y}}) - \frac{\partial L}{\partial y} = 0$ is satisfied along that curve.

The motions of the mechanical system $\ddot{\mathbf{X}} + \frac{\partial U}{\partial \mathbf{X}} = 0$ coincide with the extremals of the functional $\Phi(\gamma) = \int_{t_0}^{t_1} L dt$ where $L = T - U$ is the difference between the kinetic energy $T = \frac{1}{2} \dot{\mathbf{X}} \cdot \dot{\mathbf{X}}$ and the potential energy $U(\mathbf{X})$. (This is because $\frac{\partial L}{\partial \dot{\mathbf{X}}} = \dot{\mathbf{X}}$ and $\frac{\partial L}{\partial \mathbf{X}} = -\frac{\partial U}{\partial \mathbf{X}}$). Therefore the evolution of the position vector $\mathbf{X}(t)$ in the configuration space is subject to the Euler-Lagrange (Lagrange) equation

$$\frac{d}{dt}(\frac{\partial L}{\partial \dot{\mathbf{X}}}) - \frac{\partial L}{\partial \mathbf{X}} = 0, \quad L = T - U. \quad (2.1.3)$$

The function L is called the Lagrangian of the system.

Now assume, for example, that the system is constrained by the functionally independent equations $f_1(\mathbf{X}) = 0, \dots, f_k(\mathbf{X}) = 0$, then $n = 3s - k$ is the number of degrees of freedom. Let $\mathbf{q} = (q_1, q_2, \dots, q_n)$ be a position vector in the configuration space of that constrained system. That is let $\mathbf{q} \in R^n$ and $\dot{\mathbf{q}} \in R^n$ be the vector position and velocity over all the degrees of freedom. We consider the system of Lagrange's equations

$$\dot{\mathbf{p}} = \frac{\partial L}{\partial \mathbf{q}} \quad \text{where} \quad \mathbf{p} = \frac{\partial L}{\partial \dot{\mathbf{q}}}, \quad (2.1.4)$$

and we assume that $L = \frac{1}{2}\dot{\mathbf{X}} \cdot \dot{\mathbf{X}} - U(\mathbf{q})$ is convex with respect to $\dot{\mathbf{q}}$ (i.e. $\frac{\partial^2 L}{\partial \dot{\mathbf{q}}^2} d\dot{\mathbf{q}} d\dot{\mathbf{q}}$ is positive definite). The system of Lagrange's equations is equivalent to the system of $(2n + 1)$ -first order equations (called Hamilton's equations)

$$\dot{\mathbf{p}} = -\frac{\partial H}{\partial \mathbf{q}}, \quad \dot{\mathbf{q}} = \frac{\partial H}{\partial \mathbf{p}}, \quad \frac{\partial H}{\partial t} = -\frac{\partial L}{\partial t} \quad (2.1.5)$$

where

$$H(\mathbf{p}, \mathbf{q}, t) = \mathbf{p} \cdot \dot{\mathbf{q}} - L(\mathbf{q}, \dot{\mathbf{q}}, t), \quad (2.1.6)$$

is the Legendre transformation of the Lagrangian function L viewed as a function of $\dot{\mathbf{q}}$. The function H is called the Hamiltonian.

If, in particular, $\frac{\partial H}{\partial t} = 0$, the Hamiltonian H is conserved :

$$H(\mathbf{q}(t), \mathbf{p}(t)) = E \text{ (constant)}, \quad (2.1.7)$$

which defines a $(2n - 1)$ -dimensional surface S_E called the energy surface.

The use of the coordinates \mathbf{q} and momenta \mathbf{p} (in (2.1.5)) as independent variables allows a greater freedom in selecting the physical quantities to be designated as \mathbf{q} and \mathbf{p} . As a result, the Hamiltonian formulation gives more abstract ways of presenting the physical content of mechanics and constructing the more modern theories of mathematical physics (optics, quantum mechanics, etc.). Moreover, it has even greater value for the approximate methods of perturbation theory for understanding the general character of motion in complicated mechanical systems. This formulation proves to be very powerful in giving more far reaching theoretical development than any other means.

The $2n$ -dimensional space with coordinates $q_1, q_2, \dots, q_n; p_1, p_2, \dots, p_n$ is called phase space. The phase flow is the one-parameter group of

transformations of phase space

$$g^t : (\mathbf{q}(0), \mathbf{p}(0)) \rightarrow (\mathbf{q}(t), \mathbf{p}(t)), \quad (2.1.8)$$

where $\mathbf{q}(t)$, $\mathbf{p}(t)$ are solutions of Hamilton's equations (Arnold 1978).

We see that Lagrange's equations are derived from a variational principle (2.1.2), with fixed end conditions, in the space of events $QT \in R^{n+1}$ whose coordinates are \mathbf{q} , t . Hamilton's equations also can be derived from a variational principle, with free end conditions, in the space of states $QTP \in R^{2n+1}$ whose coordinates are \mathbf{q} , t , \mathbf{p} . This follows from the important theorem of Poincare Cartan: "The integrals of the form $\mathbf{p} \cdot d\mathbf{q} - H dt$, along two curves γ_1 and γ_2 which circle the same tube of the phase trajectories of (2.1.5), are the same" (see Gantmacher, 1970 also Arnold, 1978).

i.e.

$$\delta I = \delta \oint (\mathbf{p} \cdot d\mathbf{q} - H dt) = 0. \quad (2.1.8)$$

The phase tube and the Poincare's integral invariant are explained diagrammatically in figure (2.1).

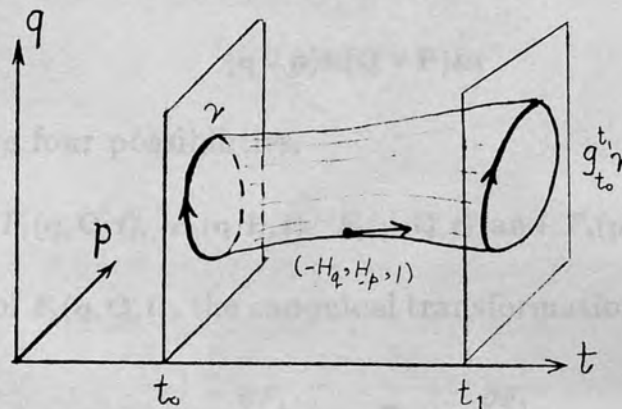


Figure (2.1). A phase tube,
(an explanation of the Poincare integral invariant)

(2.2) Canonical transformations.

Let q, p be any set of $2n$ variables whose time evolution is given by equations of the form (2.1.5). These variables are said to be canonical, with q_i and p_i as conjugate variables. Let Q, P be another set of $2n$ variables

$$\begin{aligned} Q &= Q(q, p, t), \\ P &= P(q, p, t). \end{aligned} \quad (2.2.1)$$

If Q, P are again canonical and with a new Hamiltonian (K) we have

$$\frac{dQ}{dt} = \frac{\partial K}{\partial P}, \quad \frac{dP}{dt} = -\frac{\partial K}{\partial Q}. \quad (2.2.2)$$

Then equations (2.2.1) represent a canonical transformation.

The canonical transformation is useful when the function K is in a simpler form than H . In this case, the system of equations (2.2.2) is less difficult to solve than the original system.

The method of generating canonical transformations depends on the fact that the variational principle (2.1.8) must be satisfied for both (q, p) and (Q, P) . This yields generating functions of $(q$ or $p)$ and $(Q$ or $P)$ and of the time t , explicitly, of the logical formula

$$(q \vee p) \& (Q \vee P) \& t$$

i.e. there are four possibilities:

$$F_1(q, Q, t), F_2(q, P, t), F_3(p, Q, t) \text{ and } F_4(p, P, t). \quad (2.2.3)$$

In the case of $F_1(q, Q, t)$, the canonical transformation is accomplished by

$$p = \frac{\partial F_1}{\partial q}, \quad P = -\frac{\partial F_1}{\partial Q}, \quad (2.2.4)$$

The four possibilities for canonical transformations are collected in table (2.2)

Table (2.2). Summary of canonical transformation in the phase space.

Generating function	$q =$	$p =$	$Q =$	$P =$	$K =$
$F_1(q, Q, t)$		$\frac{\partial F_1}{\partial q}$		$-\frac{\partial F_1}{\partial Q}$	$H + \frac{\partial F_1}{\partial t}$
$F_2(q, P, t)$		$\frac{\partial F_2}{\partial q}$	$\frac{\partial F_2}{\partial P}$		$H + \frac{\partial F_2}{\partial t}$
$F_3(p, Q, t)$	$-\frac{\partial F_3}{\partial p}$			$-\frac{\partial F_3}{\partial Q}$	$H + \frac{\partial F_3}{\partial t}$
$F_4(p, P, t)$	$-\frac{\partial F_4}{\partial p}$		$\frac{\partial F_4}{\partial P}$		$H + \frac{\partial F_4}{\partial t}$

Canonical transformations are commonly used throughout the developed structure of classical mechanics particularly the Hamilton-Jacobi theory which is extensively explained by Goldstein (1980) and briefly, but elegantly, by Landau and Lifshitz (1976).

(2.3) Volume preservation of phase flow.

An important theorem (Liouville's theorem) states that the volume of any portion D of phase space ($\int_D dq \cdot dp$) is conserved when the representative points which compose it move in accordance with Hamilton's equations (see Synge, 1960, for absolute integral invariants in phase space p.172 also Arnold, 1978 p.238).

(2.4) The extended phase space,

A simpler and more geometric variational principle can be obtained by taking appropriate particles in the phase space of $2n$ dimensions to higher dimensionality. One of these is the so-called extended phase

If $\mathcal{D} = \mathcal{D}(\mathbf{q}, \mathbf{p}, t)$ is the probability of a given ensemble or density distribution of system points in the phase space, the continuity equation (see Lichtenberg and Lieberman 1983)

$$\text{Div}(\mathcal{D}\mathbf{v}) + \frac{\partial \mathcal{D}}{\partial t} = 0 \quad (2.3.1)$$

holds, where

$$\mathbf{r} = (\mathbf{q}, \mathbf{p})$$

and

$$\mathbf{v} = \dot{\mathbf{r}} = \left(\frac{\partial H}{\partial \mathbf{p}}, -\frac{\partial H}{\partial \mathbf{q}} \right)$$

are the system point and the phase velocity vector respectively.

Another important theorem is the Poincaré's recurrence theorem :

"Let g be a volume-preserving continuous one-to-one mapping which maps a bounded region D of Euclidian space onto itself : $gD = D$. Then in any neighbourhood B of any point of D there is a point $x \in B$ which returns to B , i.e. $g^n x \in B$ for some $n > 0$ ".

Liouville's theorem has many applications in mechanics. For example, the volume preservation property makes it possible to apply the Poincaré's recurrence theorem to the phase flow g^t of a two-dimensional system with potential $|U(q_1, q_2)| \rightarrow \infty$ as $(q_1, q_2) \rightarrow \infty$ (Arnold 1978). This condition is valid for the quadratic Zeeman potential (5.31) ^{except when $z=0$} and in the bounded region defined by $D = \{\mathbf{q}, \mathbf{p} : T + U \leq E\}$ almost every point returns repeatedly to the vicinity of its initial point. This seems to be paradoxical but the resolution of this paradox lies in the fact that the returns may be in extremely long periods of time. For further applications to methods of ergodic theory see Arnold(1978).

(2.4) The extended phase space.

A simpler and more symmetric variational principle can be obtained by taking representative points in the phase space of $2n$ dimensions to higher dimensionality. One of these is the so-called extended phase space of $(2n + 2)$ dimensions (called by some authors the space of states and energy (*QTPH*)). This is again a step forward to more abstraction by which dynamical theories are better illustrated.

Following Synge (1960) and also Szebehely (1967), we consider a dynamical system of n degrees of freedom with generalised coordinates and momenta $q_1, \dots, q_n, p_1, \dots, p_n$. Consider a space (*QTPH*) whose points are represented by the coordinates

$$\begin{aligned}x_\rho &= q_\rho, & x_{n+1} &= t, \\y_\rho &= p_\rho, & y_{n+1} &= -H,\end{aligned}\tag{2.4.1}$$

where we use the suffix ρ for the range $1, 2, \dots, n$. The suffix i will be reserved for the range $1, 2, \dots, n + 1$. A dynamical system with y_i , conjugate to x_i is defined by assigning a $(2n + 1)$ -dimensional energy surface to which the representative points in (*QTPH*) are confined

$$\Gamma(x_1, \dots, x_{n+1}, y_1, \dots, y_{n+1}) = 0.\tag{2.4.2}$$

Solving (2.4.2) for y_{n+1} , Γ can be written in the form

$$\Gamma = y_{n+1} + \nu(x_1, \dots, x_{n+1}, y_1, \dots, y_n) = 0.\tag{2.4.3}$$

Equivalently;

$$H = \nu(\mathbf{q}, t, \mathbf{p}).\tag{2.4.4}$$

In this new space we use " ν " (equation (2.4.4)) rather than " H " to remove the confusion arising from the appearance of H as a coordinate and as a functional symbol.

"Using an energy function $\Gamma(\mathbf{x}, \mathbf{y})$ instead of merely an energy surface enlarges the scope of dynamics. To a given energy function there corresponds a unique energy surface with equation $\Gamma(\mathbf{x}, \mathbf{y}) = 0$; to a given energy surface there corresponds an infinity of energy functions."
(Synge (1960)).

We define trajectories in (QTPH) by the variational principle

$$\delta \int \sum y_i \delta x_i = 0, \quad (2.4.5)$$

and

$$\Gamma(x, y) = \text{constant}. \quad (2.4.6)$$

We introduce now a special parameter ϖ so that the new $(n + 1)$ th coordinate $t = x_{n+1}$ and the independent variable $t = \varpi$ may be distinguished. Hence we obtain the canonical equations

$$\frac{dx_i}{d\varpi} = \frac{\partial \Gamma}{\partial y_i}, \quad \frac{dy_i}{d\varpi} = -\frac{\partial \Gamma}{\partial x_i}. \quad (2.4.7)$$

In the case of 2 degrees of freedom let us consider the Hamiltonian

$$H = H(q_1, q_2, p_1, p_2). \quad (2.4.8)$$

Hamilton's equations of motion are

$$\frac{dq}{dt} = \frac{\partial H}{\partial p_i} \quad \text{and} \quad \frac{dp}{dt} = -\frac{\partial H}{\partial q_i} \quad i = 1, 2. \quad (2.4.9)$$

In the 6-dimensional extended phase space we have

$$\Gamma = p_3 + \nu(q_1, q_2, p_1, p_2), \quad (= 0) \quad (2.4.10)$$

where the relation to the previous formulation is given by

$$p_3 = -H \quad \text{and} \quad \nu(q_1, q_2, p_1, p_2) = H(q_1, q_2, p_1, p_2) \quad (2.4.11)$$

The equations of motion in the extended phase space are

$$\frac{dq_i}{d\varpi} = \frac{\partial \Gamma}{\partial p_i}, \quad \frac{dp_i}{d\varpi} = -\frac{\partial \Gamma}{\partial q_i} \quad i = 1, 2, 3. \quad (2.4.12)$$

For $i = 3$, we have

$$\frac{dt}{d\varpi} = 1 \quad \text{and} \quad p_3 = \text{constant}. \quad (2.4.13)$$

Note that because the original Hamiltonian does not contain the time explicitly, Γ does not contain q_3 and this leads to $p_3 = -H = \text{constant}$.

(2.5) Canonical transformation in the extended phase space.

Parallel to what we have described (in section (2.2)) for the phase space, we still have a variational principle (equation (2.4.5)) which is even simpler and more symmetric than (2.1.8). For a canonical transformation, (2.4.5) must be satisfied for both the old coordinates (x_1, \dots, x_{n+1}) and the new coordinates (X_1, \dots, X_{n+1}) say. Consequently; table (2.2) is also applicable in the extended phase space except that we replace the independent variable t by ϖ .

(2.6) Generalised time transformation.

Without loss of generality we consider the case of two degrees of freedom with the Hamiltonian given in (2.4.8), which for the purpose of this section, we assume to have singularities that usually cause computational difficulties. A powerful technique for removing these singularities (a regularisation) is to use a time transformation in the form

$$dt = f(q_1, q_2) d\tau. \quad (2.6.1)$$

We show that if Γ (equation (2.4.10)) is replaced by

$$\begin{aligned} \Gamma^* &= f(q_1, q_2)\Gamma \\ &= p_3 f(q_1, q_2) + f(q_1, q_2) \nu(q_1, q_2, p_1, p_2). \quad (= 0), \end{aligned} \quad (2.6.2)$$

we get the following canonical set

$$\frac{dq_i}{d\tau} = \frac{\partial \Gamma^*}{\partial p_i},$$

$$\frac{dp_i}{d\tau} = -\frac{\partial \Gamma^*}{\partial q_i}, \quad i = 1, 2, 3. \quad (2.6.3)$$

We verify this: for $i=3$

$$\frac{dq_3}{d\tau} = f(q_1, q_2) \quad \text{then} \quad dt = f(q_1, q_2) d\tau, \quad (2.6.4)$$

$$\frac{dp_3}{d\tau} = 0 \quad \text{then} \quad p_3 = \text{constant}. \quad (2.6.5)$$

The verification for $i = 1, 2$ leads to Hamilton's equations of motion

$$\frac{dq_i}{dt} = \frac{\partial H}{\partial p_i}, \quad \frac{dp_i}{dt} = -\frac{\partial H}{\partial q_i},$$

which completes the proof.

The function f is to be chosen in a suitable form so as to remove the singularities from the right hand side of (2.6.2). Here, we must notice that the introduction of the extended phase space is essential for using this method. But it cannot be used, in general, in the phase space (Szebehely (1967)). This method will be applied to a ten-dimensional extended phase space (in section (6.2)).

CHAPTER (3)

Regular and irregular motion (I)

(3.1) Integrable systems and invariant tori.

In a conservative Hamiltonian system with n degrees of freedom (i.e. with a $2n$ -dimensional phase space) assume that there exist n independent analytic single-valued first integrals

$$F_i(\mathbf{q}, \mathbf{p}) = \alpha_i, \quad i = 1, 2, \dots, n \quad (3.1.1)$$

i.e. along any phase trajectory, any function F_i takes a constant value α_i . If a canonical transformation $\mathbf{q}, \mathbf{p} \rightarrow \mathbf{Q}, \mathbf{P}$ is performed* such that $\mathbf{P} = \boldsymbol{\alpha}$ (a constant), we get (from (2.2.2))

$$0 = \dot{\mathbf{P}} = -\frac{\partial K}{\partial \mathbf{Q}}, \quad (3.1.2)$$

i.e. K does not depend on \mathbf{Q} . Then

$$\dot{\mathbf{Q}} = \frac{\partial K(\boldsymbol{\alpha})}{\partial \boldsymbol{\alpha}} = \text{constant}, \quad (3.1.3)$$

or

$$\mathbf{Q} = \left(\frac{\partial K}{\partial \boldsymbol{\alpha}}\right)t + \boldsymbol{\delta}, \quad (3.1.4)$$

where $\boldsymbol{\delta}$ is a constant.

A generating function of the form $S(\mathbf{q}, \mathbf{P})$ (see table (2.2)) yields

$$\mathbf{Q} = \frac{\partial S(\mathbf{q}, \mathbf{P})}{\partial \mathbf{P}}, \quad (3.1.5)$$

with

$$S = \int_{\mathbf{q}_0}^{\mathbf{q}} \mathbf{p}(\mathbf{q}, \boldsymbol{\alpha}) \cdot d\mathbf{q} = S(\mathbf{q}, \boldsymbol{\alpha}), \quad (3.1.6)$$

where the integrand $\mathbf{p}(\mathbf{q}, \boldsymbol{\alpha})$ can be derived by solving (3.1.1) for \mathbf{p} . From (3.1.4), (3.1.5) and (3.1.6) we get the solution

$$\mathbf{q} = \mathbf{q}(t, \boldsymbol{\alpha}, \boldsymbol{\delta}),$$

* Such a transformation exists if (3.1.7) is satisfied.

(α and δ are the $2n$ constants required to define a solution)

All exactly-soluble systems in classical mechanics are integrable in this sense (the Kepler problem and the n -dimensional oscillator are examples of such integrable systems). When $F_i(\mathbf{q}, \mathbf{p})$ are in involution i.e. the Poisson brackets

$$\{F_r, F_s\} = \frac{\partial F_r}{\partial \mathbf{p}} \cdot \frac{\partial F_s}{\partial \mathbf{q}} - \frac{\partial F_s}{\partial \mathbf{p}} \cdot \frac{\partial F_r}{\partial \mathbf{q}} = 0, \quad r, s = 1, 2, \dots, n \quad (3.1.7)$$

then n further such functions may be found and any complete set of functions of the α 's, such as the action variables (defined below), are a set of isolating integrals.

By virtue of (3.1.1), the trajectory of the system can explore at most an n -dimensional manifold \mathcal{M} defined by the (smooth) level set

$$\mathcal{M} = \{(\mathbf{q}, \mathbf{p}) : F_i(\mathbf{q}, \mathbf{p}) = \alpha_i, \quad i = 1, 2, \dots, n\}. \quad (3.1.8)$$

Topologically, if \mathcal{M} is connected and compact, then it is diffeomorphic to the n -dimensional torus (i.e. a direct product of n circles, (Arnold (1978))):

$$T^n = \{(\phi_1, \phi_2, \dots, \phi_n) \bmod 2\pi\}.$$

Introduce n independent variables $J_i(\alpha)$ defined by

$$J_i = \frac{1}{2\pi} \oint_{\gamma_i} \mathbf{p} \cdot d\mathbf{q} \quad (3.1.9)$$

as the new momenta, where γ_i are the n independent irreducible circuits on the torus (i.e. which cannot be shrunk to 0). The relation (3.1.9) defines the J_i 's in terms of the α_i 's and vice versa.

By analogy to the canonical transformation used above

$(\mathbf{q}, \mathbf{p}) \rightarrow (\mathbf{Q}, \mathbf{P})$, with a change of symbols, a canonical transformation $(\mathbf{q}, \mathbf{p}) \rightarrow (\boldsymbol{\theta}, \mathbf{J})$ can be performed. Then

$$H = K(\mathbf{J}), \quad (3.1.10)$$

(since H itself is a constant of the motion and equal to one of the α_i 's) and

$$S(\mathbf{q}, \mathbf{J}) = \int_{\mathbf{q}_0}^{\mathbf{q}} \mathbf{p}(\mathbf{q}, \mathbf{J}) \cdot d\mathbf{q}, \quad (3.1.11)$$

$$\dot{\theta} = \frac{\partial K(\mathbf{J})}{\partial \mathbf{J}} = \text{constant vector } \boldsymbol{\omega}, \quad (3.1.12)$$

$$\dot{\mathbf{j}} = -\frac{\partial K(\mathbf{J})}{\partial \boldsymbol{\theta}} = \mathbf{0}. \quad (3.1.13)$$

When these equations are integrated,

$$\theta = \boldsymbol{\omega} t + \boldsymbol{\beta}, \quad (3.1.14)$$

$$\mathbf{J} = \text{constant}, \quad (3.1.15)$$

\mathbf{J} is called the action, θ the angle (because $(\Delta\theta_i)_{\gamma_i} = 2\pi$, see Berry 1978) and $\boldsymbol{\omega}$ the frequency vector of the motion. From (3.1.14) and (3.1.15) the motion is on a surface labelled by \mathbf{J} on which the position of a phase point of the system is specified by θ . This surface (the torus) is invariant with respect to the phase flow of the system in the sense that an orbit starting on it remains on it for all times t (Arnold 1978). This is immediately obvious in a system of 2-degrees of freedom. Because \mathbf{q} and \mathbf{p} are periodic functions of θ with period 2π , Fourier expansion yields

$$\mathbf{p}(t) = \sum_{\mathbf{m}} p_{\mathbf{m}}(\mathbf{J}) \exp[i \mathbf{m} \cdot (\boldsymbol{\omega} t + \boldsymbol{\beta})], \quad (3.1.16)$$

$$\mathbf{q}(t) = \sum_{\mathbf{m}} q_{\mathbf{m}}(\mathbf{J}) \exp[i \mathbf{m} \cdot (\boldsymbol{\omega} t + \boldsymbol{\beta})], \quad (3.1.17)$$

where \mathbf{m} is a vector with n integer components. That is the motion on \mathcal{M} is generally multiply (or conditionally) periodic with n periods $T_i = \frac{2\pi}{\omega_i}$.

(3.2) Resonant and non-resonant tori.

Let I^n be the field of all vectors with n integer components. If the frequencies $\omega_1, \omega_2, \dots, \omega_n$ are such that

$$\mathbf{m} \cdot \boldsymbol{\omega} \neq 0 \quad \forall \mathbf{J} \quad (3.2.1)$$

for all non-zero $\mathbf{m} \in I^n$, then the invariant tori (with n frequencies) form a dense set in phase space. Such tori are called non-resonant (or proper) tori. The frequencies $\boldsymbol{\omega}$ which satisfy (3.2.1) are said to be linearly independent or non-degenerate. A necessary condition for linear independence is

$$\det \left| \frac{d\boldsymbol{\omega}}{d\mathbf{J}} \right| = \det \left| \frac{\partial^2 H}{\partial \mathbf{J}^2} \right| \neq 0, \quad (3.2.2)$$

usually called the non-degeneracy condition (Lichtenberg and Lieberman 1983). If, however, s relations of the form

$$\mathbf{m} \cdot \boldsymbol{\omega} = 0 \quad \forall \mathbf{J} \quad (3.2.3)$$

hold, where $s \leq n-1$, the phase trajectory lies on an $(n-s)$ -dimensional invariant torus. Such tori are called resonant tori and they too are dense in phase space. The system in this case is said to be s -fold degenerate. In the particular case when $s = n-1$, we get closed orbits. The frequencies $\boldsymbol{\omega}$ in this case are said to be commensurable and the system is completely degenerate. The number of independent frequencies is then 1 i.e. $\boldsymbol{\omega} = k\Omega$, $k \in I^n$. Closure occurs after a period

$$T = \frac{2\pi}{\Omega} = \frac{2\pi k_i}{\omega_i} = \frac{k_i}{T_i} \quad i = 1, 2, \dots, n. \quad (3.2.4)$$

As an example, the case of 2-degrees of freedom (3.2.3) gives

$$\frac{\omega_1}{\omega_2} = \frac{r}{s}, \quad r, s \in I$$

for a resonant torus where r and s are relatively prime. For a proper torus, $\frac{\omega_1}{\omega_2} = \sigma =$ an irrational number. Arithmetically, σ can be

approximated arbitrarily closely by a rational number. Therefore, proper tori can be arbitrarily close to resonant ones (Berry 1978). Nevertheless, a random choice of initial conditions in the phase space of an integrable system gives a zero probability of landing on a resonant torus (since the probability of picking out a rational number by a random choice of a real number is zero). A further property is that non-resonant tori form a set of full measure, i.e. the union of all invariant resonant tori is a set of measure zero (in the sense of Lebesgue) (Arnold 1978).

(3.3) Canonical perturbation theorem.

The class of systems which are known to us as solvable integrable problems is only a small proportion of the total number of systems. Nevertheless, they are helpful: The properties of some non-integrable systems can be studied if these systems can be considered to follow from a small perturbation of integrable ones. In this case we consider the integrable system as a first approximation.

If an integrable system, which in angle action variables (θ, \mathbf{J}) has a Hamiltonian $H_0(\mathbf{J})$, is perturbed to a system with Hamiltonian

$$H(\theta, \mathbf{J}) = H_0(\mathbf{J}) + \epsilon H_1(\theta, \mathbf{J}), \quad |\epsilon| \ll 1 \quad (3.3.1)$$

\mathbf{J} is no longer a constant of the motion for the new system. We seek angle-action variables θ', \mathbf{J}' of the perturbed system H , by a transformation: $(\theta, \mathbf{J}) \rightarrow (\theta', \mathbf{J}')$, generated by the function $S(\theta, \mathbf{J}')$, defined in (3.1.11), such that $H(\theta, \mathbf{J}) = H'(\mathbf{J}')$. Since $\mathbf{J} = (\partial S / \partial \theta)$ (see table (2.2)),

$$H\left(\theta, \frac{\partial S(\theta, \mathbf{J}')}{\partial \theta}\right) = H'(\mathbf{J}'). \quad (3.3.2)$$

Expanding S as a power series in ϵ :

$$S = \theta \cdot \mathbf{J}' + \epsilon S_1(\theta, \mathbf{J}') + O(\epsilon^2) \quad (3.3.3)$$

(As $\epsilon = 0$, the zeroth order $S = S_0 = \theta \cdot \mathbf{J}'$ generates the identity $\theta' = \theta$; $\mathbf{J}' = \mathbf{J}$). Substituting from (3.3.3) into (3.3.2) where H is given by (3.3.1), we get

$$H'(\mathbf{J}') = H_0(\mathbf{J}') + \epsilon(\omega_0 \cdot \frac{\partial S_1}{\partial \mathbf{J}'} + H_1(\theta, \mathbf{J}')), \quad (3.3.4)$$

where $\omega_0 = \frac{\partial H(\mathbf{J}')}{\partial \mathbf{J}'}$ is the unperturbed frequency vector. H_1 and S_1 are periodic in θ so that in terms of Fourier series we have

$$H_1(\theta, \mathbf{J}') = \sum_{\mathbf{m}} H_{1\mathbf{m}}(\mathbf{J}') \exp(i\mathbf{m} \cdot \theta), \quad (3.3.5)$$

$$S_1(\theta, \mathbf{J}') = \sum_{\mathbf{m} \neq 0} S_{1\mathbf{m}}(\mathbf{J}') \exp(i\mathbf{m} \cdot \theta). \quad (3.3.6)$$

Substituting from (3.3.5) and (3.3.6) into (3.3.4) and equating coefficients of $\exp(i\mathbf{m} \cdot \theta)$ we get

$$\mathbf{m} = 0 \Rightarrow H'(\mathbf{J}') = H_0(\mathbf{J}') + \epsilon H_{10}(\mathbf{J}') + O(\epsilon^2), \quad (3.3.7)$$

$$\mathbf{m} \neq 0 \Rightarrow S_{1\mathbf{m}}(\mathbf{J}') = \frac{i H_{1\mathbf{m}}(\mathbf{J}')}{\mathbf{m} \cdot \omega_0(\mathbf{J}')} + O(\epsilon). \quad (3.3.8)$$

Then correct to the first order in ϵ the generating function for an integrable motion undergoing perturbation (i.e. for new tori) is

$$S(\theta, \mathbf{J}') = \theta \cdot \mathbf{J}' + i\epsilon \sum_{\mathbf{m} \neq 0} \frac{H_{1\mathbf{m}}(\mathbf{J}')}{\mathbf{m} \cdot \omega_0(\mathbf{J}')} \exp(i\mathbf{m} \cdot \theta). \quad (3.3.9)$$

So if the frequencies of the unperturbed invariant tori are degenerate i.e. if there are $\mathbf{m} \neq 0$ such that $\mathbf{m} \cdot \omega_0 = 0$ * for some \mathbf{J}' , the series (3.3.9) will diverge (unless $H_{1\mathbf{m}}(\mathbf{J}') = 0$). Even for incommensurable ω_0 (i.e. $\mathbf{m} \cdot \omega_0 \neq 0 \forall \mathbf{m} \neq 0$; the case of proper tori), there are \mathbf{m} 's for which $\mathbf{m} \cdot \omega_0$ is arbitrarily small. So we are left with the problem of small divisors and hence convergence is not guaranteed. This problem was avoided by the KAM theorem technique (section 3.4). The most important application of the perturbation series (3.3.9) is in celestial mechanics where H_0 in (3.3.1) is the Hamiltonian of the motion of a

* i.e. the case of resonant tori.

** There is also the problem of convergence of the iteration process when higher orders in ϵ are included.

planet considering the gravitational potential of the sun alone (the Keplerian problem is integrable). The perturbation ϵH_1 represents the gravitational interaction of other planets.

(3.4) The KAM theorem.

Following a conjecture by Kolmogorov in 1954, Arnold (1962) and Moser (1962) proved what has become widely known as the KAM theorem.

This theorem answers the *question about the fate of some invariant proper tori* if an integrable system is slightly perturbed. It proves that most non-resonant tori do not vanish (but persist though in a distorted form). We know that this answer could not be obtained from the series (3.3.9) as the small denominators create difficulties regarding the question of its convergence. The KAM's technique is basically a replacement of *the iterative scheme associated with (3.3.9) by a different scheme*, which is rapidly convergent. This technique is based on Newton's method of tangents for finding roots of algebraic equations. With initial error ϵ , the method gives, after n approximations, an error of order ϵ^{2^n} . This is sufficient to paralyze the influence of small denominators and shows the convergence of the entire procedure.

There are conditions for the KAM tori to exist

- (1) non-degeneracy condition (sufficient non-linearity)

$$\det \left| \frac{\partial \omega}{\partial \mathbf{J}} \right| \neq 0, \quad (3.4.1)$$

where $\omega = (\partial H_0 / \partial \mathbf{J})$, so that the unperturbed tori depend uniquely on ω .

- (2) a smoothness condition of the perturbation (a sufficient number, M , of continuous derivatives of H_1).

(3) initial conditions sufficiently far from any resonance of low order. This can be satisfied by fixing a set of independent frequencies ω which, for $\epsilon > 0$, implies the existence of $C(\epsilon)$ such that

$$|\mathbf{m} \cdot \omega| > C(\epsilon) \cdot |\mathbf{m}|^{-\gamma} \quad \forall \mathbf{m} \neq \mathbf{0}, \quad \mathbf{m} \in I^n. \quad (3.4.2)$$

C is independent of \mathbf{m} but tends to zero with the perturbation parameter ϵ , and γ is dependent on M .

(4) sufficiently small perturbation (ϵH_1).

In the original proof, H was assumed to be analytic (see for example Arnold 1978). Chirikov (1979) has proved, for N degrees of freedom, that the necessary smoothness condition for the existence of KAM surfaces is

$$M \geq 2N - 2. \quad (3.4.3)$$

Moser (1966) has also determined a rigorous sufficient condition

$$M \geq 2N + 2. \quad (3.4.4)$$

Since γ can be identified as $\frac{M}{2}$ (Lichtenberg and Lieberman 1983), then the condition (3.4.2) takes the form

$$|\mathbf{m} \cdot \omega| > C(\epsilon) |\mathbf{m}|^{-(N+1)}. \quad (3.4.5)$$

Formally, the theorem as stated by Arnold (1978) is: "If an unperturbed system is non-degenerate, then for sufficiently small conservative Hamiltonian perturbations, most non-resonant invariant tori do not vanish, but are only slightly deformed, so that in the phase space of the perturbed system, too, there are invariant tori densely filled with phase curves winding around them conditionally-periodically, with a number of independent frequencies equal to the number of degrees of freedom. The invariant tori form a majority in the sense

that the measure of the complement of their union is small when the perturbation is small".

In the case of *two degrees of freedom* a torus survives perturbations if

$$\left| \sigma - \frac{r}{s} \right| > \frac{C(\epsilon)}{2^{2.5}} \quad \forall \text{ relatively prime integers } r, s \quad (3.4.6)$$

where $\sigma = \frac{\omega_1}{\omega_2}$ is the frequency ratio of an unperturbed torus. The torus with

$$\sigma = \frac{1}{1 + \frac{1}{1 + \frac{1}{1 + \dots}}} = 0.61803 = \frac{\sqrt{5} - 1}{2} \quad (3.4.7)$$

survives the largest perturbation (see Berry 1978). This value of σ is called the *golden mean*. Numerical experiments show that non-resonant tori exist for perturbations larger than those allowed by the KAM theorem (this is because of the restrictive condition of small ϵ in the theorem).

Percival (1988) has recently given a measure of the magnitude of ϵ for which the theory is valid.

CHAPTER (4)

Regular and irregular motion (II)

(4.1) The surface of section.

This is a technique, originally suggested by Poincaré (1892), for investigating the structure of the phase space of two-dimensional Hamiltonian systems. The fascination and importance of this method lies in observing and studying the breakdown of integrability and the motion in gaps between the destroyed tori. The surface of section is generally defined for systems of n -degrees of freedom (see Arnold and Avez 1968) but the method *best suits the two-dimensional problems, which we consider here.*

The phase space trajectories are confined to the three-dimensional energy surface, S_E , defined by

$$H(u, p_u, v, p_v) = E. \quad (4.1.1)$$

The surface of section (or the Poincaré surface of section) S_v is defined as the intersection of S_E with

$$v = 0, \quad p_v > 0, \quad (4.1.2)$$

and has (u, p_u) as coordinates. Each point on S_v uniquely defines initial conditions which determine (together with Hamilton's equations of motion) a unique phase trajectory. In other words, any point on S_v specifies completely the state of the system. In a bounded region of phase space a trajectory $\mathbf{X}(t)$ starting at $\mathbf{X}_0 = (u^0, p_u^0)$ crosses S_v repeatedly at points $\mathbf{X}_1 = (u^1, p_u^1)$, $\mathbf{X}_2 = (u^2, p_u^2)$, ... (see figure (4.1.1)). This defines a map (called the Poincaré map) $T : S_v \rightarrow S_v$ which takes

a point X_n on S_v to the next trajectory's intersection X_{n+1} :

$$T : \quad \begin{aligned} u^{n+1} &= f_n(u^n, p_u^n), \\ p_u^{n+1} &= g_n(u^n, p_u^n), \end{aligned} \quad (4.1.3)$$

where f_n and g_n are functions determined by the system.

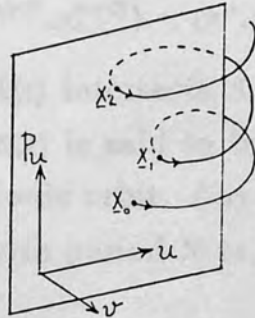


Figure (4.1.1). A trajectory starting at a point X_0 on the surface of section intersects it, successively, at points X_1, X_2, \dots

Because of the Hamiltonian character of the dynamics of the system its state (u^1, p_u^1, v^1, p_v^1) at time t_1 can be obtained from its state (u^0, p_u^0, v^0, p_v^0) at time t_0 by a canonical transformation. This gives the map T an important character as an *area preserving* homeomorphism i.e.

$$\left| \frac{du^{n+1} dp_u^{n+1}}{du^n dp_u^n} \right| = \frac{\partial(u^{n+1}, p_u^{n+1})}{\partial(u^n, p_u^n)} = \begin{bmatrix} \frac{\partial u^{n+1}}{\partial u^n} & \frac{\partial u^{n+1}}{\partial p_u^n} \\ \frac{\partial p_u^{n+1}}{\partial u^n} & \frac{\partial p_u^{n+1}}{\partial p_u^n} \end{bmatrix} = 1. \quad (4.1.4)$$

The manner in which the successive iterates $X_0, X_1, \dots, X_n, \dots$ are distributed suggests three different types of orbits

- (1) a regular trajectory (or quasi periodic orbit): the successive iterates X_0, X_1, \dots fill a closed curve C on S_v which is an invariant curve of the map T i.e., $T(C) = C$. So the trajectory is confined to a two-dimensional torus and fills it densely. For integrable systems the surface of sections are formed of invariant curves and

we have conditionally periodic motion (Arnold 1978, also Landau and Lifshitz 1976).

- (2) a periodic orbit: the successive iterates $\mathbf{X}_0, \mathbf{X}_1, \dots$ produce a cycle of N points. i.e. there is a least finite positive integer N such that

$$(u^{n+N}, p_u^{n+N}) = (u^n, p_u^n), \quad \forall n \in I \quad (4.1.5)$$

i.e. the trajectory $\mathbf{X}(t)$ intersects S_v in N points before closing itself. In this case $\mathbf{X}(t)$ is said to be a periodic orbit of period N or an N -cycle periodic orbit. Any of the points \mathbf{X}_n is called a periodic point of T with period N or, alternatively, called a fixed point of T^N i.e.

$$T^N(u^n, p_u^n) = (u^n, p_u^n). \quad (4.1.6)$$

- (3) an irregular (or stochastic) trajectory: the successive iterates $\mathbf{X}_0, \mathbf{X}_1, \dots$ fill in a two-dimensional set on S_v , a so-called chaotic (or irregular) area. So the trajectory explores densely a three-dimensional submanifold of S_E . This corresponds to a non-integrable motion where invariant curves on S_v (and in turn invariant tori) do not exist.

The three types of orbits are seen, schematically, in figure (4.1.2) but can all be seen, realistically, for the quadratic Zeeman potential (figures (7.2)).

The computation of the trajectory $\mathbf{X}(t)$ is subject to numerical errors. Therefore, only a finite number of the iterates \mathbf{X}_n on the surface of section can suggest, but not prove, the nature of $\mathbf{X}(t)$.

The surface of section method has been used widely to determine

the large scale structure of phase space, for various one parameter systems, following Hénon and Heiles (1964). We use it for the Zeeman potential (5.31) (Al-Laithy *et al* 1985 and also section (7.2) of this thesis).

This technique is best suited to studying the macroscopic properties of the phase space. In contrast, methods of locating periodic orbits and studying their stability allow an investigation of the microscopic structure of phase space (see chapter (10))

Twist maps

(4.2.1) The twist mapping.

A convenient way of studying the phase space trajectories around fixed points is to study area preserving mappings in the neighbourhood of these points.

For a two-dimensional time-independent integrable Hamiltonian in action-angle variables we have

$$H_0(J_x, J_y) = E, \quad (4.2.1.1)$$

$$\theta_x = \omega_x t + \delta_x, \quad \omega_x = \frac{\partial H_0}{\partial J_x}, \quad (4.2.1.2)$$

$$\theta_y = \omega_y t + \delta_y, \quad \omega_y = \frac{\partial H_0}{\partial J_y}, \quad (4.2.1.3)$$

and the motion lies on a 2-torus $J_x = \text{constant}$, $J_y = \text{constant}$. We choose a surface of section S_{θ_y} defined by $\theta_y = \text{const} \pmod{2\pi}$ and $J_y > 0$ with $J_x - \theta_x$ as coordinates.

On S_{θ_y} , over the invariant curves (see figure (4.2.1.1)) we have

$$\begin{aligned}\oint \mathbf{p} \cdot d\mathbf{q} &= \oint p_x d\theta_x = \pi \rho^2 \\ &= 2\pi J_x,\end{aligned}\tag{4.2.1.4}$$

where $\rho = \sqrt{2J_x}$ and θ are polar coordinates on S_{θ_y} . For convenience we write θ for θ_x since we are using only invariant circles on S_{θ_y} . Successive intersections of a trajectory on the torus with S_{θ_y} have $J_x = \text{constant}$ (i.e. ρ is conserved). These intersections are separated by the same time interval $\Delta t = \frac{2\pi}{\omega_y}$. Then an intersection point $\mathbf{X}_0 = (\rho_0, \theta_0)$ on S_{θ_y} is followed by its next $\mathbf{X}_1 = (\rho_1, \theta_1)$ such that

$$\rho_1 = \rho_0,\tag{4.2.1.5}$$

$$\theta_1 = \theta_0 + \omega_x \Delta t = \theta_0 + \omega_x \left(\frac{2\pi}{\omega_y}\right) = \theta_0 + 2\pi \alpha(\rho_0),\tag{4.2.1.6}$$

where the frequency ratio $\alpha = \frac{\omega_x}{\omega_y}$ is a function of ρ because for a fixed E in (4.2.1.1) J_y can be given in terms of J_x . Therefore, α is a function of J_x and consequently of ρ . It is called the rotation (or the winding) number,

$$\alpha(\rho) = \frac{\omega_x}{\omega_y}.\tag{4.2.1.7}$$

Thus we have reduced the integrable system to a mapping $T : S_{\theta_y} \rightarrow S_{\theta_y}$,

$$T(\mathbf{X}_n) = \mathbf{X}_{n+1}, \quad \mathbf{X}_n = \begin{pmatrix} \rho_n \\ \theta_n \end{pmatrix}, \quad n = 0, 1, 2, \dots\tag{4.2.1.8}$$

defined by

$$\rho_{n+1} = \rho_n,\tag{4.2.1.9}$$

$$\theta_{n+1} = \theta_n + 2\pi \alpha(\rho_n).\tag{4.2.1.10}$$

T is area-preserving ($\det T = 1$) and maps circles into circles with a rotation number α dependent on the radius of the circle.

For α irrational the successive iterates $\mathbf{X}_0, \mathbf{X}_1, \dots, \mathbf{X}_n, \dots$ fill the circle densely as $n \rightarrow \infty$. For a rational number $\alpha = \frac{r}{s}$ with r and s relatively

prime integers we get s fixed points of the mapping T^s , i.e.

$$T^s(\mathbf{X}_n) = \mathbf{X}_n. \quad (4.2.1.11)$$

That is when ω_x and ω_y are commensurate, the motion degenerates into a periodic orbit which closes on itself after r revolutions in θ_x and s revolutions in θ_y . If C is the circle on which the s fixed points lie, we get for every $\mathbf{X} = (r, \theta)$ on C ,

$$T^s \left(\begin{array}{c} \rho \\ \theta + 2\pi\alpha(\rho) \end{array} \right) = \left(\begin{array}{c} \rho \\ \theta + 2\pi r \end{array} \right) = \left(\begin{array}{c} \rho \\ \theta \end{array} \right) \quad (4.2.1.12)$$

i.e. any point \mathbf{X} on C is a fixed point of the mapping T^s .

(4.2.2) Perturbed twist mapping.

If the integrable system, defined in section (4.2.1), is slightly perturbed such that the Hamiltonian takes the form

$$H(\theta_x, \theta_y, J_x, J_y) = H_0(J_x, J_y) + \epsilon H_1(\theta_x, \theta_y, J_x, J_y), \quad (4.2.2.1)$$

the twist mapping changes to the perturbed twist mapping T_ϵ defined by

$$\rho_{n+1} = \rho_n + \epsilon f(\rho_n, \theta_n), \quad (4.2.2.2)$$

$$\theta_{n+1} = \theta_n + 2\pi\alpha(\rho_n) + \epsilon g(\rho_n, \theta_n), \quad (4.2.2.3)$$

where f and g have period 2π in θ_n and are related in such a way that T_ϵ is area preserving and O remains a fixed point (i.e. $f = g = 0$ at $\rho = 0$). The unperturbed mapping T and the perturbed mapping T_ϵ are viewed as stating the perturbation problem in a geometrical language. This language is more general in that T and T_ϵ can be any two area preserving mappings not necessarily arising from a Hamiltonian and f , g and α need not be analytic but only smooth in the first 333 derivatives (Moser 1973)*. According to the KAM theorem, any irrational circle sufficiently away from the unperturbed rational

* This seems somewhat surprising, in comparison with the condition for the KAM theorem (3.4.4).

circle C survives the perturbation from T to T_ϵ . But the KAM theorem is silent about the fate of the unperturbed rational circle C itself. This fate is determined by the Poincaré fixed point theorem which we explain, in a separate section, as follows

(4.2.3) Poincaré fixed point theorem.

This theorem states that an even multiple of s , i.e. $2ks$ ($k = 1, 2, 3, \dots$), fixed points remain under perturbation and each of them is a fixed point of T_ϵ^s .

Proof: Let the unperturbed mapping T^s have an invariant circle C on which $\alpha(\rho_0) = \frac{r}{s}$ for some $\rho_0 \in R$. Then

$$T^s(\mathbf{X}) = \mathbf{X}, \quad \forall \mathbf{X} \in C.$$

Since T^s is continuous and has zero twist on C (i.e. unchanged angular coordinate on C), then it, in general, induces opposite twists on the annulus

$$C = \{\mathbf{X}(\rho) : \rho_1 \leq \rho \leq \rho_2, \quad \rho_0 \in (\rho_1, \rho_2)\}. \quad (4.2.3.1)$$

Figure (4.2.3.1) shows such twists with circles C_1 , and C_2 , the boundary of C . On C_1 the rotation number $\alpha(\rho_1) < \frac{r}{s}$ and on C_2 , $\alpha(\rho_2) > \frac{r}{s}$. For ϵ sufficiently small these opposite twists are maintained. Since T_ϵ^s is a continuous map, there exists a closed curve D_1 , close to C , which has a zero twist. Let D_2 be the image of D_1 under T_ϵ^s i.e. $T_\epsilon^s D_1 = D_2$. Since T_ϵ^s is area preserving, then D_1 and D_2 intersect at an even number of points (see figure (4.2.3.2)). Each one of these points is a fixed point of T_ϵ^s . If \mathbf{X}_i is one of them, then $T_\epsilon^s(\mathbf{X}_i) = \mathbf{X}_i$ i.e. the points

$$\mathbf{X}_i, T_\epsilon(\mathbf{X}_i), T_\epsilon^2(\mathbf{X}_i), \dots, T_\epsilon^{s-1}(\mathbf{X}_i)$$

are fixed points of T_ϵ^s . Therefore, there are $2ks$ points which are fixed points of T_ϵ^s .

We conclude that under perturbation all fixed points (on the unperturbed circle C) are destroyed except for a finite number $2ks$ which are preserved. This completes the proof.

Thus unlike the KAM theorem, the twist theorem enables us to understand more about the fate of the unperturbed rational circles under perturbation (i.e. the fate of the 1-dimensional tori or closed orbits). The types of these fixed points are explained in section (4.3).

(4.3) Linear stability in area-preserving maps.

The structure of invariant curves in the neighbourhood of a fixed point determines its type. This depends on the stability of the fixed point.

A fixed point X_0 is stable under an area preserving mapping A if for a given neighbourhood U of the point X_0 , there is a subneighbourhood $V \subset U$ such that

$$A^n V \subseteq U \quad \forall n \in I.$$

(4.3.1) Linearization of an area-preserving map.

Let X_0 be a fixed point of period s of an area preserving mapping T defined on the plane (q, p) . Without loss of generality, we take X_0 as the origin O and assume that $s = 1$. We can almost always classify the stability/instability of O by examining the 2×2 matrix \mathcal{M} whose elements \mathcal{M}_{ij} are given by linearizing the mapping equations, of the mapping T at O . Then

$$\begin{pmatrix} q_1 \\ p_1 \end{pmatrix} = \begin{pmatrix} \mathcal{M}_{11}q_0 + \mathcal{M}_{12}p_0 \\ \mathcal{M}_{21}q_0 + \mathcal{M}_{22}p_0 \end{pmatrix} = \mathcal{M} \begin{pmatrix} q_0 \\ p_0 \end{pmatrix}, \quad (4.3.1.1a)$$

or

$$\xi_1 = \mathcal{M}\xi_0, \quad (4.3.1.1b)$$

where $\xi_0 = \delta X_0 = (q_0, p_0)^t \in V$, for a neighbourhood, V , of O . The type of O depends on the curves generated by the iterates $\xi_n = (q_n, p_n)^t$, $n = 1, 2, 3, \dots$. This is determined by the eigenvalues λ_1, λ_2 of \mathcal{M} which are the roots of the equation

$$\det \begin{bmatrix} \mathcal{M}_{11} - \lambda & \mathcal{M}_{12} \\ \mathcal{M}_{21} & \mathcal{M}_{22} - \lambda \end{bmatrix} = 0, \quad (4.3.1.2)$$

or

$$\lambda^2 - \lambda \text{Tr} \mathcal{M} + 1 = 0, \quad (4.3.1.3)$$

where $\det \mathcal{M} = 1$ in (4.3.1.3) since T is area-preserving. $\text{Tr} \mathcal{M}$ is the trace $\mathcal{M}_{11} + \mathcal{M}_{22}$ of the matrix \mathcal{M} . The solutions for λ are

$$\lambda_{1,2} = \frac{\text{Tr} \mathcal{M}}{2} \pm i \left[1 - \left(\frac{\text{Tr} \mathcal{M}}{2} \right)^2 \right]^{\frac{1}{2}}. \quad (4.3.1.4)$$

We have $\lambda_1 \lambda_2 = 1$ and $\lambda_1 + \lambda_2 = \text{Tr} \mathcal{M} =$ a real number. We show that the value of $\text{Tr} \mathcal{M}$ can be used to classify the linear stability of a fixed point. We have three possibilities

- (1) $|\text{Tr} \mathcal{M}| < 2$: the eigenvalues are complex conjugates and lie on the unit circle

$$1 = \lambda_1 \lambda_2 = \lambda_1 \bar{\lambda}_1 = |\lambda_1|^2.$$

- (2) $|\text{Tr} \mathcal{M}| > 2$: the eigenvalues are real and distinct; one of them has absolute value greater than 1, and the other absolute value less than 1.

- (3) $|\text{Tr} \mathcal{M}| = 2$: the eigenvalues are real and equal ($\lambda_1 = \lambda_2 = \pm 1$).

These different types are shown with respect to the unit circle (figure (4.3.1.1)). We can always make a linear change of coordinates by means of a non-singular matrix B and obtain

$$D = B \mathcal{M} B^{-1}. \quad (4.3.1.5)$$

Since

$$\text{Tr}D = \text{Tr}(\mathcal{M}B^{-1}B) = \text{Tr}\mathcal{M} = \lambda_1 + \lambda_2, \quad (4.3.1.6)$$

$$\det D = \det B \det \mathcal{M} \det B^{-1} = \det \mathcal{M} = \lambda_1 \lambda_2, \quad (4.3.1.7)$$

then the type of transformation represented by D is the same as the type for \mathcal{M} . The matrix B can be chosen, depending on \mathcal{M}_{ij} , such that D is in a simple standard form (Percival and Richards 1982).

Elliptic Points.

For type (1), we can write

$$\lambda_1 = e^{i\theta}, \quad \lambda_2 = e^{-i\theta}. \quad (4.3.1.8)$$

The matrices B and D are

$$B = \begin{pmatrix} \mathcal{M}_{21} & \cos \theta - \mathcal{M}_{11} \\ 0 & \sin \theta \end{pmatrix}, \quad D = \begin{pmatrix} \cos \theta & -\sin \theta \\ \sin \theta & \cos \theta \end{pmatrix}. \quad (4.3.1.9)$$

Then \mathcal{M} is reduced by this linear change of coordinates and we obtain in the transformed coordinates

$$\begin{pmatrix} \bar{q}_1 \\ \bar{p}_1 \end{pmatrix} = \begin{pmatrix} \bar{q}_0 \cos \theta - \bar{p}_0 \sin \theta \\ \bar{q}_0 \sin \theta + \bar{p}_0 \cos \theta \end{pmatrix}. \quad (4.3.1.10)$$

Thus for the n th iteration $\xi_n = (\bar{q}_n, \bar{p}_n)^t$, $n = 0, 1, 2, \dots$ we have

$$\bar{q}_n^2 + \bar{p}_n^2 = \bar{q}_0^2 + \bar{p}_0^2 = \text{constant}, \quad (4.3.1.11)$$

i.e. the invariant curves are circles. But in general, for type 1, the invariant curves are ellipses (figure (4.3.1.2)) and the fixed point is said to be elliptic. Since ξ_n are confined to an ellipse near O , then elliptic fixed points are stable.

Hyperbolic Points.

For type (2), $\lambda_1 = \lambda$ (a real number where $|\lambda| > 1$) and $\lambda_2 = \lambda^{-1}$,

$$B = \begin{pmatrix} \mathcal{M}_{21} & \lambda_1 - \mathcal{M}_{11} \\ \mathcal{M}_{21} & \lambda_2 - \mathcal{M}_{11} \end{pmatrix}, \quad D = \begin{pmatrix} \lambda_1 & 0 \\ 0 & \lambda_2 \end{pmatrix}, \quad (4.3.1.12)$$

and we get the reduced form

$$\begin{pmatrix} \bar{q}_1 \\ \bar{p}_1 \end{pmatrix} = \begin{pmatrix} \lambda \bar{q}_0 \\ \frac{1}{\lambda} \bar{p}_0 \end{pmatrix}. \quad (4.3.1.13)$$

For the n th iteration we have

$$\bar{p}_n \bar{q}_n = \bar{p}_0 \bar{q}_0 = \text{constant}, \quad (4.3.1.14)$$

i.e. the invariant curves are hyperbolae $\bar{p} = \frac{\text{constant}}{\bar{q}}$. The fixed point in this case is said to be a hyperbolic point. There are two kinds of hyperbolic points depending on the sign of λ . If $\lambda > 0$, the iterates ξ_n remain on the same invariant curve. The fixed point in this case is said to be an ordinary hyperbolic point (figure (4.3.1.3)). If however $\lambda < 0$, the iterates ξ_n alternate between two opposite invariant curves (figure (4.3.1.4)). The fixed point in this case is an inversion hyperbolic point or hyperbolic point with reflection. Hyperbolic points are unstable because ξ_n move away from the fixed point O as n increases.

Type (3) represents a boundary for types (2) and (3) and the fixed points in this case are either stable or unstable. This is decided by non-linear analysis. The various kinds of fixed points we discussed in this section are listed in section (10.3) (table (10.3.1)). where the letter R in this table denotes the residue of the fixed point which we define in next section (section 4.3.2)

A good description of area-preserving linear mappings from the plane onto itself and various kinds of stability are given by Percival and Richards (1982).

(4.3.2) The residue.

Let $X_0(t)$ be a periodic orbit which has s intersection points, p_1, p_2, \dots, p_s , with the surface of section. Each of these points is a fixed point of T^s , where T is the Poincaré map. Following Greene (1979a), we calculate the 2×2 matrix \mathcal{M} which is the linearization of T^s about one of these fixed points p_i , say. It is convenient to consider instead of the trace $\text{Tr}\mathcal{M}$ a quantity defined by Greene (1968) as

$$R = \frac{1}{4}(2 - \text{Tr}\mathcal{M}). \quad (4.3.2.1)$$

By (4.3.2.1) we can identify the types (1), (2) and (3) of stability and instability given in section (4.3.1) in terms of R . To characterize the type of the fixed point p_i :

- (1) if $0 < R < 1$, p_i is an elliptic point of T^s and $X_0(t)$ is linearly stable (except for $R = \frac{3}{4}$ and sometimes $R = \frac{1}{2}$ corresponding to $\lambda^3 = 1$ and $\lambda^4 = 1$) (see Greene *et al* 1981).
- (2) if $R < 0$, p_i is an ordinary hyperbolic fixed point, and if $R > 1$, p_i is an inversion hyperbolic fixed point. In both cases $X_0(t)$ is unstable.
- (3) the cases $R = 1$ and $R = 0$ define a boundary between the other cases and the orbit may be either stable or unstable.

By Lichtenberg and Lieberman (1983) we may express \mathcal{M} by

$$\mathcal{M} = \prod_{i=1}^s \mathcal{M}_i, \quad (4.3.2.2)$$

where \mathcal{M}_i is the linearization of T about p_i . Since the trace of a product of matrices is not changed by cyclic permutation of the factors, then all the fixed points p_1, p_2, \dots, p_s have the same residue.

In this thesis we use the residue (4.3.2.1) to identify the stability of

periodic orbits for the one parameter map arising from the quadratic Zeeman potential in chapter (10)

(4.3.3) The Poincaré-Birkhoff theorem and the microcosmic structure under perturbations.

It only remains to present an addition to the Poincaré-Birkhoff theorem. It is obvious from the continuity of arrows in figure (4.2.3.2) that fixed points on the curve D_1 are alternately elliptic and hyperbolic. In other words, we give figure (4.3.3.1) which is a part of figure (4.2.3.2) and depicts only two successive fixed points. The directions of the arrows around each fixed point suggest its type

Thus the *corollary* of the theorem, formally, states that *of the $2ks$ fixed points of T_ϵ^s that remain after the break-up of the curve with rotation number $\frac{r}{s}$, precisely ks are elliptic and ks are hyperbolic, the two types form an alternating sequence.* This is depicted in figure (4.3.3.2).

This suggests the following.

About every elliptic point there will also be invariant circles. Whenever a rational circle exists it breaks up, under perturbation, to give a chain of alternating elliptic and hyperbolic points and so on down to any arbitrarily smaller scale. Thus the theorem, wonderfully, reveals the microcosmic structure (Berry (1978)).

For small perturbation amplitudes, the alternation of elliptic and hyperbolic fixed points about the rational curve is a generic property of the system. (Lichtenberg and Lieberman 1983).

A property is said to be *generic* in a class of systems if it holds on a countable intersection of open dense sets in that class. We will often

use the words *generic* and *non-generic* in this thesis particularly, for describing the bifurcation behaviour of periodic orbits in classes of one parameter systems (sections (4.3.5) and (10.4)).

(4.3.4) Complexity of structure around hyperbolic points and chaotic motion.

What we have described in the last section is not a complete picture of what happens to an integrable system under perturbation. To understand how the chaotic motion can arise, we explain how this motion is connected with the hyperbolic fixed points. The invariant curves at a hyperbolic fixed point X_i of T^s in the perturbed twist mapping may be incoming or outgoing from X_i . These are the asymptotes of the hyperbola. One may ask how does an outgoing curve, generated by T^n , behave as $n \rightarrow \infty$, or how did an incoming curve behave as $n \rightarrow -\infty$. It may happen that one outgoing curve from a hyperbolic point X_i becomes an incoming one for another, X_j . This happens in the pendulum problem (see for example Lichtenberg and Lieberman 1983 also Whiteman 1977) but this is exceptional, nongeneric. What happens, generically, is that an outgoing curve from one hyperbolic point intersects an invariant curve through a neighbouring hyperbolic point, which belonged to the same rational curve (i.e. the same s -cycle periodic orbit) an infinite number of times. The points of intersection are called *homoclinic points* (see figure (4.3.4.1)). If, however, the two hyperbolic points were situated on two different rational curves (i.e. belonged to two different periodic orbits) of the twist mapping, the intersections are then called *heteroclinic points* (Arnold and Avez 1968, Whiteman 1977, Berry 1978).

In the particular case $s = 1$ i.e. X is a hyperbolic point of T , one outgoing asymptote of the hyperbola may join smoothly an incoming asymptote of the same hyperbola (i.e. at X), but this is non-generic. The generic situation is that they intersect each other at an infinite number of homoclinic points. This is depicted in figure (4.3.4.2).

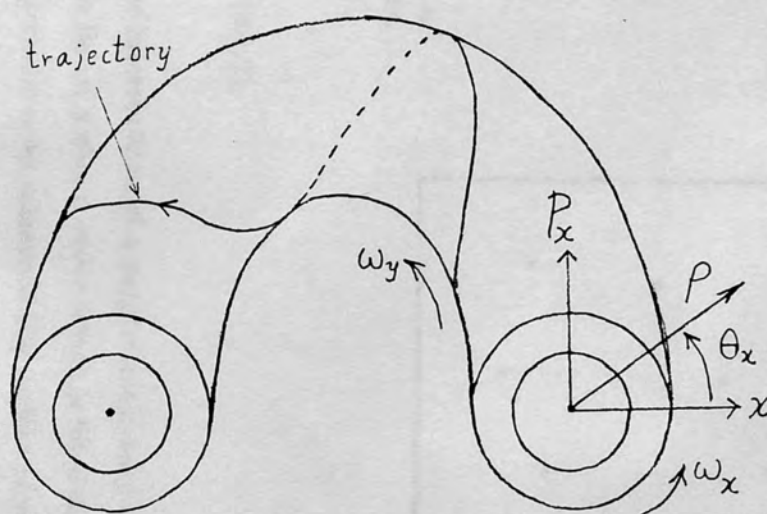


Figure (4.2.1.1). For the system defined by the Hamiltonian (4.2.1.1), any trajectory is confined to a 2-torus.

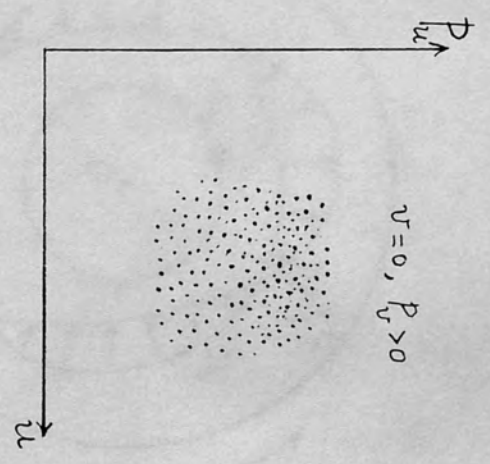
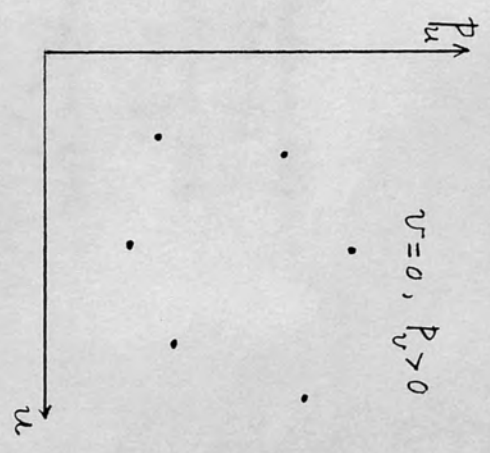
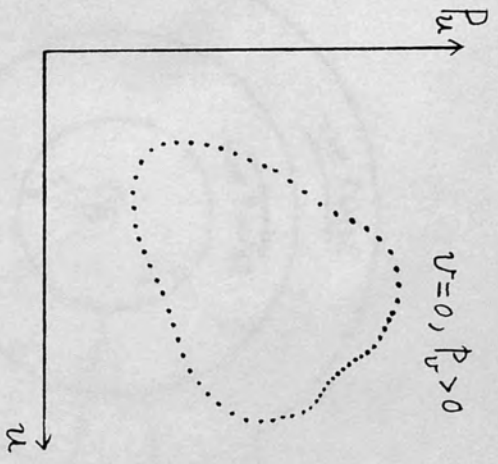


Figure (4.1.2).

- a- The intersections of a regular trajectory with the surface of section lie on a closed curve which is filled densely as $t \rightarrow \infty$.
- b- A periodic orbit intersects the surface of section in 6 points. The orbit is 6-cycle.
- c- A chaotic area is filled in densely by an infinite number of intersections of an irregular trajectory with the surface of section.

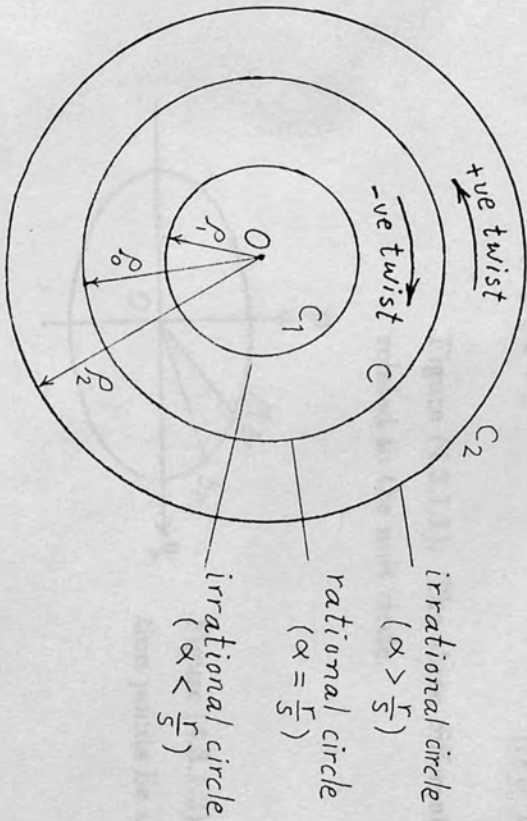


Figure (4.2.3.1). Invariant circles under T^s for the unperturbed integrable system.

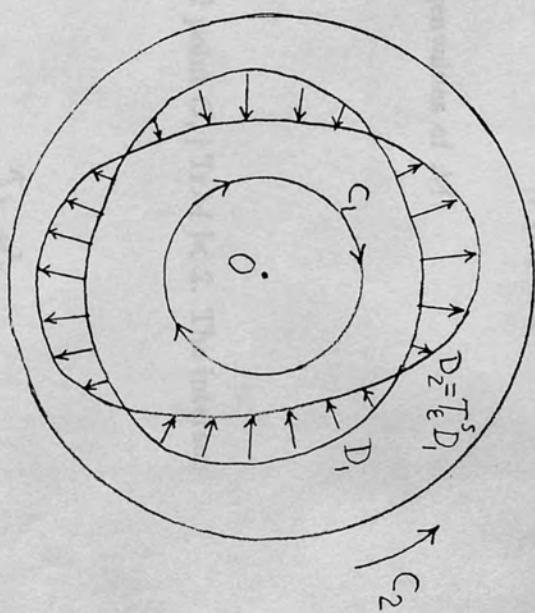


Figure (4.2.3.2). The perturbed case.

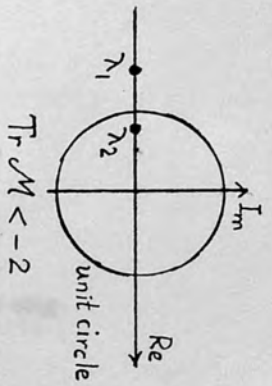


Figure (4.3.1.1). The three different types of the eigenvalues of M related to the unit circle.

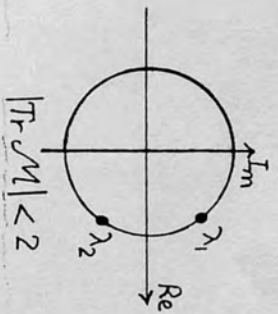


Figure (4.3.1.2). An elliptic fixed point O , $|\text{Tr}M| < 2$. The intersection points lie on an ellipse.

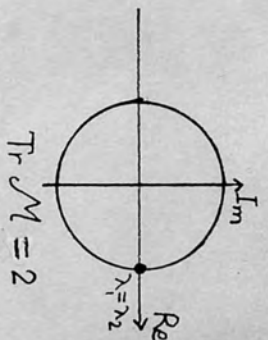


Figure (4.3.1.3). O is an ordinary hyperbolic point, $\text{Tr}M > 2$. The intersection points lie on the same branch of the hyperbola.

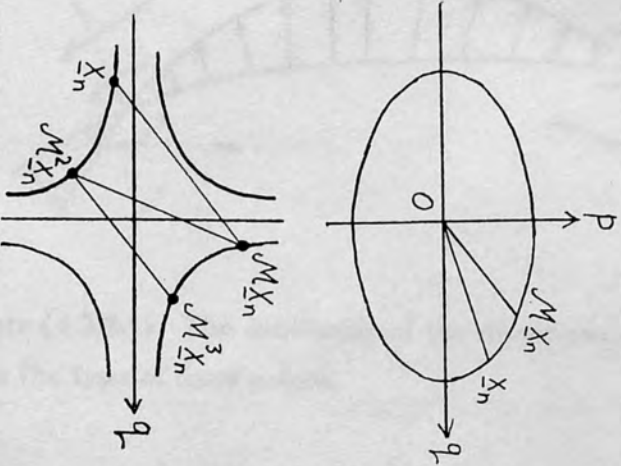
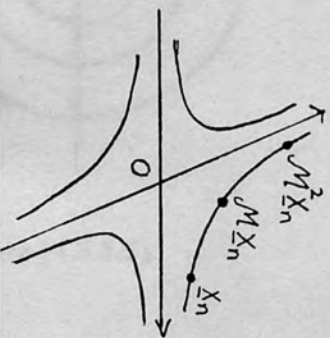


Figure (4.3.1.4). O is an inversion hyperbolic point, $\text{Tr}M < -2$. The intersection points alternate between two opposite branches of the hyperbola.



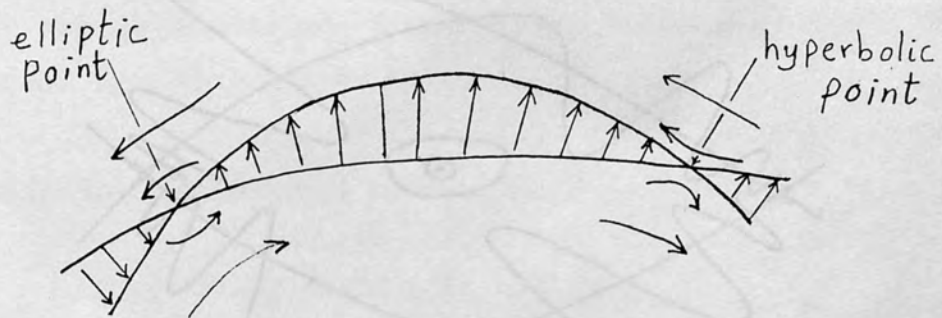


Figure (4.3.3.1). The continuity of the directions of the arrows suggests the type of fixed points.

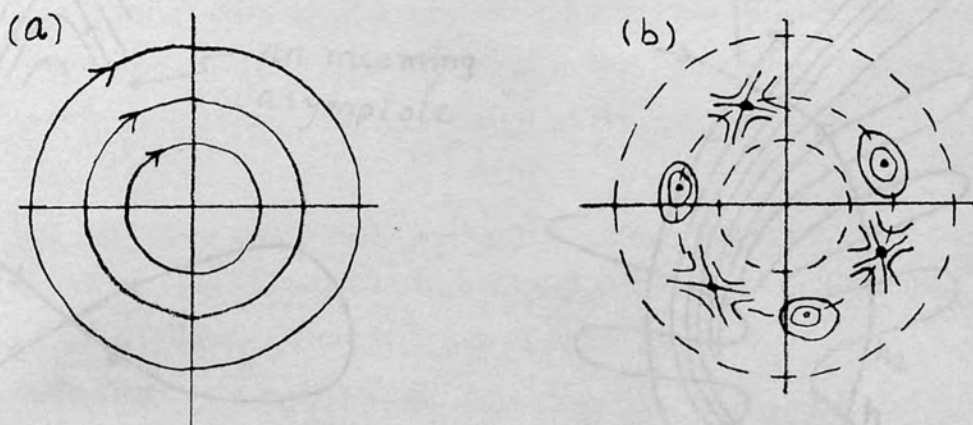


Figure (4.3.3.2).

- a- Unperturbed rational invariant circles of a twist mapping.
 b- Under perturbation a rational curve breaks up into a sequence of elliptic and hyperbolic fixed points (O and X points).

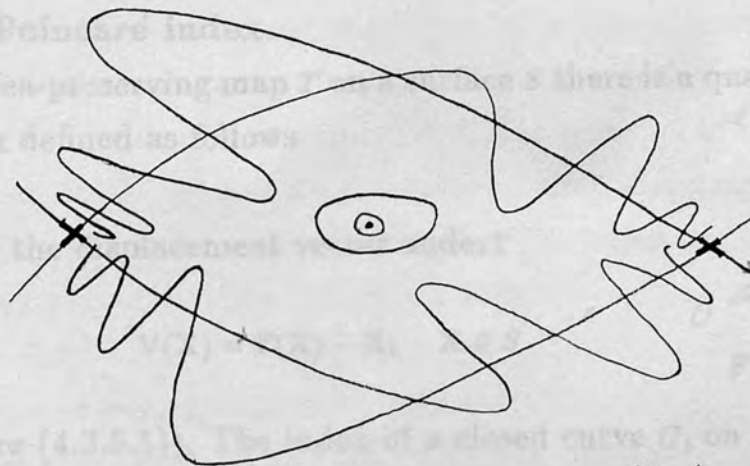


Figure (4.3.4.1). Invariant curves from two hyperbolic ^{fixed} points intersect at an infinite number of homoclinic points. (Taken from Whiteman (1977)).

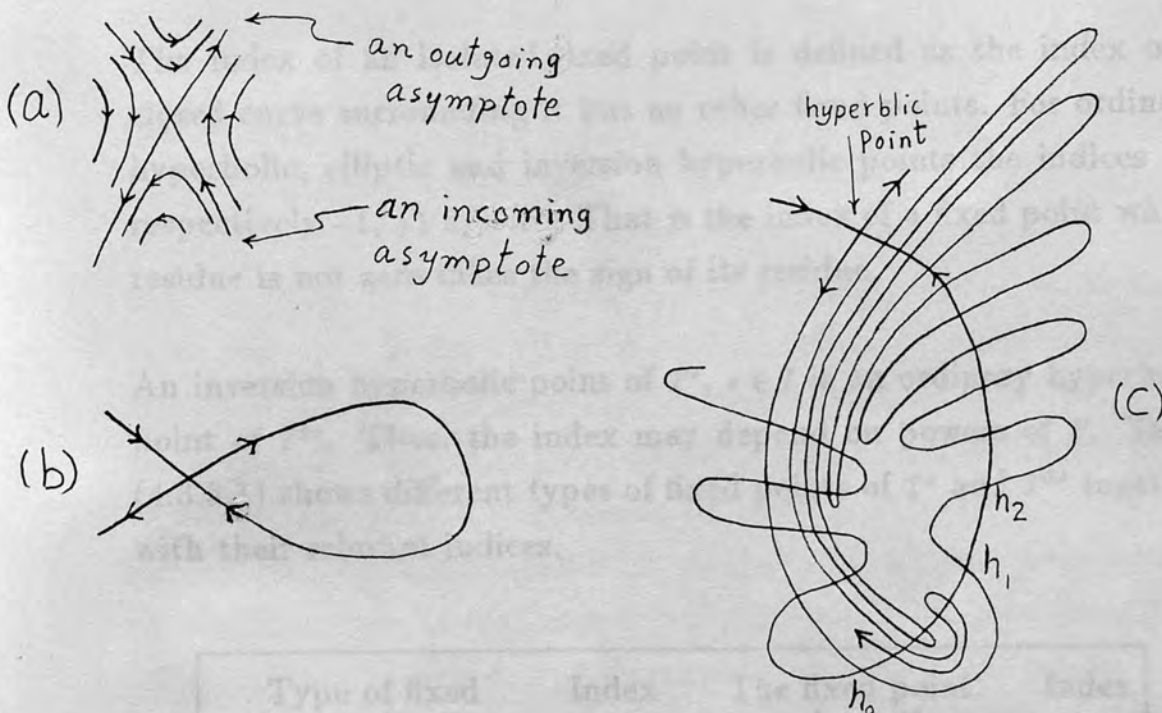


Figure (4.3.4.2). (a) Invariant curves around a hyperbolic fixed point. (b) Smooth joining of the outgoing and the incoming asymptotes, (a nongeneric behaviour). (c) The outgoing and the incoming asymptotes intersect at an infinite number of homoclinic points h_1, h_2, h_3, \dots , (a generic behaviour). (Taken from Robnik 1982).

(4.3.5) Poincaré index.

For an area-preserving map T on a surface S there is a quantity called the index defined as follows

Consider the displacement vector under T

$$V(X) = T(X) - X, \quad X \in S$$

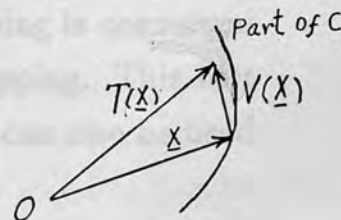


Figure (4.3.5.1).

(see figure (4.3.5.1)). The index of a closed curve C , on S , which passes through no ^{fixed} points is defined as the number of complete rotations that $V(X)$ makes as X traverses C . If the rotation of V and the traversal of X (on C) are in the same direction, the index is taken to be positive and vice versa. The index is a continuous function of C . Then being integer-valued it is a constant.

The index of an isolated fixed point is defined as the index of a closed curve surrounding it but no other fixed points. For ordinary hyperbolic, elliptic and inversion hyperbolic points the indices are respectively -1 , $+1$ and $+1$. That is the index of a fixed point whose residue is not zero takes the sign of its residue.

An inversion hyperbolic point of T^s , $s \in I$ is an ordinary hyperbolic point of T^{2s} . Thus, the index may depend on powers of T . Table (4.3.5.1) shows different types of fixed points of T^s and T^{2s} together with their relevant indices.

Type of fixed point of T^s	Index	The fixed point under T^{2s}	Index
ordinary hyperbolic	-1	ordinary hyperbolic	-1
elliptic	$+1$	elliptic	$+1$
inversion hyperbolic	$+1$	ordinary hyperbolic	-1

Table (4.3.5.1)

The index is summable i.e. the index of a closed curve C is the sum of the indices of the fixed points contained in C (Greene 1968). Moreover, the index of a closed curve C , for a mapping is conserved with respect to changes in a parameter of that mapping. This last property is useful in bifurcation analysis. The index can also be used for locating periodic orbits (MacKay 1982a).

(4.3.6) Fixed point bifurcations.

In the previous sections we have explained different techniques for investigating the stability/instability of a fixed point. It is often useful and interesting to follow the behaviour of fixed points of a mapping as some parameter is changed and in particular finding where they are created or absorbed or collide. These events are called bifurcations and occur at discrete values of the parameter. So, they are occasional, but significant events.

For an area-preserving mapping T , consider a closed curve C surrounding a finite number of fixed points of T^s , $s \in I$, and passing through no fixed points. The conservation of the Poincaré index of C with respect to a parameter p of the mapping constrains the fixed point behaviour inside C . This is used as a check in a neighbourhood of a fixed point X_0 before and after its bifurcation. In what follows we enumerate some well known bifurcations of a fixed point X_0 of T^s . They are classified according to whether the residue R of the fixed point passes through 1 or 0. For all future bifurcation figures we show the type of fixed point: solid lines indicate linear stability (elliptic fixed points), dotted lines inversion hyperbolic points. The horizontal and vertical axes are to be considered as the parameter p and the position of the fixed point respectively.

The residue R of a fixed point X_0 of T^s may increase steadily passing through 1. We have two possibilities:

p1- an elliptic fixed point X_0 of T^s becomes an inversion hyperbolic point as R increases through 1, and two elliptic fixed points of T^{2s} (i.e. of twice the period) are created (figure (4.3.6.1)). The behaviour of R is shown in figure (4.3.6.2). This behaviour may occur in the same way over a finite range of the parameter p . The successive bifurcations take place at the ends of a sequence of decreasing intervals of p which converges to a point called the accumulation point (Greene *et al* 1981)). This type of bifurcation is generic and called *period doubling bifurcation*. This type is found in section (10.4.1).

p2- an elliptic fixed point X_0 of T^s becomes an inversion hyperbolic point as R passes through 1, and two ordinary hyperbolic points of T^{2s} (i.e. of twice the period) are absorbed (figure (4.3.6.3)).

The two types of bifurcations p1 and p2 are known respectively as *direct* and *inverse* period-doubling bifurcations.

The residue R may decrease steadily from positive values to negative values passing through zero. At $R = 0$ we may have one of the following types of bifurcation.

T1- an elliptic fixed point X_0 of T^s becomes an ordinary hyperbolic point, and two elliptic fixed points of T^s (i.e. of the same period) are created (figure (4.3.6.4)). The behaviour of R is shown in figure (4.3.6.5). This type of bifurcation is frequently found in section (10.4.2).

T2- an elliptic fixed point X_0 of T^s becomes an ordinary hyperbolic one and two hyperbolic points of T^s (i.e. of the same period) are absorbed (figure (4.3.6.6)).

The two types T1 and T2 are known as *direct Rimmer* and *inverse Rimmer* bifurcations respectively (MacKay 1982a).

At $R = 0$ we may have also the following two types

T3- as R increases passing through zero, one elliptic fixed point of T^s is created from one ordinary hyperbolic fixed point of T^s and two other elliptic fixed points of T^s (i.e. of the same period) are absorbed. This is known as *inverse bifurcation*.

T4- at $R = 0$ there may be also a type of bifurcation known as *tangent bifurcation*, one elliptic fixed point and one hyperbolic fixed point of T^s are created in a region where previously no fixed point of T^s existed.

The bifurcations of types T1, T2 and T4 were analysed by Rimmer (1978, 1979) for symmetric periodic orbits in reversible area-preserving maps.

A system is reversible if it is conjugate to its time reverse, by a coordinate change whose square is the identity (called an involution). For example, Hamiltonians which are even in momenta (or positions) are reversible (MacKay 1982a).

Notice that the Poincare index is conserved for all the bifurcations described above.

(4.3.7). Renormalization.

One of the properties found to be common to one parameter area-preserving maps is *renormalization*. It means looking at the behaviour on successively longer time scales and smaller spatial scales. The important result obtained from studying renormalization has been the discovery of universal aspects of asymptotically exact self-similarity in area-preserving maps. An extremely important example is when this behaviour represents that of an interesting class of Hamiltonian systems (see section (10.4.1)). Following Greene *et al* (1981), we describe this behaviour briefly.

Typically, as the perturbation parameter P of the map, T , is varied, an initially stable periodic orbit loses stability at some parameter value P_1 and gives birth to stable periodic orbits of twice the original period. An infinite sequence of such *period doubling bifurcations* occurs at values P_1, P_2, \dots . This sequence has a universal limiting behaviour:

The intervals in the parameter between successive bifurcations form a geometric progression with a ratio

$$\frac{P_{k+1} - P_k}{P_k - P_{k-1}} = \frac{1}{\delta} \quad (4.3.7.1)$$

as $k \rightarrow \infty$, $\delta \simeq 8.72$. The infinite sequence converges rapidly in a finite parameter range, accumulating at a parameter value P^* (called the accumulation value). The explanation for this universal behaviour, which is independent of the particular map, is attributed (in the limit) to the existence of a universal map, T^* , of the plane, as its two coordinates x, y are rescaled by $\alpha \simeq -4.2$ and $\beta \simeq 16.36$, respectively. Not only does the pattern of periodic points of periods 2^n repeat itself (asymptotically) on rescaling by α and β (at $P = P^*$), but also does the whole map, on squaring and rescaling. This operation can

be written as follows

$$A(T) = BT^2B^{-1}, \quad \text{where } B = \begin{bmatrix} \alpha & 0 \\ 0 & \beta \end{bmatrix} \quad (4.3.7.2)$$

In a period doubling sequence, each bifurcation produces as many unstable fixed points as the previous bifurcation. The successive intervals of stability of these fixed points becomes shorter and shorter as P is varied (see figure (4.3.7.1)). So, the area consisting of invariant circles around the newly born stable fixed points following each bifurcation diminishes as P is varied. As P approaches P^* , the regular region associated with the initial fixed point of the sequence shrinks by a factor $f \simeq \frac{\alpha\beta}{2}$ at each period doubling (Greene *et al* (1981)). However, the hypothesis that the invariant circles produced by period doubling beyond P^* is of zero measure was disproved by MacKay (1982b) who showed that islets of stability produced by tangent bifurcations always exist in the universal map T^* .

Such universal aspects in various dynamical systems are found in Cvitanovic (1984).

(4.4) Ergodicity.

As the perturbation increases, more and more hyperbolic points are created in the manner we described in section (4.3.3). In the neighbourhood of each hyperbolic point the homoclinic points form densely (see section (4.3.4)). Consequently, the proportion of phase space occupied by regions of irregular motion increases. This has been found in both two-dimensional potentials (for example, see section(7.2)) and abstract area-preserving maps (see, for example Greene *et al* 1981). It is common that numerical integration in irregular regions is very sensitive to the minutest change in initial conditions. This might happen even for short intervals of time, because

irregular trajectories which are initially close diverge exponentially in time as they evolve. The loss of determinancy arising in such cases can be dealt with statistically. Stochastic orbits cause ergodicity, mixing and rapid transport. In this thesis we only define and explain ergodicity in autonomous Hamiltonian systems. The other aspects of irregular motion are not relevant to our present discussion.

To generalize we consider the volume-preserving continuous transformation g_t , induced by Hamilton's equations of motion on an $(2n-1)$ -dimensional energy surface rather than merely considering a discrete area-preserving map on the plane.

For a time independent Hamiltonian system the motion is confined to an energy surface S_E . The time average of a continuous (or merely Riemann integrable) function f on S_E is defined as

$$f^*(\mathbf{r}) = \lim_{T \rightarrow \infty} \frac{1}{T} \int_0^T f(g_t \mathbf{r}) dt, \quad (4.4.1)$$

where $g_t : S_E \rightarrow S_E$ is the continuous canonical mapping induced by the system.

The phase space average of $f(\mathbf{r})$ over S_E is defined by

$$\bar{f} = \int_{S_E} f(\mathbf{r}) d\Omega, \quad (4.4.2)$$

where $d\Omega$ is the invariant measure on S_E and is given by (see Arnold and Avez 1968)

$$d\Omega = \frac{d\mathbf{r}}{\left\| \frac{\partial H}{\partial \mathbf{r}} \right\|}, \quad (4.4.3)$$

where $\left\| \frac{\partial H}{\partial \mathbf{r}} \right\|$ is the norm (length), in R^{2n} , of the gradient of the Hamiltonian, on S_E and $d\mathbf{r}$ is the volume element of S_E induced by the metric of R^{2n} . It can be shown that (Nemytskii and Stepanov (1960)).

- a) f^* exists almost everywhere i.e. except, possibly, on a set of measure zero
- b) f^* is summable and invariant almost everywhere, i.e. is independent of initial conditions on a given orbit. Or

$$f^*(g_t \mathbf{r}) = f^*(\mathbf{r}) \quad \forall t.$$

c)

$$\int_{S_E} f^*(\mathbf{r}) d\Omega = \int_{S_E} f(\mathbf{r}) d\Omega \quad (4.4.4)$$

The system is said to be ergodic on S_E if

$$f^*(\mathbf{r}) = \bar{f}, \quad (4.4.5)$$

almost everywhere. According to this definition of ergodicity on S_E we conclude

- 1) the time average of an ergodic system is independent of \mathbf{r} .
- 2) a system can only be ergodic if over the course of time the system explores the whole of S_E i.e. covers it densely (The converse is not true).

If the system includes KAM curves, it can not be considered as ergodic on S_E but is said to be decomposable.

The definition of an ergodic system must be related to a subspace over which ergodicity is defined. For example,

- 1) An autonomous Hamiltonian system given by

$$H(\mathbf{r}) = H(\mathbf{q}, \mathbf{p}) = E_1, \quad (4.4.6)$$

for which (4.4.5) holds is ergodic on S_{E_1} but not ergodic on the whole phase space for all energies. i.e. is not ergodic on

$$\{S_E : E \in R\}. \quad (4.4.7)$$

- 2) A system undergoing conditionally-periodic motion is ergodic on any irrational (i.e. non-resonant) torus.

A rigorous proof of (4.4.5) on an n -dimensional ^{proper} torus can be found in Arnold (1978). In this case

$$\bar{f} = (2\pi)^{-n} \int_0^{2\pi} \dots \int_0^{2\pi} f(\theta) d\theta_1 \dots d\theta_n, \quad (4.4.8)$$

and

$$f^*(\theta_0) = \lim_{T \rightarrow \infty} \frac{1}{T} \int_0^T f(\theta_0 + \omega t) dt, \quad (4.4.9)$$

where

$$g_t(\theta_0) = \theta = \theta_0 + \omega t. \quad (4.4.10)$$

is the trajectory on the torus.

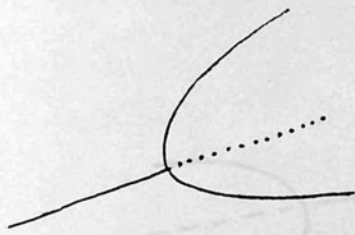


Figure (4.3.6.1). Direct period doubling bifurcation (Type P1 in the text).

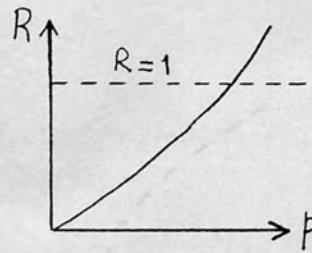


Figure (4.3.6.2). As the residue R of a fixed point passes through 1, period doubling bifurcation occurs.

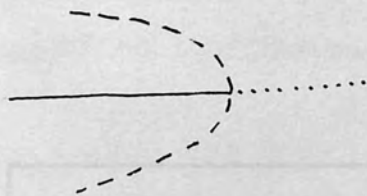


Figure (4.3.6.3). Inverse period doubling bifurcation (Type P2).



Figure (4.3.6.4). Direct Rimmer bifurcation (Type T1).

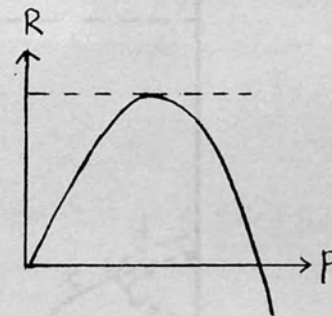


Figure (4.3.6.5). The behaviour of the residue for same-period bifurcation as R decreases passing through 0.

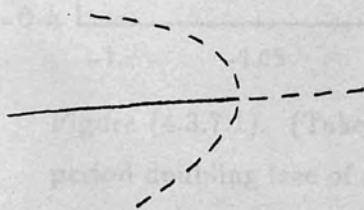


Figure (4.3.6.6). Inverse Rimmer bifurcation (Type T2).

CHAPTER 3

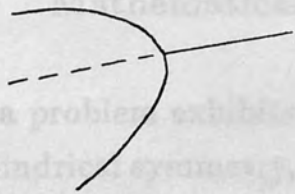


Figure (4.3.6.7). Inverse bifurcation (Type T3).

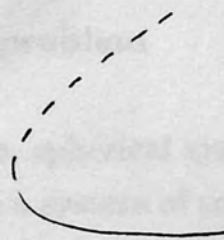


Figure (4.3.6.8). Tangent bifurcation (Type T4).

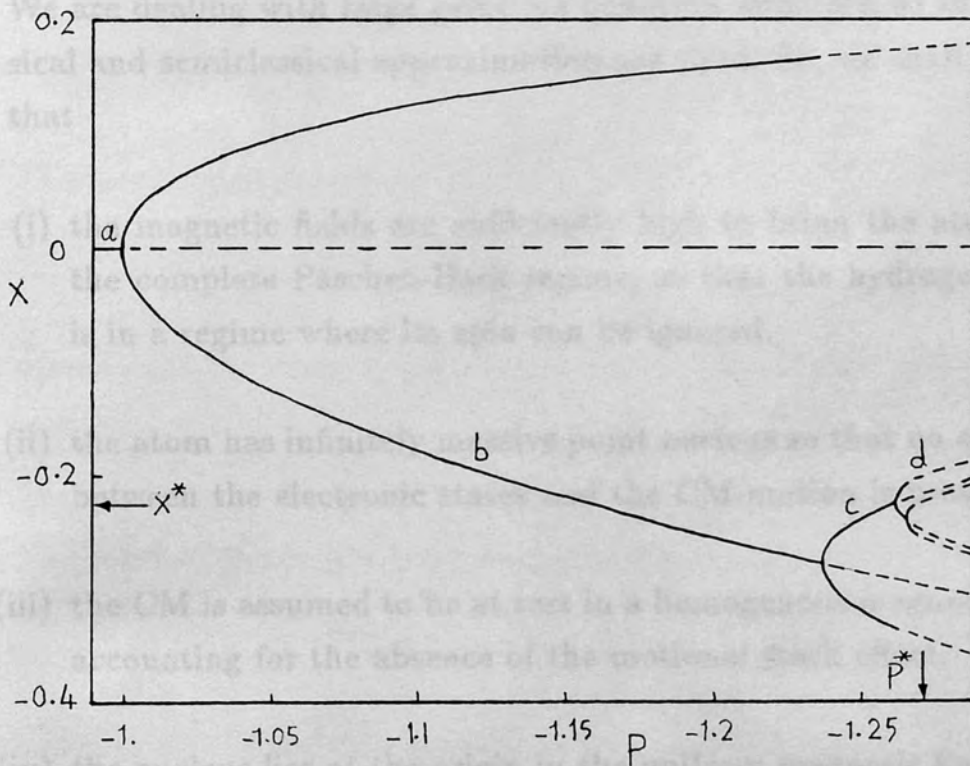


Figure (4.3.7.1). (Taken from Greene *et al* (1981)). A part of the period doubling tree of an area preserving map (studied by Greene *et al* (1981)). The curve *a* represents the initial fixed point and the curves *b*, *c* and *d* represent the subsequent bifurcated fixed points with periods 2, 4, and 8 respectively.

CHAPTER(5)

Mathematical formulation of the problem

When a problem exhibits symmetry, for example, spherical symmetry, cylindrical symmetry, this allows us to choose a system of coordinates q in such a way that the Hamiltonian function is independent of some of these coordinates. In these cases we can find integrals of the motion and thereby reduce the problem to one involving a smaller number of coordinates. This is demonstrated, here, by deriving the Hamiltonian and the equations of motion in both spherical and cylindrical coordinates.

We are dealing with large principle quantum numbers, so that classical and semiclassical approximations are valid. So, we shall assume that

- (i) the magnetic fields are sufficiently high to bring the atom into the complete Paschen-Back regime, so that the hydrogen atom is in a regime where its spin can be ignored.
- (ii) the atom has infinitely massive point nucleus so that no coupling between the electronic states and the CM-motion is present.
- (iii) the CM is assumed to be at rest in a homogenous magnetic field, accounting for the absence of the motional Stark effect.
- (iv) the nucleus lies at the origin in the uniform magnetic field B .

The classical potential, U , for this one-electron system contains two terms, the first Coulombic and the second due to the magnetic field.

(i) In spherical polar coordinates (r, θ, ϕ) taking the z-axis along the magnetic field, we define the vector potential \mathbf{A} for a uniform magnetic field \mathbf{B} as

$$\mathbf{A} = \frac{1}{2}(\mathbf{B} \wedge \mathbf{r}) = \frac{1}{2}Br \sin \theta \hat{e}_\phi, \quad \nabla \cdot \mathbf{A} = 0 \quad (5.1)$$

where \hat{e}_ϕ is a unit vector in the direction of ϕ increasing. Then, letting \mathbf{v} be the velocity vector

$$\mathbf{v} = (r, r\dot{\theta}, r \sin \theta \dot{\phi}), \quad (5.2),$$

we have the generalized potential

$$\begin{aligned} U(r, \theta, \phi) &= -\frac{e^2}{r} + \frac{|e|}{c}(\mathbf{v} \cdot \mathbf{A}) \\ &= -\frac{e^2}{r} + \frac{|e|B}{2c}r^2 \sin^2 \theta \dot{\phi}. \end{aligned} \quad (5.3)$$

The Lagrangian \mathcal{L} is given by

$$\mathcal{L} = \frac{1}{2}m_e(\dot{r}^2 + r^2\dot{\theta}^2) + \frac{e^2}{r} + \frac{m_e}{2}r^2 \sin^2 \theta \left[\left(\dot{\phi} - \frac{\omega_c}{2} \right)^2 - \frac{\omega_c^2}{4} \right], \quad (5.4)$$

where m_e is the mass of the electron and ω_c , the cyclotron frequency, is given by

$$\omega_c = \frac{|e|B}{m_e c}. \quad (5.5)$$

The form of the Lagrangian suggests the angular velocity transformation

$$\dot{\phi}' = \dot{\phi} - \frac{\omega_c}{2} \quad (5.6)$$

which is equivalent to a coordinate transformation

$$\phi' = \phi - \frac{\omega_c}{2}t + \phi'_0 \quad (5.7)$$

where ϕ'_0 is a constant.

This implies the use of a coordinate frame rotating with a constant angular velocity $\frac{\omega_c}{2}$, along the magnetic field \mathbf{B} (called the rotating Larmor frame).

This choice of the rotating Larmor frame is also understood from Larmor's theorem which states that the effect of a ^{small} constant magnetic field \mathbf{B} on a classical system is to superimpose on its normal motion a uniform precession with angular frequency given by

$$\omega_L = \frac{|e| \mathbf{B}}{2mc} = \frac{\omega_c}{2} \hat{e}_z \quad (5.8)$$

known as the Larmor's frequency (Jackson (1975)). Now substituting for $\dot{\phi}$ by $\dot{\phi}' = \dot{\phi} - \frac{\omega_c}{2}$ in equation(5.4), the Lagrangian takes the form

$$\mathcal{L} = \frac{m_e}{2}(\dot{r}^2 + r^2\dot{\theta}^2 + r^2 \sin^2 \theta \dot{\phi}'^2) - \frac{m_e \omega_c^2}{8} r^2 \sin^2 \theta + \frac{e^2}{r}. \quad (5.9)$$

The conjugate momenta are defined by

$$p_i = \frac{\partial \mathcal{L}}{\partial \dot{q}_i} \quad (5.10)$$

where

$$q_1 = r, \quad q_2 = \theta, \quad q_3 = \phi' \quad (5.11)$$

so that

$$p_r = m_e \dot{r}, \quad p_\theta = m_e r^2 \dot{\theta}, \quad p_{\phi'} = m_e r^2 \sin^2 \theta \dot{\phi}'. \quad (5.12)$$

Then in terms of the coordinates r, θ, ϕ' and their conjugate momenta given by (5.12), the Hamiltonian \mathcal{H} , defined by

$$\mathcal{H} = \sum p_i \dot{q}_i - \mathcal{L}, \quad (5.13)$$

takes the form

$$\mathcal{H} = \frac{1}{2m_e} \left(p_r^2 + \frac{p_\theta^2}{r^2} + \frac{p_{\phi'}^2}{r^2 \sin^2 \theta} \right) + \frac{m_e \omega_c^2}{8} r^2 \sin^2 \theta - \frac{e^2}{r}, \quad (5.14)$$

and consequently Hamilton's equations of motion are

$$\begin{aligned} \dot{r} &= \frac{p_r}{m_e}, \\ \dot{\theta} &= \frac{p_\theta}{m_e r^2}, \\ \dot{\phi}' &= \frac{p_{\phi'}}{m_e r^2 \sin^2 \theta}, \\ -\dot{p}_r &= -\frac{1}{m_e r^3} \left(p_\theta^2 + \frac{p_{\phi'}^2}{\sin^2 \theta} \right) + \frac{m_e \omega_c^2}{4} r \sin^2 \theta + \frac{e^2}{r^2}, \\ -\dot{p}_\theta &= -\frac{p_{\phi'}^2 \cos \theta}{m_e r^2 \sin^3 \theta} + \frac{m_e \omega_c^2}{4} r^2 \sin \theta \cos \theta, \\ -\dot{p}_{\phi'} &= 0. \end{aligned} \tag{5.15}$$

The last equation in (5.15) indicates the constancy of the motion of $p_{\phi'}$.

Gajewski (1970) pointed out that the equations of motion for an electron in the Coulomb field of the nucleus and a uniform magnetic field \mathbf{B} can be reduced to a parameter free form by appropriate scaling of the space and time coordinates with

$$t = T t^*, \quad \mathbf{r} = \ell \mathbf{r}^* \tag{5.16}$$

where

$$T = \frac{2}{\omega_c}, \quad \ell = 2 \left(\frac{m_e c^2}{B^2} \right)^{\frac{1}{3}}. \tag{5.17}$$

Some appreciation of the magnitude of the scaling parameters can be derived from the observation that the characteristic length ℓ is the radius of a sphere containing magnetic field energy $(\frac{B^2}{8\pi}) \cdot (\frac{4\pi\ell^3}{3})$, which

is comparable to the rest mass energy $m_e c^2$ of the electron. Energy is then measured in units of $\frac{2e^2}{l}$ and angular momentum in units of $\frac{m_e l^2}{T}$. In terms of the dimensionless parameters E and L , the energy \mathcal{E} and the angular momentum $p_{\phi'}$, are

$$\mathcal{E} = 12.415 E B^{\frac{2}{3}} \text{ cm}^{-1}, \quad (5.18)$$

$$p_{\phi'} = 265.9 L \hbar B^{-\frac{1}{3}}, \quad (5.19)$$

where B is in kG.

Introducing the notation H for the Hamiltonian in terms of the dimensionless coordinates, we have, following Gajewski,

$$H = \frac{1}{2} \left(p_r^{*2} + \frac{p_\theta^{*2}}{r^{*2}} + \frac{L^2}{r^{*2} \sin^2 \theta} \right) + \frac{1}{2} r^{*2} \sin^2 \theta - \frac{1}{2r^*} \quad (5.20)$$

where

$$p_r^* = \frac{dr^*}{dt^*}, \quad p_\theta^* = r^{*2} \frac{d\theta}{dt^*}, \quad p_{\phi'}^* = r^{*2} \sin^2 \theta \frac{d\phi'}{dt^*},$$

$$\phi' = \phi - t^* \quad (5.21)$$

and we have taken

$$p_{\phi'}^* = L \quad (5.22)$$

since $p_{\phi'}^*$ is a constant of the motion.

(ii) In cylindrical coordinates (ρ, θ, ϕ) , taking the z -axis along the magnetic field, the potential U takes the form

$$U = -\frac{e^2}{\sqrt{\rho^2 + z^2}} + \frac{|e| B}{2c} \rho^2 \dot{\phi} \quad (5.23)$$

and the velocity \mathbf{v} is

$$\mathbf{v} = (\dot{\rho}, \rho \dot{\phi}, \dot{z}). \quad (5.24)$$

Then in the rotating Larmor frame and using (5.6), the Lagrangian takes the form

$$\mathcal{L} = \frac{m_e}{2} (\dot{\rho}^2 + \rho^2 \dot{\phi}'^2 + \dot{z}^2) + \frac{m_e \omega_c^2}{8} \rho^2 + \frac{e^2}{(\rho^2 + z^2)^{\frac{1}{2}}}. \quad (5.25)$$

All The momenta conjugate to the coordinates (ρ, ϕ', z) are

$$p_\rho = m_e \dot{\rho}, \quad p_{\phi'} = m_e \rho^2 \dot{\phi}', \quad p_z = m_e \dot{z}. \quad (5.26)$$

Thus the Hamiltonian takes the form

$$\mathcal{H} = \frac{1}{2m_e} (p_\rho^2 + \frac{p_{\phi'}^2}{\rho^2} + p_z^2) + \frac{m_e \omega_c^2}{8} \rho^2 - \frac{e^2}{(\rho^2 + z^2)^{\frac{1}{2}}} \quad (5.27)$$

and consequently Hamilton's equations are

$$\dot{\rho} = \frac{p_\rho}{m_e},$$

$$\dot{\phi}' = \frac{p_{\phi'}}{m_e \rho^2},$$

$$\dot{z} = \frac{p_z}{m_e},$$

$$-\dot{p}_\rho = -\frac{p_{\phi'}^2}{m_e \rho^3} + \frac{m_e \omega_c^2}{4} \rho + \frac{e^2 \rho}{(\rho^2 + z^2)^{\frac{3}{2}}},$$

$$-\dot{p}_{\phi'} = 0,$$

$$-\dot{p}_z = \frac{e^2 z}{(\rho^2 + z^2)^{\frac{3}{2}}}. \quad (5.28)$$

Using the scaling units (equations (5.16) and (5.17)), the dimensionless momenta are given by

$$p_\rho^* = \frac{d\rho^*}{dt^*}, \quad p_{\phi'}^* = \rho^{*2} \frac{d\phi'}{dt^*}, \quad p_z^* = \frac{dz^*}{dt^*} \quad (5.29)$$

where ρ^* and z^* are the dimensionless cylindrical coordinates. The dimensionless Hamiltonian H is

$$H = \frac{1}{2} [p_\rho^{*2} + p_z^{*2} + \frac{L^2}{\rho^{*2}} + \rho^{*2} - (\rho^{*2} + z^{*2})^{-\frac{1}{2}}]. \quad (5.30)$$

Alternatively we define an effective potential

$$V(\rho^*, z^*; L) = \frac{1}{2} \left[\rho^{*2} + \frac{L^2}{\rho^{*2}} - (\rho^{*2} + z^{*2})^{-\frac{1}{2}} \right], \quad (5.31)$$

so that

$$H = \frac{1}{2} (p_\rho^{*2} + p_z^{*2}) + V(\rho^*, z^*; L). \quad (5.32)$$

Thus the fact that ϕ' is a cyclic coordinate (i.e. $\frac{\partial H}{\partial \phi'} = 0$) has reduced the system to a two-dimensional one, and the problem of classical motion has now been reduced to the study of orbits in a four-dimensional phase space (ρ, p_ρ, z, p_z) .

For convenience, from now on, we drop the asterisks. Thus (5.20) and (5.30) becomes

$$H = \frac{1}{2} \left(p_r^2 + \frac{p_\theta^2}{r^2} + \frac{L^2}{r^2 \sin^2 \theta} \right) + \frac{1}{2} r^2 \sin^2 \theta - \frac{1}{2r}, \quad (5.33)$$

and

$$H = \frac{1}{2} \left[p_\rho^2 + p_z^2 + \rho^2 + \frac{L^2}{\rho^2} - (\rho^2 + z^2)^{-\frac{1}{2}} \right] \quad (5.34)$$

respectively, and Hamilton's equations of motion derived from (5.34) are

$$\frac{d\rho}{dt} = p_\rho,$$

$$\frac{dz}{dt} = p_z,$$

$$\frac{dp_\rho}{dt} = \frac{L^2}{\rho^3} - \rho - \frac{1}{2} \rho (\rho^2 + z^2)^{-\frac{3}{2}},$$

$$\frac{dp_z}{dt} = -\frac{1}{2} z (\rho^2 + z^2)^{-\frac{3}{2}}. \quad (5.35)$$

Figure (5.1) shows the equipotential lines $V(\rho, z; L) = \text{constant}$ with $L = 0.4$ and scaled energies ranging from $E = -0.5$ to $E = 0.2$.

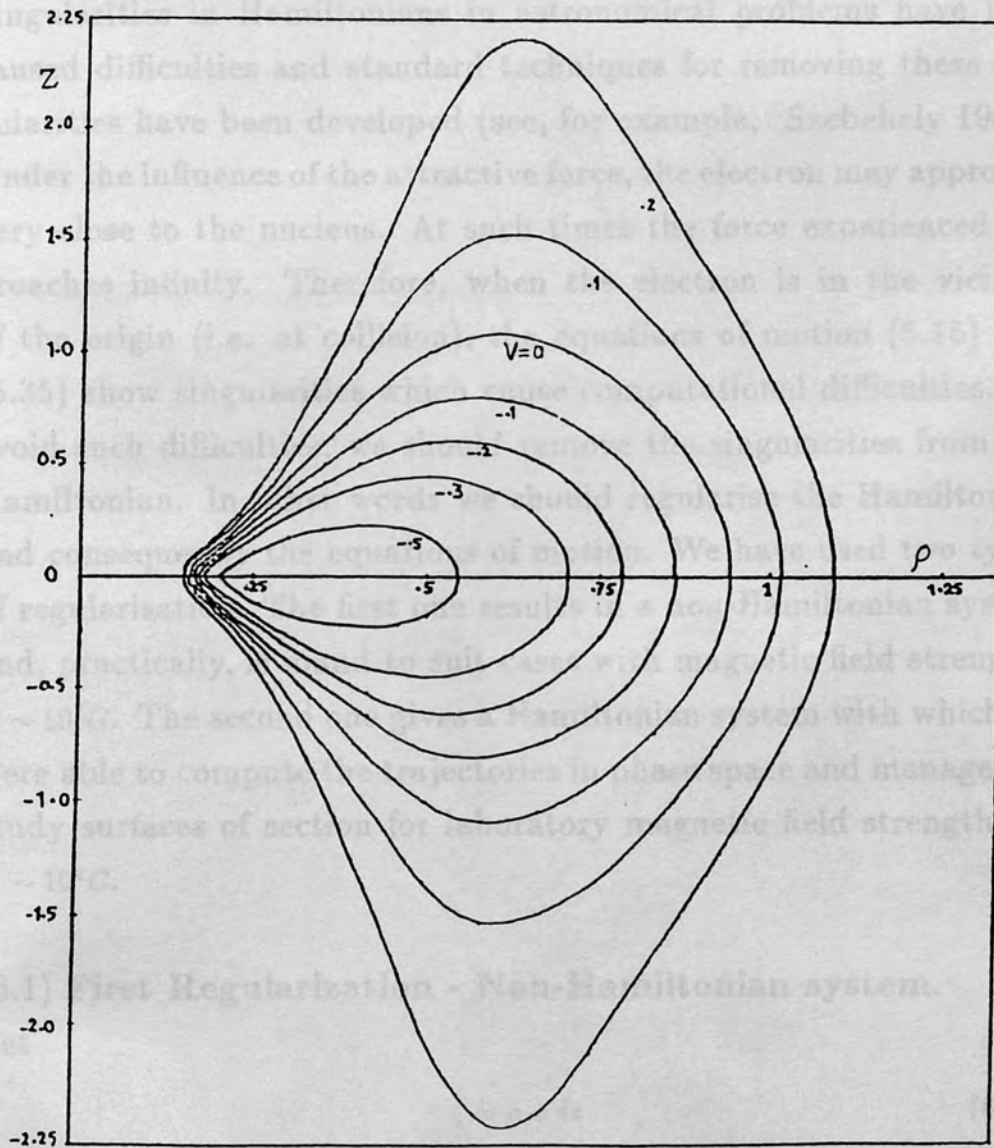


Figure (5.1). Equipotential surfaces $V(\rho, z) = \text{const.}$, $L = 0.4$.

CHAPTER (6)

REGULARISATION

Singularities in Hamiltonians in astronomical problems have long caused difficulties and standard techniques for removing these singularities have been developed (see, for example, Szebehely 1967). Under the influence of the attractive force, the electron may approach very close to the nucleus. At such times the force experienced approaches infinity. Therefore, when the electron is in the vicinity of the origin (i.e. at collision), the equations of motion (5.15) and (5.35) show singularities which cause computational difficulties. To avoid such difficulties, we should remove the singularities from the Hamiltonian. In other words we should regularise the Hamiltonian and consequently the equations of motion. We have used two types of regularisation. The first one results in a non-Hamiltonian system and, practically, is found to suit cases with magnetic field strengths $B \sim 10^7 G$. The second one gives a Hamiltonian system with which we were able to compute the trajectories in phase space and managed to study surfaces of section for laboratory magnetic field strengths i.e. $B \sim 10^4 G$.

(6.1) First Regularization - Non-Hamiltonian system.

Let

$$\zeta = \rho + iz \quad (6.1.1)$$

be an arbitrary vector in the ζ - plane. Then equation (5.32) can be written as

$$|\dot{\zeta}|^2 = 2\mathcal{K} \quad (6.1.2)$$

where the “.” stands for $\frac{d}{dt}$ and

$$\mathcal{K} = E - V \quad (6.1.3)$$

is the kinetic energy.

The equations of motion derived from (5.35) take the form

$$\ddot{\zeta} = \nabla_{\zeta} \mathcal{K} \quad (6.1.4)$$

where

$$\nabla_{\zeta} = \left(\frac{\partial}{\partial \rho} + i \frac{\partial}{\partial z} \right).$$

Let us use the conformal mapping

$$\zeta = f(w), \quad \zeta = \rho + iz, \quad w = u + iv, \quad (6.1.5)$$

from the w -plane to the ζ -plane and assume that

$$\frac{dt}{d\tau} = g(w) = \bar{h}(w) h(w) \quad (6.1.6)$$

where h is an analytic function and \bar{h} is the conjugate of h . So g is a real function of w .

It can be proved that (see Szebehely p. 78-91)

$$\frac{1}{2} \left| \frac{dw}{d\tau} \right|^2 = |f'|^{-2} |h|^4 \mathcal{K} \quad (6.1.7)$$

and

$$\begin{aligned} \frac{d^2 w}{d\tau^2} + 2i \frac{dw}{d\tau} \mathcal{Jm} \left[\frac{dw}{d\tau} \frac{d}{dw} \ln(f'/h) \right] \\ = \nabla_w |f'|^{-2} |h|^4 \mathcal{K} \end{aligned} \quad (6.1.8)$$

where $f' = \frac{df}{dw}$ and \mathcal{Jm} stands for “imaginary part of”.

For any choice of the analytic functions f and h , equations (6.1.5) and (6.1.6) define a transformation from the coordinate system $t, \rho(t), z(t)$

to a new coordinate system $\tau, u(\tau), v(\tau)$ whose energy equation and equations of motion are (6.1.7) and (6.1.8) respectively.

By choosing

$$h^2 = ff'(f + \bar{f}), \quad (6.1.9)$$

evaluation of $\frac{d}{dw} \ln\left(\frac{f'}{h}\right)$ gives

$$\frac{d}{dw} \ln\left(\frac{f'}{h}\right) = \frac{f''f(f + \bar{f}) - f'^2(f + \bar{f}) - f'f(f' + \bar{f}')}{2f'f(f + \bar{f})}. \quad (6.1.10)$$

Then choosing

$$f = e^w, \quad (6.1.11)$$

the right hand side of (6.1.10) reduces to $-\frac{1}{2}$.

The new energy equation and equations of motion then take the form

$$\frac{1}{2} \left| \frac{dw}{d\tau} \right|^2 = 2e^{3u}(1 + 2Ee^u) \cos^2 v - 2e^{6u} \cos^4 v - 2L^2 e^{2u}, \quad (6.1.12)$$

$$\frac{d^2w}{d\tau^2} - i \left(\frac{dv}{d\tau} \right) \left(\frac{dw}{d\tau} \right) = \frac{1}{2} \nabla_w \left| \frac{dw}{d\tau} \right|^2. \quad (6.1.13)$$

Thus we have the following transformation

$$\rho = e^u \cos v, \quad z = e^u \sin v, \quad \frac{dt}{d\tau} = 2e^{3u} \cos v, \quad (6.1.14)$$

with which the regularized energy equation is

$$\frac{1}{2} \left[\left(\frac{du}{d\tau} \right)^2 + \left(\frac{dv}{d\tau} \right)^2 \right] = 2e^{3u}(1 + 2Ee^u) \cos^2 v - 2e^{6u} \cos^4 v - 2L^2 e^{2u} \quad (6.1.15)$$

and the regularized equations of motion are

$$\frac{d^2u}{d\tau^2} + \left(\frac{dv}{d\tau} \right)^2 = 2e^{3u}(3 + 8Ee^u) \cos^2 v - 12e^{6u} \cos^4 v - 4L^2 e^{2u},$$

$$\frac{d^2v}{d\tau^2} - \left(\frac{du}{d\tau} \right) \left(\frac{dv}{d\tau} \right) = -2e^{3u}(1 + 2Ee^u) \sin 2v + 8e^{6u} \cos^3 v \sin v. \quad (6.1.16)$$

We notice from equations (6.1.15) and (6.1.16) that this technique of regularisation has established regularized equations but the system is not Hamiltonian.

We can retrieve the original phase space by the inverse transformation

$$\rho = e^u \cos v,$$

$$z = e^u \sin v,$$

$$p_\rho = \frac{1}{2} e^{-2u} \left[\frac{du}{d\tau} - \frac{dv}{d\tau} \tan v \right]$$

$$p_z = \frac{1}{2} e^{-2u} \left[\frac{dv}{d\tau} + \frac{du}{d\tau} \tan v \right]. \quad (6.1.17)$$

We integrated the regularized equations (6.16) to get u , v , $\frac{du}{d\tau}$ and $\frac{dv}{d\tau}$. Then by means of equations (6.1.17) we converted to the canonical variables ρ , p_ρ , z , p_z . Using this technique we obtained, for strong magnetic fields, a classical picture quite similar to that given by Robnik (1981).

Following Edmonds and Pullen (1980), we assume that the constant of the motion p_ϕ is quantized by the relation

$$p_\phi = m \hbar, \quad m = 0, \pm 1, \pm 2, \dots \quad (6.1.18)$$

which with (5.19) give the correlation between the magnetic quantum number m , the parameter L and the magnetic field strength B (see table (6.1.1)).

We obtained surfaces of sections for values of L comparable with 0.1 and consequently values of $B \sim 10^7 G$ which are smaller than those used by Robnik who generated surfaces of section at $B \sim 10^9 G$ (Robnik (1981)). We analyse the surfaces of section in section (7.2). However, the values of B we considered above are far from the laboratory field strength for which $L \sim 0.01$. So this transformed system best suits strong magnetic fields.

Table (6.1.1)

Values of the unscaled angular momentum parameter L corresponding to various values of the magnetic quantum number m and the magnetic field strength B .

m	B [kG]	L
0	B	0
1	27	0.0113
2	27	0.0226
3	27	0.0338
1	42	0.0131
2	42	0.0261
3	42	0.0392
1	60	0.0147
2	60	0.0294
3	60	0.0442

(6.2) Second regularisation - Hamiltonian system

However the Hamiltonian formalism being the most powerful technique established in classical mechanics, we employed another transformation which is canonical (Richards 1984 and Cornish 1984). Then we could tackle the problem within the Hamiltonian framework and with the Hamiltonian and the equations of motion regularised. The canonical transformation to be performed will be given by a generating function of the second type (see table (2.2)).

$$\begin{aligned} F(P_i, q_i) = & P_1 r^{\frac{1}{2}} \cos \frac{\theta}{2} \cos\left(\frac{\sigma + \phi}{2}\right) + \\ & P_2 r^{\frac{1}{2}} \cos \frac{\theta}{2} \sin\left(\frac{\sigma + \phi}{2}\right) + \\ & P_3 r^{\frac{1}{2}} \sin \frac{\theta}{2} \cos\left(\frac{\sigma - \phi}{2}\right) + \\ & P_4 r^{\frac{1}{2}} \sin \frac{\theta}{2} \sin\left(\frac{\sigma - \phi}{2}\right), \end{aligned} \quad (6.2.1)$$

where the independent variable σ is introduced as an additional coordinate and is to be defined below.

Then

$$\begin{aligned} p_r = \frac{\partial F}{\partial r}, \quad p_\theta = \frac{\partial F}{\partial \theta}, \quad p_\phi = \frac{\partial F}{\partial \phi}, \quad p_\sigma = \frac{\partial F}{\partial \sigma}, \\ Q_i = \frac{\partial F}{\partial P_i}, \quad i = 1, 2, 3, 4. \end{aligned} \quad (6.2.2)$$

The second four of these equations give

$$Q_1 = r^{\frac{1}{2}} \cos\left(\frac{\theta}{2}\right) \cos\left(\frac{\sigma + \phi}{2}\right),$$

$$Q_2 = r^{\frac{1}{2}} \cos\left(\frac{\theta}{2}\right) \sin\left(\frac{\sigma + \phi}{2}\right),$$

$$Q_3 = r^{\frac{1}{2}} \sin\left(\frac{\theta}{2}\right) \cos\left(\frac{\sigma - \phi}{2}\right),$$

For any chosen pair of the complex variables ζ_A and ζ_B , a unique set of values for the cartesian coordinates x, y, z is determined, and for a given choice of x, y, z , the complex variables ζ_A and ζ_B are determined.

$$Q_4 = r^{\frac{1}{2}} \sin\left(\frac{\theta}{2}\right) \sin\left(\frac{\sigma - \phi}{2}\right). \quad (6.2.3)$$

Note that the transformation equations (6.2.3) connect the new and the old coordinates directly without involving the momenta.

The first four equations of (6.2.2) give
The old coordinates r, θ , and ϕ can be retrieved in terms of the Q_i 's.
We get

$$r = \sum_{i=1}^4 Q_i^2, \quad (6.2.4a)$$

$$\theta = \tan^{-1}\left(\frac{Q_3^2 + Q_4^2}{Q_1^2 + Q_2^2}\right),$$

$$\phi = \tan^{-1}\left(\frac{Q_2 Q_3 - Q_1 Q_4}{Q_1 Q_3 + Q_2 Q_4}\right). \quad (6.2.4a)$$

Moreover

$$z = (Q_1^2 + Q_2^2) - (Q_3^2 + Q_4^2)$$

$$\rho^2 = 4(Q_1^2 + Q_2^2)(Q_3^2 + Q_4^2). \quad (6.2.4b)$$

Let us define the two complex variables

$$\begin{aligned} \zeta_A &= Q_1 + i Q_2 \\ &= r^{\frac{1}{2}} \cos \frac{\theta}{2} \exp\left[i \frac{(\sigma + \phi)}{2}\right], \end{aligned}$$

$$\begin{aligned} \zeta_B &= Q_3 + i Q_4 \\ &= r^{\frac{1}{2}} \sin \frac{\theta}{2} \exp\left[i \frac{(\sigma - \phi)}{2}\right]. \end{aligned} \quad (6.2.5)$$

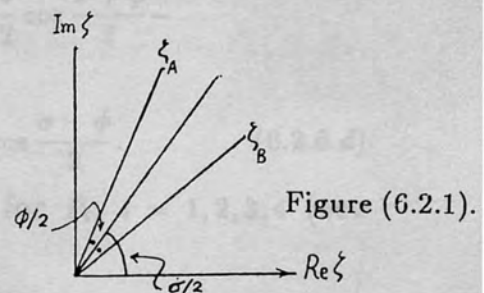


Figure (6.2.1).

Hence we get the geometrical meaning of σ

$$\sigma = \arg \zeta_A + \arg \zeta_B = \arg(\zeta_A \zeta_B). \quad (6.2.7)$$

For any chosen pair of the complex variables ζ_A and ζ_B a unique set of values for the cartesian coordinates x, y, z is determined, and for any given choice of x, y, z , the complex variables ζ_A and ζ_B are determined to within an arbitrary value for the angle σ .

The first four equations of (6.2.2) give

$$2r^{\frac{1}{2}}p_r = P_1 \cos \frac{\theta}{2} \cos \frac{\sigma + \phi}{2} + P_2 \cos \frac{\theta}{2} \sin \frac{\sigma + \phi}{2} + P_3 \sin \frac{\theta}{2} \cos \frac{\sigma - \phi}{2} + P_4 \sin \frac{\theta}{2} \sin \frac{\sigma - \phi}{2}, \quad (6.2.6.a)$$

$$2r^{-\frac{1}{2}}p_\theta = -P_1 \sin \frac{\theta}{2} \cos \frac{\sigma + \phi}{2} - P_2 \sin \frac{\theta}{2} \sin \frac{\sigma + \phi}{2} + P_3 \cos \frac{\theta}{2} \cos \frac{\sigma - \phi}{2} + P_4 \cos \frac{\theta}{2} \sin \frac{\sigma - \phi}{2}, \quad (6.2.6.b)$$

$$2r^{-\frac{1}{2}}p_\phi = -P_1 \cos \frac{\theta}{2} \sin \frac{\sigma + \phi}{2} + P_2 \cos \frac{\theta}{2} \cos \frac{\sigma + \phi}{2} + P_3 \sin \frac{\theta}{2} \sin \frac{\sigma - \phi}{2} - P_4 \sin \frac{\theta}{2} \cos \frac{\sigma - \phi}{2}, \quad (6.2.6.c)$$

$$2r^{-\frac{1}{2}}p_\sigma = -P_1 \cos \frac{\theta}{2} \sin \frac{\sigma + \phi}{2} + P_2 \cos \frac{\theta}{2} \cos \frac{\sigma + \phi}{2} - P_3 \sin \frac{\theta}{2} \sin \frac{\sigma - \phi}{2} + P_4 \sin \frac{\theta}{2} \cos \frac{\sigma - \phi}{2}. \quad (6.2.6.d)$$

The system of equations (6.2.6) are solved for P_i , $i = 1, 2, 3, 4$ (see Appendix).

Furthermore we have

$$\sum_{i=1}^4 P_i^2 = 4r[p_r^2 + \frac{p_\theta^2}{r^2} + \frac{L^2}{r^2 \sin^2 \theta}] + \frac{4}{r \sin^2 \theta} [p_\sigma^2 - 2Lp_\sigma \cos \theta]. \quad (6.2.7)$$

Since σ , the angle between the two complex vectors ζ_A and ζ_B , is arbitrary, we set

$$p_\sigma \equiv 0 \quad (6.2.8)$$

and get

$$\sum_{i=1}^4 P_i^2 = 4r[p_r^2 + \frac{p_\theta^2}{r^2} + \frac{L^2}{r^2 \sin^2 \theta}]. \quad (6.2.9)$$

Substituting from (6.2.9) into (5.33) we get $K = K(Q_i, P_i)$ or

$$K = \frac{1}{8r} \left(\sum_{i=1}^4 P_i^2 \right) + \frac{1}{2} \rho^2 - \frac{1}{2r}, \quad (6.2.10)$$

where r and ρ are expressed as functions of Q_1, Q_2, Q_3, Q_4 (see equations (6.2.4a) and (6.2.4b)).

Now, we have the Hamiltonian (6.2.10) which does not contain the time t explicitly and contains a singularity at $r = 0$. For the purpose of regularization we use the method of the generalised time transformation explained in section (2.6). It is essential in this case to introduce the concept of extended phase space (explained in section (2.4)):

Introducing as the fifth generalised coordinate Q_5 the time t , then its conjugate momentum P_5 becomes $-K$. Thus, we have a ten-dimensional extended phase space with coordinates $Q_1, \dots, Q_5, P_1, \dots, P_5$.

We use the Hamiltonian function

$$\Gamma = P_5 + \nu(Q_1, \dots, Q_4, P_1, \dots, P_4) \quad (= 0) \quad (6.2.11)$$

where

$$\nu = K = H,$$

$$Q_5 = t \quad \text{and} \quad P_5 = -K = -E \quad (6.2.12)$$

where E is the dimensionless energy parameter.

The equations of motion in the extended phase space are

$$\frac{dQ_i}{d\varpi} = \frac{\partial \Gamma}{\partial P_i}, \quad (6.2.10)$$

Then, the new regularized potential is given by

$$\frac{dP_i}{d\varpi} = -\frac{\partial \Gamma}{\partial Q_i}, \quad i = 1, 2, 3, 4, 5. \quad (6.2.13)$$

Having constructed the extended phase space, the method of generalised time transformation (section (2.6)) is ready for use: The extended phase space Hamiltonian Γ is transformed into

$$\begin{aligned} \Gamma^* &= f(Q_1, \dots, Q_4)\Gamma \\ &= f\left[\frac{1}{8r}\left(\sum_{i=1}^4 P_i^2\right) + \frac{1}{2}\rho^2 - \frac{1}{2r}\right] \end{aligned} \quad (6.2.14)$$

and simultaneously a parameter τ is introduced by

$$d\varpi = dt = f(Q_1, \dots, Q_4)d\tau. \quad (6.2.15)$$

Then the canonical character of the equations is preserved by the transformed system

$$\frac{dQ_i}{d\tau} = \frac{\partial \Gamma^*}{\partial P_i}, \quad (6.2.16)$$

Thus, the system of equations (6.2.15) is regular. The canonical integration of these equations, to get the Q_i and P_i (including

One of the choices of f which removes the singularity from Γ^* (i.e. from the right hand side of (6.2.14)) is

$$f = 4r \left(= 4 \sum_{i=1}^4 Q_i^2 \right). \quad (6.2.17)$$

Then

$$\Gamma^* = \frac{1}{2} \sum_{i=1}^4 P_i^2 + 4\lambda \sum_{i=1}^4 Q_i^2 - 2 \quad (= 0) \quad (6.2.18)$$

where

$$\lambda = P_5 + 2(Q_1^2 + Q_2^2)(Q_3^2 + Q_4^2). \quad (6.2.19)$$

Then, the new regularized potential is given by

$$V_Q = 4\lambda \sum_{i=1}^4 Q_i^2 - 2. \quad (6.2.20)$$

Equations (6.2.16) can be written as

$$\frac{dQ_i}{d\tau} = P_i, \quad i = 1, 2, 3, 4 \quad (6.2.21)$$

$$\frac{dt}{d\tau} = 4 \sum_{i=1}^4 Q_i^2,$$

$$\frac{dP_1}{d\tau} = -8Q_1\lambda - 16Q_1(Q_3^2 + Q_4^2) \sum_{i=1}^4 Q_i^2,$$

$$\frac{dP_2}{d\tau} = -8Q_2\lambda - 16Q_2(Q_3^2 + Q_4^2) \sum_{i=1}^4 Q_i^2,$$

$$\frac{dP_3}{d\tau} = -8Q_3\lambda - 16Q_3(Q_1^2 + Q_2^2) \sum_{i=1}^4 Q_i^2,$$

$$\frac{dP_4}{d\tau} = -8Q_4\lambda - 16Q_4(Q_1^2 + Q_2^2) \sum_{i=1}^4 Q_i^2. \quad (6.2.21)$$

Thus, the system of equations (6.2.21) has no singularities. Numerical integration of these equations, to get the Q_i and P_i (including the time t), is feasible by using a suitable numerical method to be discussed in section (7.3).

In cylindrical coordinates the momenta (equations (5.29)) can be obtained in terms of Q_i and P_i (see Appendix) as

$$p_\rho = \frac{1}{2\rho} \sum_{i=1}^4 P_i Q_i - \frac{z}{2\rho r} (P_1 Q_1 + P_2 Q_2 - P_3 Q_3 - P_4 Q_4)$$

$$p_z = \frac{1}{2r}(P_1Q_1 + P_2Q_2 - P_3Q_3 - P_4Q_4)$$

$$p_\phi = \frac{1}{2}(-P_1Q_2 + P_2Q_1 + P_3Q_4 - P_4Q_3). \quad (6.2.22)$$

We again use the shorthand p_ϕ for $p_{\phi'}$.

We shall also need the identity

$$p_\sigma = \frac{1}{2}(-P_1Q_2 + P_2Q_1 - P_3Q_4 + P_4Q_3). \quad (6.2.23)$$

Going back to equations (6.1.7) and (6.1.8) we find the canonical mapping (6.1.5), with the choice $\kappa = \pi$ is a canonical transformation since, with the new Hamiltonian

$$F = \frac{1}{2} \left(\frac{dq}{dt} \right)^2 - q \omega^2 \kappa, \quad (6.2.24)$$

we have

$$\frac{d^2q}{dt^2} = -\nabla_q(q \omega^2 \kappa) = -\omega^2 \kappa. \quad (6.2.25)$$

Explicitly,

$$F = \frac{1}{2}(p_u^2 + p_v^2) - \omega^2(u^2 + v^2) + \omega^2(u^2 + v^2)\cos\pi = \frac{1}{2}(p_u^2 + p_v^2) - \omega^2(u^2 + v^2),$$

$$\frac{4L^2(u^2 + v^2)}{(u^2 - v^2)^2} = 2, \quad (6.2.26)$$

where

$$p_u = \frac{dq}{dt}, \quad p_v = \frac{dq}{dt} \cos\pi = -\frac{dq}{dt} \quad (6.2.27)$$

so we get

$$\frac{4L^2(u^2 + v^2)}{(u^2 - v^2)^2} = 2, \quad (6.2.28)$$

CHAPTER (7)

Surface of section calculation for the quadratic Zeeman Hamiltonian

(7.1) More visible surfaces of section.

For the quadratic Zeeman potential, the surface of section in the phase space ρ, p_ρ, z, p_z is found to be concentrated in narrow regions of space when the angular momentum parameter L is comparable with 0.01 i.e. for those L for which the Hamiltonian system in section (6.2) is used. Therefore, we find it appropriate to obtain surfaces of section in a phase space given by a canonical transformation which we derive as follows

Going back to equations (6.1.7) and (6.1.8) we see that the conformal mapping (6.1.5), with the choice $h = 2w$ is a canonical transformation since, with the new Hamiltonian

$$\Gamma = \frac{1}{2} \left| \frac{dw}{d\tau} \right|^2 - 4|w|^2 \mathcal{K}, \quad (= 0) \quad (7.1.1)$$

we have

$$\frac{d^2 w}{d\tau^2} = \nabla_w (4|w|^2 \mathcal{K}) = -\nabla_w \Gamma \quad (7.1.2)$$

Explicitly,

$$\Gamma = \frac{1}{2}(p_u^2 + p_v^2) - 4E(u^2 + v^2) + 2(u^2 + v^2)(u^2 - v^2)^2 + \frac{4L^2(u^2 + v^2)}{(u^2 - v^2)^2} - 2, \quad (= 0) \quad (7.1.3)$$

where

$$p_u = \frac{du}{d\tau}, \quad p_v = \frac{dv}{d\tau}, \quad (7.1.4)$$

so we get

$$\frac{dp_u}{d\tau} = -\frac{\partial \Gamma}{\partial u},$$

$$\frac{dp_v}{d\tau} = -\frac{\partial\Gamma}{\partial v}. \quad (7.1.5)$$

Therefore the transformation

$$\rho = u^2 - v^2, \quad z = 2uv, \quad \frac{dt}{d\tau} = 4\tau \quad (7.1.6)$$

is canonical. Furthermore, we notice from (7.1.3) that for the particular case $L = 0$, we obtain a regularised Hamiltonian and regularised equations of motion.* For $L \neq 0$ the Hamiltonian (7.1.3) and the canonical equations (7.1.5) still have singularities. They are not meant to be integrated. We instead integrate Hamilton's equations (6.2.21) and then use equations (6.2.4) to get a phase trajectory in ρ, p_ρ, z, p_z . The following step is to convert from a phase point (ρ, p_ρ, z, p_z) in the original phase space to the phase point (u, p_u, v, p_v) in the transformed one:

Differentiating the first two equations in (7.1.6) with respect to τ we get

$$uu' - vv' = \frac{\rho'}{2} \quad (7.1.7)$$

$$vu' + uv' = \frac{z'}{2} \quad (7.1.8)$$

where the prime "''" stands for $\frac{d}{d\tau}$.

Solving (7.1.7) and (7.1.8) for u' and v' we get

$$u' = \frac{1}{2r}(u\rho' + vz'), \quad (7.1.9)$$

$$v' = \frac{1}{2r}(uz' - v\rho'). \quad (7.1.10)$$

Also we have

$$\rho' = \frac{d\rho}{d\tau} = \frac{d\rho}{dt} \frac{dt}{d\tau}, \quad (7.1.11)$$

$$z' = \frac{dz}{d\tau} = \frac{dz}{dt} \frac{dt}{d\tau}. \quad (7.1.12)$$

* This is the regularisation scheme used by Edmonds and Pullen (1980) and is equivalent to the Cornish scheme for $L=0$.

Substituting for $\frac{d\rho}{dt}$, $\frac{dz}{dt}$ and $\frac{dt}{d\tau}$ by p_ρ , p_z and $4r$ respectively, we get

$$\rho' = 4rp_\rho, \quad z' = 4rp_z \quad (7.1.13)$$

and hence from (7.1.9) and (7.1.10),

$$p_u (= \frac{du}{d\tau}) = 2(up_\rho + vp_z), \quad (7.1.14)$$

$$p_v (= \frac{dv}{d\tau}) = 2(up_z - vp_\rho). \quad (7.1.15)$$

Solving (7.1.14) and (7.1.15) for p_ρ and p_z we get

$$p_\rho = \frac{1}{2r}(up_u - vp_v), \quad (7.1.16)$$

$$p_z = \frac{1}{2r}(up_v + vp_u), \quad (7.1.17)$$

where

$$r = u^2 + v^2.$$

The surface of section pictures in the up_u -plane, defined by

$$v = 0, \quad p_v > 0 \quad (7.1.18)$$

in this scheme are much clearer and easier to investigate than those in the original phase space, particularly when $|L|$ is small (for example when $|L|$ is comparable with 0.01).

Figures (7.1.1a) and (7.1.1b) show two curves: the first is the bounding curve of a surface of section in the ρp_ρ -plane and the second is the bounding curve of the corresponding surface of section in the up_u -plane. The area enclosed by the latter curve is seen to be quite spacious, while the area enclosed by the former is narrow.

(7.2) The surface of section for the quadratic Zeeman potential

The Poincaré map, T , (see section (4.1)) reduces the study of a Hamiltonian system with two degrees of freedom (i.e. a system of four first-order differential equations) to a study of surfaces of section generated by T^s for a finite integer s . By means of the surfaces of section we can investigate, macroscopically, the various regions in phase space, and thus view the overall classical motion of the system. In this section we study the Poincaré map, T , arising from the Zeeman potential by applying the surface of section method to the transformed system given by (7.1.3). The integration difficulties due to the singularity are avoided by integrating instead the regularized system given by (6.2.18).

For a fixed value E in (7.1.3) a phase orbit can be plotted in a three dimensional space, parametrised by (u, p_u, v) . The boundary of this space is given by

$$p_v^2 \equiv -p_u^2 + 8E(u^2 + v^2) - 4(u^2 + v^2)(u^2 - v^2)^2 - \frac{8L^2(u^2 + v^2)}{(u^2 - v^2)^2} + 4 = 0. \quad (7.2.1)$$

Thus for a fixed E , the three-dimensional energy surface S_E given by (7.1.3) intersects the plane $v = 0$ in a two-dimensional region

$$R = \{(u, p_u) : v = 0, p_v^2 > 0\}. \quad (7.2.2)$$

We choose our surface of section to be the subset $S_v \subset R$ and defined by

$$S_v = \{(u, p_u) : v = 0, p_v > 0\}, \quad (7.2.3)$$

on which the Poincaré map T is defined. So our initial conditions should be in S_v .

It is convenient to display the surfaces of section at some arbitrary fixed value of the parameter L at a fixed value of E . If X_0 is an initial point on the surface of section (7.2.2), we calculate the iterates

$X_i = T^i(X_0), i=1,2,\dots,s$ on the surface of section (7.2.2). The maximum s we used was $s = 400$. The possibilities of how the iterates X_1, X_2, \dots, X_s are distributed was explained in section (4.1). If all the iterates lie on a curve (i.e. an invariant curve of the mapping), then there exists a third integral of the motion I_3 which intersects the plane $v = 0$ in that curve. If X_0 is a fixed point of some least iterate $N \in I$ of the mapping T , then we have discovered an N -cycle periodic orbit in the phase space. If however, the iterates fill a two-dimensional area on the surface of section, then the motion is stochastic and possibly ergodic in some region in the phase space. By repeating this process for a sufficient finite number of initial points in the area bounded by (7.2.1), the resulting trajectories, in view of (7.2.3), produce a surface of section picture, labelled by L and E . This picture, generally, reveals the macroscopic features of the surface of section. At a fixed value of L we repeat the same procedure for discrete values of E , to obtain a series of surfaces of section which are clearly observed to vary with E over some interval of E .

For laboratory magnetic field strengths ($B \sim 10^4$ G) we give four series of surfaces of section at $m=0, 1, 2, 3$. Figure(7.2.1) shows the surfaces of section generated by trajectories at $m=0$ (i.e. $L = 0$) at various values of E . The initial conditions for these trajectories are chosen in such a way that they exhibit the features of each surface of section. The values of E are chosen so as to show the change of the structure of the phase space, starting from the regular regime at $E = -1.0$ up to the chaotic regime at $E = -0.37$ (i.e. ranging between -111.73 cm^{-1} up to -41.34 cm^{-1} , $B = 27 \text{ kG}$). Figures (7.2.2), (7.2.3) and (7.2.4) are like figure (7.2.1) but at $m = 1, 2, 3$ respectively (for which we have, for example, $B = 27 \text{ kG}$, $L = 0.011, 0.022,$ and 0.033 respectively). These values were chosen because of the analogy with

the experiments on Cs by Gay *et. al.* (1980), for 27kG , $m=3$.

Apart from slight displacement of the motions from the z -axis for $m = 1, 2, 3$, all the four series have similar surface of section features. So, we choose to explain the first: ($m = 0$).

For low energies, such as $E = -1.0$, we have four different families of invariant simply connected curves on the surface of section. One family, f_1 , is situated round the point $(0, 0)$, the second, f_2 , round $(0, \sqrt{2})$ and the third, f_3 , round $(0, -\sqrt{2})$. The fourth family, f_4 , consists of invariant curves which encompass the families f_1, f_2 and f_3 altogether. These families (for $m = 0$) were first discovered by Edmonds and Pullen (1980). The innermost invariant curves of the family f_1 and the outermost of the family f_4 are found to be the most persistent curves and correspond to orbits oscillating with big amplitudes along the ρ -axis and small ones along the z -axis. The latter decrease as we approach the fixed point $(0, 0)$ or alternatively as we approach the largest invariant curve in the family f_4 . This curve was found to be the longest surviving one which together with the fixed point $(0, 0)$ correspond to a planar orbit (see chapter 8). The stability of this planar orbit is studied, quantitatively, in section (10.4) and results from that section show that the planar orbits are linearly stable for $E < -0.127$ and lose stability permanently beyond this value. This value can be considered as the last plausible limit of the macroscopic features in the phase space.

The families f_2 and f_3 correspond, respectively, to two similar non-planar motions up and down the z -axis. The inner invariant curves of the family f_2 correspond to orbits which oscillate with big amplitudes along the positive z -axis and small amplitudes along the

ρ -axis. The latter amplitudes decrease as we approach the fixed point $(0, +\sqrt{2})$. This point corresponds to a periodic orbit which is, to a good approximation, a linear motion along the positive z -axis. The linear stability of this orbit is studied, quantitatively, in section (10.4.2). Results from that section reveal the importance of this orbit as it behaves and bifurcates non-generically. The families of invariant curves f_i , $i = 1, 2, 3, 4$ are separated from each other by a trajectory called the separatrix (whose invariant curve is depicted as a solid line in figure (7.2.1) at $E = -1.0$). There are two ordinary hyperbolic points (X points) on both sides of the figure. Results from section (10.4.1) show that it is unstable throughout the whole range of E .

For lower values of E (for example $E = -1.0$) surfaces of section, within the accuracy of numerical computation, seem to be wholly occupied by invariant curves. Roughly speaking, this implies that a third integral I_3 exists. Furthermore, it is an isolating integral in the sense that given initial conditions (u_0, p_u^0, v_0, p_v^0) restrict (or isolate) the trajectory to a limited region of phase space (i.e. a specific torus). Each invariant curve on the surface of section is the intersection of the integral

$$I_3(u, p_u, v, p_v) = \text{constant}, \quad (7.2.4)$$

with the plane $(u, p_u, v = 0)$ for a single value of that constant.

Like many other maps defined by a two-dimensional potential the map T exhibits an increase in stochasticity in phase space with respect to a continuously varying parameter. In the present case this parameter is the energy parameter E .

Back to figure (7.2.1), at $E = -0.48$ we notice that three invariant

curves belonging to different families are destroyed. Each one breaks up into six islands centered at six elliptic points (of T^6) indicating the existence of three six-cycle periodic orbits. The islands are separated by a separatrix trajectory passing through six hyperbolic fixed points (of T^6) (see the solid curve drawn by hand in figure (7.2.1) at $E = -0.4$). But it is worth noting that such separatrices round island chains are not, typically, curves but stochastic layers (figure (7.2.5)). In figure (7.2.1) at $E = -0.37$ the two elliptic points situated above and below the point $(0, +\sqrt{2})$ indicate a special occurrence; a bifurcation (see section (4.3.6)). The elliptic fixed point which existed for lower energies becomes a hyperbolic fixed point and two other elliptic fixed points are created. This bifurcation and others are studied in section (10.4.2). In this figure (figure (7.2.1)) we notice that irregular motion occupies a considerable proportion of the whole surface of section. Figure (7.2.6) is a schematic diagram showing the regular and irregular areas on the surface of section and the corresponding potential contour. The growth of irregularity, in between the regions which remain regular of the four families f_i , $i = 1, 2, 3, 4$ (figure (7.2.6a)), increases with E . This is to be expected, since the trajectories associated with these regions pass close to the convex parts C_1, C_2, C_3 , and C_4 , which are depicted in figure (7.2.6b).

In all the series of surfaces of section (figures (7.2.1)-(7.2.4)) we notice that there is a transition from regular motion to a chaotic motion. If we agree to be specific or more quantitative and define a value of E at which this transition takes place we then may call this value the *critical energy*. In fact there are several definitions which are all roughly equivalent in view of the fact that the transition, particularly in generic behaviour, is fairly sharp. For example, one definition refers to the destruction of the large scale torus, another one involves

a global property of the phase flow; the Kolmogorov entropy. However, a definition of a critical energy is considered by some people, like Berry, a misleading idea (Berry 1987). We adopt the criterion that the critical energy E_c is reached when the two proportions of a surface of section occupied by the regular and the chaotic motions are approximately the same. Fortunately, we found this definition convenient for our surfaces of section because each invariant curve belonging to one of the families f_1 and f_4 is found to be approximately elliptic whilst stochastic regions grow up between these two families. For all fields of laboratory strengths and small magnetic quantum numbers ($m = 0, 1, 2, 3$) $E_c \simeq -0.4$. There is only a slight variation in E_c for the range $|L| \leq 0.033$.

For strong magnetic fields ($B \sim 10^7$ G) the technique discussed in section (6.1) proves to be efficient. Figure (7.2.7) shows surfaces of section defined by

$$S_z = \{(\rho, p_\rho) : z = 0 \text{ and } p_z > 0\}, \quad (7.2.6)$$

at fixed value $L = 0.4$ (for which we have for example $m = 3$, $B = 44563$ kG). At low energies (such as $E = -0.3$) the surface of section is wholly occupied by one family, f , of invariant curves. What happens as L increases from zero is that the two families f_2 and f_3 , described above, shrink until they vanish. So we are left only with the union of the two families f_1 and f_4

$$f = f_1 \cup f_4. \quad (7.2.7)$$

This implies, from the discussion above, that planar orbits (in the $z = 0$ plane), and in turn the σ -spectra, are the clearest feature as L increases (i.e. for astrophysical magnetic field strengths). This is to be expected, since the quasi Landau resonance $1.5 \hbar \omega_c$ which was

discovered experimentally by Garton and Tomkins (1969) merely at laboratory magnetic fields has been attributed to the planar motions (see the introduction of this thesis).

The elliptic fixed point seen in the regular regime is situated along the ρ -axis and drifts away from the origin as E increases until eventually it coalesces with the boundary of the energetically available phase space at the farthest point on the ρ -axis. The breaking up of invariant curves into island chains centered at fixed points is shown in the figure for different energies. The critical energy is found to be $E_c \simeq -0.225$. The most persistent invariant curve is the shell curve which bounds the motion.

To conclude, there is no rigorous proof regarding the existence of an analytic integral, I_3 , of the motion (Zaslaviskii and Chirikov 1972, Whiteman 1977, Robnik 1981). But within the accuracy of numerical calculations the existence of an isolating integral, when the calculated invariant curves always seem to fill in the surface of section, can be suggested (Henon and Heiles 1964). Based on results from the KAM theorem it has been conjectured that the measure of invariant curves is approximately 1 (Robnik 1981). Strictly speaking, this does not imply that the invariant curves are dense almost everywhere in the surface of section since the measure of the complement is not exactly zero. Such a conjecture implies the existence of orbits of certain stability/instability properties which are jammed between nearby exact invariant curves. In the light of this discussion the attribute of a regime, through studying surfaces of section, as being *integrable* may be accepted in that sense. For values of E just below and beyond E_c the integral I_3 has a diminishing role. It is effective only in limited regions of phase space and may be considered as

an approximate integral of the motion. The rapid rate of increase of stochasticity in phase space with E beyond this last transition regime indicates the rapid rate of the non-existence of I_3 .

(7.3) Numerical methods and computation

We have solved the system of equations (6.2.21) numerically to calculate the trajectories in the extended phase space. Hence we can derive the trajectories in the original phase space by using equations (6.2.4) and (6.2.22) and in the transformed phase space by using (7.1.6), (7.1.14) and (7.1.15). The initial point (Q^0, P^0) should be chosen to lie on the following surfaces in the (Q, P) - space

$$p_\phi(Q, P) = L$$

$$p_\sigma(Q, P) = 0$$

$$\Gamma(Q, P) = 0. \tag{7.3.1}$$

The system of equations (7.3.1) can be written in the form

$$y'' = F(y), \quad y'(\tau_0) = \eta'_0, \quad y(\tau_0) = \eta_0 \tag{7.3.2}$$

where

$$y = \begin{bmatrix} Q_1 \\ Q_2 \\ Q_3 \\ Q_4 \\ Q_5 \end{bmatrix},$$

For the non-canonical system (Equations (6.1.15)) we used the fourth-order Runge-Kutta (Henrici, 1962) through the NAG routine D04CAF (Henrici, 1976) through in different regions. This was done by considering different values of the step length, systematically smaller. Comparing the respective results until we had agreed to six significant figures.

$$\mathbf{F} = \begin{bmatrix} -8Q_1\lambda - 16Q_1(Q_3^2 + Q_4^2) \sum_{i=1}^4 Q_i^2 \\ -8Q_2\lambda - 16Q_2(Q_3^2 + Q_4^2) \sum_{i=1}^4 Q_i^2 \\ -8Q_3\lambda - 16Q_3(Q_1^2 + Q_2^2) \sum_{i=1}^4 Q_i^2 \\ -8Q_4\lambda - 16Q_4(Q_1^2 + Q_2^2) \sum_{i=1}^4 Q_i^2 \\ 4 \sum_{i=1}^4 Q_i^2 \end{bmatrix},$$

Both the force acting on the electron and its velocity increase drastically as the electron approaches the vicinity of the origin. Thus the physical aspects of the motion become singular. The step size of numerical integration must be increased significantly in this region in order to obtain reliable results. We employed a variable step length algorithm (Henrici, 1976) on the electron's position. The convergence tests (6.1.17), A14 and A15 (see appendix) enabled us to compute the trajectories in the region $0 < r < 10^{-4}$ Å.

$$\eta'_0 = \begin{bmatrix} P_1^0 \\ P_2^0 \\ P_3^0 \\ P_4^0 \\ P_5^0 \end{bmatrix}, \quad \eta_0 = \begin{bmatrix} Q_1^0 \\ Q_2^0 \\ Q_3^0 \\ Q_4^0 \\ Q_5^0 \end{bmatrix}.$$

Let us consider the exact relative increment Δ and the increment function Φ defined by

$$\Delta(\tau, \mathbf{y}; h) = \frac{\mathbf{y}(\tau + h) - \mathbf{y}(\tau)}{h} \quad (7.3.3)$$

and trajectory contributing to the surface of action pictures depicted in Figures (7.2.1)-(7.2.4) consists of about 150 intersection points. We first computed the trajectories in the region $0 < r < 10^{-4}$ Å accurately using a large step-length of 0.0009. Near periodic orbits are quite easy to compute, as long as they remain close to a closed orbit.

$$\mathbf{y}_0 = \boldsymbol{\eta}_0, \quad (7.3.4)$$

where $\mathbf{y}(\tau)$ is the solution of (7.3.2) and \mathbf{y}_n is intended as an approximation to $\mathbf{y}(\tau_n)$.

For the canonical system, we used the Runge-Kutta Nystrom fifth-order error method (Henrici, 1962). As the total derivatives of \mathbf{F} simplify, it becomes possible to achieve an agreement in Φ and Δ , with four substitutions with an error $O(h^5)$.

For the non-canonical system (Equations (6.1.16)) we used the fourth-order Runge-Kutta Merson method (Hall and Watt, 1976) through the NAG routine DO2BBF. The accuracy of the methods was tested in different regions of the phase space for different values of energy. This was done by considering different values of the step length, systematically smaller for consecutive runs, and comparing the respective results until we got agreement correct to six significant figures.

Both the force acting on the electron and its velocity increase drastically as the electron approaches the vicinity of the origin. Thus the physical aspects of space trajectories require an increased accuracy in these critical regions near the singularities. The step size of numerical integration must be decreased significantly in this region in order to obtain reliable results. We employed a variable step length technique depending on the electron's position. The conversion relations (6.1.17), A14 and A15 (see appendix) enabled us to compute the trajectories in the original phase space, ρ, p_ρ, z, p_z .

Each trajectory contributing to the surface of section pictures depicted in Figures (7.2.1)-(7.2.4) consists of about 150 intersection points. We find that regular trajectories can be computed accurately using a large step-length of 0.0009. Near periodic orbits are quite easy to compute so long as they remain close to a closed orbit. As soon as their motions become random the difficulty in tracing them increases. Trajectories which appear to be completely chaotic, however, are very difficult to compute. On performing the quantization (see chapter 11), the NAG routine DO1GAF was called into the program to calculate integrations over unequally spaced data (Gill and Miller, 1972).

Most of the computations carried out in this work were done on a VAX 11/780. The longer runs were done on a Cray 1S and the microfilm was produced on a Calcomp 1670, both at the *University of London Computer Center*.

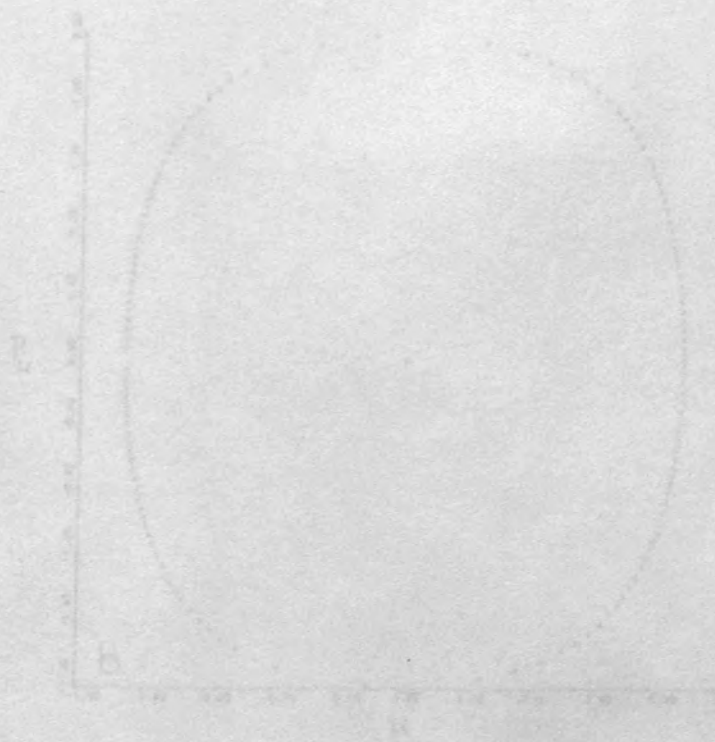
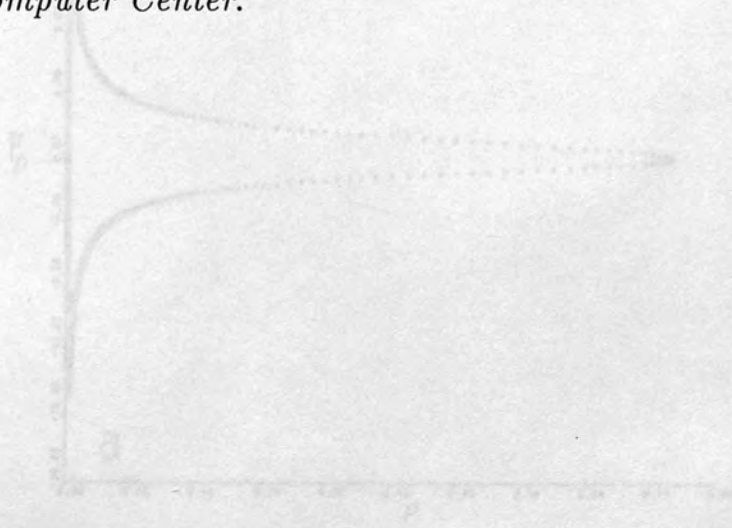


Figure (7.1). Curves based on the model in (a) the ap. plant, (b) the ap. plant, for $m = 5, 8$.

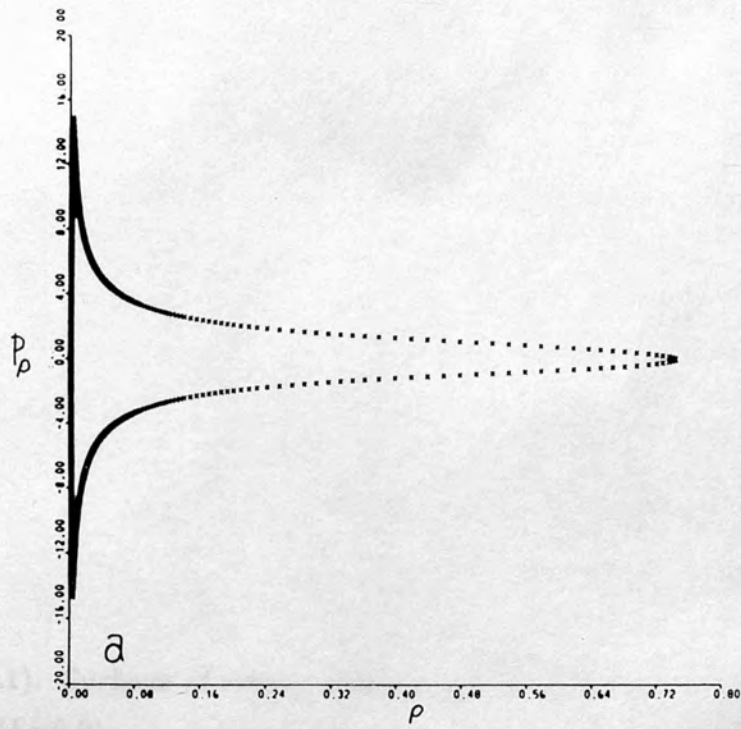


Figure (7.2.1)

$B = 27 \text{ kG}$ ($E = 0$)

Energy is given in units of $\frac{1}{2} m v^2$

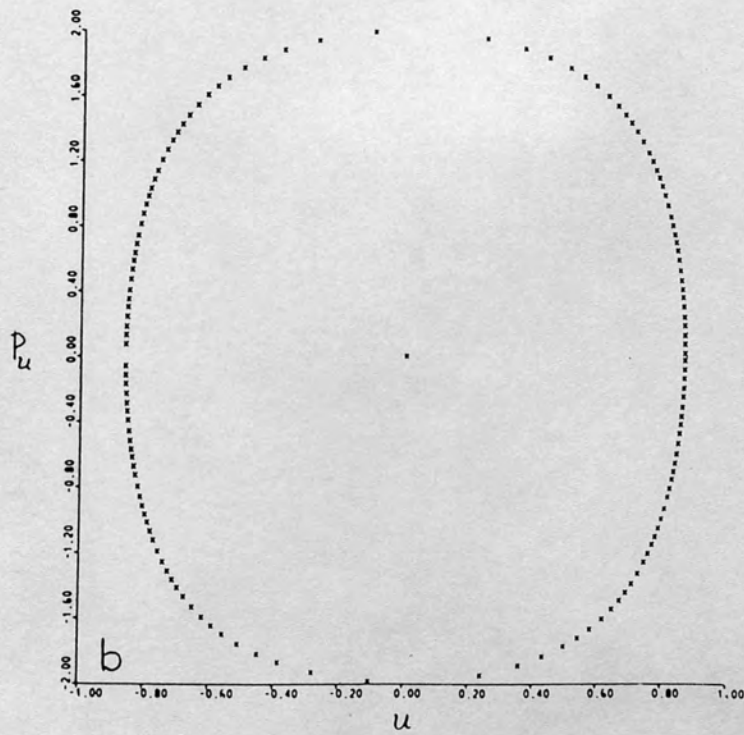


Figure (7.1). Curves bounding the motion in (a) the ρp_ρ -plane, (b) the $u p_u$ -plane, for $m = 3$, $B = 27 \text{ kG}$.

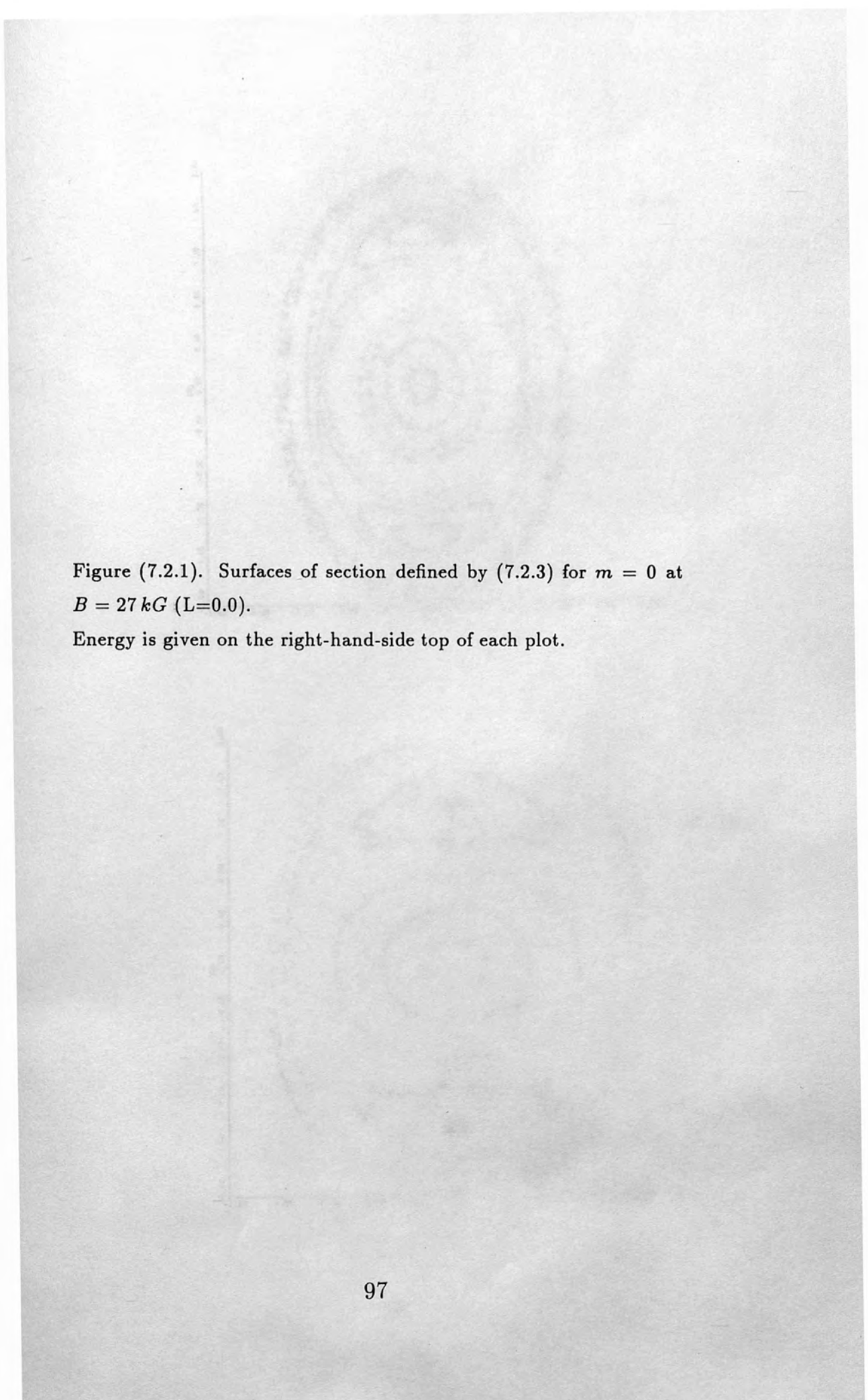
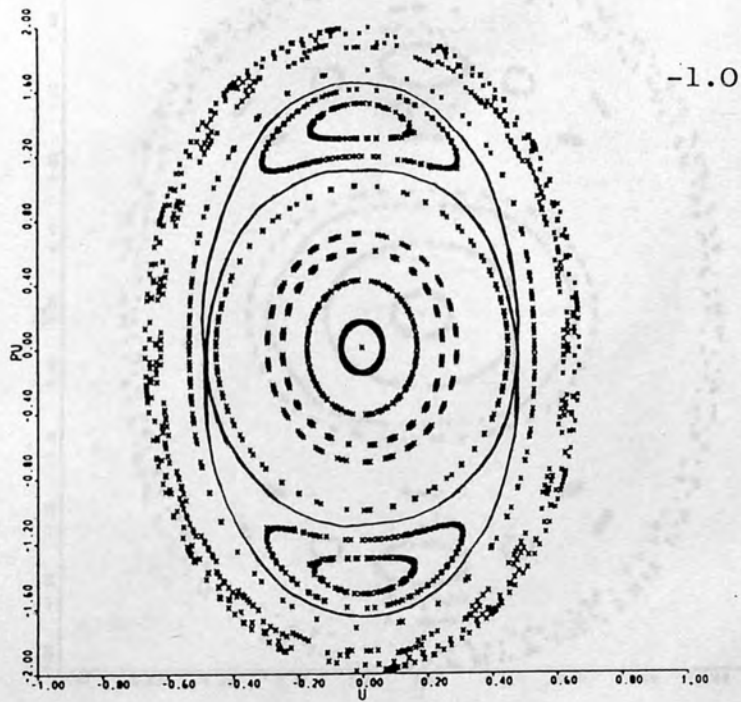
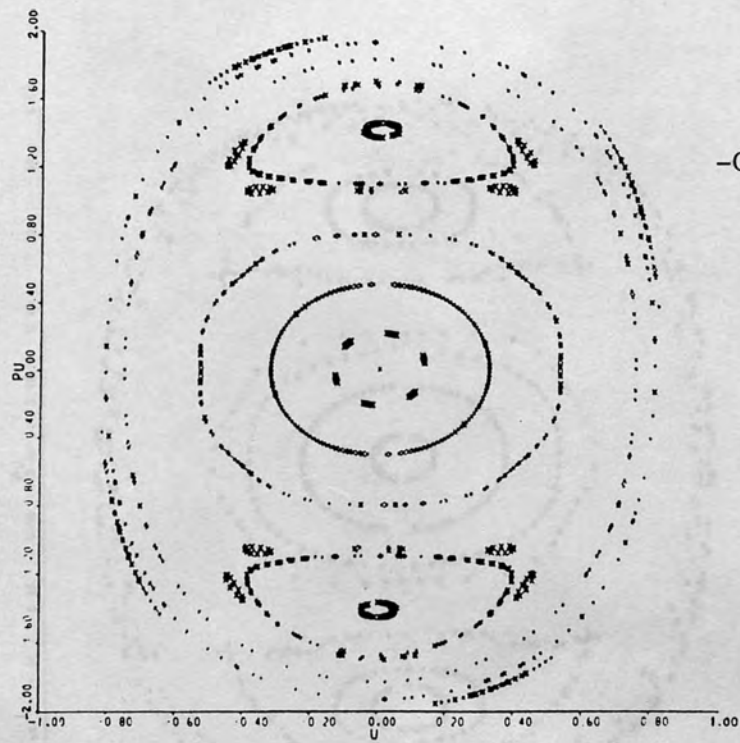


Figure (7.2.1). Surfaces of section defined by (7.2.3) for $m = 0$ at $B = 27 kG$ ($L=0.0$).

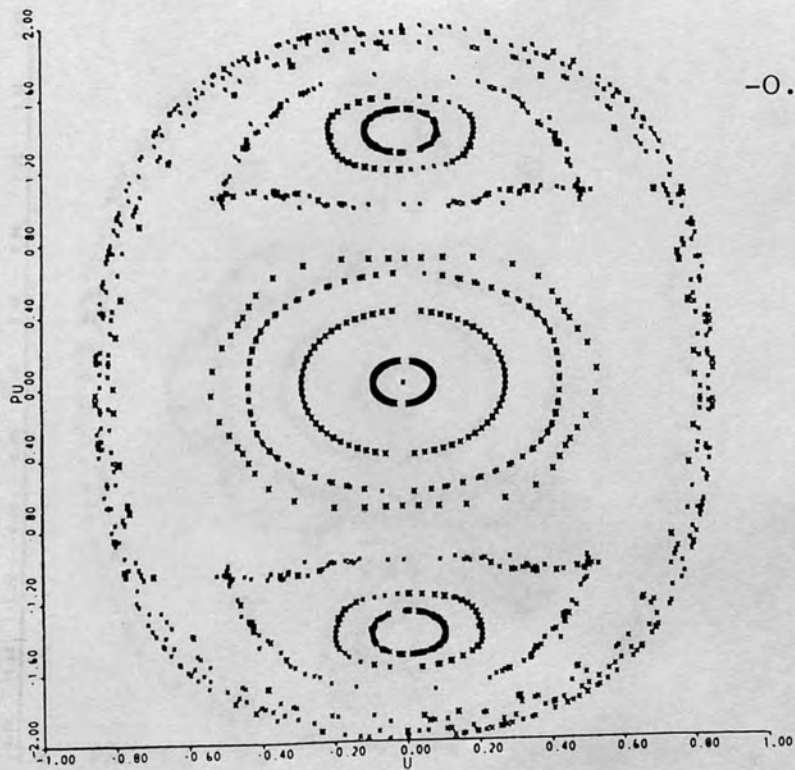
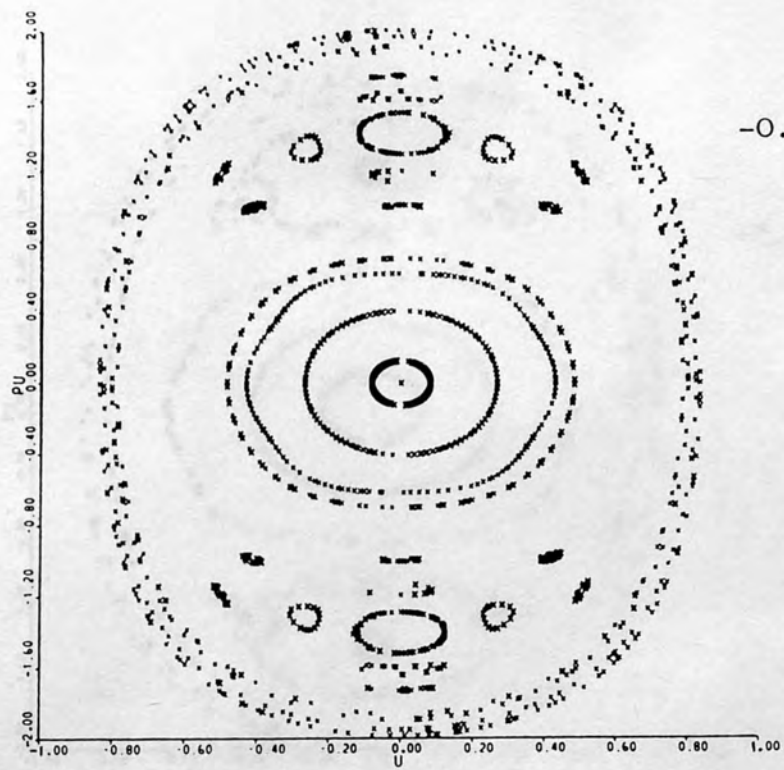
Energy is given on the right-hand-side top of each plot.

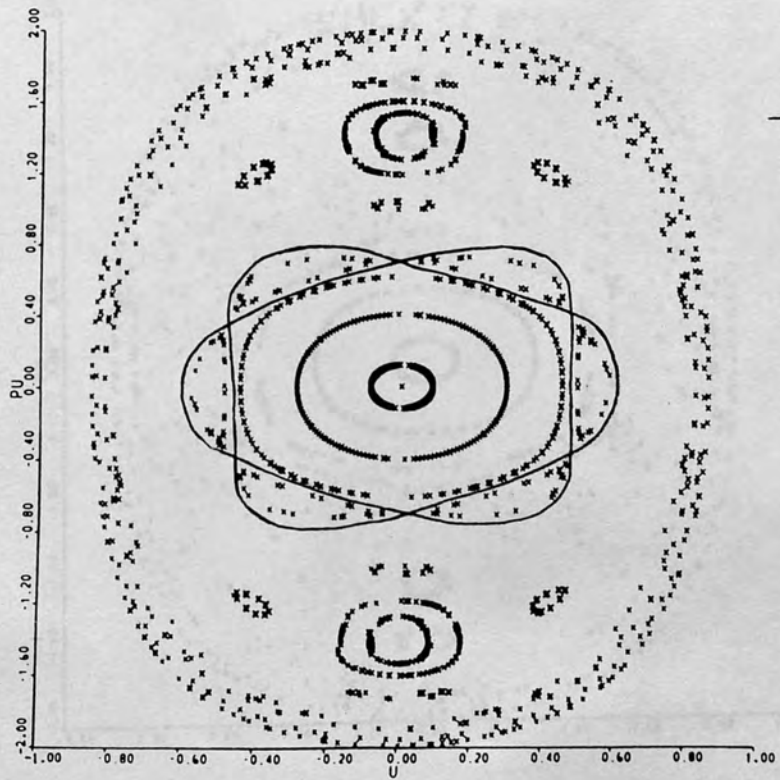
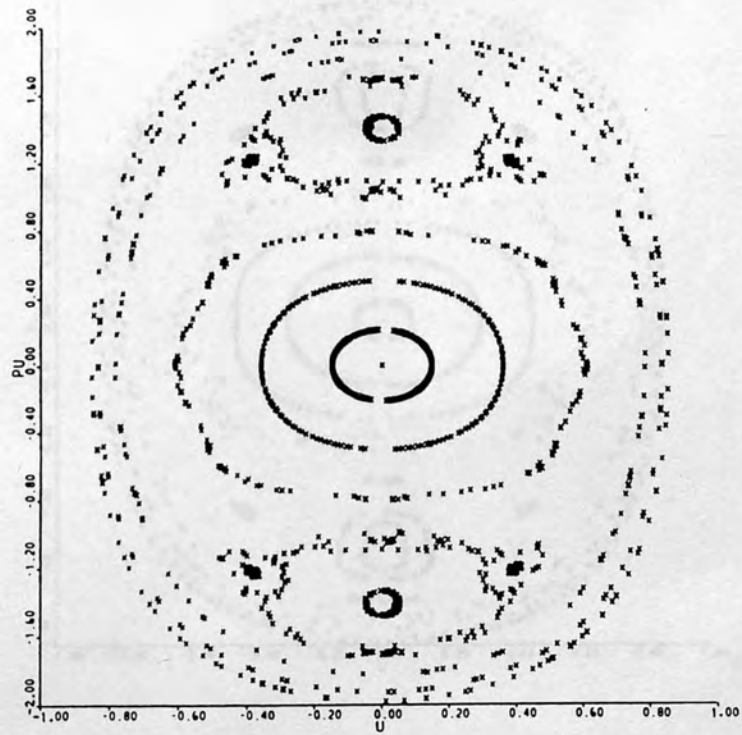


-1.0



-0.48





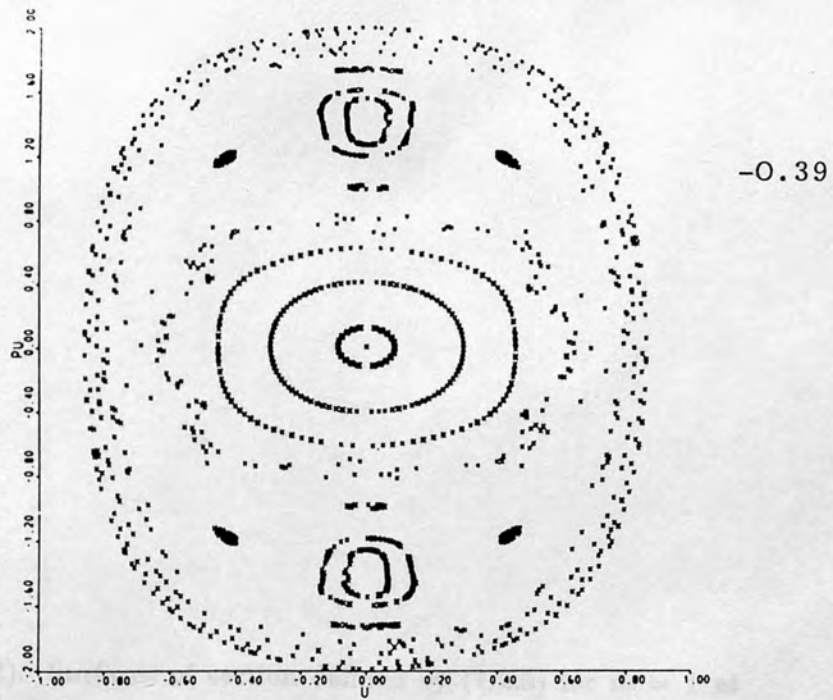


Figure (7.22)
 $B = 7740$ ($L=0.0017$)
 Energy is given on the right-hand side top of each plot.

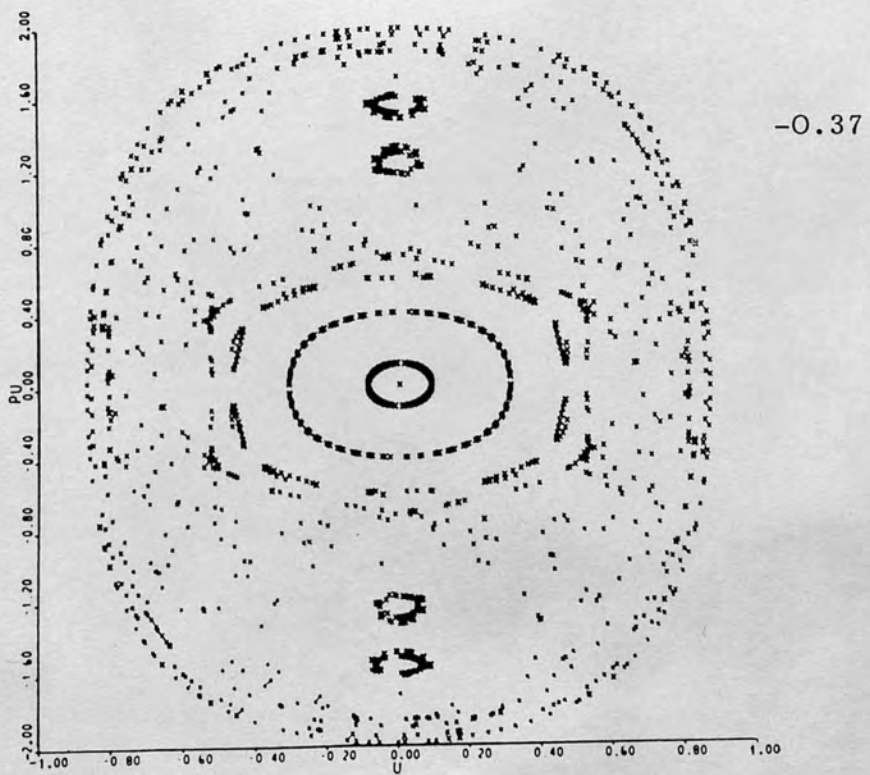
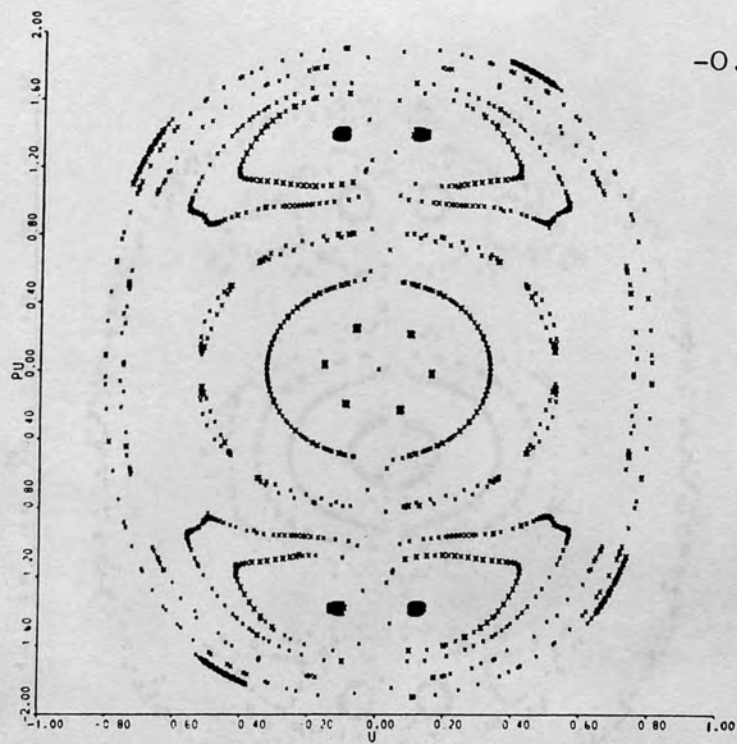
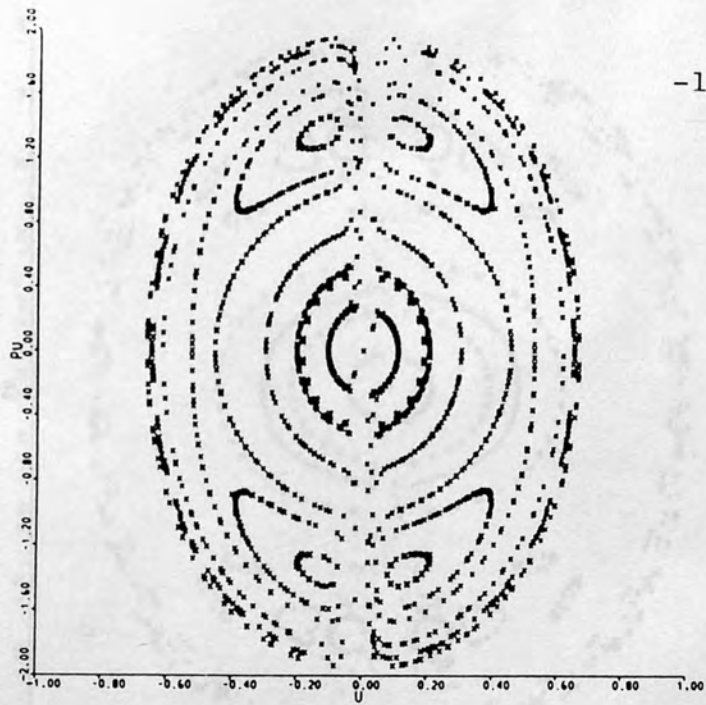


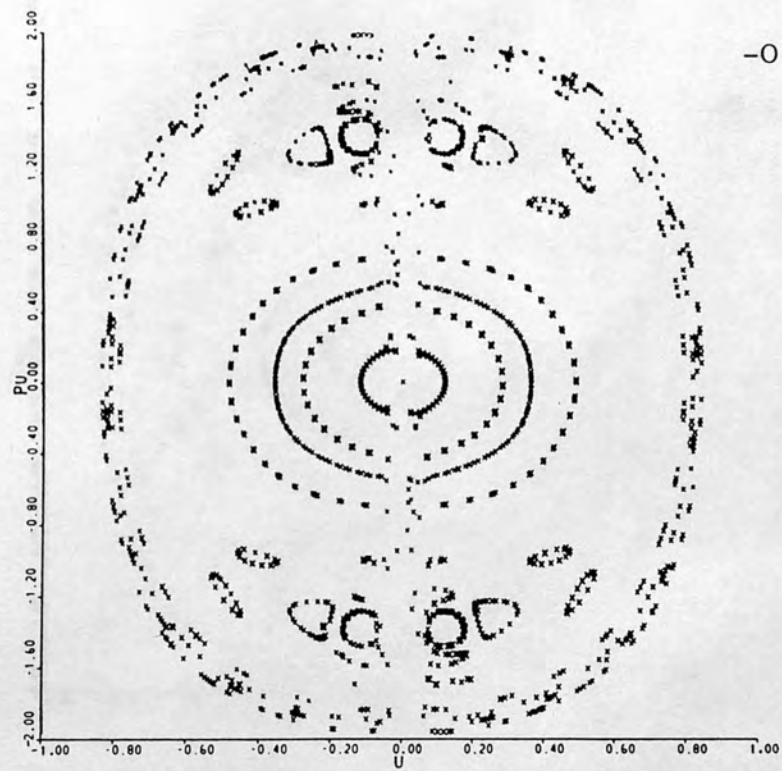


Figure (7.2.2). Surfaces of section defined by (7.2.3) for $m = 1$ at $B = 27 \text{ kG}$ ($L=0.0113$).

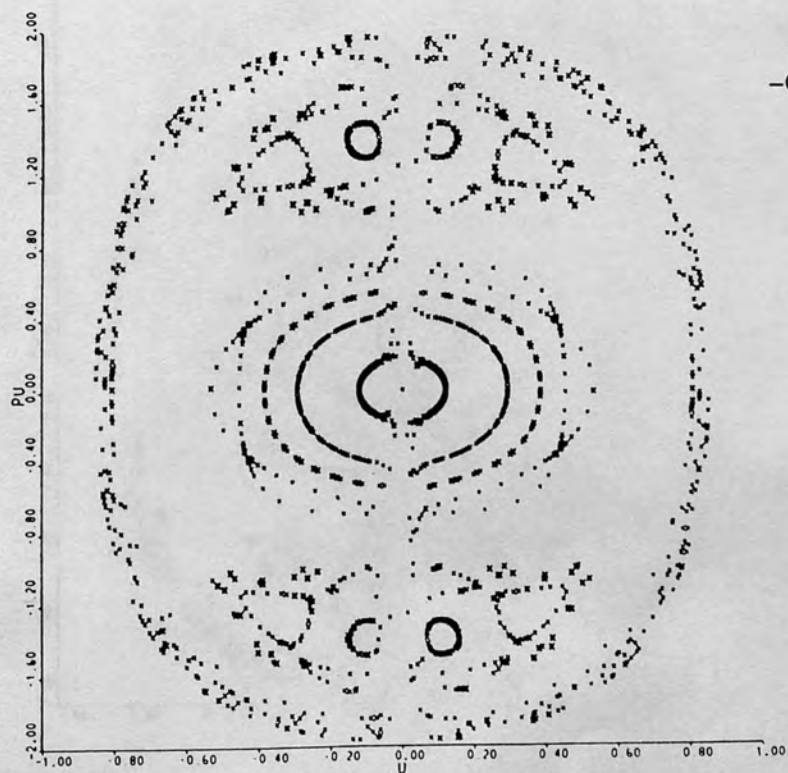
Energy is given on the right-hand-side top of each plot.



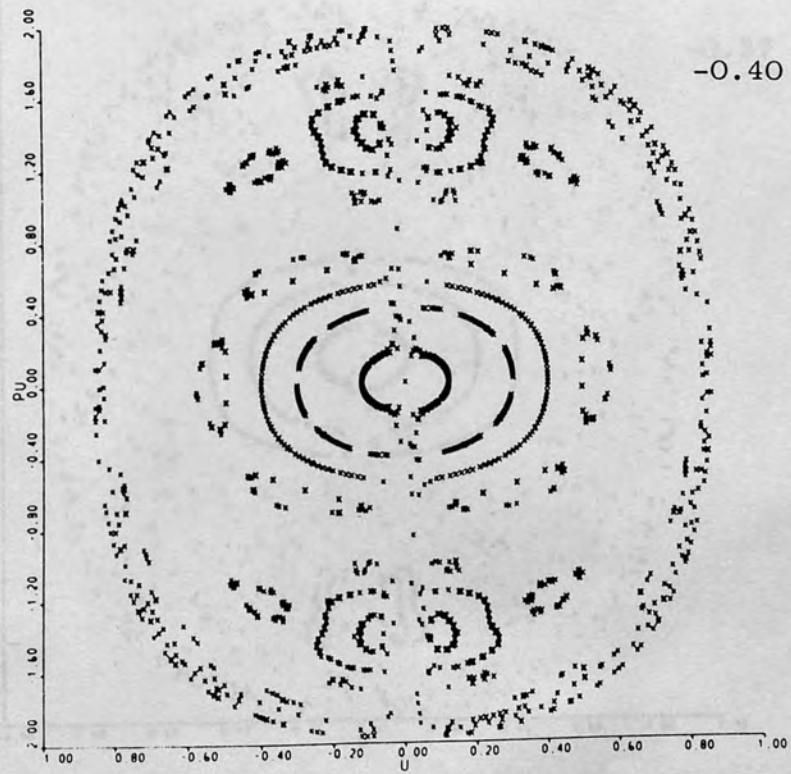
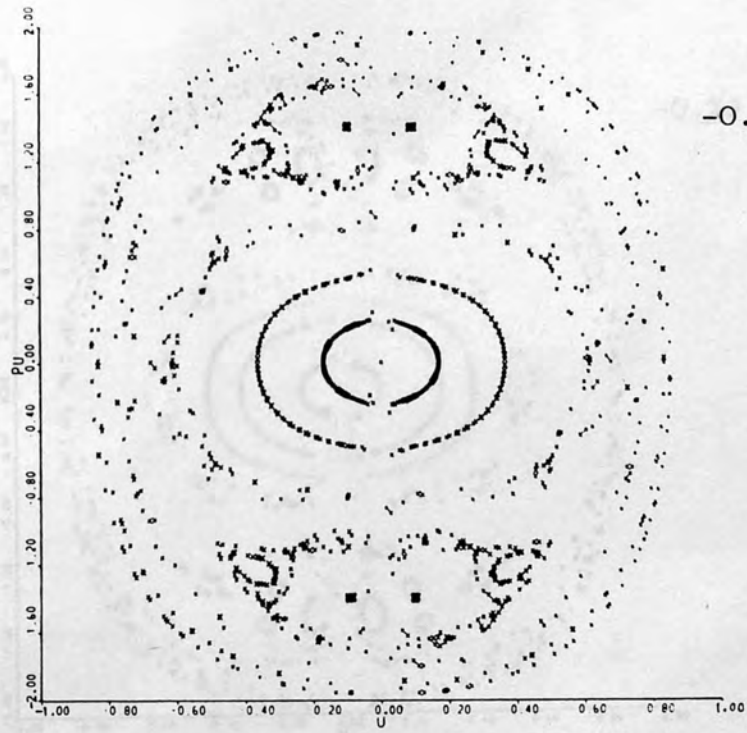


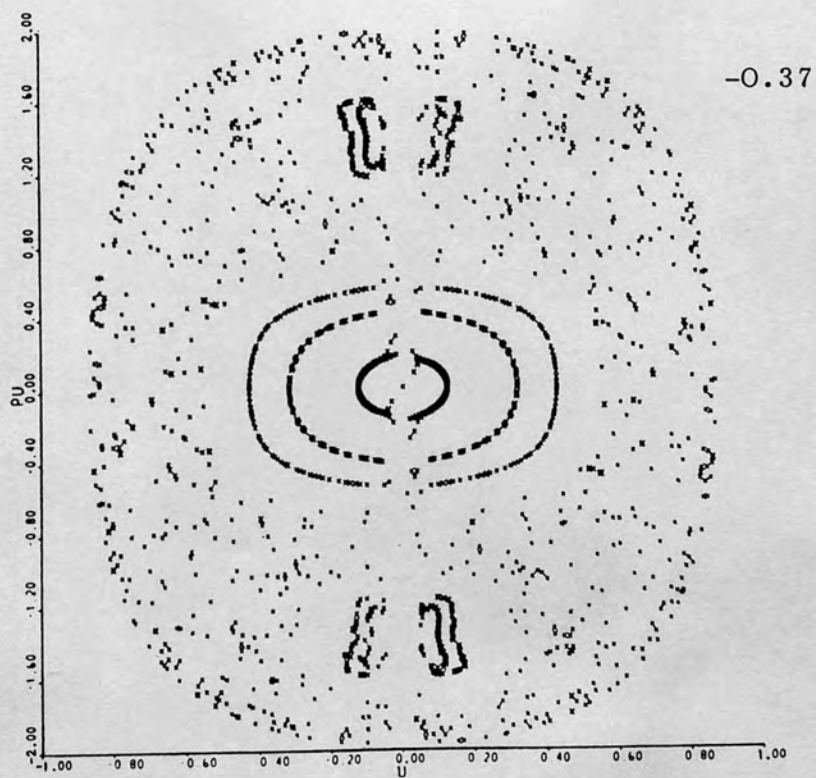
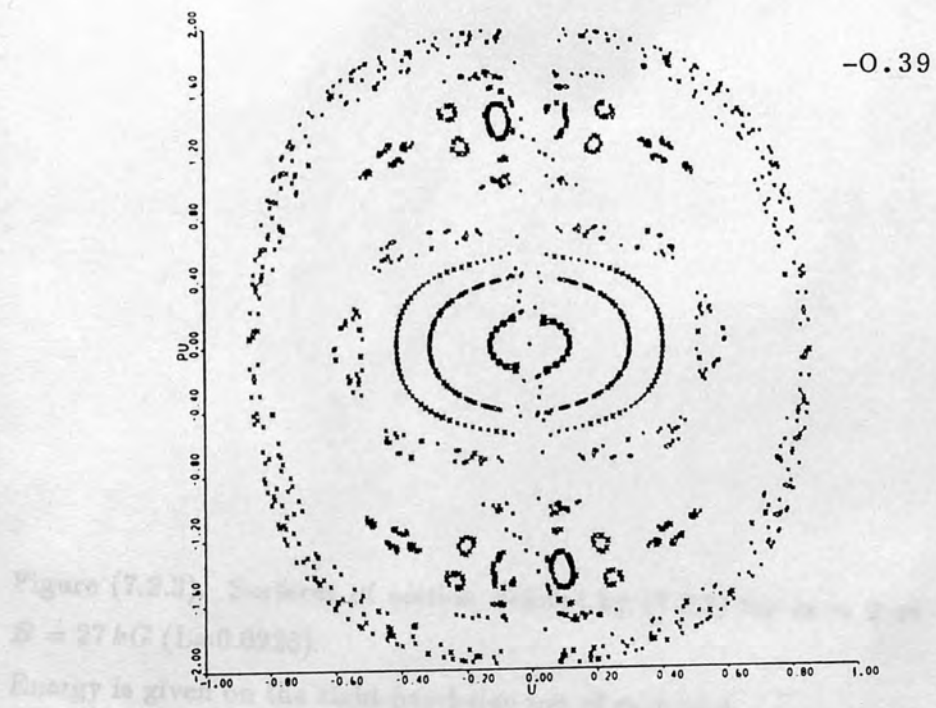


-0.45



-0.42





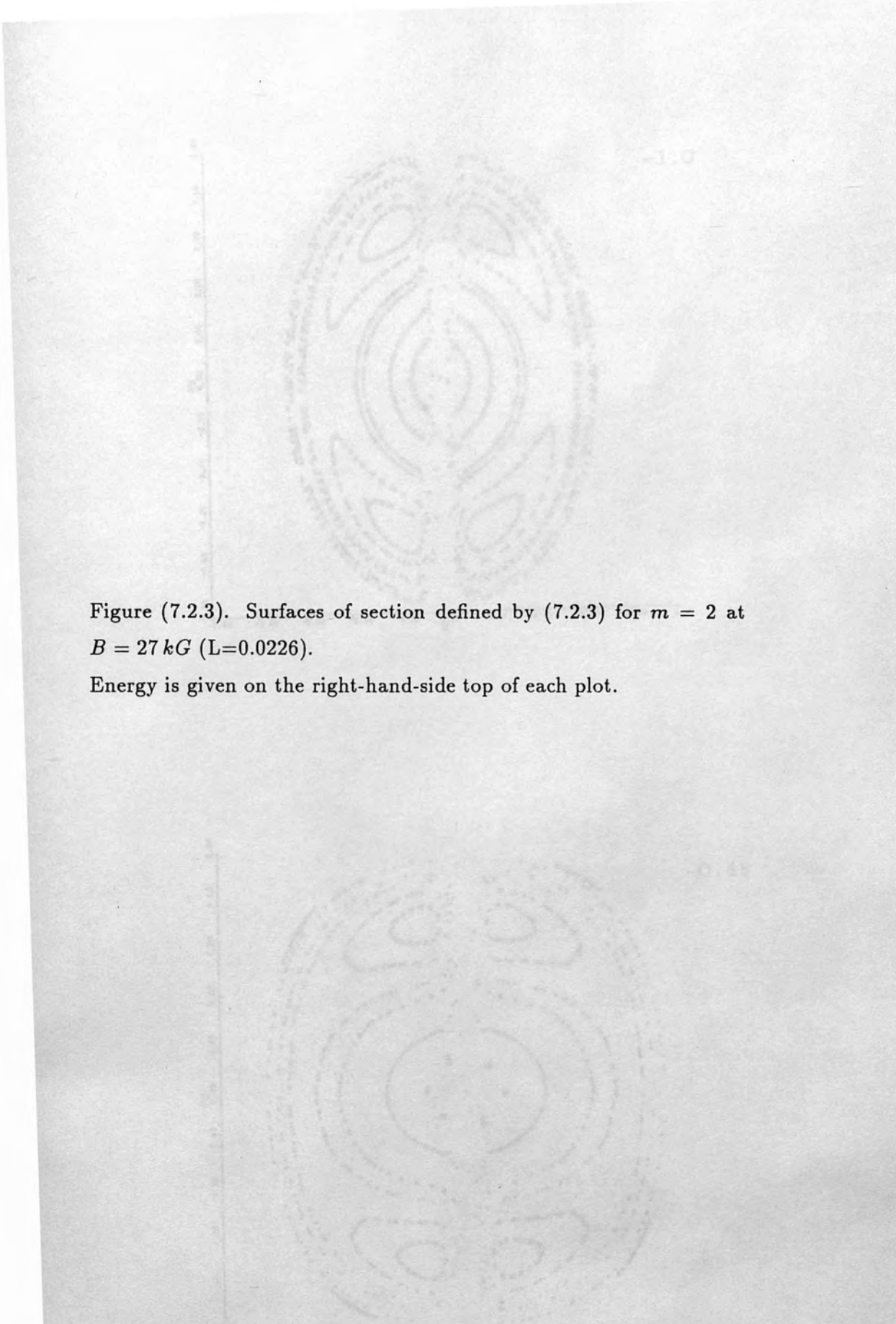
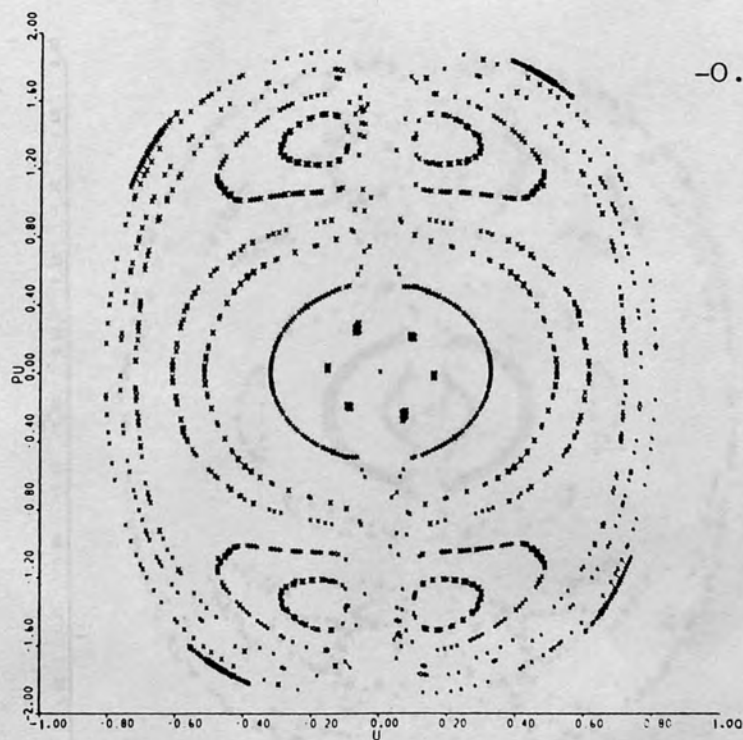
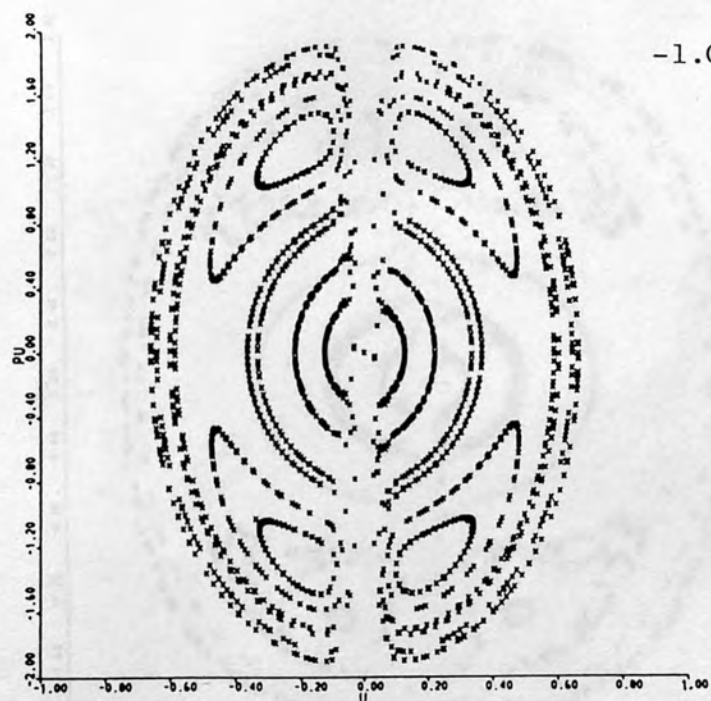
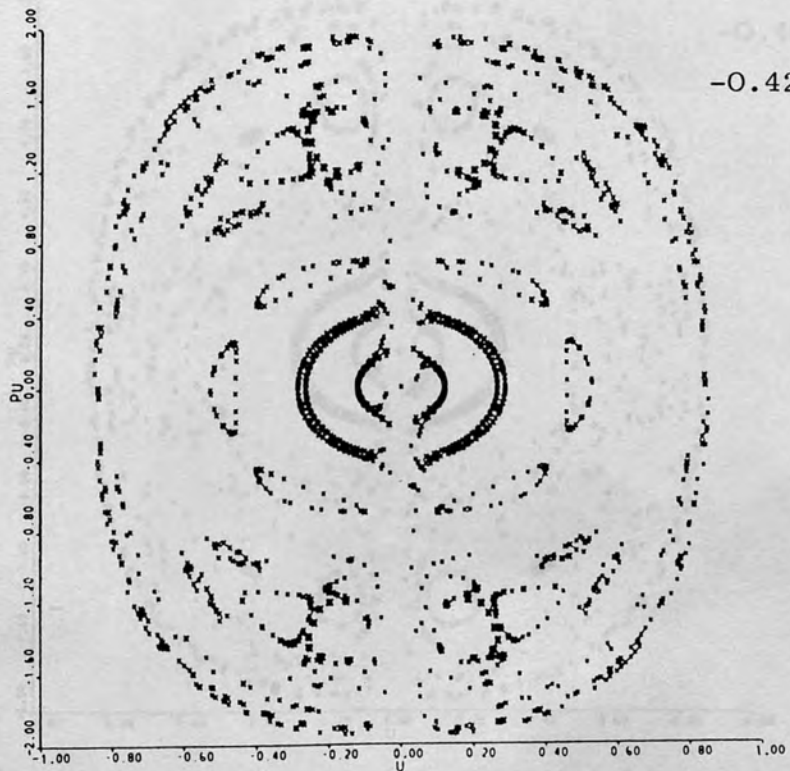
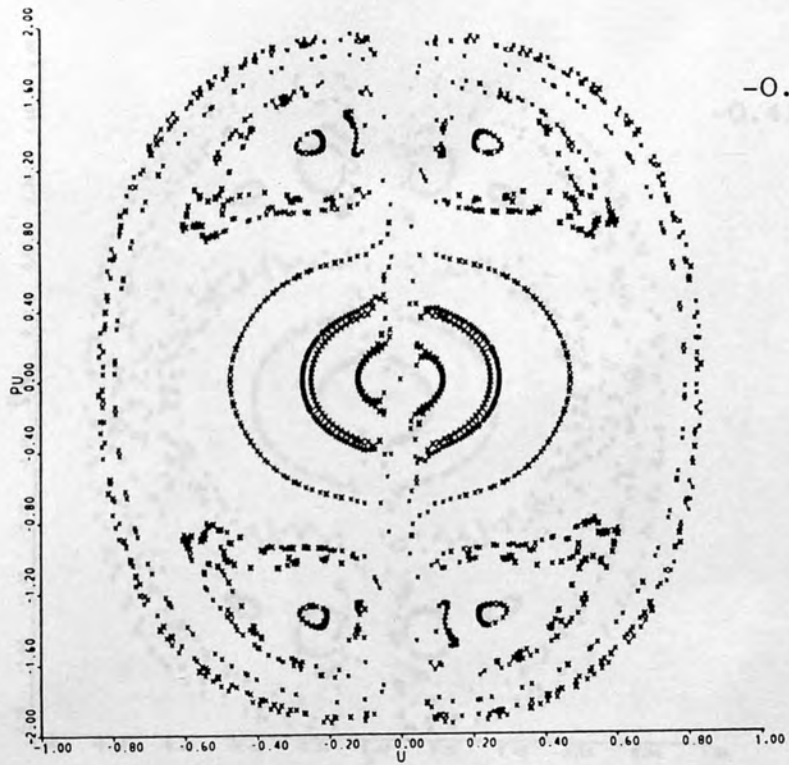
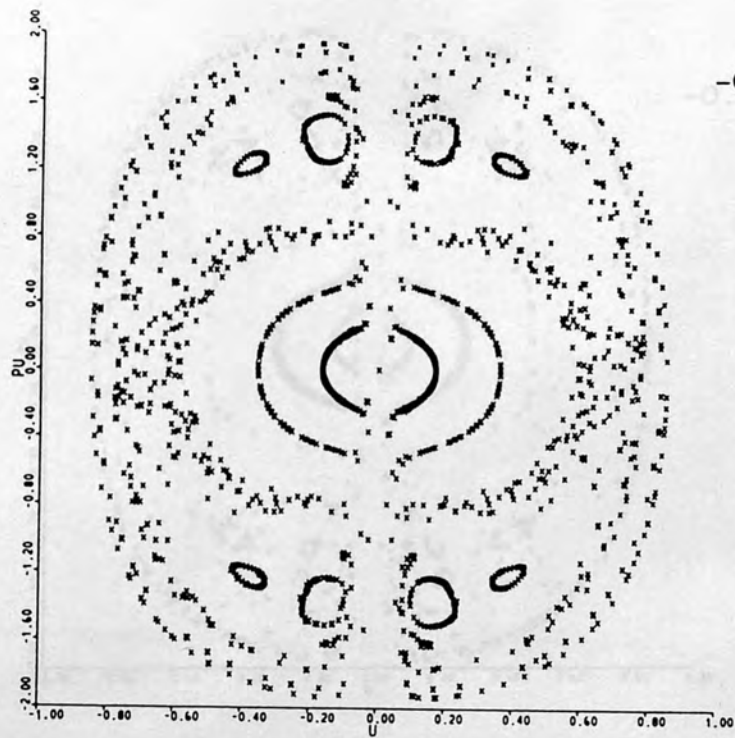


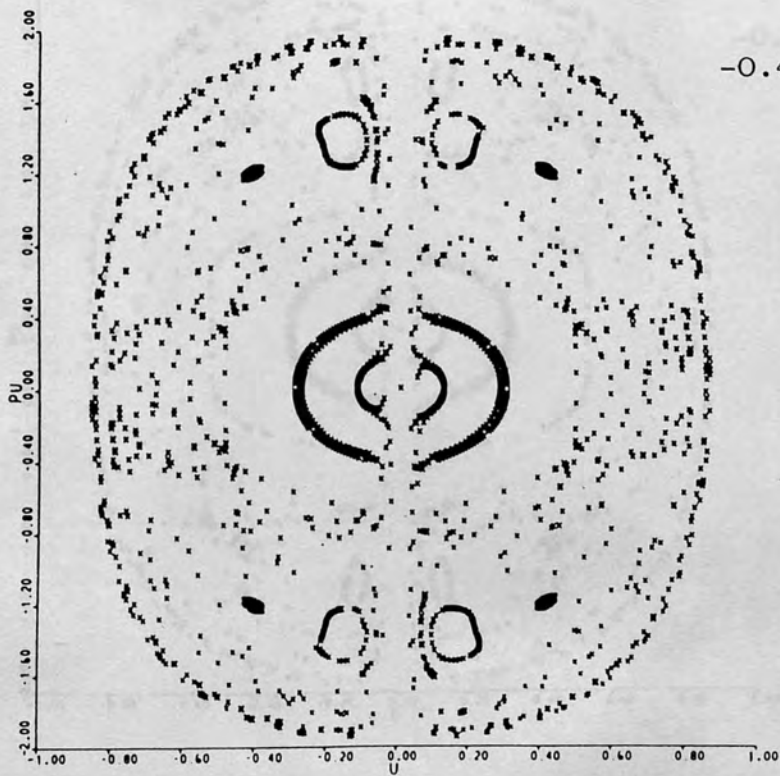
Figure (7.2.3). Surfaces of section defined by (7.2.3) for $m = 2$ at $B = 27 \text{ kG}$ ($L=0.0226$).
Energy is given on the right-hand-side top of each plot.







-0.41



-0.40

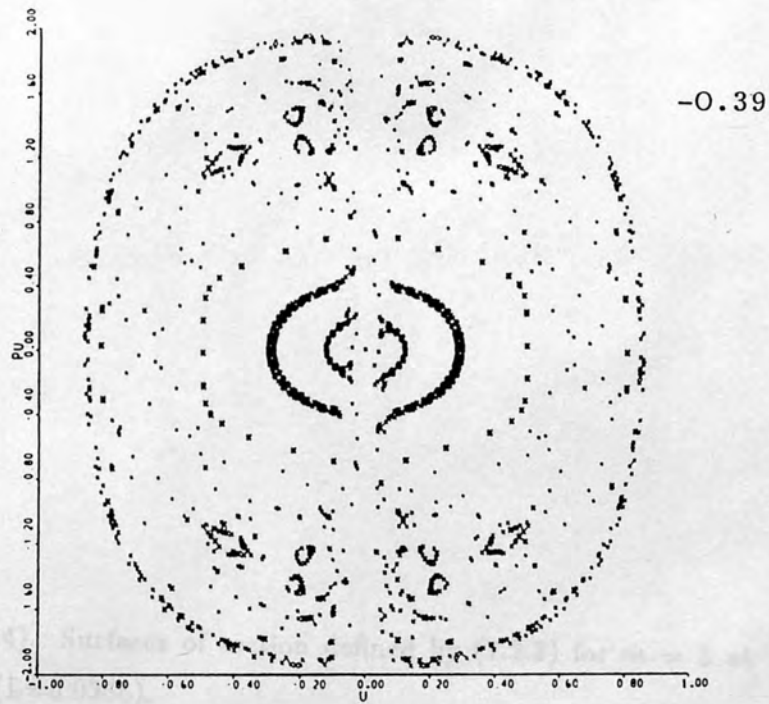
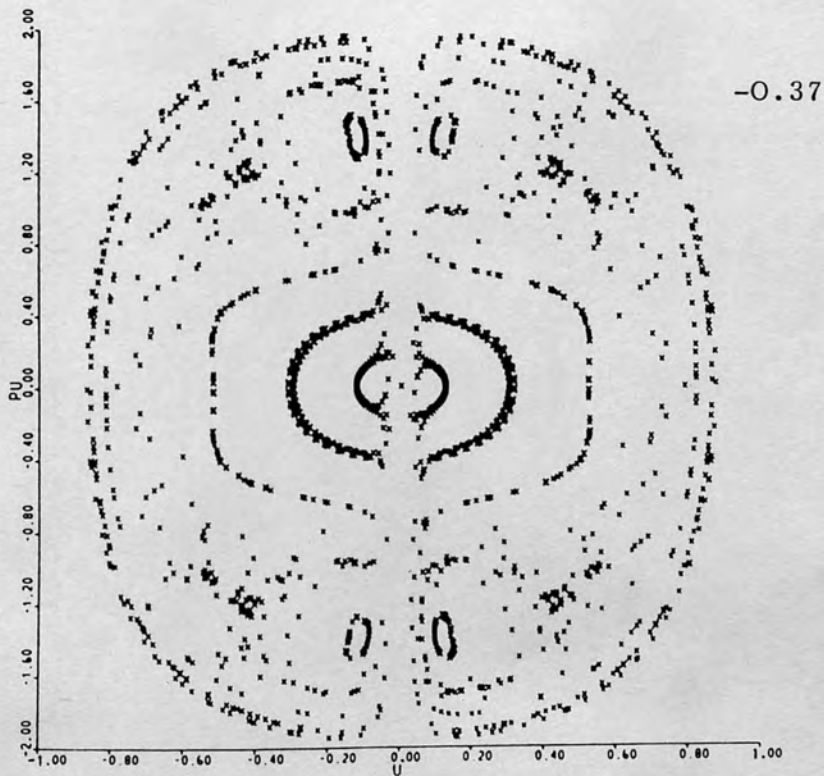


Figure (7.24) Surface ψ at $E = -0.39$ (1000 points).
 Energy is given on the right hand side top of each plot.



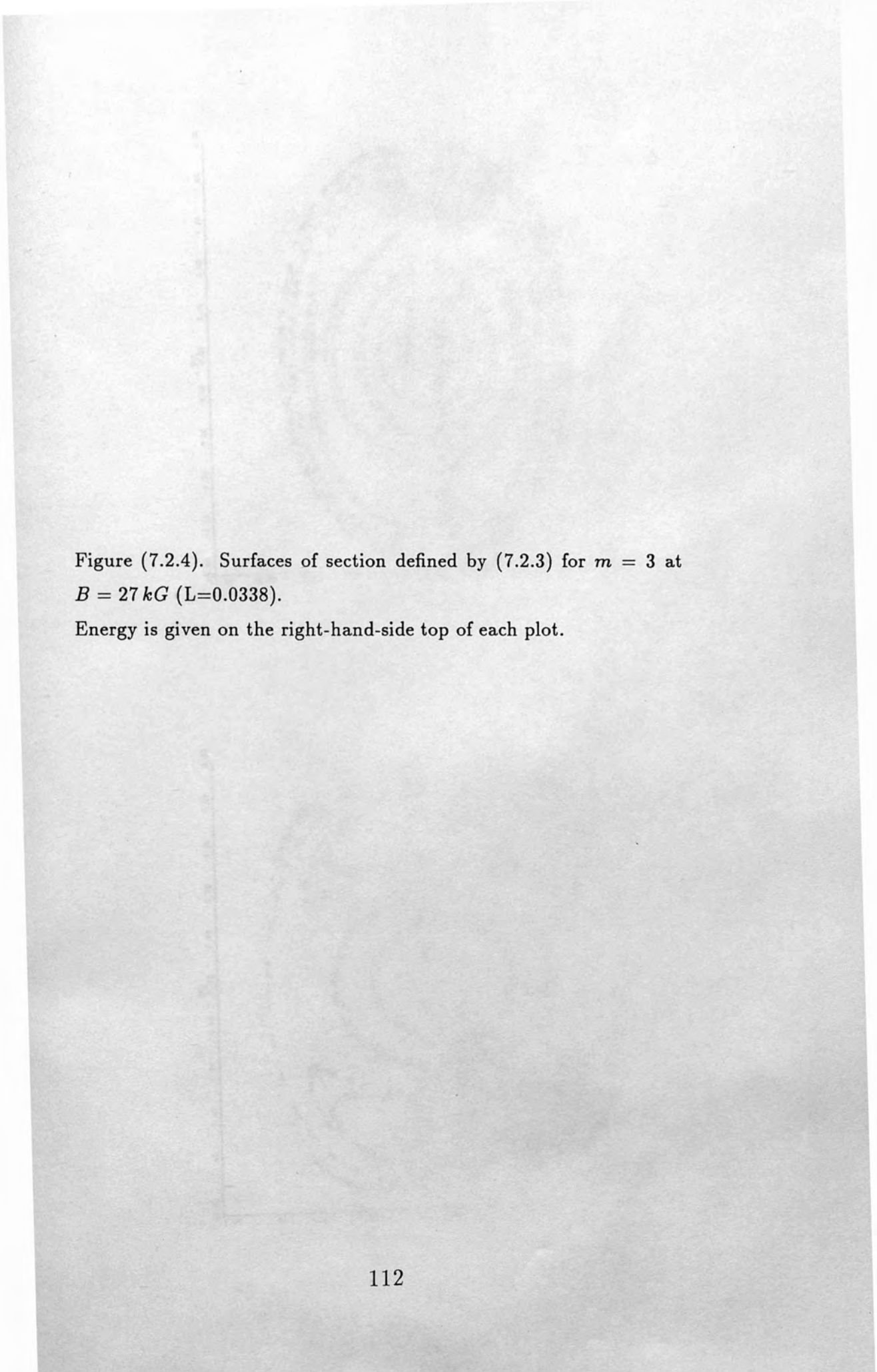
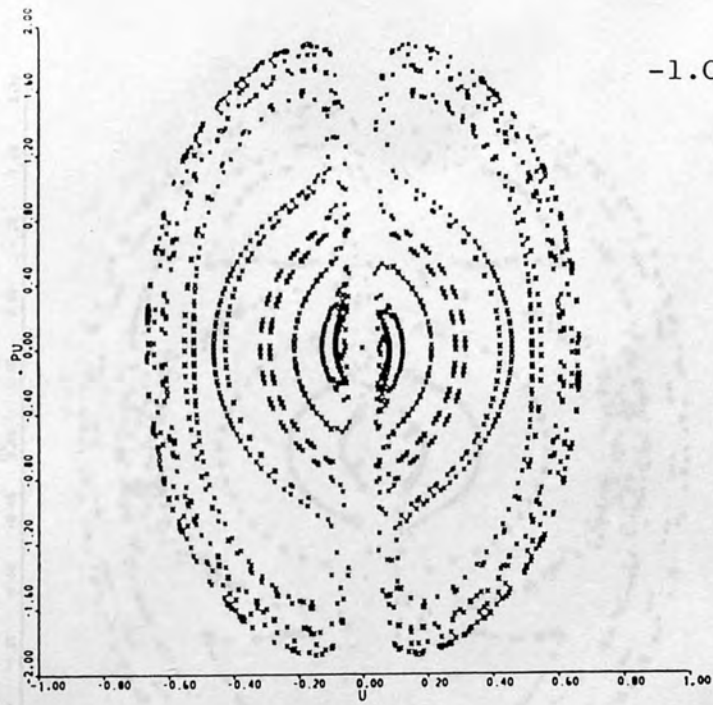
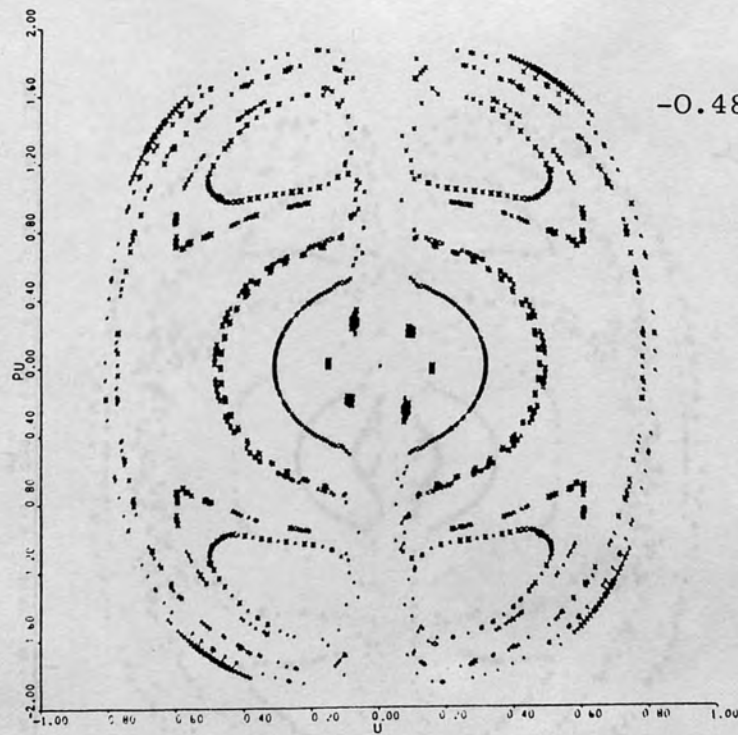


Figure (7.2.4). Surfaces of section defined by (7.2.3) for $m = 3$ at $B = 27 \text{ kG}$ ($L=0.0338$).

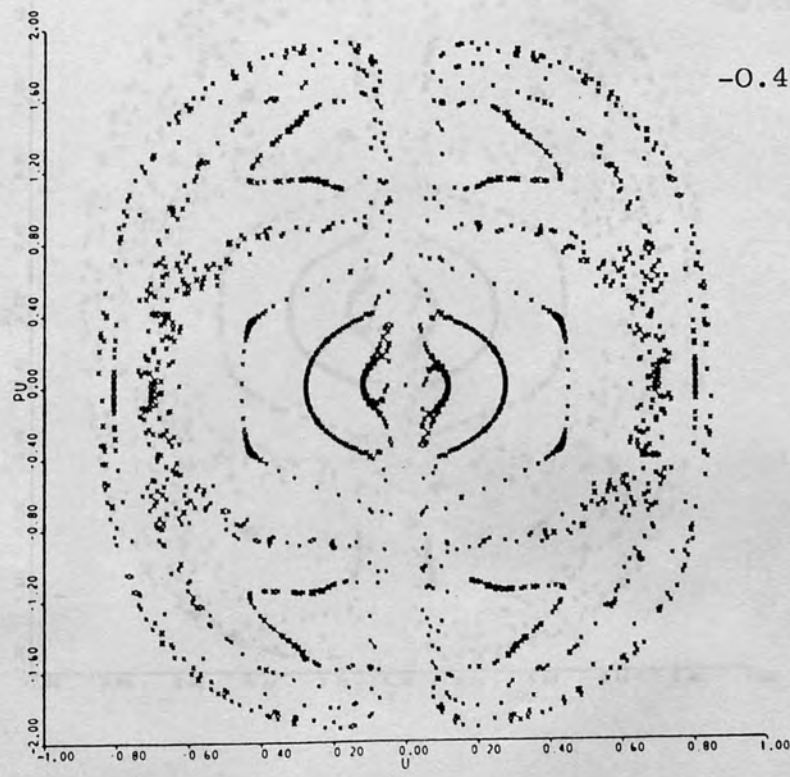
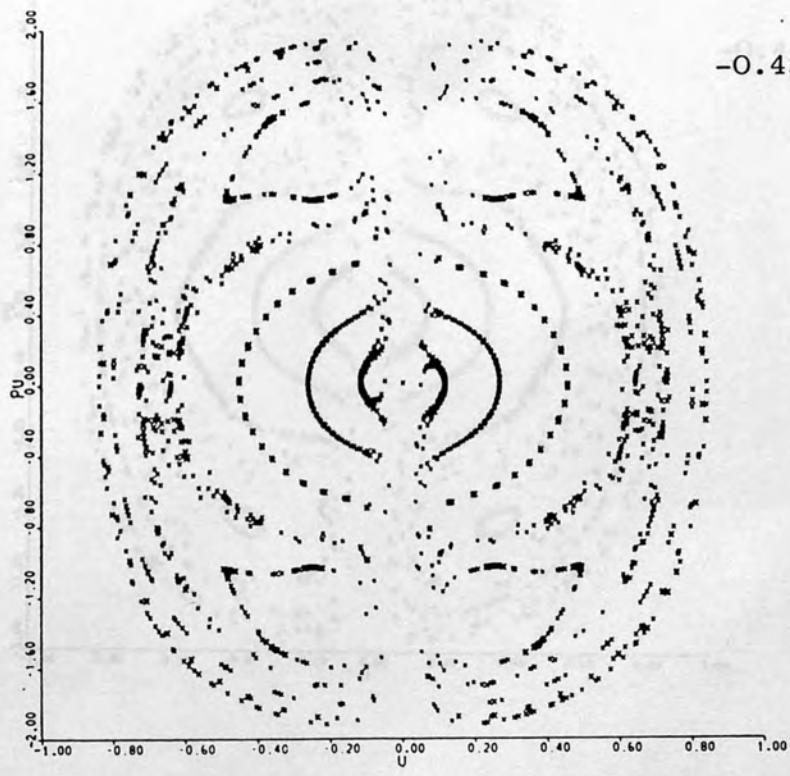
Energy is given on the right-hand-side top of each plot.

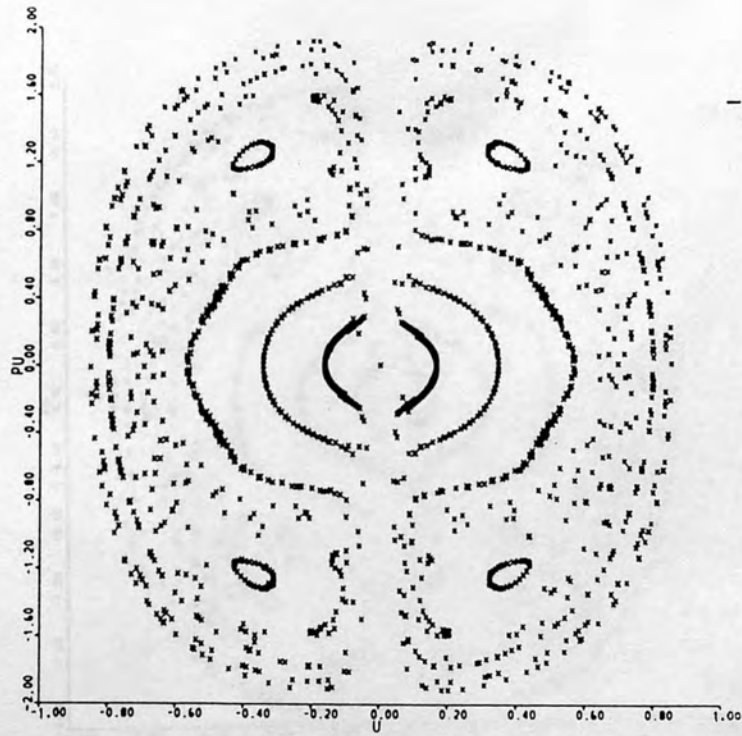


-1.0

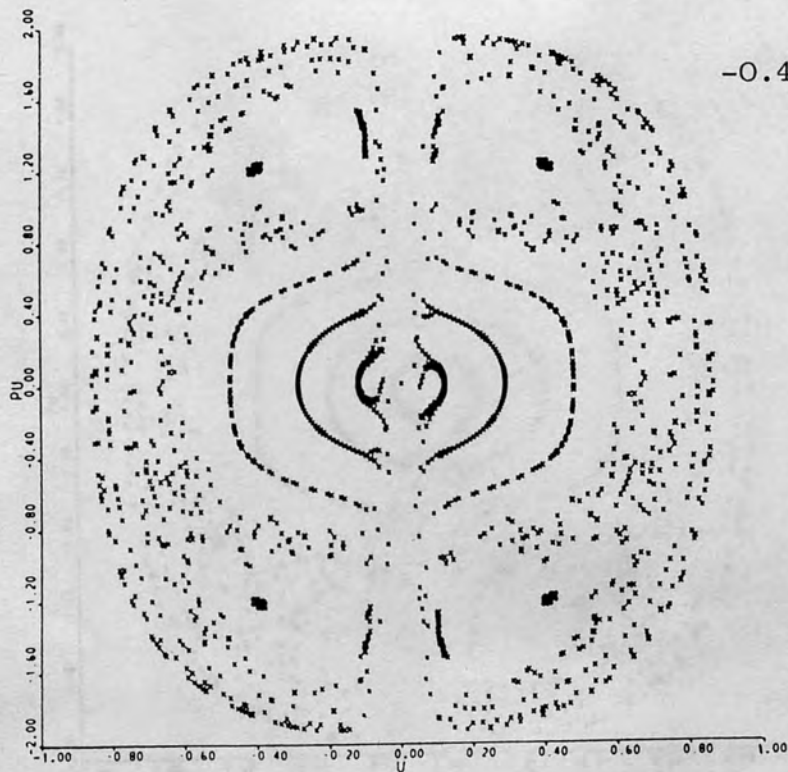


-0.48





-0.41



-0.40

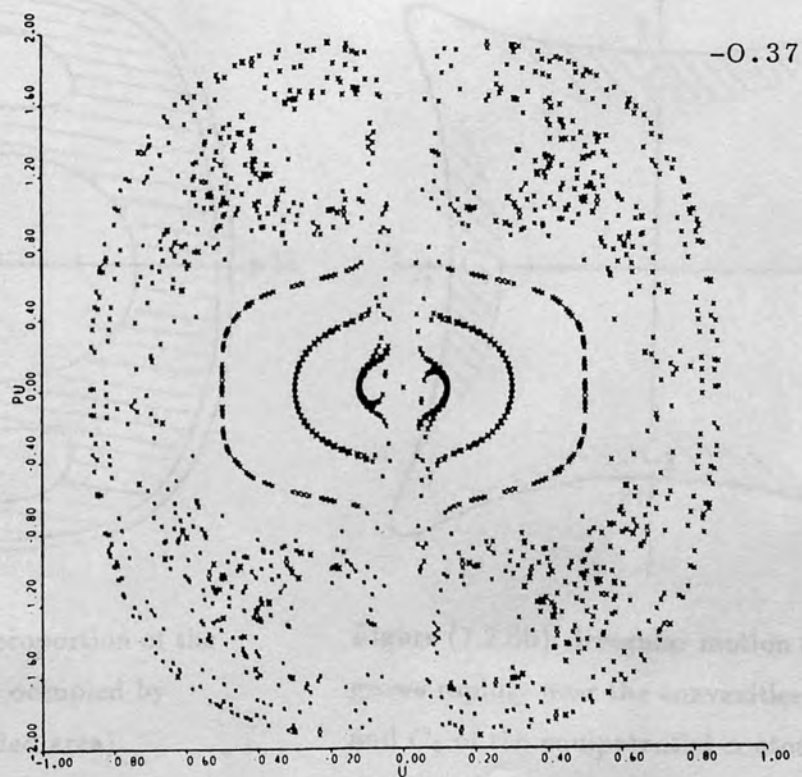
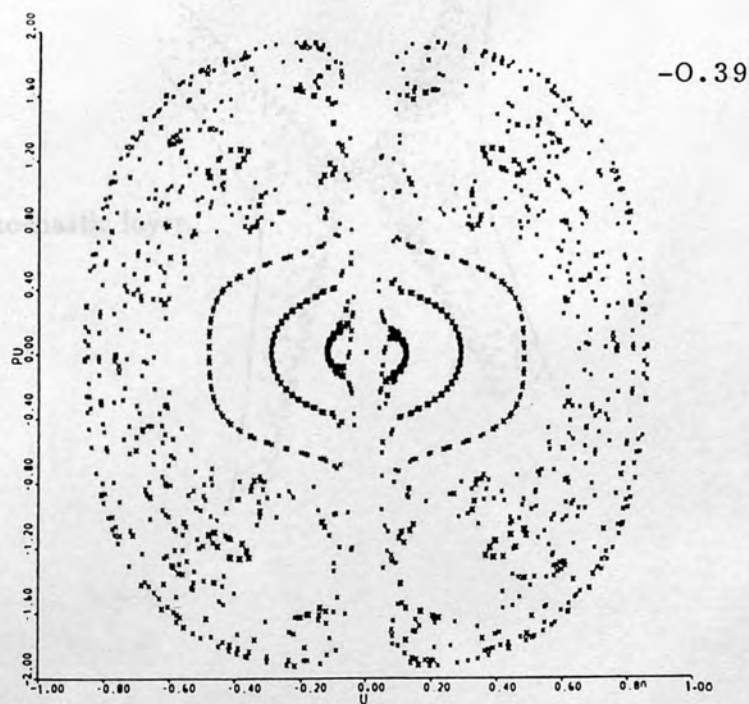


Figure (7.2.5). A stochastic layer.

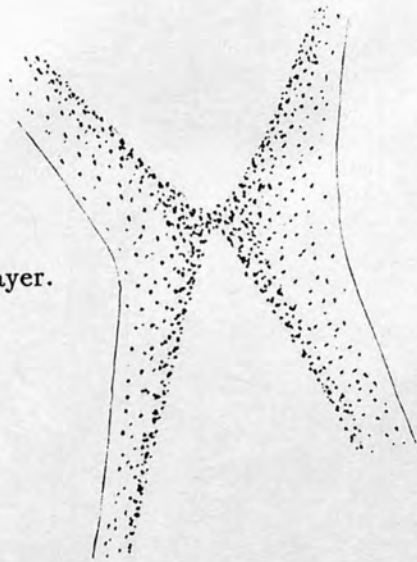


Figure (7.2.7). Surface of section of a Hamiltonian system for $\epsilon = 1$ at $B = 44562 \text{ AG}(L=0.4)$. Energy is given on the right-hand side of the plot.

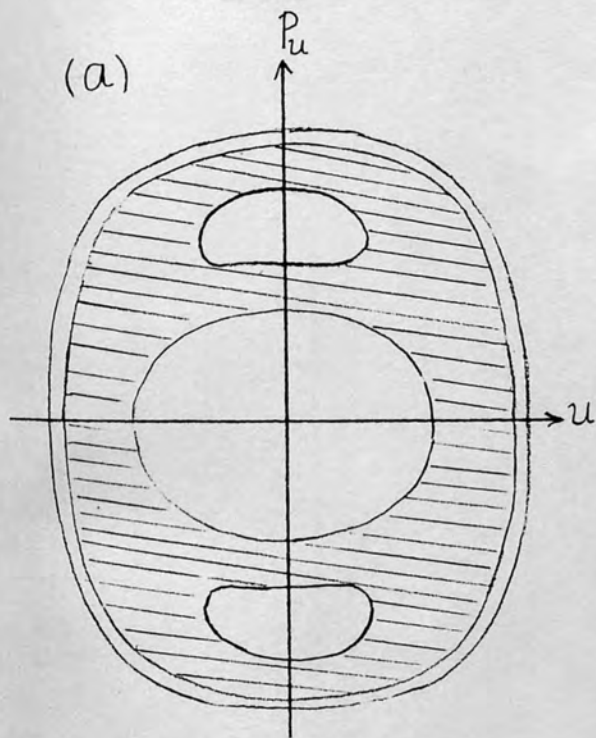


Figure (7.2.6a). The proportion of the surface of section first occupied by irregular motion (shaded area).

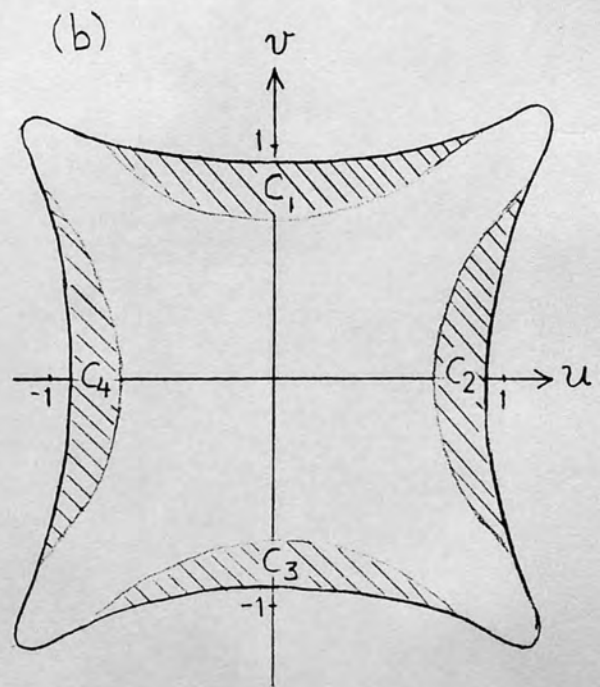


Figure (7.2.6b). Irregular motion (shaded area) grows rapidly near the convexities C_1 , C_2 , C_3 and C_4 of the equipotential contour.

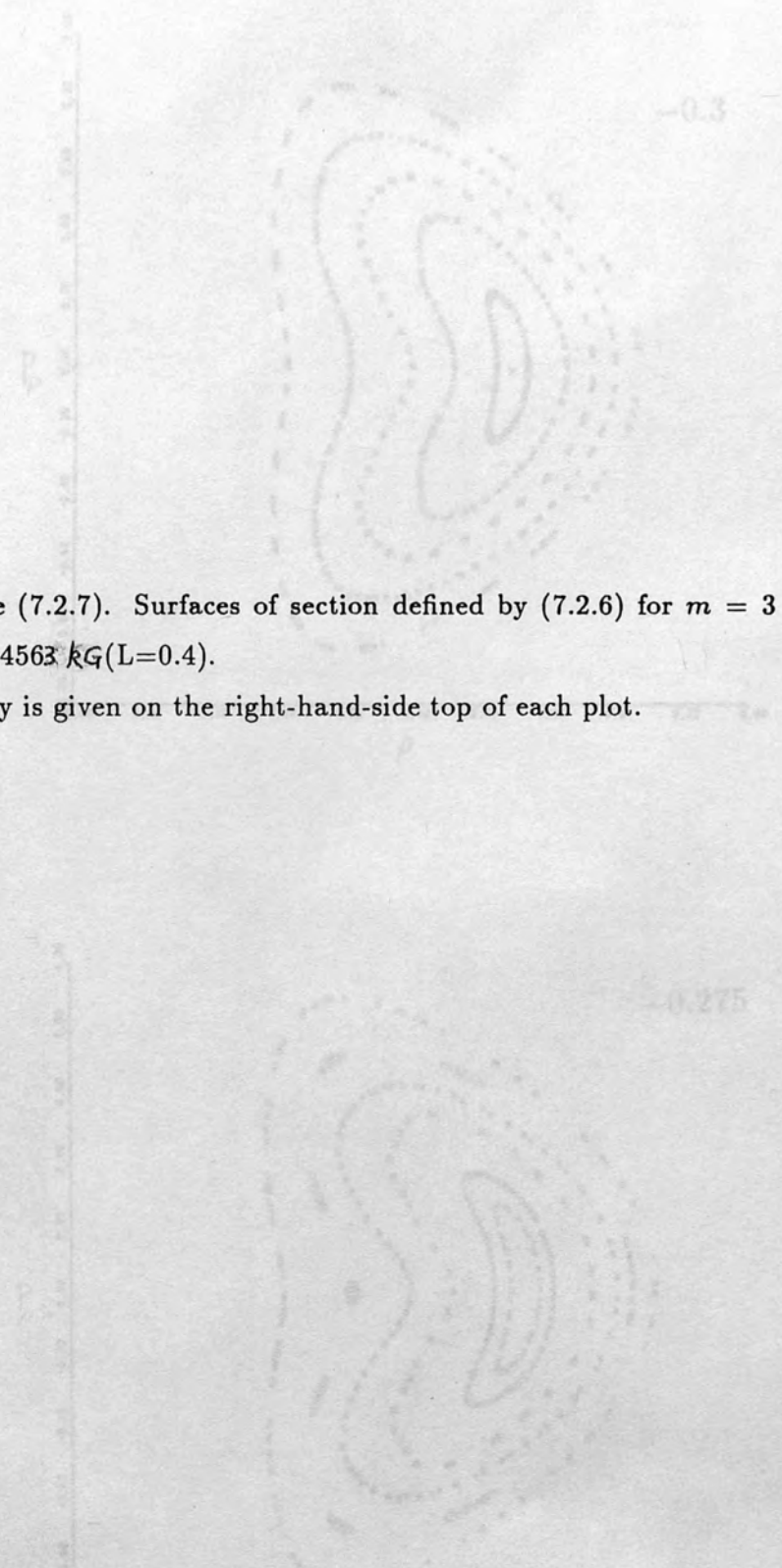
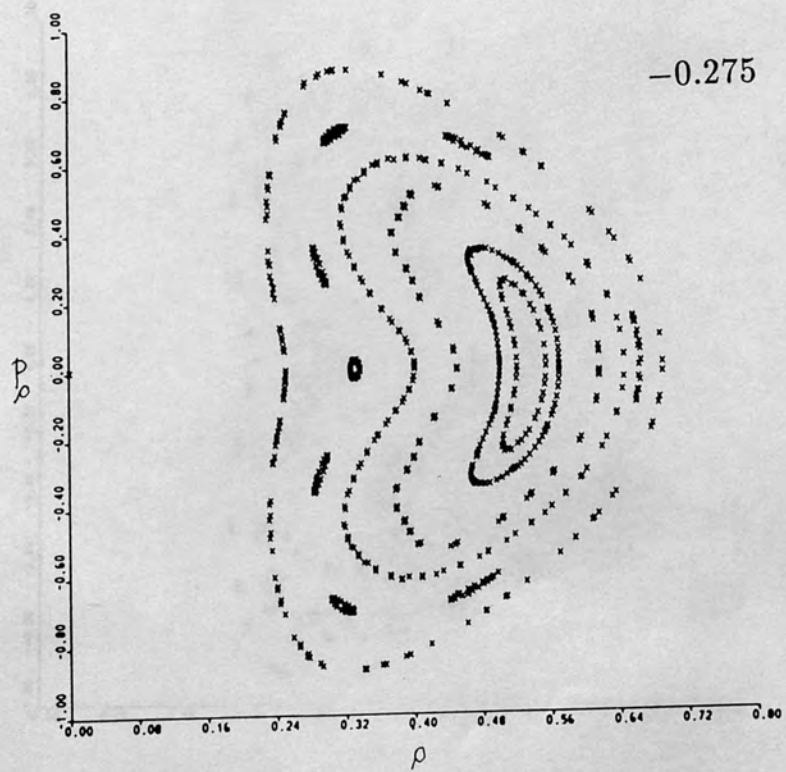
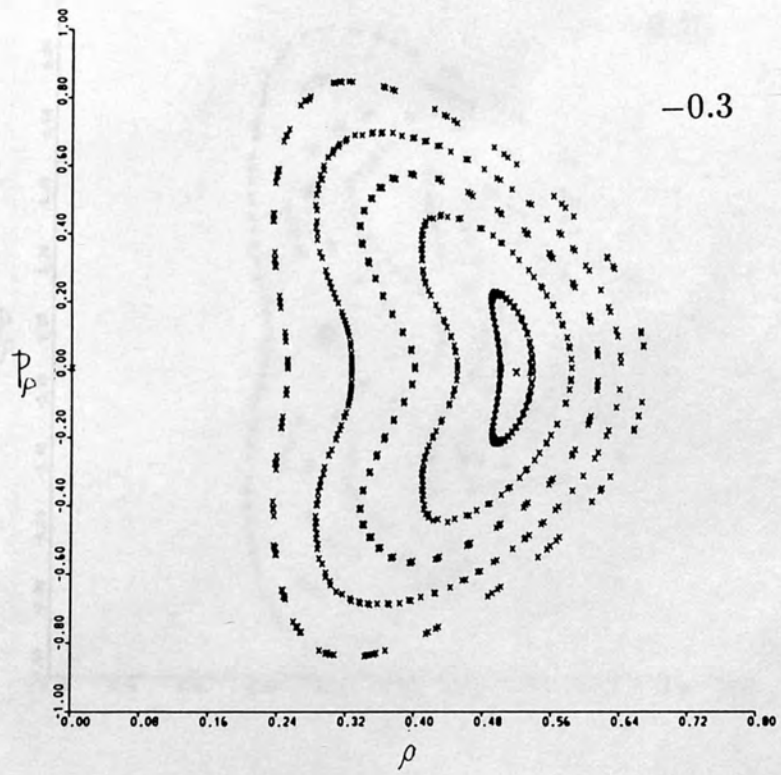
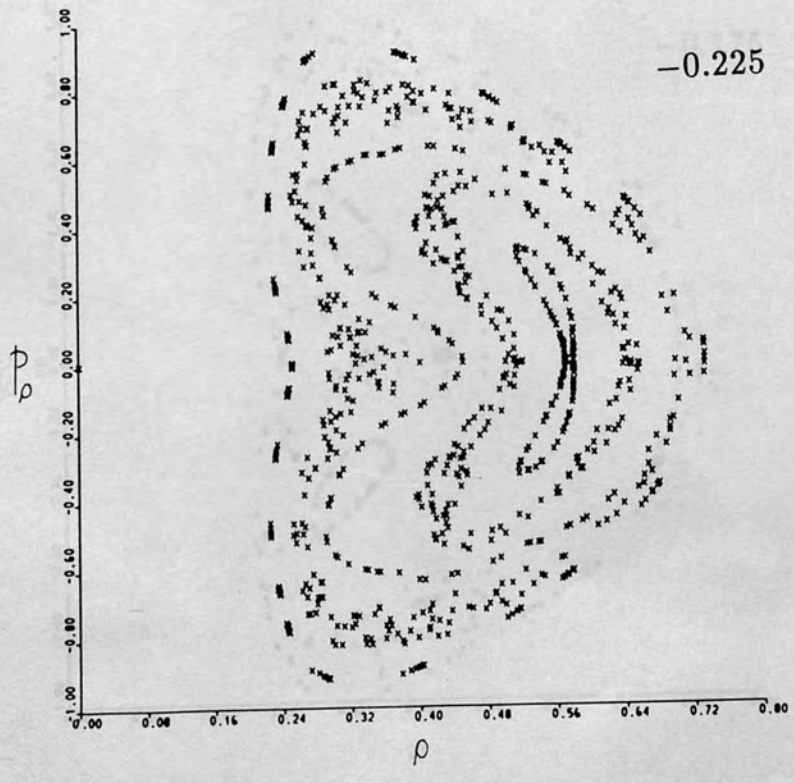
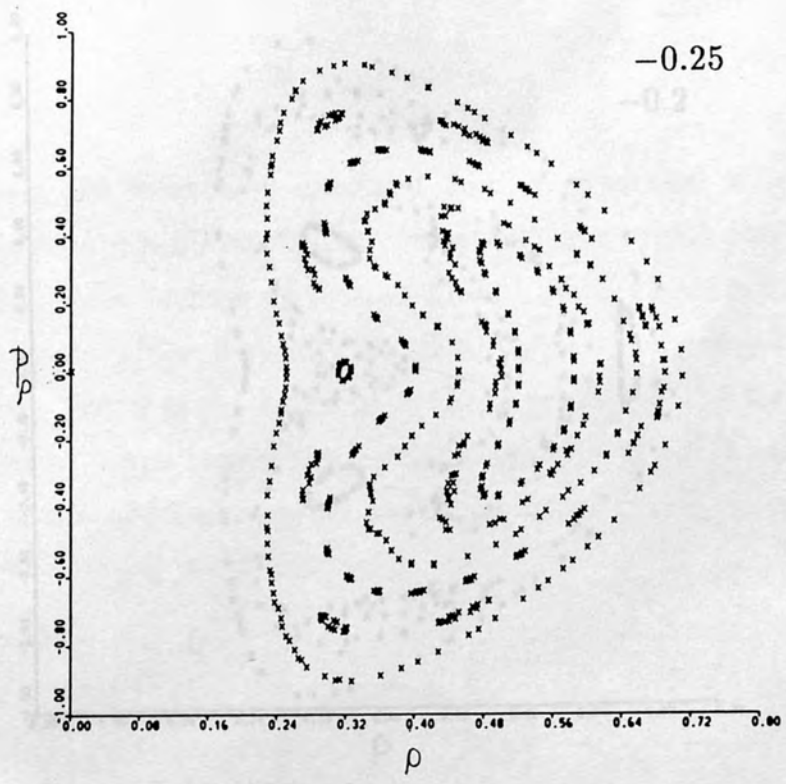


Figure (7.2.7). Surfaces of section defined by (7.2.6) for $m = 3$ at $B = 44563 \text{ kG} (L=0.4)$.

Energy is given on the right-hand-side top of each plot.

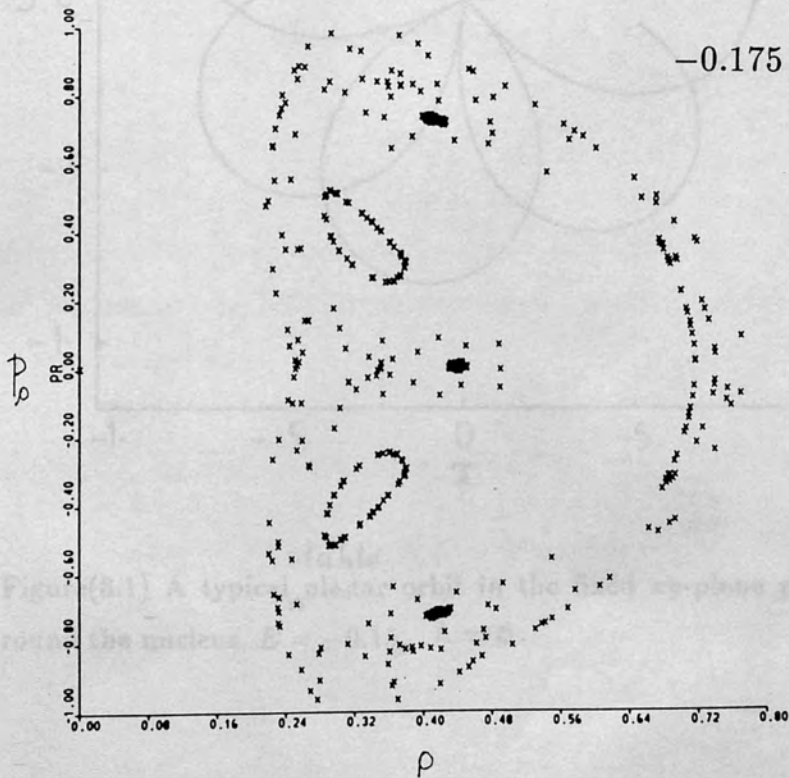
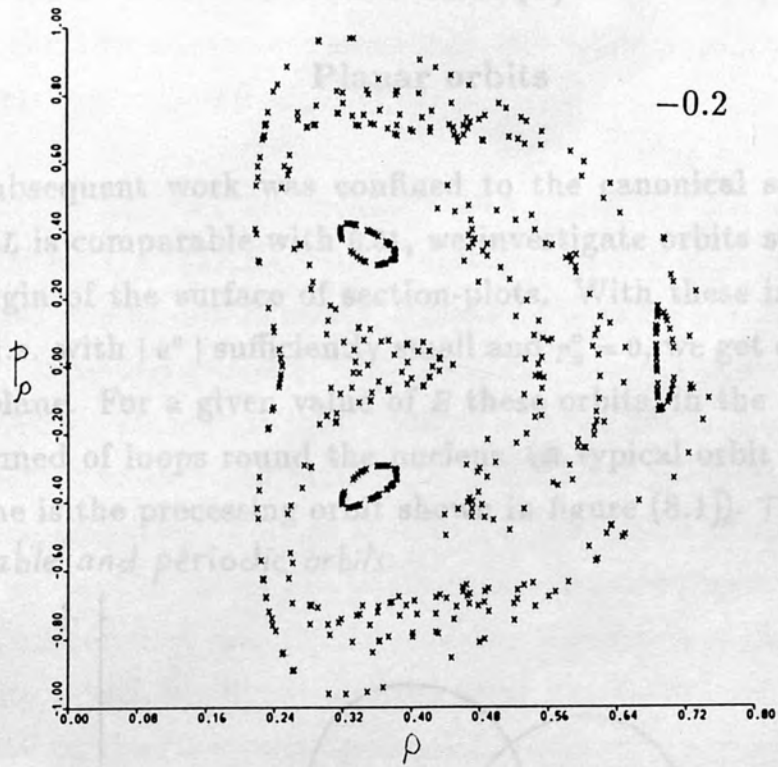




CHAPTER (8)

Planar orbits

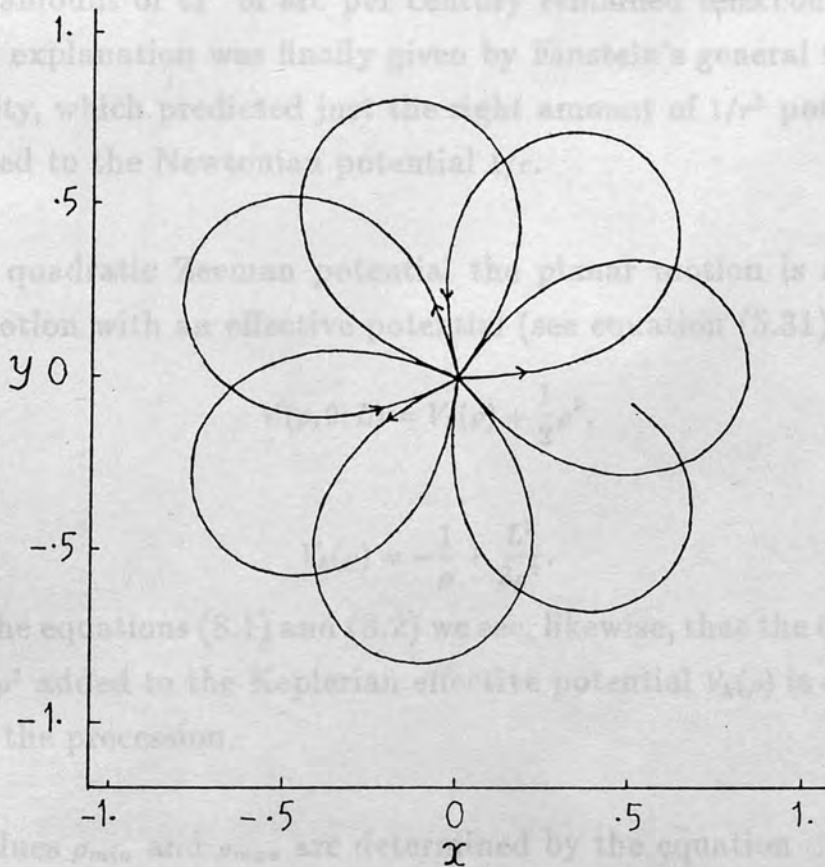
The subsequent work is confined to the canonical scheme only. When L is comparable with \hbar we investigate orbits starting near the origin of the surface of section plot. With these initial conditions, i.e. with $|a''|$ sufficiently small and $a' = 0$ we get orbits in the $\epsilon = 0$ plane. For a given value of the energy in the fixed frame, are formed of loops round the special periodic orbit in the fixed xy -plane in the process of adiabatic change (8.1). These are integrable and periodic orbits.



CHAPTER (8)

Planar orbits

The subsequent work was confined to the canonical scheme only. When L is comparable with 0.01, we investigate orbits starting near the origin of the surface of section-plots. With these initial conditions, i.e. with $|u^0|$ sufficiently small and $p_u^0 = 0$, we get orbits in the $z = 0$ plane. For a given value of E these orbits, in the fixed frame, are formed of loops round the nucleus (a typical orbit in the fixed xy -plane is the precessing orbit shown in figure (8.1)). These are *integrable and periodic orbits*.



Figure(8.1) A typical ^{stable} planar orbit in the fixed xy -plane precessing round the nucleus, $E = -0.15$, $L = 0$.

We have found, numerically, that the angle ϕ between the unit vector e_ρ and the x -axis increases monotonically while ρ oscillates periodically between ρ_{min} and ρ_{max} .

It is already known (Gasirowicz 1974) that the orbits due to the potential k/r (i.e. the Keplerian orbits) consist of ellipses that maintain their orientation in space, instead of forming precessing orbits. But small modifications of that potential cause a precession. Such modifications may arise from various sources, for example, the perturbations due to other planets, in the Kepler problem. In considering the planetary orbit of Mercury, a precession of the perihelion in the amount of $42''$ of arc per century remained unaccounted for, and an explanation was finally given by Einstein's general theory of relativity, which predicted just the right amount of $1/r^2$ potential to be added to the Newtonian potential $1/r$.

In the quadratic Zeeman potential the planar motion is a central field motion with an effective potential (see equation (5.31)).

$$V(\rho, 0; L) = V_k(\rho) + \frac{1}{2}\rho^2, \quad (8.1)$$

where

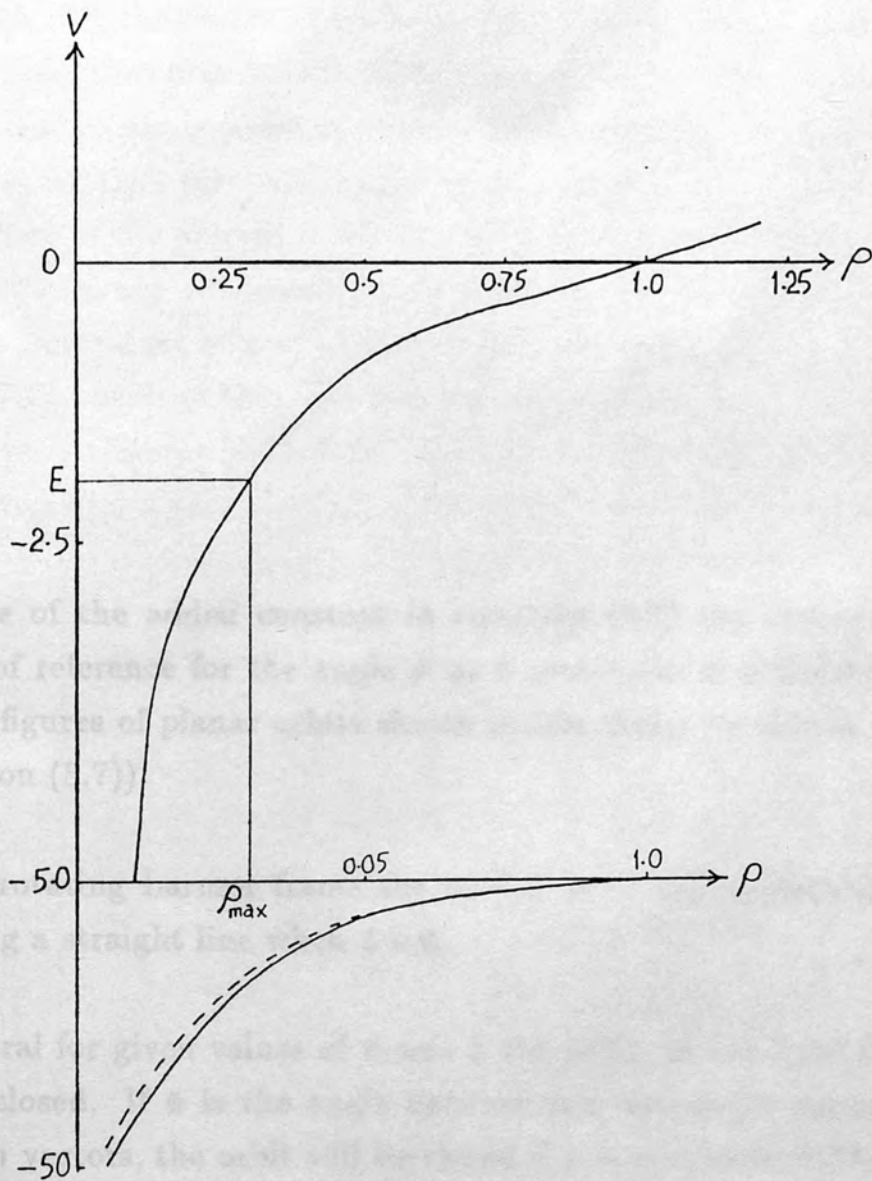
$$V_k(\rho) = -\frac{1}{\rho} + \frac{L^2}{2\rho^2}. \quad (8.2)$$

From the equations (8.1) and (8.2) we see, likewise, that the quadratic term $\frac{1}{2}\rho^2$ added to the Keplerian effective potential $V_k(\rho)$ is responsible for the precession.

The values ρ_{min} and ρ_{max} are determined by the equation

$$V(\rho, 0; L) = E. \quad (8.3)$$

(see figure (8.2)).



Figure(8.2) The effective potential energy. The broken curve (for $L = 0.02$) is shown to be distinguished from the full curve ($L = 0$) as ρ becomes nearer to zero. Furthermore, as $\rho \rightarrow 0$, $V \rightarrow \infty$ ($L = 0.02$) whereas $V \rightarrow -\infty$ ($L = 0$).

For $L \neq 0$, $\dot{\rho} \rightarrow 0$ as $\rho \rightarrow 0$. Then $\rho_{min} > 0$ and the electron will never fall into the centre of the field. Generally, there is a possibility that the electron may fall into the centre of the field (falling into the centre of the field is possible even in finite time, for example in the field $V(\rho) = -1/\rho^2$, (see Arnold, 1978 p.36)). For $L = 0$, the numerical integration of the system of regularized equations of motion (6.2.21) does not give any evidence of this possibility for the potential concerned. For values of L of the order 0.01 the points $\rho = \rho_{min}$ are so close to the nucleus that one can not see the area $\rho \leq \rho_{min}$ for the scale given in figures (8.1)-(8.4). The points where $\rho = \rho_{max}$ are called apocentres and where $\rho = \rho_{min}$ pericentres.

Because of the added constant in equation (5.7) the choice of an origin of reference for the angle ϕ' at a pericentre is arbitrary. For all the figures of planar orbits shown in this thesis we choose $\phi'_0 = 0$ (equation (5.7)).

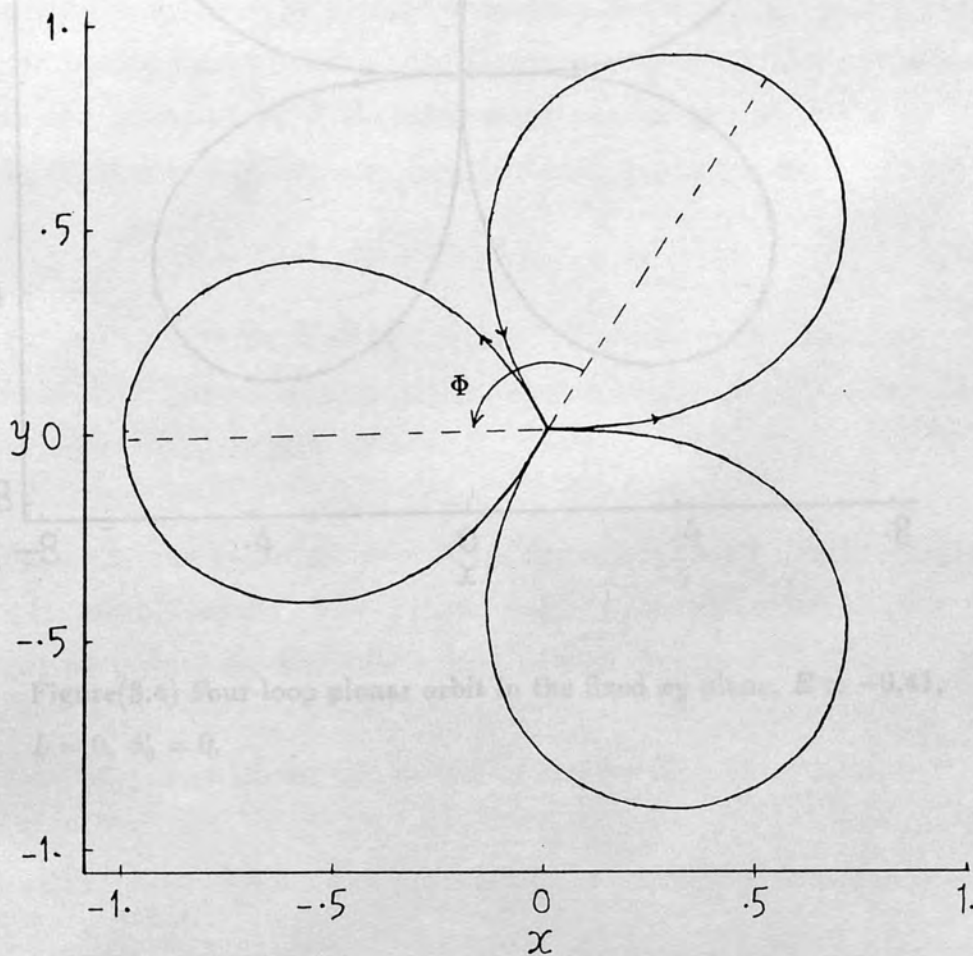
In the rotating Larmor frame the motion is found, numerically, to be along a straight line when $L = 0$.

In general for given values of E and L the orbit, in the fixed frame, is not closed. If Φ is the angle between two successive apocentral position vectors, the orbit will be closed if Φ is commensurable with 2π i.e. if $\Phi = 2\pi(p/q)$, where p and q are integers. For example $p/q = 1/3$ for the orbit shown in figure (8.3) and $p/q = 1/4$ for the orbit shown in figure (8.4). If Φ is not commensurable with 2π , the orbit is dense in the annular region $\rho_{min} \leq \rho \leq \rho_{max}$ figure(8.1).

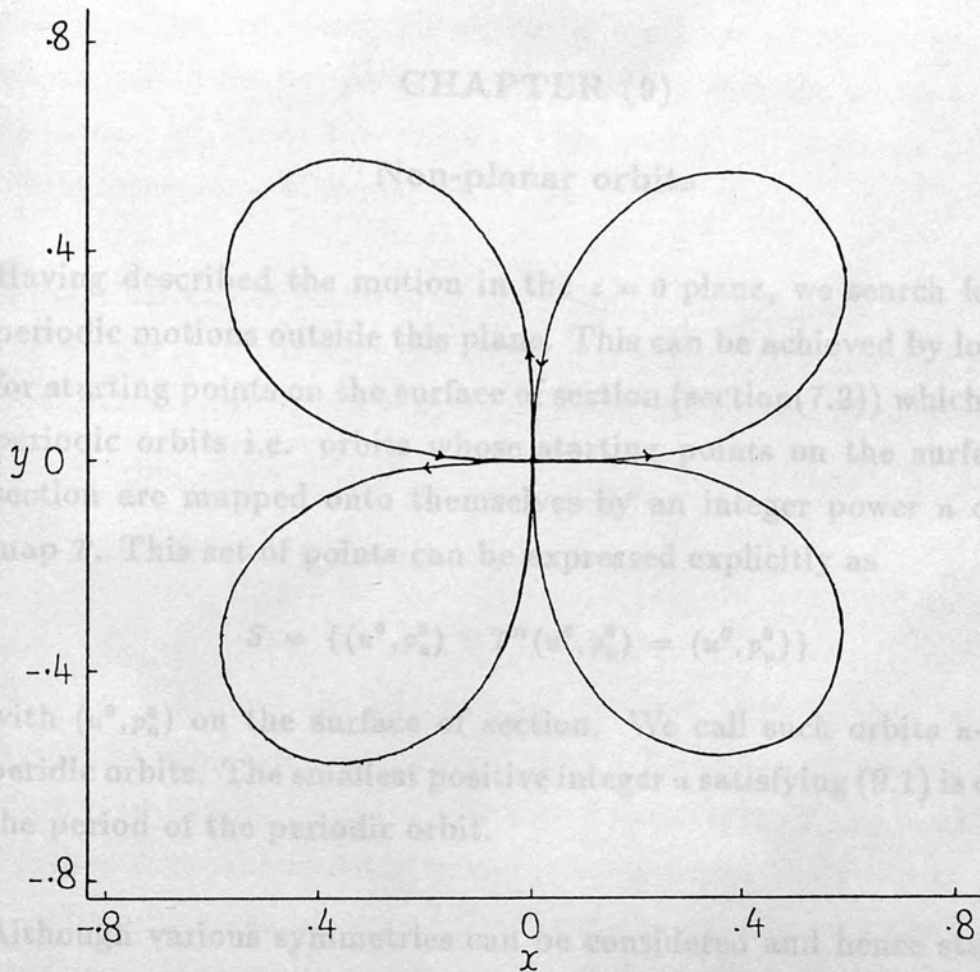
An integral number of loops is obtained at discrete values of E . For example, we have a three-loop orbit at $E \simeq 0$ (figure 8.3) and a four-

loop orbit at $E \simeq -0.41$ (figure (8.4)) and so on.

The stability of the planar orbits is studied by means of surfaces of section (section (7.2)) and also by the linearization at the corresponding fixed point (section 10.4). Results from section (10.4) indicate that the planar orbits are stable for $E < -0.127$ and unstable for $E > -0.127$.



Figure(8.3) Three-loop planar orbit in the fixed xy -plane, $E \simeq 0$, $L = 0$, $\phi'_0 = 0$.



Figure(8.4) Four-loop planar orbit in the fixed xy -plane, $E \simeq -0.41$,
 $L = 0$, $\phi'_0 = 0$.

(4.1) Periodic orbits starting along the u -axis (Class CI)
 In this case we put the condition that the momentum p_u vanishes initially at the starting point on the surface of section. In other words we assume that the initial velocity is perpendicular to the u -axis. Then we search for an initial distance, u^0 , from the origin which yields further periodic orbits with the u -axis at some distance, u^1 , from the origin. This technique produces periodic orbits symmetric with

CHAPTER (9)

Non-planar orbits

Having described the motion in the $z = 0$ plane, we search for the periodic motions outside this plane. This can be achieved by looking for starting points on the surface of section (section(7.2)) which yield periodic orbits i.e. orbits whose starting points on the surface of section are mapped onto themselves by an integer power n of the map T . This set of points can be expressed explicitly as

$$S = \{(u^0, p_u^0) : T^n(u^0, p_u^0) = (u^0, p_u^0)\} \quad (9.1)$$

with (u^0, p_u^0) on the surface of section. We call such orbits n -cycle periodic orbits. The smallest positive integer n satisfying (9.1) is called the period of the periodic orbit.

Although various symmetries can be considered and hence starting points located (Greene 1979 (a)), we confine our attention to picking up starting points for periodic orbits of two classes :

CI- Starting points along the u -axis of the surface of section,

CII- Starting points along the p_u -axis of the surface of section.

We simplify the location of periodic orbits to the search for roots of numerically calculated functions. Each one of them is a function of a single variable. We define such functions to include the following two cases :

(9.1) Periodic orbits starting along the u -axis (Class CI)

In this case we put the condition that the momentum p_u vanishes initially at the starting point on the surface of section. In other words we assume that the initial velocity is perpendicular to the u -axis. Then we search for an initial distance, u^0 , from the origin which yields a further perpendicular crossing with the u -axis at some distance u^1 , from the origin. This technique produces periodic orbits symmetric with respect to the u -axis.

A practical way of performing the technique to get periodic orbits of one period is to consider the effect of the map \sqrt{T} generated by the Hamiltonian flow which maps a point on the surface of section

$$v = 0, \quad p_v > 0, \quad (9.1.1a)$$

to the next intersection with the surface

$$v = 0, \quad p_v < 0. \quad (9.1.1b)$$

We have borrowed the square root notation from Greene, 1979a although he used the notations \sqrt{T}_+ and \sqrt{T}_- as two operators which follow a trajectory from the plane $v = 0$ back to itself. He used them together with a symmetry operator to factorize the Poincare map T . The advantage of using \sqrt{T} is that the calculations are half as expensive. Meanwhile, we checked the effect of T and T^2 .

The above method proves to be very successful and efficient. It reveals clearly and easily the existence of the nongeneric behaviour which is particularly dominant for the orbits in class CII. This will be explained in chapter (10).

Let

$$\sqrt{T}(u^0, 0) = (u, p_u). \quad (9.1.2)$$

for some point (u, p_u) on the surface (9.1.1b) The relation (9.1.2) motivates the definition of a function $F_I(u^0)$ as the u -component of the

momentum of the image of the point $(u^0, 0)$ under \sqrt{T} ; i.e. $F_I(u^0) = p_u$. We calculate the zeros of $F_I(u^0)$ to get the set

$$A = \{u^0 : \sqrt{T}(u^0, 0) = (u^1, 0) \text{ for some value } u^1 \text{ of } u.\} \quad (9.1.3)$$

The starting points on the surface of section (9.1.1a) for periodic orbits of class CI take their u -values from the set of zeros A . We have found numerically that \sqrt{T} is a one-to-one mapping from A onto itself. And this is confirmed by the fact that the Hamiltonian (7.1.3) is reversible since it is even in the momenta (and positions also).

The set A can be partitioned into three subsets: two of them, A_1 and A_2 have equal numbers of elements such that \sqrt{T} maps either of them onto the other. The third subset A_3 is mapped onto itself under \sqrt{T} . In other words periodic orbits starting from an element of A_1 are described in the opposite sense to those beginning from the corresponding element of A_2 and each one of them intersects the plane $v = 0$ at two different points. But each periodic orbit starting from A_3 intersects the plane $v = 0$ at one point.

It should be noted that these starting points satisfy the relations $p_\rho = 0$ and $p_z \neq 0$, which are evident from (7.1.16) and (7.1.17). This implies that the corresponding periodic orbits in the original coordinates (ρ, z) are symmetric about the ρ -axis.

For example, figure (9.1.1) shows the zeros at $E = -0.1$ (with $B = 60$ kG, and $m = 0$). For these fixed values of B and m we express all zeros at $E = -0.1$ in an explicit set form

$$A = \{o, a_1^+, a_1^-, b^+, b^-, a_2^+, a_2^-, s^+, s^-\}, \quad (9.1.4)$$

where the value of u at a_1^- is the negative of its value at a_1^+ , ... and so on. The zero denoted o is at the origin of the surface of section

and corresponds to a linear periodic motion in the ρ -direction and in the fixed frame to a motion in the $z = 0$ plane. This motion was discussed in detail in chapter (8). We call the subclass containing these periodic orbits in the ρ -direction Co.

The subsets of A , as described above, are

$$A_1 = \{a_1^+, a_1^-, s^+\}, \quad A_2 = \{a_2^+, a_2^-, s^-\}, \quad A_3 = \{o, b^+, b^-\}, \quad (9.1.5)$$

so that

$$\sqrt{T}(a_1^+) = a_2^+, \quad \sqrt{T}(a_1^-) = a_2^-, \quad \sqrt{T}(s^+) = s^-, \quad (9.1.6a)$$

and

$$\sqrt{T}(o) = o, \quad \sqrt{T}(b^+) = b^+, \quad \sqrt{T}(b^-) = b^-. \quad (9.1.6b)$$

The two points s^+ and s^- are hyperbolic points and appear clearly on the surface of section pictures of the regular regime for different values of E , B and m (Figures (7.2)). At a fixed value of E the points s^+ and s^- exist along the u -axis equidistant from the origin and such that $-s^+ = s^-$. A magnification of the point s^+ is shown in chapter (10), where we shall be discussing the stability of the periodic orbits which start from these points. We mentioned in chapter (7) that, in the regular regime, each of the separatrices (through points very near to s^+ and s^-) divided the phase space into four different families of invariant curves. But can we calculate the separatrices themselves?

Stochastic motion always occurs near the separatrices and usually, theoretically and from numerical calculations, a separatrix trajectory does not have the smooth nature to be found in the integrable problems (for example the pendulum problem). By numerical integration we calculate the two orbits through the points s^+ and s^- even in the chaotic regime. We mentioned in chapter (7) that the

more complicated separatrices, like those round the island chains, were typically not curves, but stochastic layers (see figure (7.2.5)).

Figures (9.1.2a) and (9.1.2b) show the orbits through s^+ and s^- respectively. Each is shown at two different values of the energy parameter E . The first is at $E = -1.0$ i.e. in the regular regime and the second is at $E = -0.1$ i.e. in the chaotic regime. At fixed values of E , B and m both separatrices are similar in shape but differ in the senses in which they are described. From now on we call the subclass containing them CIs.

From our numerical calculations we found that each orbit is generally an ellipse whose equation is

$$\frac{\rho^2}{a^2} + \frac{z^2}{b^2} = 1, \quad (9.1.7)$$

where the functional form of the major and minor axes $a(E)$ and $b(E)$ are plotted against the energy E (Figure 9.1.3). From this figure we see that

$$a(E) \simeq b(E) \quad \text{for} \quad E < -0.9. \quad (9.1.8)$$

That is these orbits are practically circular orbits below the energy parameter value $E = -0.9$.

Good descriptions of separatrices for different Hamiltonian systems, particularly in the one-dimensional problems, exist in the literature (see for example Percival and Richards, 1982 also Lichtenberg and Lieberman 1983).

Figures (9.1.4a) and (9.1.4b) show two periodic orbits in the original coordinates $\rho-z$ with starting points at b^+ and b^- respectively. These orbits have the same shape and period but they are described in the different senses. We call this subclass of orbits CI1.

Figures (9.1.5a-d) show the periodic orbits in the ρz -plane with the starting points at a_1^+ , a_1^- , a_2^+ and a_2^- respectively. They also have the same shape and period. The different senses in which these orbits are described are illustrated by the arrows. We call this subclass of orbits CI2.

It remains, in this section, to point out that all these orbits of class CI were investigated for different values of the magnetic quantum number m ($m = 0, 1, 2, 3$) and we found no significant change in their shape or period but they are very slightly displaced away from the z -axis (see section (7.2)). The maximum displacement is of order 10^{-3} scaled units in the u -direction.

(9.2) Periodic orbits starting along p_u -axis (Class CII)

The periodic orbits which pass through the origin of the u, v coordinates and in turn are emitted from the origin in the ρ, z coordinates are the most important. Some of the results available from experiments on the spectrum of the hydrogen-like atoms in external magnetic fields are, in the chaotic regime, related to these orbits.

We mentioned in chapter 1 that in this regime the $1.5 \hbar \omega_c$ had been attributed to planar orbits which approach close to the nucleus.

Later in this chapter and also in chapter (11) we shall see that other orbits belonging to this class (class II) are important in understanding recent ionization experiments on hydrogen in the presence of a uniform magnetic field.

The condition that the orbit starts on the surface of section (9.1.1a) along the p_u -axis will ensure an emission from the origin with a mo-

momentum vector $\mathbf{p}^0 = (p_u^0, p_v^0)$ which is constant in magnitude but arbitrary in direction. This is because a direct substitution with this initial position in phase space in the energy surface equation (7.1.3) gives

$$|\mathbf{p}^0|^2 = (p_u^0)^2 + (p_v^0)^2 = 4. \quad (9.2.1)$$

Therefore, the search for a periodic orbit turns out to be a problem of locating the direction, through changes in p_u^0 , which results in the orbit returning to the origin. As p_u^0 changes from $p_u^0 = -2$ to $p_u^0 = +2$ over the interval $[-2, +2]$, the initial momentum changes direction from $\psi_0 = \frac{-\pi}{2}$ to $\psi_0 = \frac{\pi}{2}$, sweeping the whole semi-circle, where ψ_0 is the angle between the vector \mathbf{p}^0 and the v -axis.

Applying this technique for every value of the energy parameter E , we get a finite number of periodic orbits. We give an explanation to this technique similar to that given in the last section (9.1)

Let

$$\sqrt{T}(0, p_u^0) = (u, p_u), \quad (9.2.2)$$

for some point (u, p_u) on the surface (9.1.1b). The relation (9.2.2) motivates the definition of a function $F_{II}(p_u^0)$ as the coordinate u of the image of the point $(0, p_u^0)$ under \sqrt{T} ; i.e. $F_{II}(p_u^0) = u$. We calculate the zeros of $F_{II}(p_u^0)$ to get the set

$$B = \{p_u^0 : \sqrt{T}(0, p_u^0) = (0, p_u^1) \text{ for some } p_u^1\}. \quad (9.2.3)$$

The starting points on the surface of section (9.1.1a) for periodic orbits of class CII take their p_u^0 values from the set of zeros B .

The set B defined in (9.2.3) has the same partition properties as the set A in section (9.1.4) under \sqrt{T} . We illustrate this by giving an example:

At $E = -0.2$ (with $B = 60$ kG, and $m=0$), Figure (9.2.1) shows the zeros of the function $F_{II}(p_u^0)$. The set B defined in (9.2.2) contains fifteen points and can be expressed explicitly as

$$B = \{0, c_1^+, c_1^-, d_1^+, d_1^-, e_1^+, e_1^-, f^+, f^-, e_2^+, e_2^-, d_2^+, d_2^-, c_2^+, c_2^-\} \quad (9.2.4)$$

The subsets of B are

$$B_1 = \{c_1^+, c_1^-, d_1^+, d_1^-, e_1^+, e_1^-\},$$

$$B_2 = \{c_2^+, c_2^-, d_2^+, d_2^-, e_2^+, e_2^-\},$$

$$B_3 = \{o, f^+, f^-\}.$$

so that

$$\sqrt{T}(c_1^+) = c_2^+, \quad \sqrt{T}(c_1^-) = c_2^-, \quad \sqrt{T}(d_1^+) = d_2^+, \dots \text{etc.} \quad (9.2.5a)$$

and

$$\sqrt{T}(o) = o, \quad \sqrt{T}(f^+) = f^+, \quad \sqrt{T}(f^-) = f^- \quad (9.2.5b)$$

Here again the origin o corresponds to a planar motion and is discussed in chapter(8). The two points $f^+ \equiv (0, \sqrt{2})$ and $f^- \equiv (0, -\sqrt{2})$ correspond, macroscopically, in the ρ, z - coordinates to linear motions along the z -axis in the regions $z > 0$ and $z < 0$ respectively. The oscillations in the ρ direction are so minute that they can be qualitatively neglected. However, a quantitative analysis of these oscillations reveals the importance of them as responsible for a non-generic stability behaviour and giving rise to a sequence of bifurcations from the same orbit. Because of that, these orbits are important as we shall see when we study their stability in section (10.4.2) and (10.4.4). We call the subclass containing these orbits CIIz.

Figure (9.2.2) shows four periodic orbits, in the ρ, z -coordinates, starting with initial positions on the surface of section at the points c_1^+ ,

c_1^- , c_2^+ and c_2^- . These orbits are illustrated in this figure by a, b, c, and d respectively and have the following features

- (a) They are symmetric about the z -axis.
- (b) They have the same shape and period but differ in orientation and in the sense in which they are described.
- (c) Each orbit crosses the z -axis at one point.

We call this subclass of orbits, from now on, CII1

Figure (9.2.3) shows another four periodic orbits which constitute a subclass CII2. These orbits have initial positions on the surface of section (9.1.1a) at the points d_1^+ , d_1^- , d_2^+ and d_2^- . These orbits are illustrated in the figure by a, b, c and d respectively.

The orbits of this subclass have the following features:

- (a) They are not symmetric but each has a vanishing velocity at a point off the z -axis. This point is the highest (or lowest) point on the orbit.
- (b) They have the same shape and period but differ in orientation and the sense in which they are described.
- (c) Each orbit crosses the z -axis at one point.

Figure (9.2.4) shows a third subclass containing four periodic orbits which start at the points e_1^+ , e_1^- , e_2^+ and e_2^- . They have the same

features like the subclass CII1 except that there are two crossing points on the z -axis. One of them is the highest (or lowest) point of the orbit. We call this subclass CII3.

At a higher energy ($E = -0.15$, say) four more zeros exist and the set B of zeros contains nineteen elements. The additional zeros produce four new periodic orbits shown in figure (9.2.5). They have the same features as the subclass CII2 except that there are two crossing points with the z -axis. We call this subclass CII4.

To sum up, the class CII has been divided into distinct subclasses:

$$\text{CII} = \{ \text{Co}, \text{CIIz}, \text{CII1}, \text{CII2}, \text{CII3}, \dots, \text{CII}n, \dots \} \quad (9.2.5)$$

where Co is the subclass containing the planar orbits in the $z = 0$ plane. The subclasses $\text{CIIz}, \text{CII1}, \text{CII2}, \dots$ are defined above.

Each of the subclasses $\text{CII}n$, $n = 1, 2, 3, \dots$ contains four periodic orbits. We have the following two cases:

- (a) If n is odd, the four periodic orbits contained in $\text{CII}n$ are symmetric about the z axis. They have the same shape and period but differ in the sense in which they are described and orientation. For each, the number of crossing points on the z -axis is $\frac{n+1}{2}$.
- (b) If n is even, the four periodic orbits contained in $\text{CII}n$ are not symmetric. They have the same shape but differ in the sense in which they are described and orientation. The velocity of each orbit vanishes at the highest (or lowest) point which is not one of the crossing points on the z -axis. The number of the crossing points on the z -axis is $\frac{n}{2}$.

We, further, notice that the planar motions in the $z = 0$ plane belong to both classes i.e. $CI \cap CII = Co$. Presumably because of that it was easy to locate and recognize its relevance to the $1.5 \hbar \omega_c$ spacing near $E = 0$.

(9.3) Change of the periodic orbits with the energy parameter.

For fixed values of B , and m we locate the periodic orbits of classes CI and CII at different energies. In this case the functions $F_I(u^0)$ and $F_{II}(p_u^0)$ are dependent on E and consequently the sets A in (9.1.3) and B in (9.2.3) will depend on E . In general, this dependence implies: Firstly a change in the initial positions of the periodic orbits on the surface of section (i.e. a shift for each zero of the functions $F_I(u^0; E)$ and $F_{II}(p_u^0; E)$). Secondly it implies the possibility, if the increase of E is big enough, of an affiliation of new members to the sets A and B . What happens in fact is that these new orbits are born at some intermediate value of E and survive beyond this value.

We determine the sets $A(E)$ and $B(E)$ starting from the regular regime where the invariant tori seem to occupy all the surface of section pictures. With a gradual increase in E we can follow the change of the elements of $A(E)$ and $B(E)$. As we reach the chaotic regime we take finer steps of E to locate the newly created members. And so on.

For locating periodic orbits of multiple periods and the period doubling we consider the zeros of the functions $F_I(u^0; E)$ and $F_{II}(p_u^0; E)$ defined for higher integral powers of the map T . This will be seen when we study the stability of the orbits in the following chapter.

For the class CI we have figure (9.3.1) which is a plot of the zeros u^0 of the function F_I , defined in (9.1.3), against E . For example

$$\begin{aligned} A(-0.16) &= \{s^+, o, s^-\} \\ A(-0.12) &= \{s^+, o, s^-, b^+, b^-\} \\ A(-0.10) &= \{s^+, o, s^-, b^+, b^-, a_1^+, a_1^-, a_2^+, a_2^-\}. \end{aligned} \quad (9.2.3.1)$$

From (9.2.3.1) we notice that two zeros b^+ and b^- must have been created at some value of E between $E = -0.16$ and $E = -0.12$. Four more zeros a_1^+ , a_1^- , a_2^+ , a_2^- must have been created at some value of E between $E = -0.12$ and $E = -0.10$. The stability of such zeros (or fixed points) is studied in chapter (10) and surfaces of section surrounding them are displayed when necessary. Furthermore, the specific values of E at which the creation of new fixed points takes place is given in chapter (10).

Similarly, for the class CII we have figure (9.3.2): a plot of the zeros p_u^0 of the function F_{II} , defined in (9.2.3), against E . The zeros shown in (9.2.4) are depicted in the figure. This figure shows that the subclasses of periodic orbits CII1, CII2, CII3, ... are all born from the two orbits of the subclass CIIz. This nongeneric behaviour is exciting and needs a study of the stability of the various orbits particularly those of subclass CIIz. This will be described in the following chapter.

It may be useful to know the extent of an orbit in both dimensions ρ and z , particularly when the parameter E changes. For the class of orbits CI, we see in (9.1) that each of the subclasses CIs, CI1 and CI2 has periodic orbits which are similar in shape and size. Then the extremes $|\rho|_{max}$ and $|z|_{max}$ are the same for each subclass. Figures (9.3.3a) and (9.3.3b) depict the evolution of $|\rho|_{max}$ and $|z|_{max}$ with

the parameter E respectively. We notice from these figures that, apart from the orbits of the subclass CI2, all orbits expand in the ρ -direction as well as in the z -direction. The orbits of the subclass CI2 (shown in figure (9.1.5)) expand in the ρ -direction but shrink in the z -direction as E increases. They have gradually evolving crescent like-shapes in the sense that they become wider in the ρ -direction as E increases.

For the orbits of class CII we see in (9.2.2) that each of the subclasses CII n contains orbits similar in shape and dimension. This means that $|\rho|_{max}$ and $|z|_{max}$ are the same for all the orbits belonging to the same subclass. Figures (9.3.4a) and (9.3.4b) shows the change of $|\rho|_{max}$ and $|z|_{max}$ against E respectively for CII1, CII2, CII3, ... CII6. From these figures we notice that the two orbits in the subclass CIIz expand, along the z -axis, very rapidly as E increases (notice that $\rho \simeq 0$ for these orbits). The orbits in the subclasses CII n , $n \geq 1$ expand substantially in the ρ -direction but they nearly maintain their heights (or depths) in the z -direction as E increases.

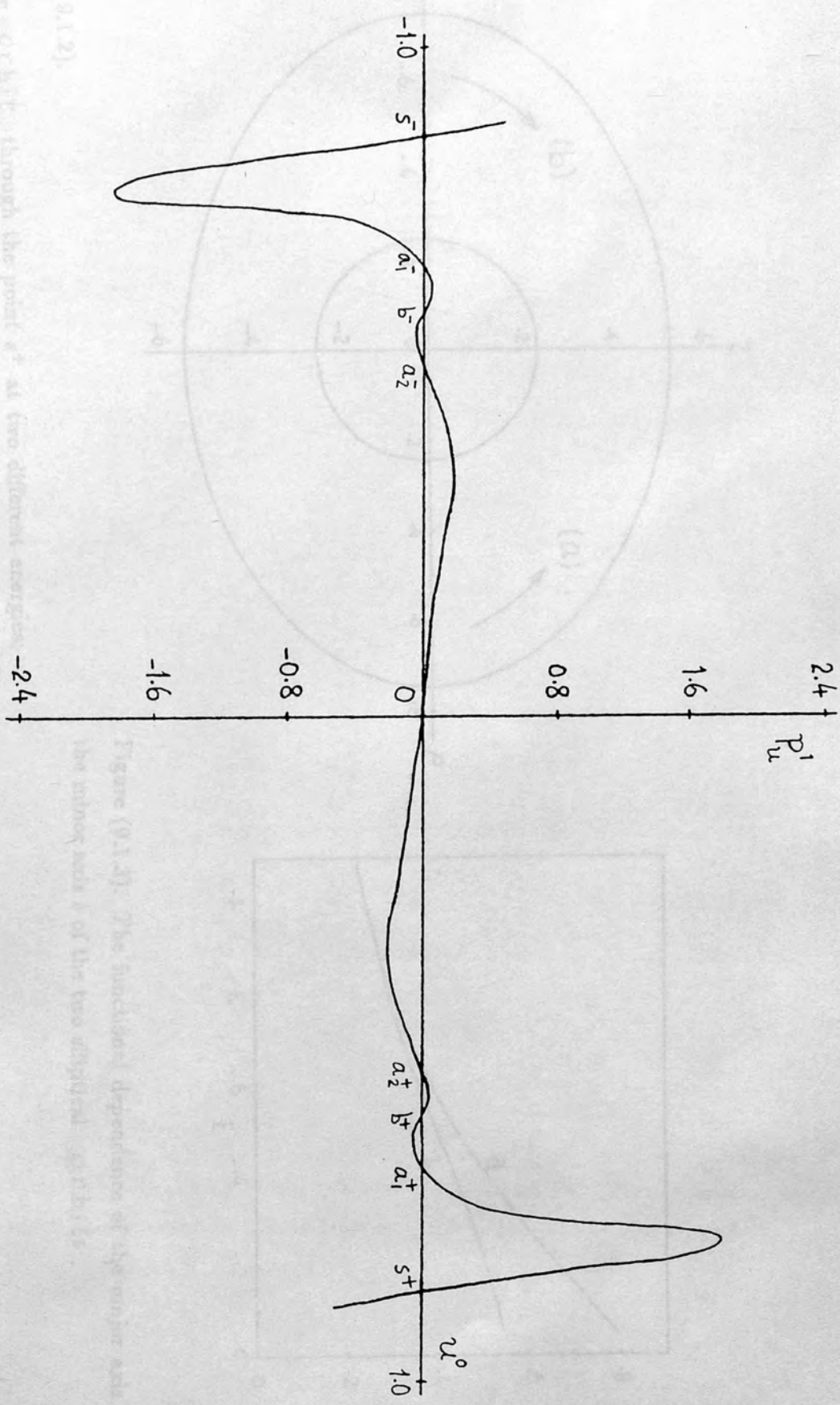


Figure (9.1.2).

(a) The orbitals through the point s^+ at two different energies: $E = -1.0$ (a circle) and $E = -0.1$ (an ellipse), $B = 60kG$ and $m = 0$. The direction of motion is indicated by the arrows.

Figure (9.1.1) The zeros of the function $p_u = F_I(u^0)$ determine the starting points of the periodic orbits of class CI. $E = -0.1$, $B = 60kG$, $m = 0$.

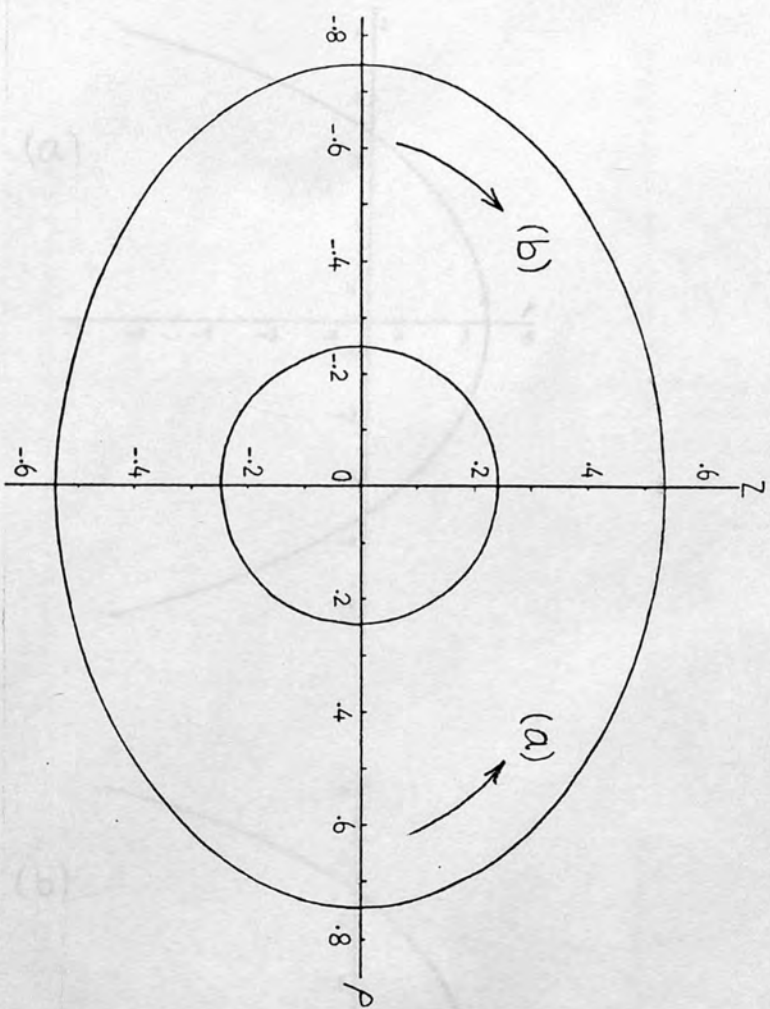


Figure (9.1.2).

- (a) The orbit through the point s^+ at two different energies; $E = -1.0$ (a circle) and $E = -0.1$ (an ellipse), $B = 60kG$ and $m = 0$. The direction of motion is anticlockwise.
- (b) The orbit through the point s^- . As (a) except that the direction of motion is clockwise.

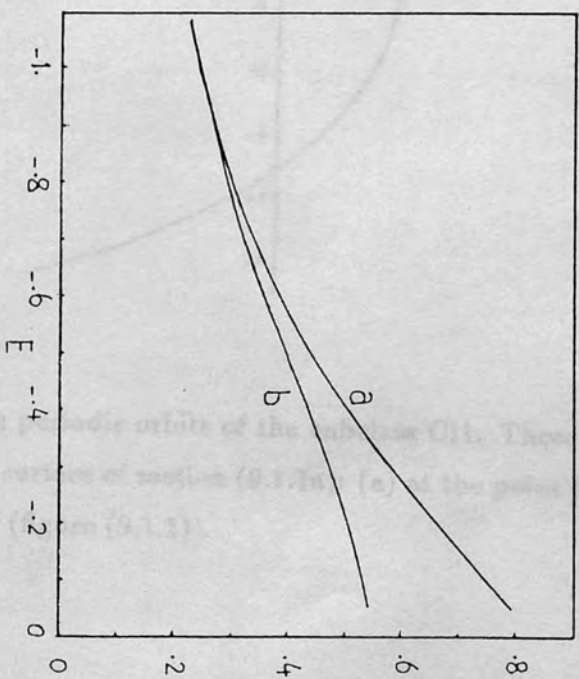


Figure (9.1.3). The functional dependence of the major axis a and the minor axis b of the two elliptical orbits.

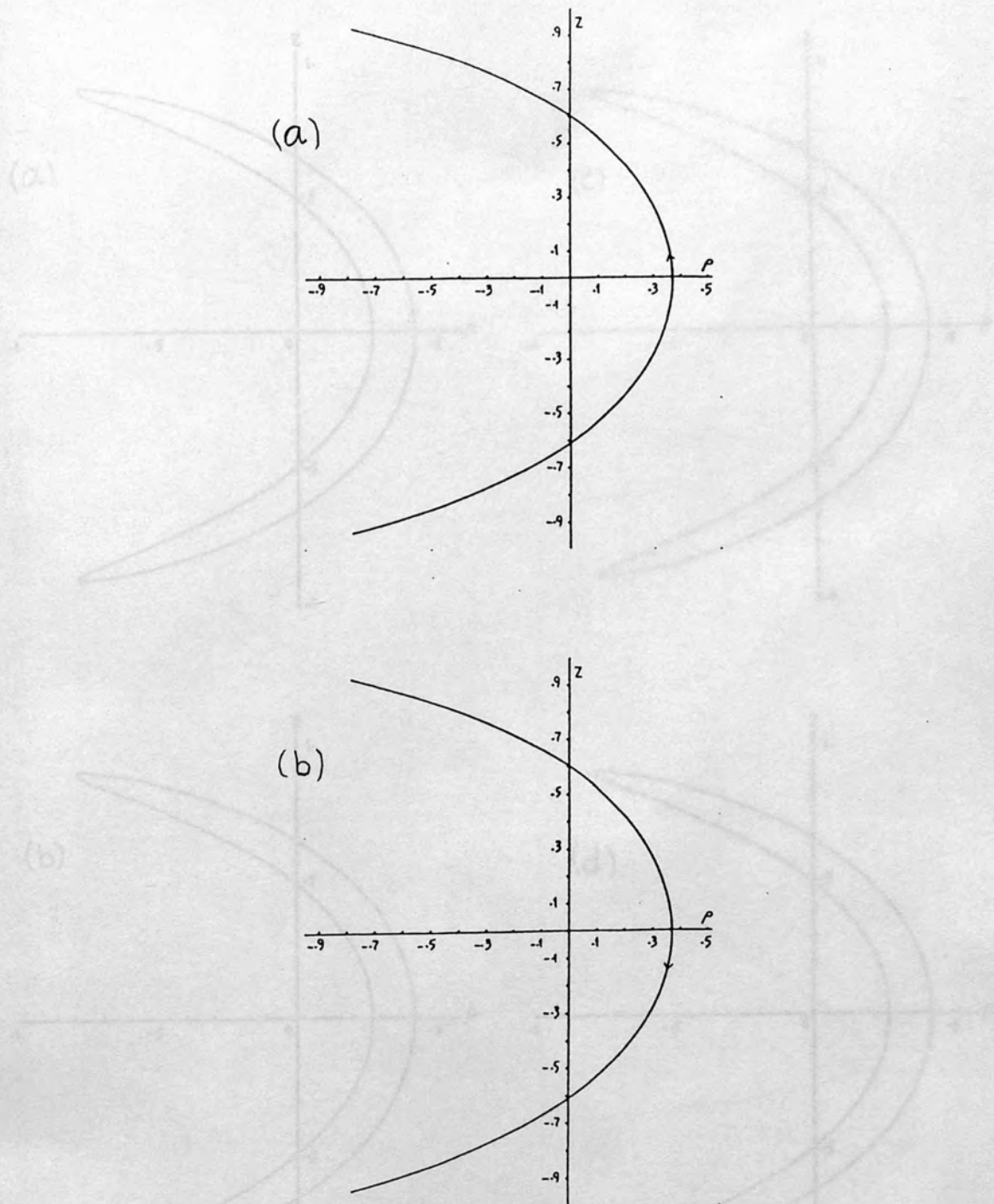


Figure (9.1.4). The periodic orbits of the subclass CII. These orbits are starting on the surface of section (9.1.1a): (a) at the point b^+ and (b) at the point b^- (figure (9.1.1)).

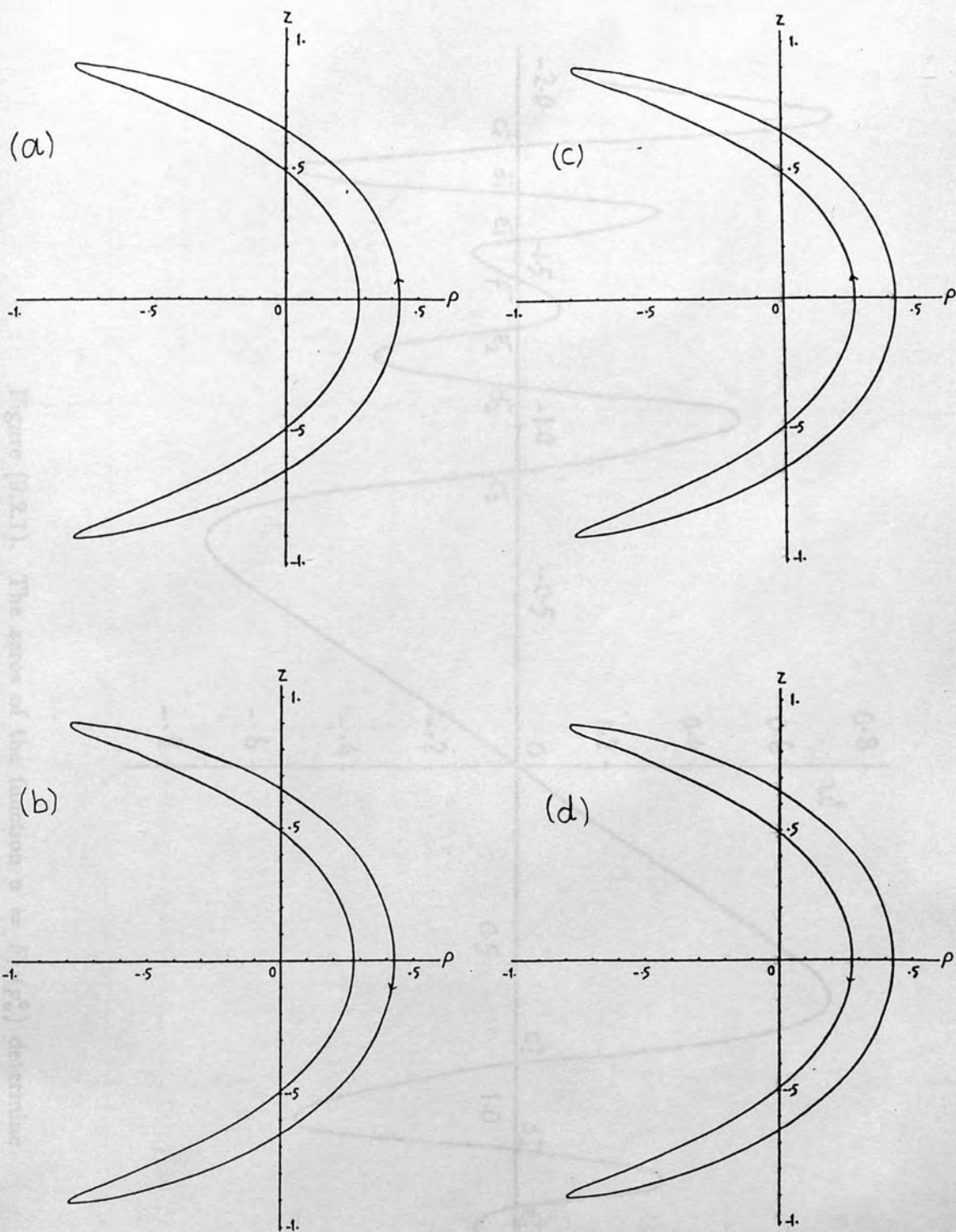


Figure (9.1.5). The periodic orbits of the subclass CI2. These orbits are starting on the surface of section (9.1.1a): (a) at the point a_1^+ , (b) at the point a_1^- , (c) at the point a_2^+ , and (d) at the point a_2^- . These points are shown in figure (9.1.1).

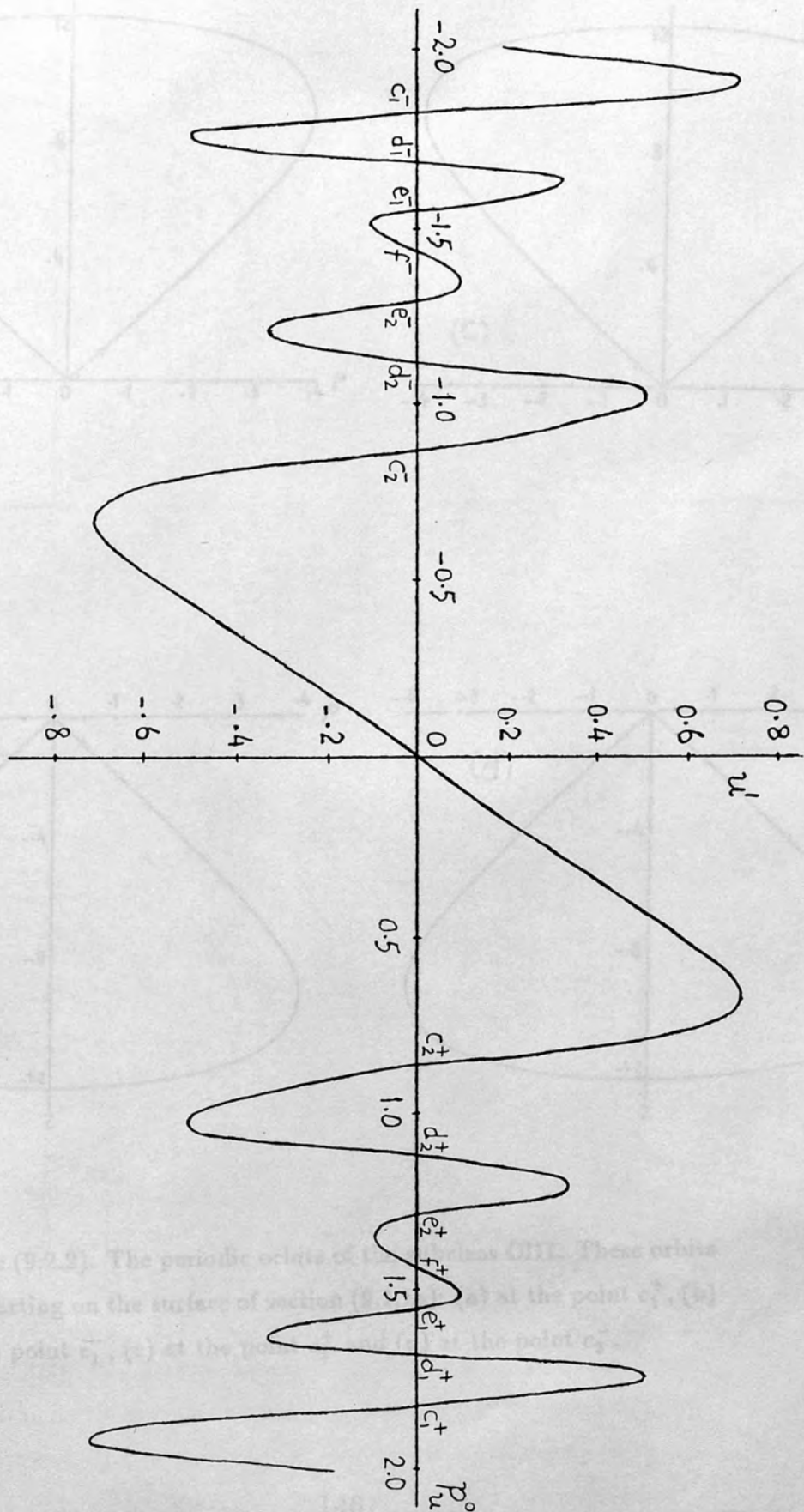


Figure (9.2.1). The zeros of the function $u = F_{II}(p_u^0)$ determine the starting points of the periodic orbits of class III, $E = -0.2$, $B = 60kG$, and $m = 0$.

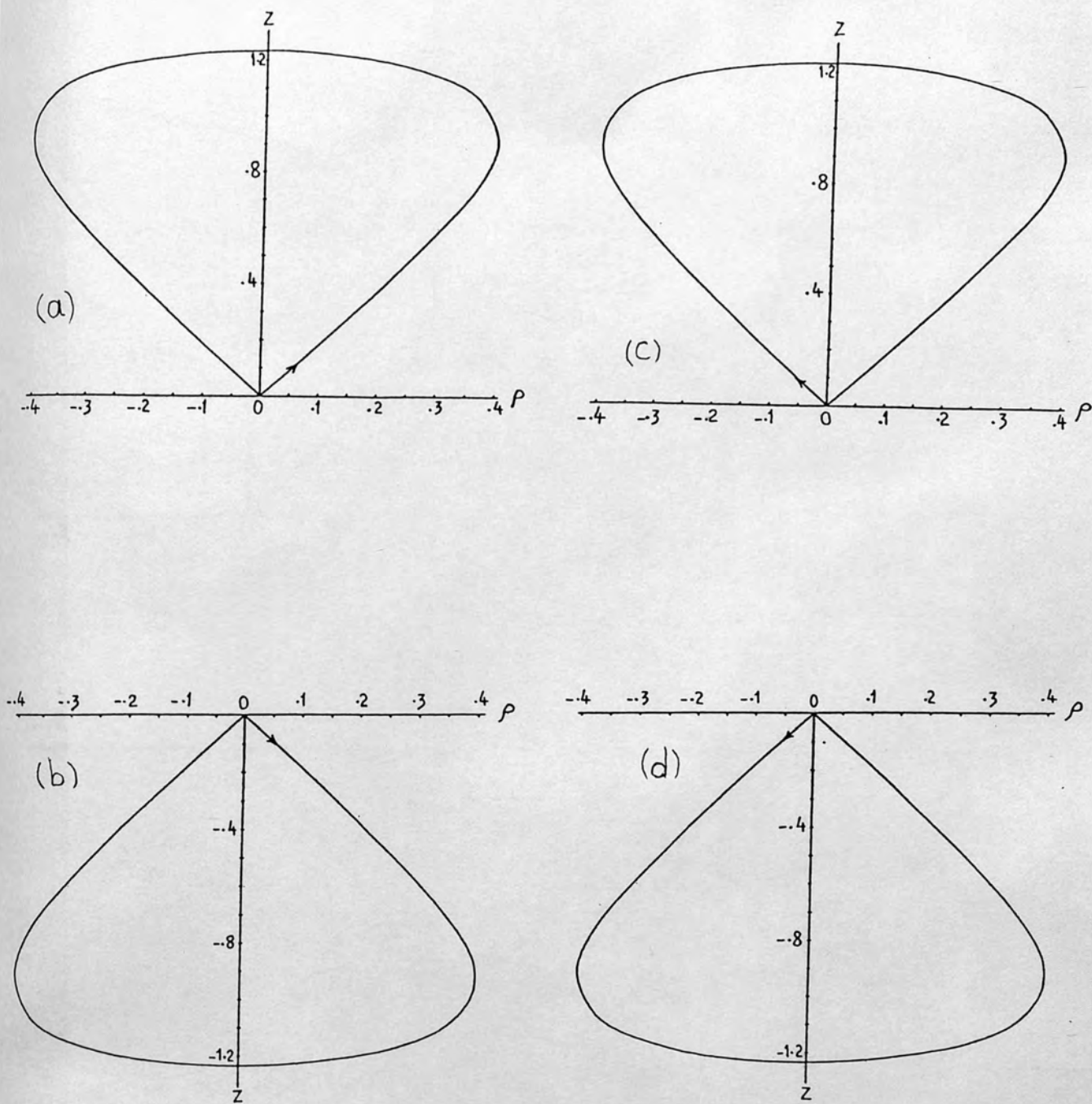


Figure (9.2.2). The periodic orbits of the subclass CIII. These orbits are starting on the surface of section (9.1.1a): (a) at the point c_1^+ , (b) at the point c_1^- , (c) at the point c_2^+ and (d) at the point c_2^- .

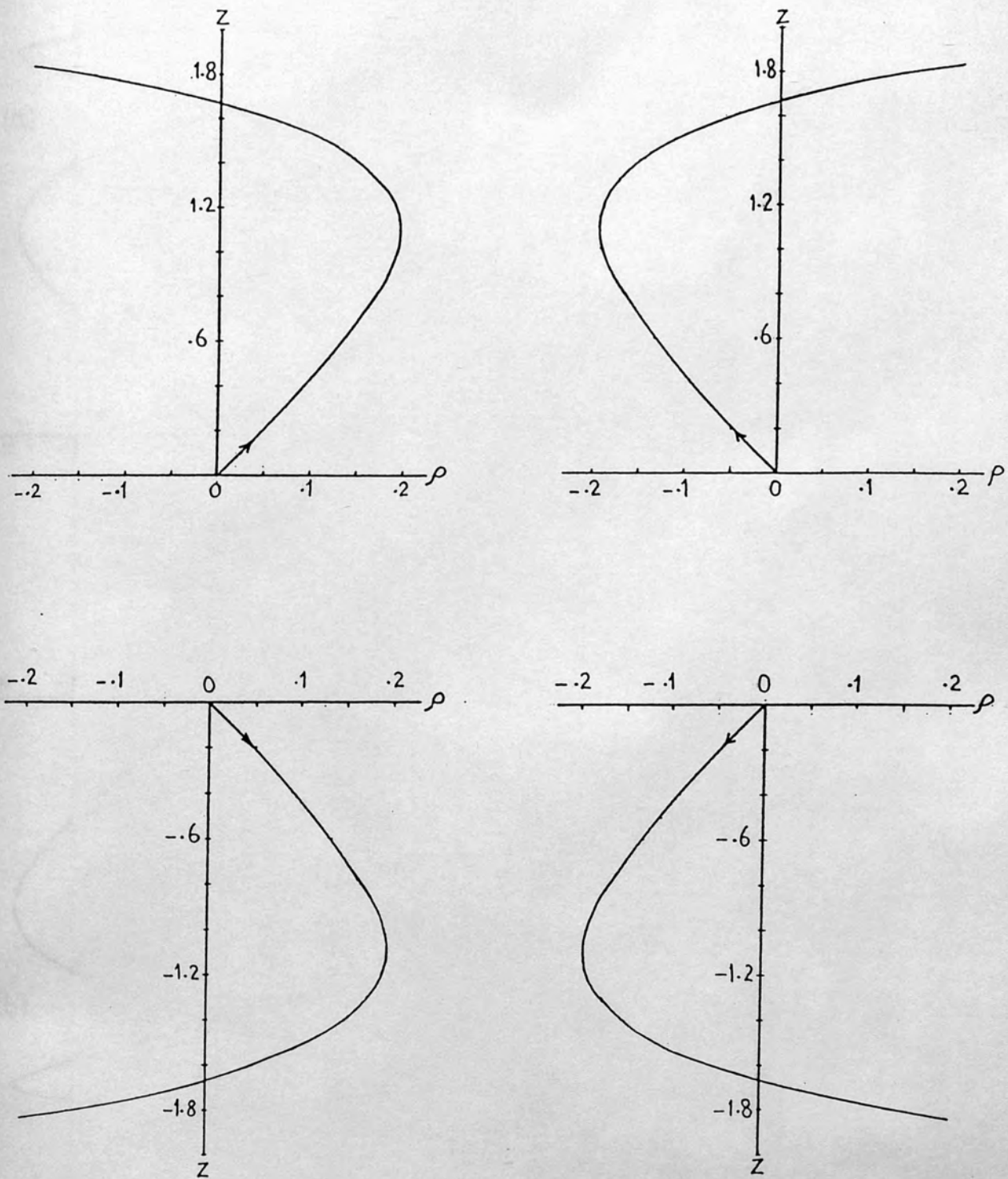


Figure (9.2.3). The periodic orbits of the subclass CII2. These orbits are starting on the surface of section (9.1.1a): (a) at the point d_1^+ , (b) at the point d_1^- , (c) at the point d_2^+ and (d) at the point d_2^- .

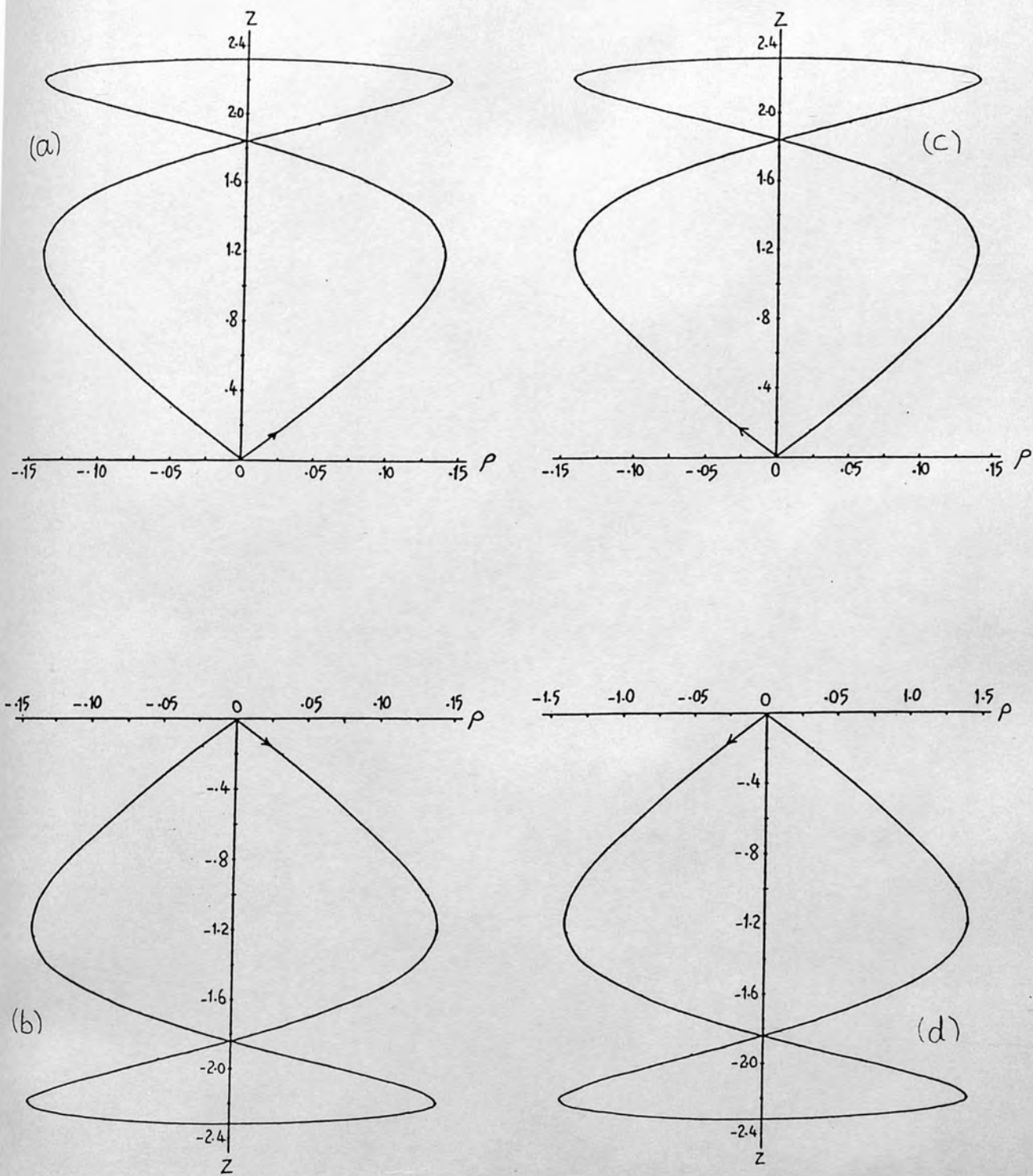


Figure (9.2.4). The periodic orbits of the subclass CII3. These orbits are starting on the surface of section (9.1.1a): (a) at the point e_1^+ , (b) at the point e_1^- , (c) at the point e_2^+ and (d) at the point e_2^- .

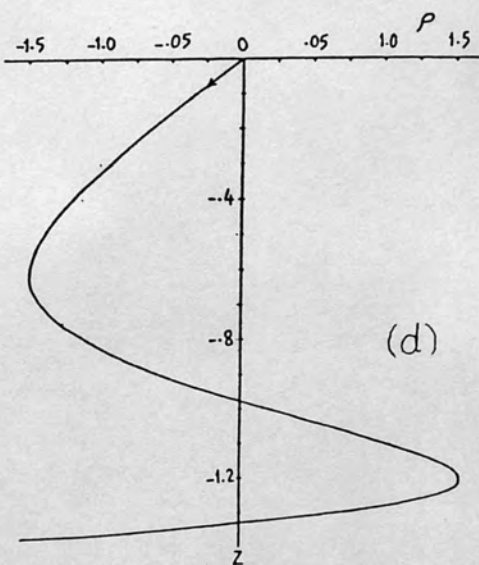
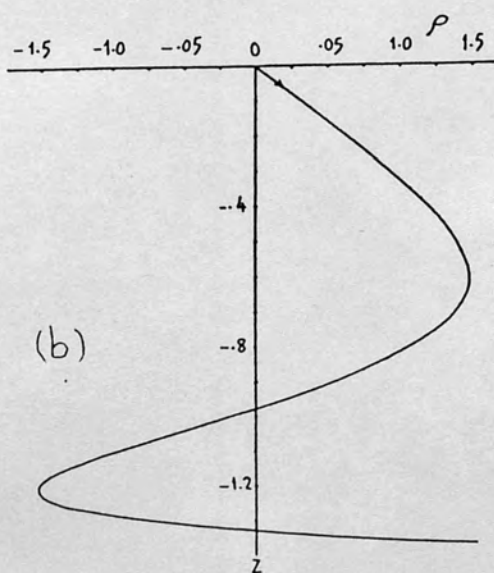
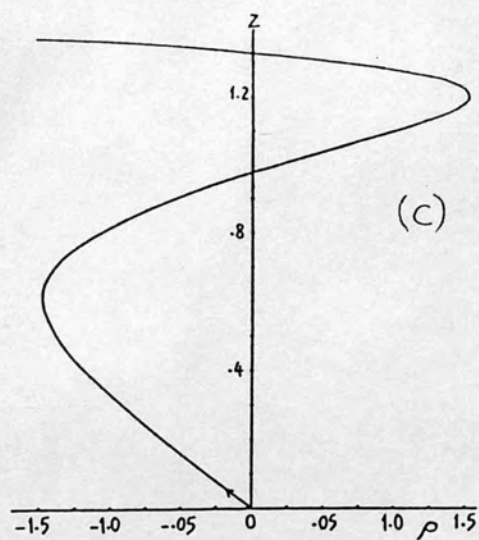
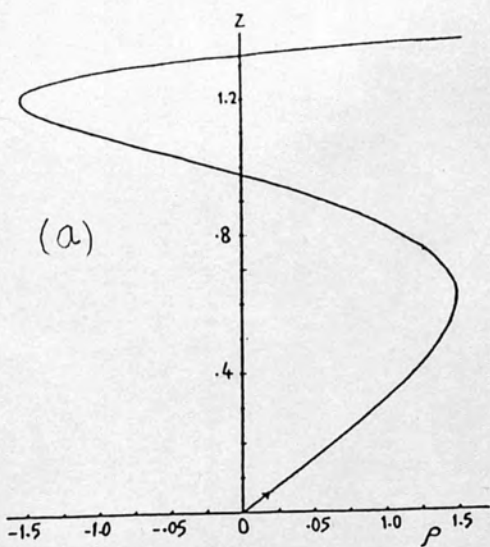


Figure (9.2.5). The periodic orbits of the subclass CII4.

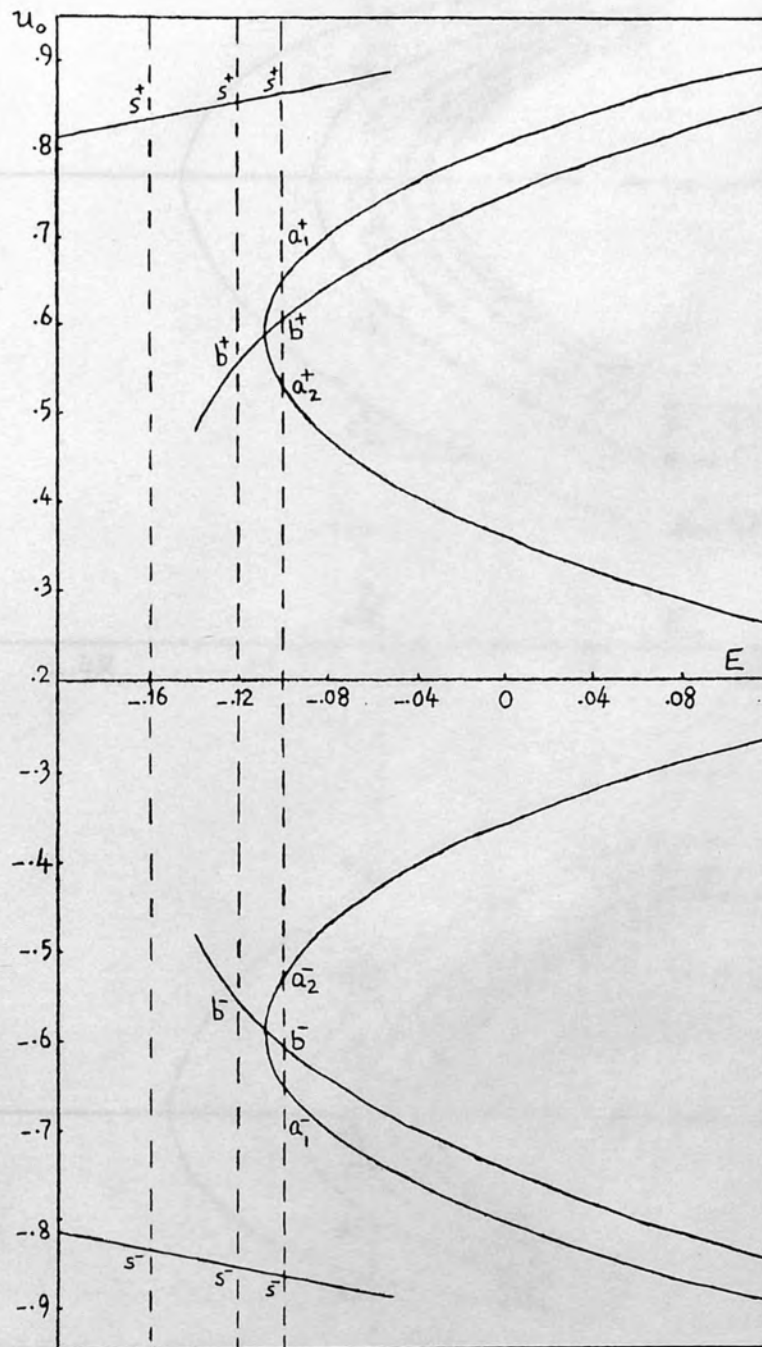


Figure (9.3.1). The zeros u^0 , defined in (9.1.3), plotted against the energy parameter E at three different energies: $E = -0.16$, $E = -0.12$ and $E = -0.1$, are shown. The elements of the last set $A(-0.1)$ is given in (9.1.4).

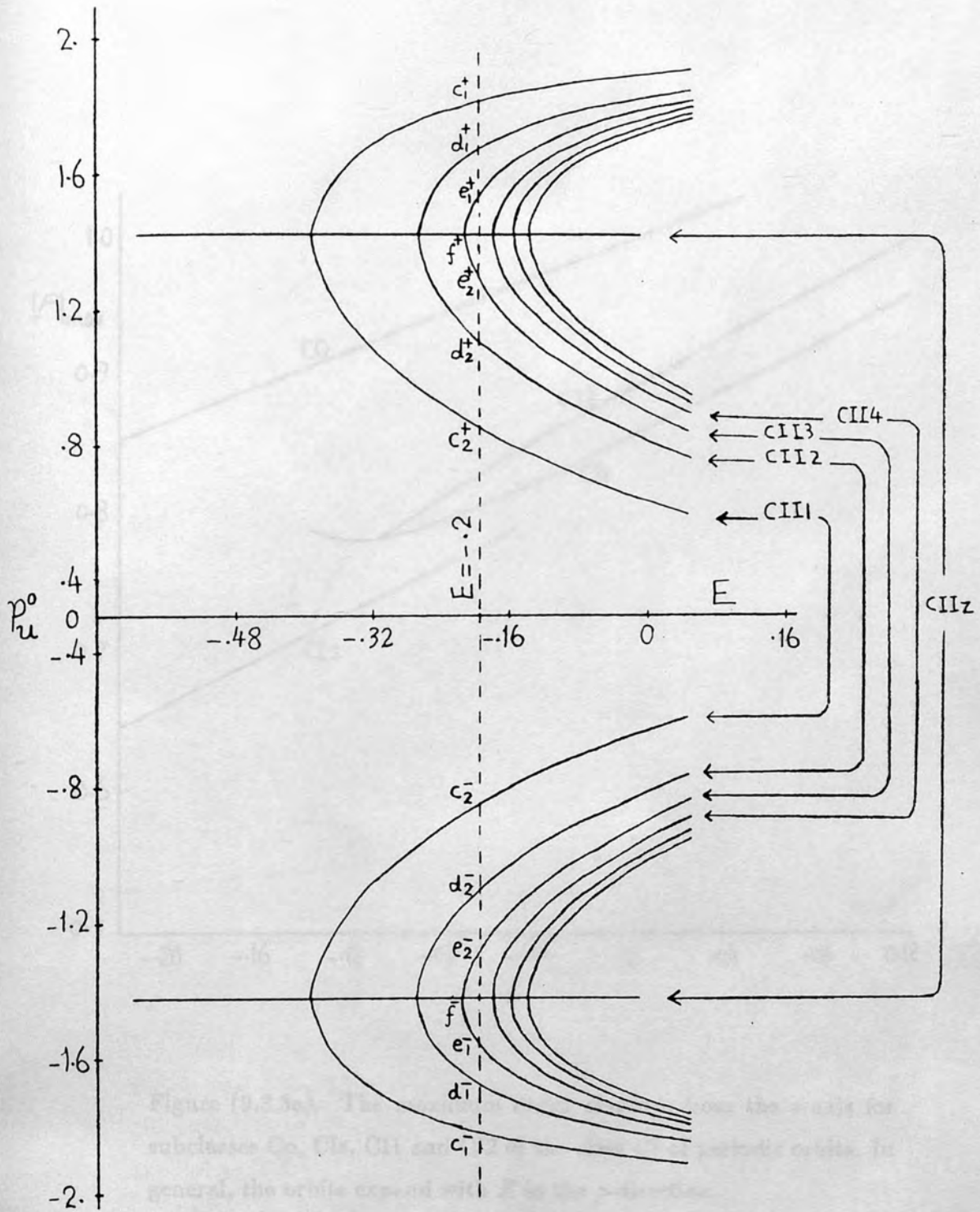


Figure (9.3.2). The zeros p_u^0 , defined in (9.2.3), plotted against the energy parameter E . The elements of the set $B(-0.2)$, in (9.2.4), are shown.

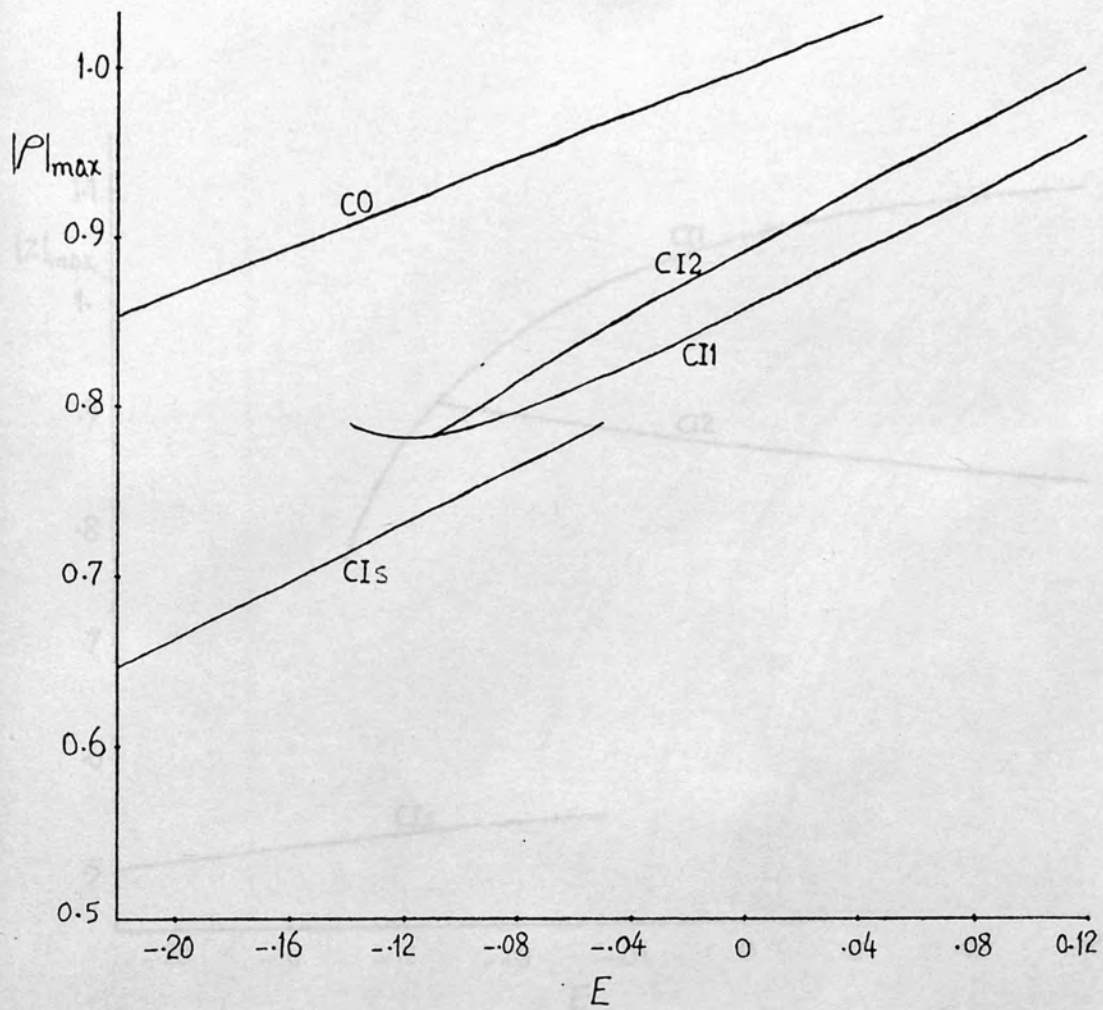


Figure (9.3.3a). The maximum radial distance from the z -axis for subclasses Co , CI_3 , CI_1 and CI_2 of the class CI of periodic orbits. In general, the orbits expand with E in the ρ -direction.

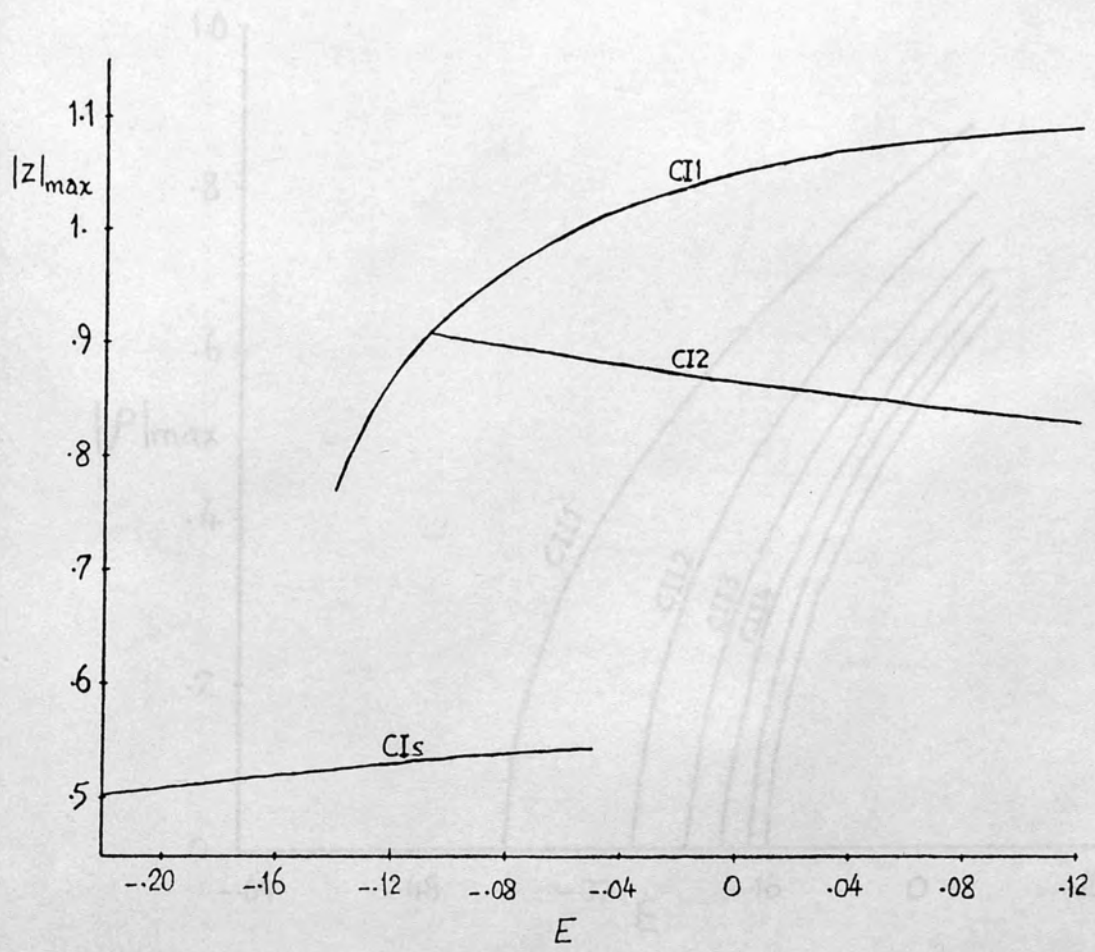


Figure (9.3.3b). A plot of $|z|_{\max}$ against E for the subclasses CI_1 , CI_2 and CI_3 of the class CI of periodic orbits. While some orbits expand with E in the z -direction, others shrink.

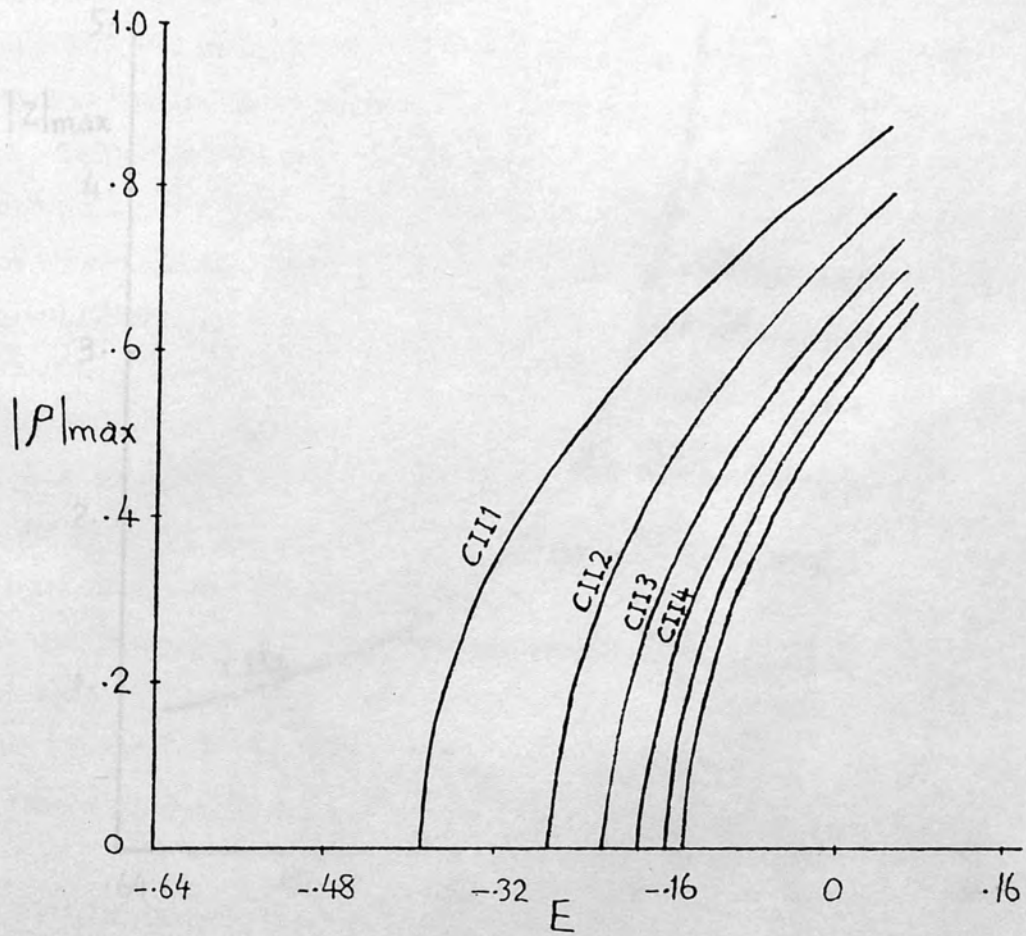


Figure (9.3.4a). The maximum distance from the z -axis for various subclasses CII_n , $n = 1, 2, \dots, 6$, of the class CII of periodic orbits. All these orbits expand substantially with E in the ρ -direction.

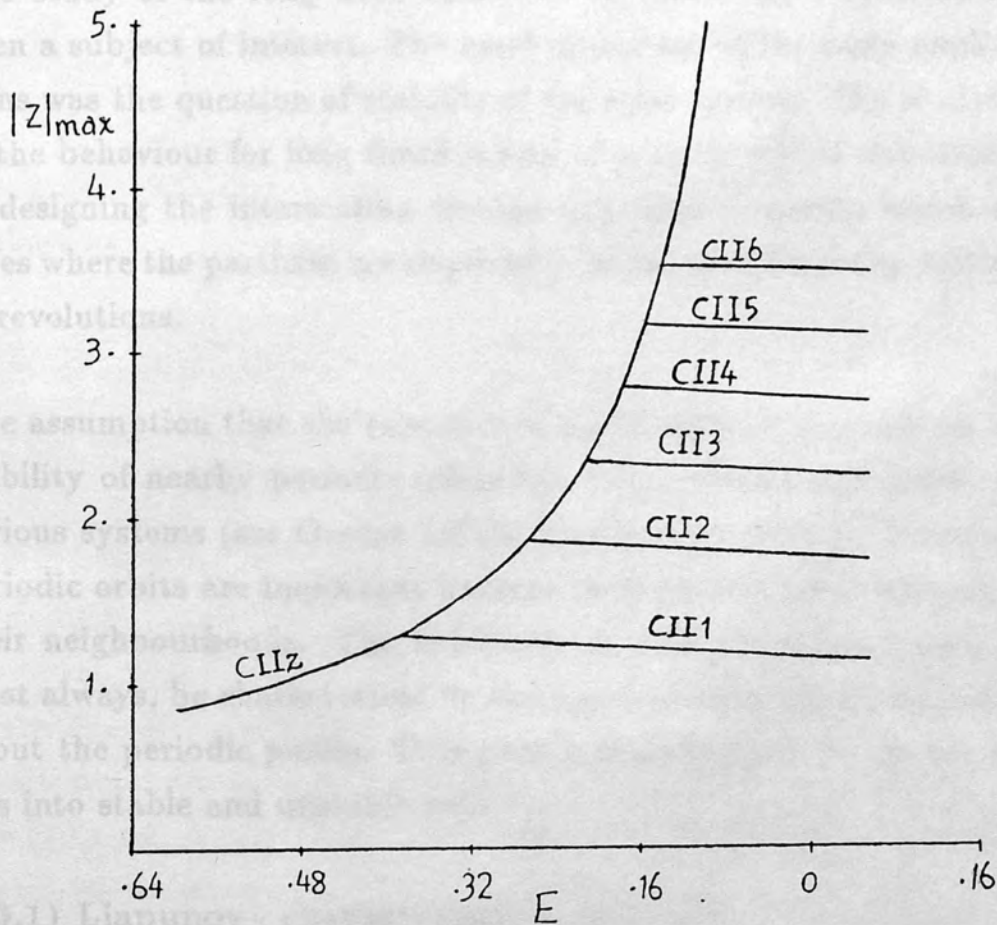


Figure (9.3.4b). A plot of $|z|_{\max}$ against E for the subclasses CIIz, CII n , $n = 1, 2, \dots, 6$, of periodic orbits. The subclasses CIIz expand along the z -axis very rapidly with E . For all other subclasses CII n , $|z|_{\max}$ decreases slightly with E .

CHAPTER (10)

Stability of periodic orbits

The study of the long time behaviour in conservative systems has been a subject of interest. The most important of the early applications was the question of stability of the solar system. The studying of the behaviour for long times is now of great practical importance in designing the intersecting storage rings and magnetic fusion devices where the particles are required to be trapped for many millions of revolutions.

The assumption that the existence of KAM surfaces depends on the stability of nearby periodic orbits has been verified and tested for various systems (see Greene 1979b, also Greene 1979a). Therefore, periodic orbits are important because they govern the behaviour in their neighbourhoods. The behaviour in a neighbourhood can, almost always, be characterised by the eigenvalues of the linearisation about the periodic points. This gives a classification of periodic orbits into stable and unstable ones.

(10.1) Liapunov characteristic exponents.

The stability of types of motion of dynamical systems may be discussed by the aid of certain constants to which Poincaré has given the name characteristic exponents (more commonly Liapunov exponents). These constants provide a computable quantitative measure of the degree of stochasticity for a trajectory. For a given trajectory they characterize the mean exponential rate of divergence of trajectories surrounding it. In this section and the following (section 10.2) we define the characteristic exponents of a periodic orbit and describe their properties placing special emphasis on autonomous

Hamiltonian systems. A detailed discussion is given by Whittaker 1964, chapter (XV).

Consider any set of differential equations

$$\frac{dx_i}{dt} = f_i \quad i = 1, 2, \dots, n \quad (10.1.1)$$

where (f_1, f_2, \dots, f_n) are functions of (x_1, x_2, \dots, x_n) and possibly also of the time t , having a period \mathcal{T} in t . In *vector* notation (10.1.1) is written as

$$\frac{dx}{dt} = f(x). \quad (10.1.2)$$

Suppose that a periodic solution is known

$$x = \Phi(t), \quad \Phi(t + \mathcal{T}) = \Phi(t). \quad (10.1.3)$$

In order to investigate solutions adjacent to this, we write

$$x = \Phi(t) + \xi \quad (10.1.4)$$

where $\xi = (\delta x_1, \delta x_2, \dots, \delta x_n)$ is the vector whose components are the infinitesimal quantities $\delta x_1, \delta x_2, \dots, \delta x_n$. Since both solutions satisfy (10.1.2), then to first order approximation of the infinitesimal quantities we have

$$\frac{d\xi}{dt} = \frac{\partial f}{\partial x} \cdot \xi \quad (10.1.5)$$

where $\frac{\partial f}{\partial x}$ is an $n \times n$ matrix: $(f_{ik})_{i,k=1}^n$ whose elements are given by

$$f_{ik} = \frac{\partial f_i}{\partial x_k}, \quad i, k = 1, 2, 3, \dots, n \quad (10.1.6)$$

The system of n equations expressed by (10.1.5) is called the variational equations of the system (10.1.2). Furthermore, (10.1.2) together with (10.1.5) may be regarded as a set of $2n$ equations in which the components $x_1, x_2, \dots, x_n, \xi_1, \xi_2, \dots, \xi_n$ are the dependent variables. If x_0 and $x_0 + \xi_0$ are nearby initial vectors, these vectors

evolve with time yielding a vector $\xi(x_0, t)$ called the tangent vector. If a *particular* solution x of (10.1.2) is known, we can substitute in (10.1.5) to determine ξ i.e. to determine the solutions of the original system (10.1.2) which are adjacent to the known particular solution.

As (10.1.5) represents a system of linear differential equations with coefficients periodic in t , it is known from the theory of linear differential equations that ξ_i will be of the form

$$\xi_i = \sum_{k=1}^n S_{ik}(t)e^{\alpha_k t}, \quad i = 1, 2, 3, \dots, n \quad (10.1.7)$$

where the coefficients S_{ik} are periodic with period T and α_k are *constants* which are called the *characteristic exponents* of the periodic solution.

If all the characteristic exponents are purely imaginary, ξ can be expressed as sums and products of purely periodic terms, while this is not the case if they are not all purely imaginary. Hence a necessary condition for stability of the periodic orbit is that all the characteristic exponents must be such that $Re(\alpha_k) \leq 0$. Furthermore, when t is not contained explicitly in the right hand side of (10.1.2), one of the characteristic exponents of every periodic solution is zero (see Whittaker, 1964 section 174).

(10.2) The characteristic exponents of a Hamiltonian system.

We consider now in particular a conservative dynamical system. For simplicity, we suppose that this system has two degrees of freedom. With generalised coordinates q_1, q_2 and generalised momenta p_1, p_2 , Hamilton's equations of motion take the form

$$\frac{dx}{dt} = J \nabla H, \quad (10.2.1)$$

where

$$\mathbf{x} = (x_1, x_2, x_3, x_4) = (q_1, p_1, q_2, p_2)$$

and

$$\mathbf{J} = \begin{bmatrix} 0 & 1 & 0 & 0 \\ -1 & 0 & 0 & 0 \\ 0 & 0 & 0 & 1 \\ 0 & 0 & -1 & 0 \end{bmatrix} \quad (10.2.2)$$

Let $\mathbf{x} = \mathbf{X}(t)$ be a periodic solution with period T and let

$$\mathbf{x} = \mathbf{X}(t) + \boldsymbol{\xi} \quad (10.2.3)$$

be an adjacent solution to the periodic solution. The variational equations (10.1.5), using Hamilton's equations of motion, take the form

$$\frac{d\boldsymbol{\xi}}{dt} = \begin{bmatrix} H_{21} & H_{22} & H_{23} & H_{24} \\ -H_{11} & -H_{12} & -H_{13} & -H_{14} \\ H_{41} & H_{42} & H_{43} & H_{44} \\ -H_{31} & -H_{32} & -H_{33} & -H_{34} \end{bmatrix} \cdot \boldsymbol{\xi} \quad (10.2.4)$$

where $\boldsymbol{\xi}$ is a vector with components $\xi_1, \xi_2, \xi_3, \xi_4$ and the elements $H_{ij}(=H_{ji})$ of the 4×4 matrix in (10.2.4)

$$H_{ij} = \frac{\partial^2 H}{\partial x_i \partial x_j}, \quad i, j = 1, 2, 3, 4,$$

are evaluated along $\mathbf{X}(t)$. For another adjacent solution we assume we have a tangent vector $\boldsymbol{\xi}'$ which satisfies (10.2.4). With a little algebra the two systems of variational equations for $\boldsymbol{\xi}$ and $\boldsymbol{\xi}'$ give

$$\xi_1 \xi_2' + \xi_3 \xi_4' - \xi_1' \xi_2 - \xi_3' \xi_4 = \text{constant}. \quad (10.2.5)$$

Let

$$\bar{\boldsymbol{\xi}} = \mathbf{M}\boldsymbol{\xi} \quad (10.2.6)$$

where $\boldsymbol{\xi}$ is the tangent vector of an orbit adjacent to a closed orbit at the beginning of a period and $\bar{\boldsymbol{\xi}}$ is its value at the end of that period and \mathbf{M} is a 4×4 matrix; $\mathbf{M} = (M_{ij})_{i,j=1}^4$. From (10.2.5) we get

$$\xi_1 \xi_2' + \xi_3 \xi_4' - \xi_1' \xi_2 - \xi_3' \xi_4 = \bar{\xi}_1 \bar{\xi}_2' + \bar{\xi}_3 \bar{\xi}_4' - \bar{\xi}_1' \bar{\xi}_2 - \bar{\xi}_3' \bar{\xi}_4. \quad (10.2.7)$$

Substituting from (10.2.6) into the right hand side of (10.2.7) and equating the coefficients, we have a set of equations which can be expressed in the matrix notation

$$\mathbf{K} = \mathbf{M}'\mathbf{K}\mathbf{M} \quad (10.2.8)$$

where

$$\mathbf{K} = \begin{bmatrix} 0 & 1 & 0 & 0 \\ -1 & 0 & 0 & 0 \\ 0 & 0 & 0 & 1 \\ 0 & 0 & -1 & 0 \end{bmatrix}$$

and \mathbf{M}' is the conjugate of \mathbf{M} . Then $(\mathbf{M}')^{-1} = \mathbf{K}\mathbf{M}\mathbf{K}^{-1}$ which shows that $(\mathbf{M}')^{-1}$ has the same eigenvalues as \mathbf{M} , and therefore that \mathbf{M}^{-1} has the same eigenvalues as \mathbf{M} , and therefore that the set of eigenvalues of \mathbf{M} (G say) is the same as the set of their reciprocals.

We notice that the matrix \mathbf{K} and the matrix \mathbf{J} (in (10.2.2)) are the same.

Now assume that

$$\bar{\xi} = \lambda\xi \quad (10.2.9)$$

From (10.2.6) and (10.2.9) we see that λ must be an eigenvalue of \mathbf{M} . From the last section, any solution of (10.2.4) is of the form

$$\xi_i = \sum_{k=1}^n S_{ik}(t) e^{\alpha_k t}, \quad i, k = 1, 2, \dots, n. \quad (10.2.10)$$

where α_k 's are the characteristic exponents and S_{ik} 's are periodic functions of period \mathcal{T} . Equation (10.2.9) can be satisfied only by considering one single characteristic exponent in (10.2.10) i.e. by

$$\xi_i = S_{ii}(t) e^{\alpha_i t}, \quad i = 1, 2, \dots, n. \quad (10.2.11)$$

Substituting from (10.2.11) into (10.2.9) we get

$$S_{ii}(\mathcal{T}) e^{\alpha_i \mathcal{T}} = \lambda S_{ii}(0),$$

or more that after a T -1 period, the orbit returns

$$\lambda = e^{\alpha_i T} \quad (10.2.12)$$

Since if $\lambda_i (= e^{\alpha_i T}) \in G$, then $\lambda_i^{-1} (= e^{-\alpha_i T}) \in G$, we conclude that for the differential equations of a Hamiltonian system, the characteristic exponents of any periodic solution may be arranged in pairs, the exponents of each pair are equal in magnitude but opposite in sign.

For an autonomous Hamiltonian system with two degrees of freedom the set of eigenvalues G takes the form

$$G = \{1, 1, e^{\alpha T}, e^{-\alpha T}\} \quad (10.2.13)$$

(10.3) Linearization of a map (calculating the characteristic exponents of periodic orbits).

In this section we derive the 2×2 linearisation matrix of the Poincaré mappings for an autonomous Hamiltonian system with two degrees of freedom. This is a technique developed by J.M.Greene (1979a) for calculating the characteristic exponents (see section (10.2)) of a periodic orbit. The method works well even for unstable periodic orbits with not very long periods (see Carnegie 1984).

Let a Hamiltonian system, with two degrees of freedom, be given by

$$H(u, p_u, v, p_v) = E.$$

For convenience we change the notation for the momenta: $\mu = p_u$ and $\vartheta = p_v$. We consider a periodic orbit $\mathbf{x}_0(t) = (u_0(t), \mu_0(t), v_0(t), \vartheta_0(t))$ with period T starting at the point p $(u_0(0), \mu_0(0))$ on the surface of section defined by

$$v = 0, \quad \vartheta > 0. \quad (10.3.1)$$

Assume that after $N \geq 1$ intersections with (10.3.1) the orbit returns to the point p . We compute the 2×2 matrix which is the linearisation of T^N about p .

Let $x_1(t)$ and $x_2(t)$ be two neighbouring orbits to $x_0(t)$ and given by

$$x_1(t) = (u_1(t), \mu_1(t), v_1(t), \vartheta_1(t))$$

$$x_2(t) = (u_2(t), \mu_2(t), v_2(t), \vartheta_2(t))$$

with starting points $x_1(0)$ and $x_2(0)$ on the surface of section (10.3.1).

Let $\delta x_1(t)$ and $\delta x_2(t)$, given by

$$\delta x_1(t) = x_1(t) - x_0(t),$$

$$\delta x_2(t) = x_2(t) - x_0(t) \quad (10.3.2)$$

be two independent linearisations of $x_0(t)$. Hamilton's equations of motion are

$$\frac{dx}{dt} = \mathbf{J} \nabla H |_{x(t)} \quad (10.3.3)$$

where \mathbf{J} is the matrix given in (10.2.2),

$\nabla = (\frac{\partial}{\partial u}, \frac{\partial}{\partial \mu}, \frac{\partial}{\partial v}, \frac{\partial}{\partial \vartheta})$ and $|_{x(t)}$ means evaluated along $x(t)$.

The variational equations for $x_0(t)$ are (see 10.2.4)

$$\frac{d\delta x(t)}{dt} = \begin{bmatrix} H_{\mu u} & H_{\mu\mu} & H_{\mu v} & H_{\mu\vartheta} \\ -H_{uu} & -H_{u\mu} & -H_{uv} & -H_{u\vartheta} \\ H_{\vartheta u} & H_{\vartheta\mu} & H_{\vartheta v} & H_{\vartheta\vartheta} \\ -H_{vu} & -H_{v\mu} & -H_{vv} & -H_{v\vartheta} \end{bmatrix} \cdot \delta x(t) \quad (10.3.4)$$

where $\delta x(t)$ is the vector $\delta x(t) = (\delta u(t), \delta \mu(t), \delta v(t), \delta \vartheta(t))$ and the matrix elements H_{ij} , $i, j = u, \mu, v, \vartheta$ are evaluated along $x_0(t)$

Since $\mathbf{x}_1(t)$ and $\mathbf{x}_2(t)$ are assumed to lie on the energy surface S_E :

$$H(u, \mu, v, \vartheta) = E,$$

$$\delta H = \nabla H |_{\mathbf{x}_0(t)} \cdot \delta \mathbf{x}_i = 0, \quad i = 1, 2 \quad (10.3.5)$$

Since we assumed that at $t = 0$ all orbits $\mathbf{x}_0(t)$, $\mathbf{x}_1(t)$ and $\mathbf{x}_2(t)$ start on the surface of section (10.3.1), then the two linearisations $\delta \mathbf{x}_1(0)$ and $\delta \mathbf{x}_2(0)$, at $t = 0$, lie on the surface $v = 0$. Therefore, $\delta v_1(0) = \delta v_2(0) = 0$. We choose $\delta \mathbf{x}_1(0)$ and $\delta \mathbf{x}_2(0)$ along the u -axis and μ -axis respectively. Then $\delta \mu_1(0) = 0$ and $\delta u_2(0) = 0$. Then

$$\delta \mathbf{x}_1(0) = (\delta u_1(0), 0, 0, \delta \vartheta_1(0))$$

$$\delta \mathbf{x}_2(0) = (0, \delta \mu_2(0), 0, \delta \vartheta_2(0))$$

With the two solutions $\delta \mathbf{x}_1(t)$ and $\delta \mathbf{x}_2(t)$ normalized we get, using (10.3.5), normalised initial conditions:

$$\begin{aligned} \delta \mathbf{x}_1(0) &= (1, 0, 0, -\frac{H_u(0)}{H_\vartheta(0)}), \\ \delta \mathbf{x}_2(0) &= (0, 1, 0, -\frac{H_\mu(0)}{H_\vartheta(0)}). \end{aligned} \quad (10.3.6)$$

At $t = T$ the two orbits $\mathbf{x}_1(t)$ and $\mathbf{x}_2(t)$ do not necessarily intersect (10.3.1) i.e. $\delta v_1(T) \neq 0$ and $\delta v_2(T) \neq 0$. We assume that they intersect the surface of section (10.3.1) at times $t_1 = T - \delta t_1$ and $t_2 = T - \delta t_2$ respectively. Then

$$\begin{aligned} \delta t_i &= \frac{\delta v_i}{\dot{v}_i} |_{t=T} \\ &= \frac{\delta v_i}{H_\vartheta} |_{\mathbf{x}_0(T)} \end{aligned} \quad (10.3.7)$$

To first order in time we get, by Taylor's expansion

$$\mathbf{x}_i(T - \delta t_i) - \mathbf{x}_i(T) = -\mathbf{J} \nabla H |_{\mathbf{x}_0(T)} \delta t_i, \quad i = 1, 2 \quad (10.3.8)$$

Substituting for δt_i from (10.3.7), (10.3.8) takes the form

$$\mathbf{x}_i(T - \delta t_i) - \mathbf{x}_i(T) = -\mathbf{J}\nabla H|_{\mathbf{x}_0(T)} \cdot \frac{\delta v_i}{H_\vartheta}|_{\mathbf{x}_0(T)} \quad i = 1, 2 \quad (10.3.9)$$

At times $t_i = T - \delta t_i$, $i = 1, 2$, the changes in u and μ due to changes in $u_0(0)$, $\mu_0(0)$, through $\delta \mathbf{x}_1(0)$ and $\delta \mathbf{x}_2(0)$, are given by the vectors $\overline{\delta \mathbf{x}}_i$ which lie on the surface $v = 0$ and are defined by

$$\begin{aligned} \overline{\delta \mathbf{x}}_i &= \delta \mathbf{x}_i(T) + [\mathbf{x}_i(T - \delta t_i) - \mathbf{x}_i(T)] \\ &= \delta \mathbf{x}_i(T) - \mathbf{J}\nabla H|_{\mathbf{x}_0(T)} \cdot \frac{\delta v_i}{H_\vartheta}|_{\mathbf{x}_0(T)} \end{aligned} \quad (10.3.10)$$

Then on (10.3.1) we have the 2×2 matrix

$$\mathcal{M} = \begin{bmatrix} \frac{\partial u}{\partial u_0} & \frac{\partial u}{\partial \mu_0} \\ \frac{\partial \mu}{\partial u_0} & \frac{\partial \mu}{\partial \mu_0} \end{bmatrix} = \begin{bmatrix} (\overline{\delta \mathbf{x}}_1)_u(T) & (\overline{\delta \mathbf{x}}_2)_u(T) \\ (\overline{\delta \mathbf{x}}_1)_\mu(T) & (\overline{\delta \mathbf{x}}_2)_\mu(T) \end{bmatrix} \quad (10.3.11)$$

where $(\overline{\delta \mathbf{x}}_1)_u(T)$ denotes the u -component of $\overline{\delta \mathbf{x}}_1$ at $t = T$, ... etc. Substituting from (10.3.10) into (10.3.11), we get

$$\mathcal{M} = \begin{bmatrix} \delta u_1(T) - \left(\frac{H_u}{H_\vartheta}\right)|_{\mathbf{x}_0(T)} \delta v_1(T) & \delta u_2(T) - \left(\frac{H_u}{H_\vartheta}\right)|_{\mathbf{x}_0(T)} \delta v_2(T) \\ \delta \mu_1(T) - \left(\frac{H_\mu}{H_\vartheta}\right)|_{\mathbf{x}_0(T)} \delta v_1(T) & \delta \mu_2(T) - \left(\frac{H_\mu}{H_\vartheta}\right)|_{\mathbf{x}_0(T)} \delta v_2(T) \end{bmatrix} \quad (10.3.12)$$

To compute the elements \mathcal{M}_{ij} of the matrix \mathcal{M} we integrate Hamilton's equations (10.3.3) with initial conditions at the fixed point p together with the variational equations (10.3.4) with initial conditions given by (10.3.6).

Since we have a Hamiltonian flow, T is area preserving. The eigenvalues of the linearised mapping are the roots of the equation

$$\det(\mathcal{M} - \lambda I) = 0,$$

where I is the 2×2 unit matrix, or

$$\lambda^2 - \lambda \text{Tr} \mathcal{M} + 1 = 0, \quad (10.3.13)$$

where we have set $\det \mathcal{M} = 1$ in (10.3.13) because of the area-preserving property. $\text{Tr} \mathcal{M}$ is the trace $\mathcal{M}_{11} + \mathcal{M}_{22}$ of the matrix \mathcal{M} . Results from section (4.3.1) give the following possibilities :

- (1) $|\text{Tr} \mathcal{M}| < 2$ and the periodic orbit is stable.
- (2) $|\text{Tr} \mathcal{M}| > 2$ and the periodic orbit is unstable.
- (3) $|\text{Tr} \mathcal{M}| = 2$ and the corresponding fixed point p is either stable or unstable and needs nonlinear stability analysis.

From section (4.3) we see that the eigenvalues λ_1 and λ_2 lie on the real axis or the unit circle, i.e. lie in the set

$$\lambda_1, \lambda_2 \in \ominus = \text{the unit circle} \cup \lambda_{Re}$$

which we denote \ominus .

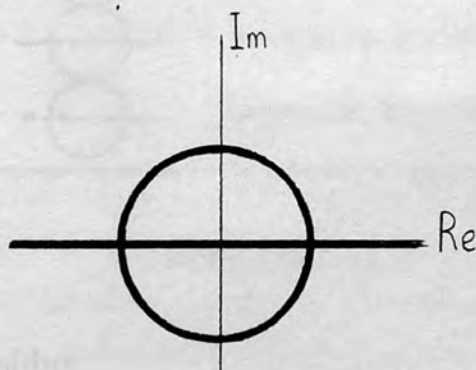


Figure (10.3.1). $\lambda_1, \lambda_2 \in \ominus$

From section (10.2) we see that $\lambda_1 = e^{\alpha T}$ and $\lambda_2 = e^{-\alpha T}$ where α and $-\alpha$ are the non-vanishing pair of characteristic exponents. This is because, in general, $\text{Tr} \mathcal{M}$ is not identically 2 for one-parametered mappings.

To sum up, if $p(u_0, \mu_0)$ is a periodic point of a map T , with period N ,

the behaviour (to first order) of nearby orbits is given by a matrix \mathcal{M} (called a tangent map) such that

$$\delta \mathbf{x} = \mathcal{M} \delta \mathbf{x}_0.$$

The exponential part (if any) of the behaviour is given by the eigenvalues of \mathcal{M} (or the multipliers of the periodic orbit). For area-preserving maps we have the following possibilities

Trace \mathcal{M}	$\lambda, \frac{1}{\lambda} \in \Theta$	Name of p	Residue
$\text{Tr} \mathcal{M} > 2$		ordinary hyperbolic	$R < 0$
$\text{Tr} \mathcal{M} = 2$		ordinary parabolic	$R = 0$
$ \text{Tr} \mathcal{M} < 2$		elliptic	$0 < R < 1$
$\text{Tr} \mathcal{M} = -2$		inversion parabolic	$R = 1$
$\text{Tr} \mathcal{M} < -2$		inversion hyperbolic	$R > 1$

Table (10.3.1)

where R is the residue

$$R = \frac{1}{4}(2 - \text{Tr} \mathcal{M}) \quad (10.3.14)$$

explained in section (4.3.2)

A good description of the dynamics of area-preserving maps is given by MacKay (1985).

(10.4) Stability of the periodic orbits in the classes CI and CII.

We study the stability of the periodic orbits shown in chapters (8) and (9) by calculating the residue (10.3.14) at gradually increasing value of E . For each orbit, $R(E)$ is calculated over a bounded range of E which is chosen to determine the general stability behaviour of that orbit through a plot of $R(E)$ versus E .

Figure (10.4.1) shows the residue $R(E)$ against E for the planar motions in the xy -plane (i.e. the subclass Co). From this figure we notice that for $E < -1.2$, $0 < R \ll 1$ and then R increases gradually to the value 1 at $E = -0.3$ where the curve touches the line $R = 1$ and then R decreases monotonically, passing through zero at $E = -0.127$, to negative values. Hence the planar motion is stable in the range $E < -0.127$ and unstable for $E > -0.127$ and the corresponding fixed point at the origin of the surface of section is an elliptic point for $E < -0.127$ (figures (7.2.1)) but an ordinary hyperbolic one for $E > -0.127$.

We found that periodic orbits belonging to the same subclass in either classes CI or CII have the same E, R -plots. Thus we were able to study the stability of these orbits by studying the stability of a single member of each subclass.

(10.4.1) Stability of periodic orbits of class CI.

Figure (10.4.1.1) is the upper (or positive) half of figure (9.3.1) It shows curves denoted by s^+ , b^+ , a_1^+ , a_2^+ , h_1^+ and h_2^+ at the middle of each curve. Each curve represents the u -component of a fixed point on the surface of section as a function of E . The full curves denote stability and the broken curves denote instability. We will

have to return to this figure, throughout this section, as we shall be describing the stability of these fixed points.

Figure (10.4.1.2) shows the residue R against E for the orbit through the point s^+ . We notice that $R < 0$ over the range $E > -0.05$ (we were not able to locate this orbit for E in the range $E < -0.05$). Since R is always negative, the fixed point s^+ is ordinary hyperbolic; a result which is confirmed by the surfaces of section plots in section (7.2). A magnified plot of the surface of section surrounding the point s^+ is shown in figure (10.4.1.3)

Figure (10.4.1.4) is a plot of the residue R versus E for the orbit shown in figure (9.1.4(a)) which corresponds to the fixed point b^+ in figure (10.4.1.1). We would expect the residue to take the value zero when the fixed point b^+ is created. However, it was difficult to locate the precise energy E at which b^+ is created because of the rapid variation of b^+ with E just after its birth. Figure (10.4.1.4) shows R increasing until it touches the line $R = 1$ and then decreases, passing through the value $R = 0$ (at $E = -0.1085$) to negative values. This means that the fixed point b^+ is elliptic over an interval δE_1 with $E \simeq -0.1085$ as an upper limit and the orbit (9.1.4(a)) is stable. Beyond this limit b^+ becomes ordinary hyperbolic and the orbit is unstable. At $E = -0.1085$, two other fixed points a_1^+ and a_2^+ (figure (10.4.1.1)) are created. Equivalently; two periodic orbits (9.1.5(a)) and (9.1.5(c)), respectively, appear at this value. They are of the same period as the original one at b^+ . This type of bifurcation is not commonly found in most maps but we find it frequently for the class of orbits CII which we describe in the next section. Figure (10.4.1.5) shows the residue of these bifurcated orbits. R increases monotonically from zero at $E = -0.1085$, then through the value $R = 1$

(at $E = -0.1017$) to higher positive values. This indicates that over the interval $\delta E_2 \equiv (-0.1085, -0.1017)$ the two fixed points a_1^+ and a_2^+ are elliptic and the orbits (9.1.5(a)) and (9.1.5(c)) are stable. For $E > -0.1017$, a_1^+ and a_2^+ are inversion hyperbolic and the orbits (9.1.5(a)) and (9.1.5(c)) are unstable. As R crosses 1 (at $E = -0.1017$), two other elliptic fixed points h_1^+ and h_2^+ (figure (10.4.1.1)) are created from a_2^+ whereas a_2^+ itself changes from an elliptic point to an inversion hyperbolic one. Equivalently; two other stable periodic orbits of twice the period (of the parent orbit) appear at $E = -0.1017$. They remain stable over an interval δE_3 shorter than δE_2 . These orbits are shown in figure (10.4.1.6). This last behaviour of the residue repeats (for these orbits) over an interval δE_4 of E which is shorter than δE_3 (figure (10.4.1.7)). This type of bifurcation (with period doubling) is common in most maps (see section (4.3.6)).

(10.4.2) Stability of periodic orbits of class CII.

As in the previous section, figure (10.4.2.1) is the upper (or the positive) half of figure (9.3.2). It shows curves denoted by c_1^+ , d_1^+ , e_1^+ , f^+ , e_2^+ , d_2^+ and c_2^+ at the middle of each curve. Each curve represents the p_u -component of a fixed point, on the surface of section, as a function of E . The full curves denote stability and the broken curves denote instability. We will have to return to this figure, throughout this section, as we describe the stability of the various fixed points.

The fixed point f^+ corresponds to a periodic orbit exhibiting, to an acceptable approximation, a linear motion along the positive z -axis. We called this orbit OZ (see section 9.2). This particular motion is of central interest because, as we shall see, it is responsible for the appearance of a sequence of periodic orbits, a phenomenon dependent on the stability of the orbit OZ .

Typically the residue of a fixed point starts at zero when the point is created and increases until the point bifurcates to produce two others of twice the period when the residue passes through unity (Greene *et al*, 1981), (see last section). However the residue of the fixed points corresponding to the orbits of this class (class CII) behaves differently.

Figure (10.4.2.2) shows the residue R , against E , for the fixed point f^+ . R oscillates about zero between constant maxima $R = 1$ and varying minima $R < 0$, indicating the existence of a sequence of stable-unstable motion. These minima decrease monotonically with E until the periodic orbit OZ escapes at $E = 0$. This figure (figure (10.4.2.2)) shows that R starts from zero in the completely regular regime and increases to unity, it then decreases, passing through zero (at $B1$) when f^+ changes from an elliptic to a hyperbolic point and two other elliptic fixed points c_1^+ and c_2^+ are created. Equivalently; OZ becomes unstable, and simultaneously bifurcates to produce two more stable periodic orbits of the same period. These two orbits are shown in figures (9.2.2(a)) and (9.2.2(c)) respectively. The orbit OZ remains unstable until R passes through zero from negative to positive values (at S_1) when it regains its stability and remains stable for some range of E until it passes through zero (at $B2$) to produce the second generation of newly born stable periodic orbits of the same period (figures (9.2.3(a)) and (9.2.3(c)) when again OZ itself becomes unstable. This process repeats many times until $E = 0$. For a conservation of Poincaré index at each point of the points S_1, S_2, \dots , we would expect the existence of a pair of elliptic fixed points which are absorbed at this point i.e. an inverse bifurcation (type $T3$ in section (4.3.6)).

The residues of the bifurcated orbits also behave in a non-generic manner: R first increases from zero to unity and then decreases monotonically through zero to negative values (figures (10.4.2.3)) indicating that each orbit remains unstable for all subsequent values of E .

This can be supported by displaying some surfaces of section: figure (10.4.2.4(a)) shows two surfaces of section before and after the bifurcation at $B1$ and figure (10.4.2.4(b)) shows two surfaces of section before and after the bifurcation at $B2$. In each case an elliptic point changes to a hyperbolic point and two other elliptic points are created.

(10.4.3) The dependence of the angles of emission of the periodic orbits of class CII on E .

We saw in chapter (9) that all the orbits of class CII start from the origins of both the uv -plane and ρz -plane. Let ψ_0 be the initial angle that an orbit, in the uv -plane, makes with the positive v -axis at the origin. Then

$$\psi_0 = \tan^{-1}\left(\frac{p_u^0}{p_v^0}\right) \quad (10.4.3.1)$$

Figure (10.4.3.1) corresponds to figure (10.4.2.1). It is a plot of the angle ψ_0 versus E and we notice that the fixed point f^+ corresponds to $\psi_0 = \frac{\pi}{4}$.

The initial polar angle θ_0 that an orbit makes with the z -axis in the ρz -plane can be derived from equations (7.1.16) and (7.1.17).

$$\tan \theta_0 = \frac{p_\rho^0}{p_z^0} = \lim_{\rho, z \rightarrow 0} \left(\frac{\mathbf{N} \cdot \mathbf{R}}{\mathbf{N} \cdot \mathbf{S}} \right), \quad (10.4.3.2)$$

where \mathbf{N} and \mathbf{R} and \mathbf{S} are the vectors defined by

$$\mathbf{N} = (u, v), \quad \mathbf{R} = (p_u, -p_v), \quad \mathbf{S} = (p_v, p_u). \quad (10.4.3.3)$$

At the origin we have $|\mathbf{R}| = |\mathbf{S}| = |\mathbf{p}^0| = 2$ (see equation (9.2.1)). Then

$$\frac{p_\rho^0}{p_z^0} = \frac{\hat{e}_N \cdot \hat{e}_R}{\hat{e}_N \cdot \hat{e}_S} = \frac{\cos(N, R)}{\cos(N, S)} \quad (10.4.3.3)$$

where \hat{e}_N , \hat{e}_R and \hat{e}_S are the unit vectors of N , R and S respectively and $\cos(N, R)$ denotes the cosine of the angle between N and R , ... etc.

Since at the origin the orbit is in the direction \hat{e}_N , then using the triangle similarity relations in figure (10.4.3.2) we get

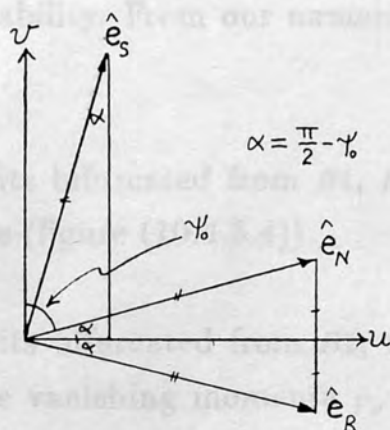


Figure (10.4.3.2).

$$\frac{p_\rho^0}{p_z^0} = -\cot 2\psi_0.$$

Hence

$$\theta_0 = \tan^{-1}(-\cot 2\psi_0). \quad (10.4.3.4)$$

In general, whenever the motion passes through the origins of the uv -plane and the ρz -plane, ψ and θ , defined analogously to ψ_0 and θ_0 satisfy the relation

$$\theta = \tan^{-1}(-\cot 2\psi). \quad (10.4.3.5)$$

Figure (10.4.3.3) is a plot of the polar angle θ_0 of emission of the periodic orbits at the origin

$$\theta_0 = \tan^{-1}\left(\frac{p_\rho^0}{p_z^0}\right), \quad (10.4.3.6)$$

against the energy and it depicts clearly the non-generic behaviour. The full and broken curves indicate stability and instability respectively.

We calculate 20 zeros of the residue of the periodic orbit OZ (table (10.4.3.1)) and classify them into points $B_1, S_1, B_2, S_2, \dots, B_{10}, S_{10}$ (see figure (10.4.2.2)) where the letter B indicates points at which bifurcation takes place and the letter S indicates points at which the orbit OZ regains stability. From our numerical study we obtain the following results

- (1) Periodic orbits bifurcated from $B_1, B_3, B_5 \dots$ are symmetric about the z -axis (figure (10.4.3.4)).
- (2) Periodic orbits bifurcated from B_2, B_4, B_6, \dots are not symmetric but have vanishing momenta $p_\rho = p_z = 0$ at maximum z (figure (10.4.3.4)).
- (3) Every bifurcated pair of orbits starts with $\theta_0 = 0$, at the bifurcation point, and then deviates with positive and negative value of $\theta_0(E)$ as E increases.
- (4) The intervals of energies over which these bifurcated orbits are stable are given in table (10.4.3.2). Beyond the upper limit of each interval the orbit is unstable.
- (5) The periodic orbits discussed above are those in the region $z > 0$. There are similar motions in the region $z < 0$.

(10.4.4) Clarification of the stable-unstable sequence of the orbit OZ

The motion along the z -axis, with initial polar angle $\theta_0 = 0$, corresponds in the uv -plane to a motion along the line $u \simeq v$ with initial angle $\psi_0 = \frac{\pi}{4}$ (see equation (10.4.3.4)). We prove that the small oscillations transverse to this linearly macroscopic motion are responsible for the stable-unstable sequence (represented by the oscillating residue R) of this particular motion.

For zero magnetic quantum number $m = 0$, Hamilton's equations of motion in the u, p_u, v, p_v space takes the form (see equations (7.1.5))

$$\frac{d^2u}{d\tau^2} = 8Eu - 4u(u^2 - v^2)(3u^2 + v^2), \quad (10.4.4.1)$$

$$\frac{d^2v}{d\tau^2} = 8Ev + 4v(u^2 - v^2)(u^2 + 3v^2). \quad (10.4.4.2)$$

Adding (10.4.4.2) to (10.4.4.1), we get

$$u'' + v'' = 8E(u + v) - 4(u - v)^2(u + v)(3u^2 + 2uv + 3v^2) \quad (10.4.4.3)$$

where "''" stands for $\frac{d}{d\tau}$. Subtracting (10.4.4.2) from (10.4.4.1) we get

$$u'' - v'' = 8E(u - v) - 4(u + v)^2(u - v)(3u^2 - 2uv + 3v^2). \quad (10.4.4.4)$$

Setting

$$\eta = u + v, \quad \xi = u - v$$

equations (10.4.4.3) and (10.4.4.4) take the form

$$\eta'' = 8E\eta - 4\eta\xi^2(2\eta^2 + \xi^2), \quad (10.4.4.5)$$

$$\xi'' = 8E\xi - 4\eta^2\xi(\eta^2 + 2\xi^2). \quad (10.4.4.6)$$

Since we are concerned with the motion in the neighbourhood of the line $u = v$, ξ is small. To first order in ξ (10.4.4.5) and (10.4.4.6) give

$$\eta'' + \omega^2\eta = 0 \quad (10.4.4.7)$$

is called the discriminant $\xi'' + (\omega^2 + 4\eta^4)\xi = 0$ (see Floquet) (10.4.4.8)

where $\omega = \sqrt{-8E}$. Then, choosing the particular solution

The discriminant $\Delta(\lambda)$ plays $\eta = \cos \omega\tau$, (10.4.4.9)

alternate intervals of stability and instability of the solutions of
(10.4.4.10) according to the following theorem (Floquet's theorem)
(10.4.4.10) $\xi'' + (\omega^2 + 4\cos^4 \omega\tau)\xi = 0.$ (10.4.4.10)

Equation (10.4.4.10) is a special form of Hill's equation defined by

Theorem. $y'' + [\lambda - q(t)]y = 0,$ (10.4.4.11)

where $\lambda_1, \lambda_2, \dots$ denote the zeros of $\Delta(\lambda) - 2$ and $\lambda_1', \lambda_2', \lambda_3', \lambda_4', \dots$ those of $\Delta(\lambda) + 3$. Then

$$q(t + \pi) = q(t).$$

We explain the properties of Hill's equation which present another verification of the existence of the stable-unstable sequence of intervals (over E) for the orbit OZ : Two linearly independent solutions of (10.4.4.11) can be defined by

$$y_1(0) = 1, \quad y_2(0) = 0, \quad (10.4.4.12)$$

$$y_1'(0) = 0, \quad y_2'(0) = 1. \quad (10.4.4.13)$$

In general we cannot expect the solution of (10.4.4.11) to be periodic merely because the coefficient is. The assumption

(ii) Over the remaining intervals of λ , i.e., for which $|\Delta(\lambda)| > 2$, all solutions of Hill's equation are bounded. These are (10.4.4.14)

$$y(t + \pi) = \rho y(t) \quad (10.4.4.14)$$

for some ρ reduces to the quadratic equation

$$\rho^2 - \Delta\rho + 1 = 0$$

or

$$\rho_{1,2} = \frac{\Delta \pm \sqrt{\Delta^2 - 4}}{2}$$

where

$$\Delta(\lambda) = y_1(\pi) + y_2'(\pi), \quad (10.4.4.15)$$

is called the discriminant of Hill's equation (see Hochstadt (1971)). We note that Δ is a function of λ since y_1 and y_2 depend on λ .

The discriminant $\Delta(\lambda)$ plays an important role because it determines alternate intervals of stability and instability of the solutions of (10.4.4.10) according to the following *oscillation theorem* (Hochstadt 1971).

Theorem.

Let $\lambda_0, \lambda_1, \lambda_2, \dots$ denote the zeros of $\Delta(\lambda) - 2$ and $\lambda'_1, \lambda'_2, \lambda'_3, \lambda'_4, \dots$ those of $\Delta(\lambda) + 2$. Then

$$\lambda_0 < \lambda'_1 \leq \lambda'_2 < \lambda_1 \leq \lambda_2 < \lambda'_3 \leq \lambda'_4 < \dots$$

Figure (10.4.4). A sequence of alternate intervals of stable and unstable solutions.

(i) For all λ in the intervals

$$(-\infty, \lambda_0), (\lambda'_1, \lambda'_2), (\lambda_1, \lambda_2), \dots$$

(i.e. for $|\Delta(\lambda)| > 2$), these intervals are instability intervals (see figure (10.4.4)).

(ii) Over the remaining intervals of λ (i.e. for which $|\Delta(\lambda)| < 2$) all solutions of Hill's equation are bounded. These are the stability intervals (see figure (10.4.4)).

Since $\lambda \propto \omega^2 = -8E$, the alternate stable-unstable sequence of the orbit OZ over the E axis can now be easily understood in the light of the properties of Hill's equation explained above.

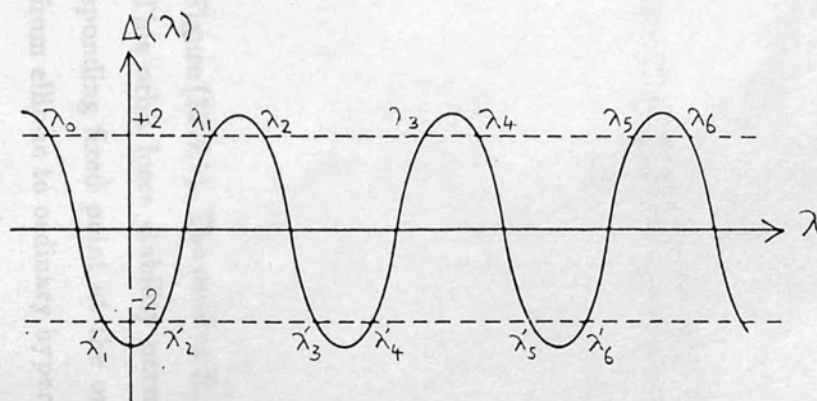


Figure (10.4.4). A sequence of alternate intervals of stable and unstable solutions of Hill's equation.

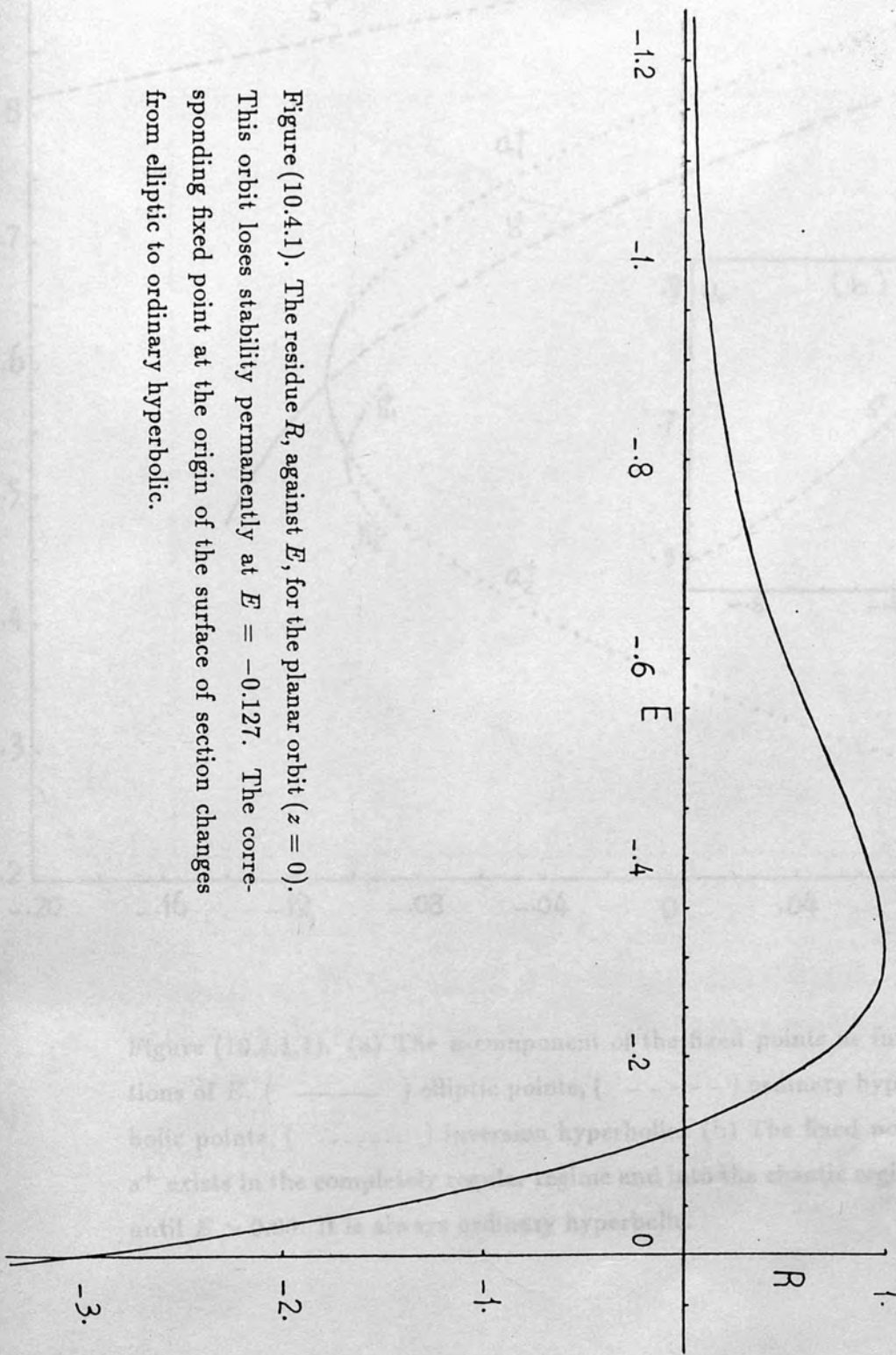


Figure (10.4.1). The residue R , against E , for the planar orbit ($z = 0$). This orbit loses stability permanently at $E = -0.127$. The corresponding fixed point at the origin of the surface of section changes from elliptic to ordinary hyperbolic.

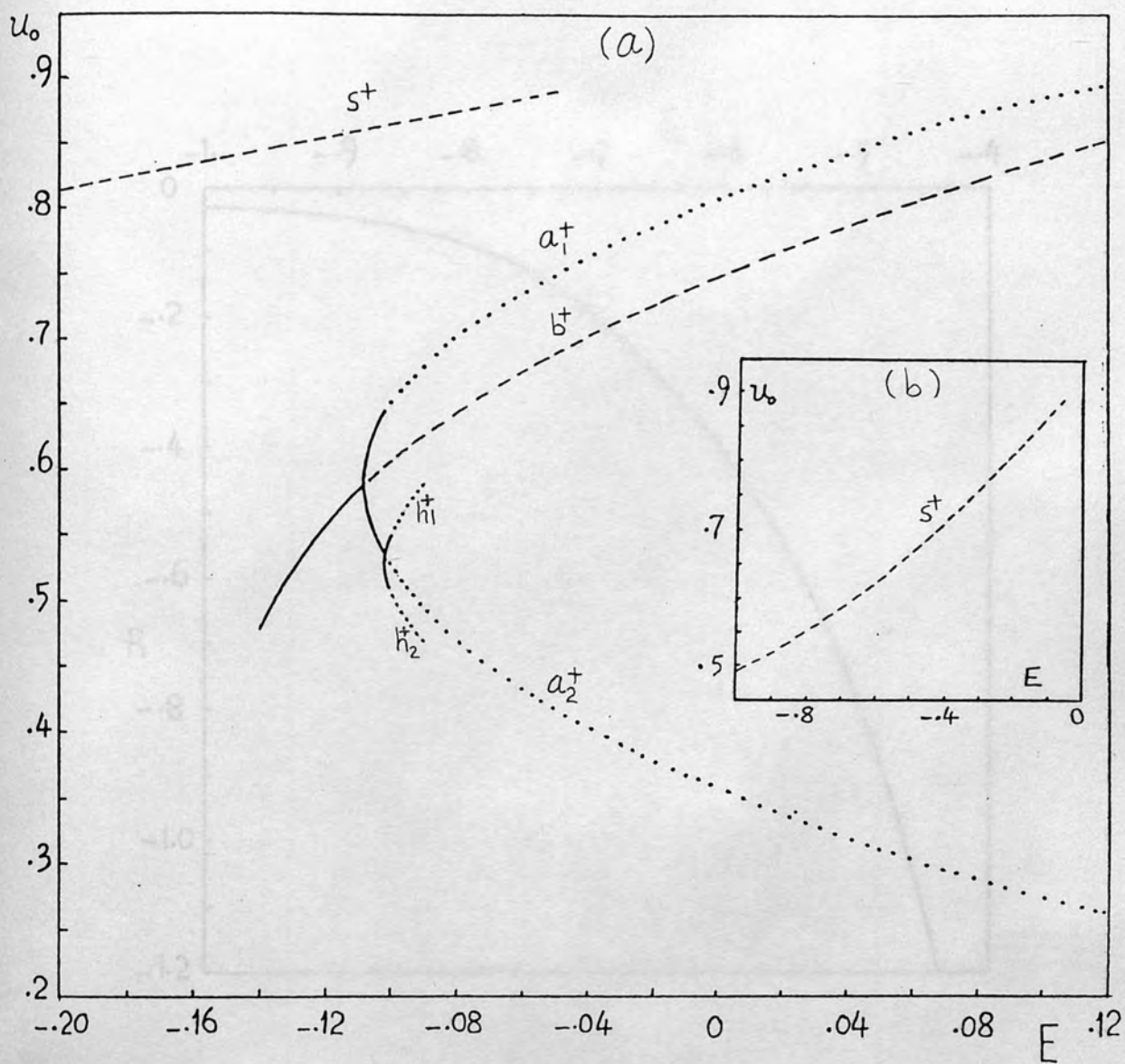


Figure (10.4.1.1). (a) The u -component of the fixed points as functions of E . (—) elliptic points, (- - -) ordinary hyperbolic points, (.) inversion hyperbolic. (b) The fixed point s^+ exists in the completely regular regime and into the chaotic regime until $E \simeq 0.05$. It is always ordinary hyperbolic.

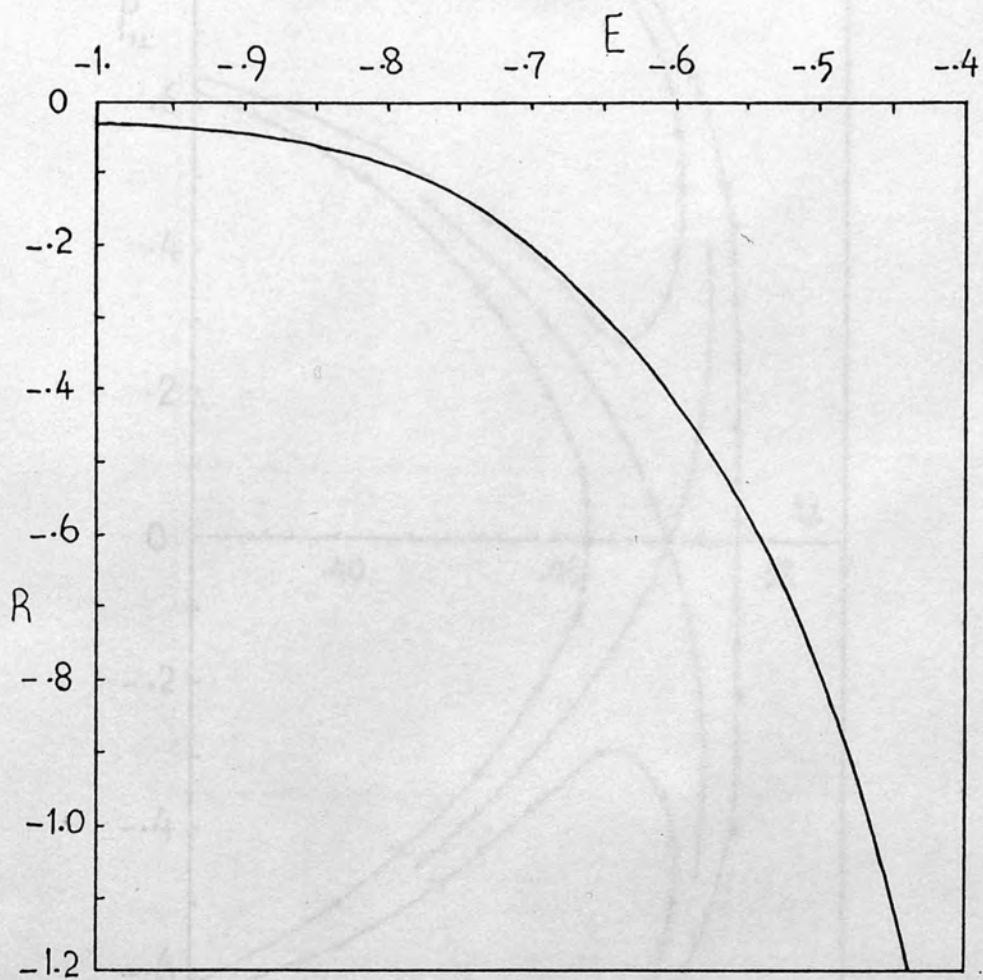


Figure (10.4.1.2). The residue R for the orbits of subclass CIs. These orbits are always unstable and the corresponding fixed points are ordinary hyperbolic.

Figure (10.4.1.3). The surface of section containing the fixed point s^* . This point is ordinary hyperbolic, $S = -1.5$.

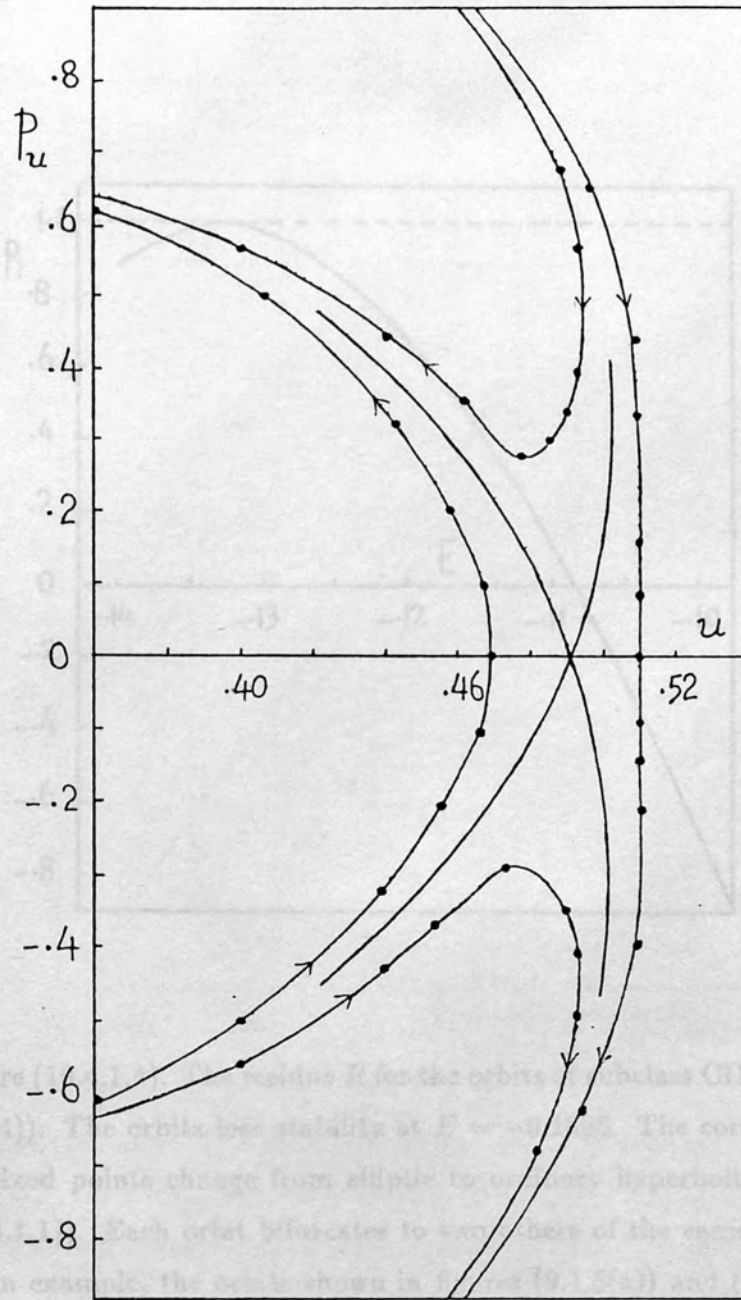


Figure (10.4.1.3). The surface of section surrounding the fixed point s^+ . This point is ordinary hyperbolic. $E = -1.0$.

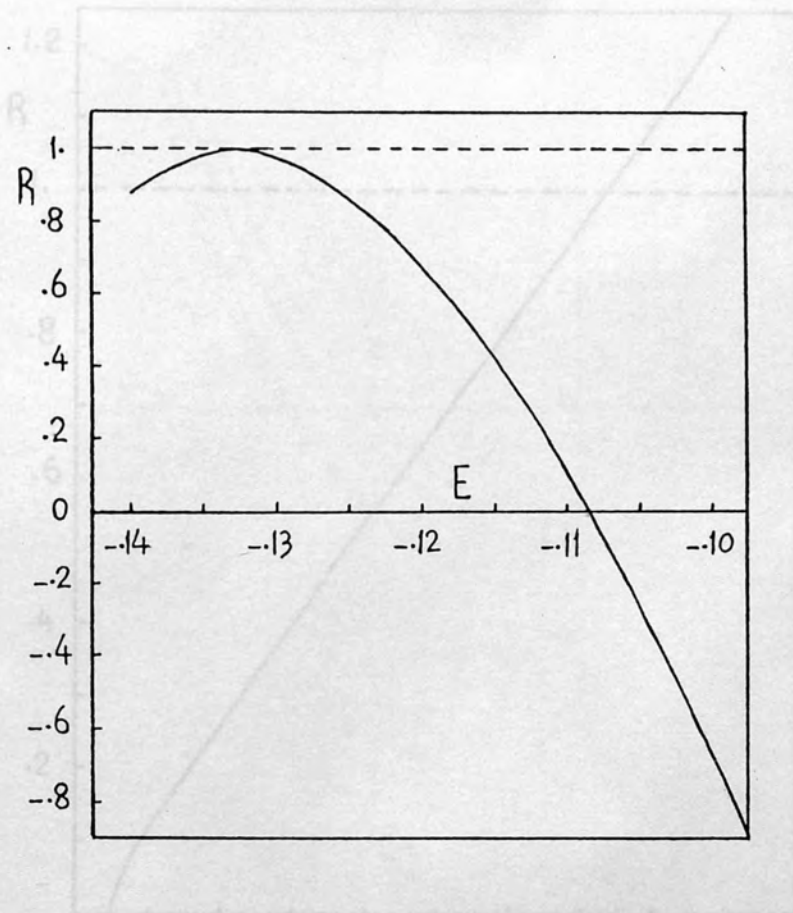


Figure (10.4.1.4). The residue R for the orbits of subclass CI1 (Figure (9.1.4)). The orbits lose stability at $E = -0.1085$. The corresponding fixed points change from elliptic to ordinary hyperbolic (figure (10.4.1.1)). Each orbit bifurcates to two others of the same period. As an example, the orbits shown in figures (9.1.5(a)) and (9.1.5(c)) bifurcate from that shown in figure (9.1.4(a)).

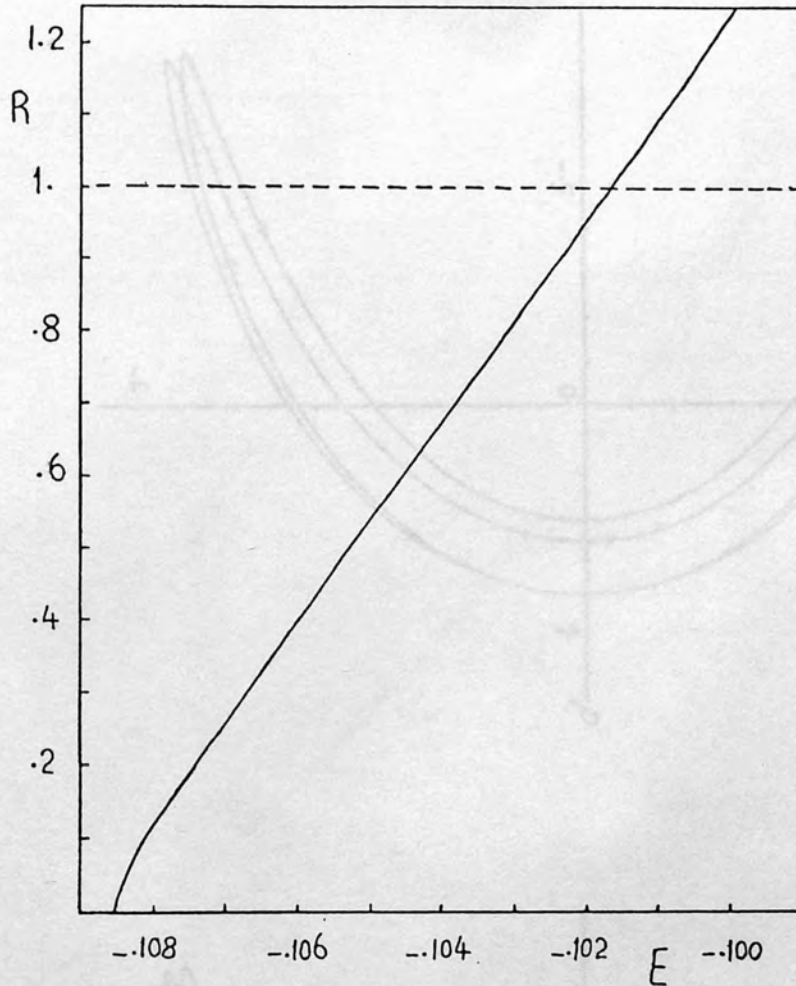


Figure (10.4.1.5). The residue R for the orbits of subclass CI2 (figure (9.1.5)). The orbits lose stability at $E \simeq -0.1017$. The corresponding fixed points change from elliptic at $E = -0.1017$ to inversion hyperbolic. Each orbit bifurcates to two others of twice the period. As an example, the orbits shown in (10.4.1.6) bifurcate from that shown in figure (9.1.5(c)). This behaviour is generic.

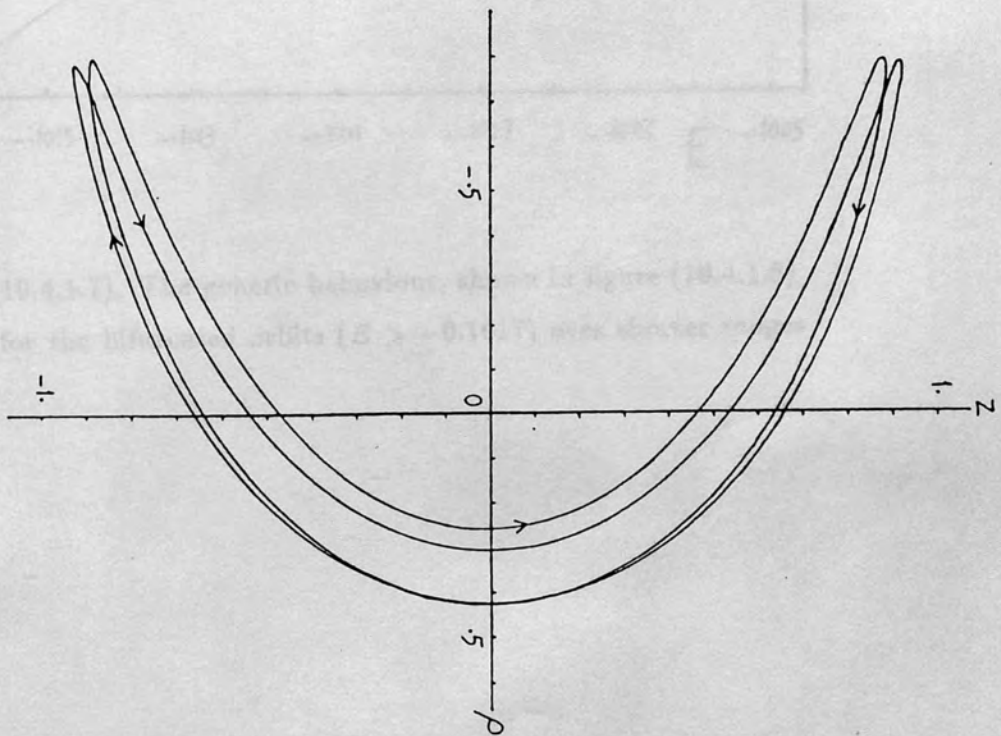
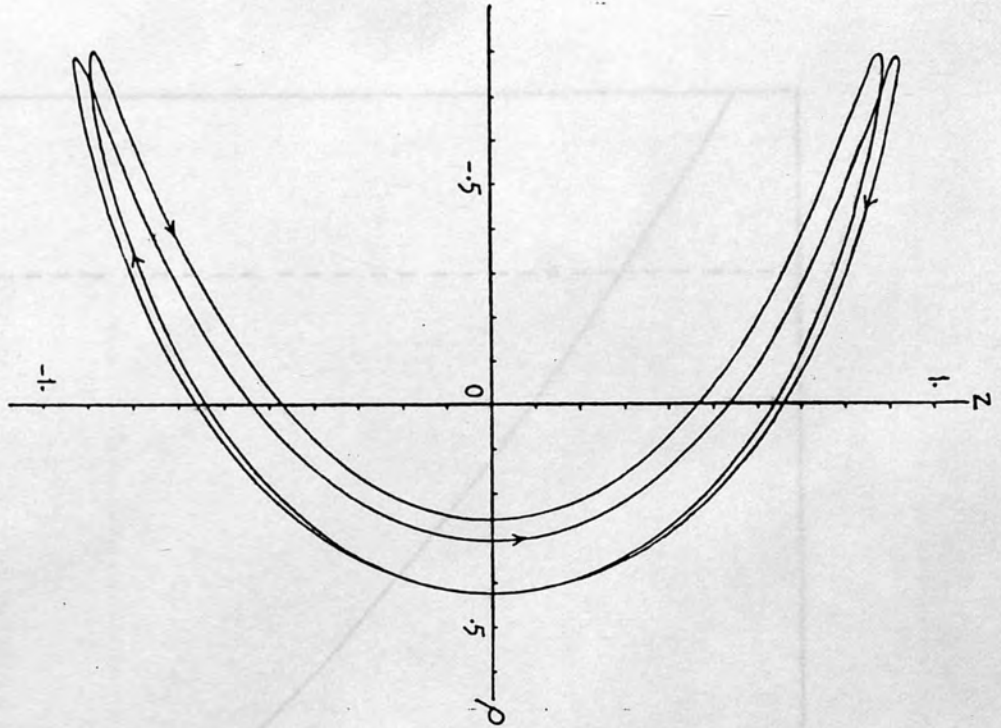


Figure (10.4.1.6). Two periodic orbits, born at $E = -0.1017$, of twice the period of the parent orbit shown in figure (9.1.5(c)). They lose stability at $E = -0.1007$, as their residue passes through unity.

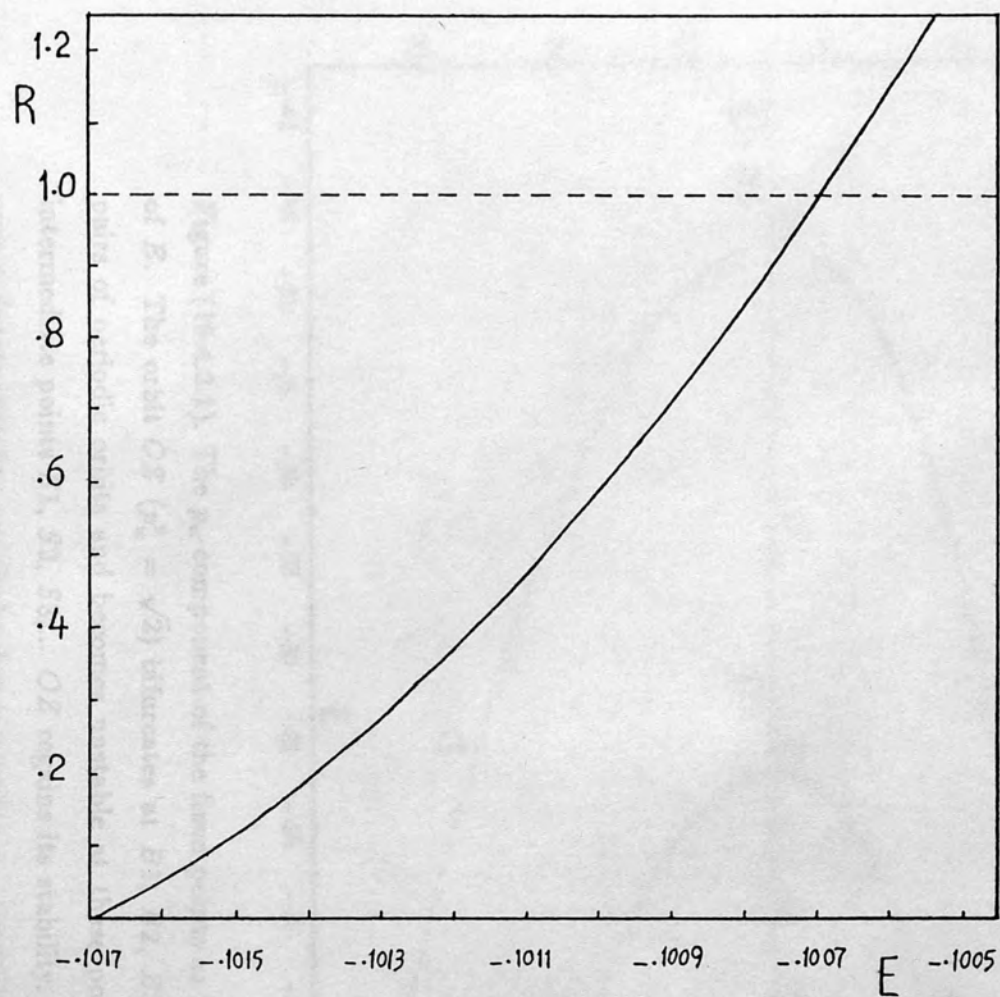


Figure (10.4.1.7). The generic behaviour, shown in figure (10.4.1.5), repeats for the bifurcated orbits ($E > -0.1017$) over shorter ranges of E .

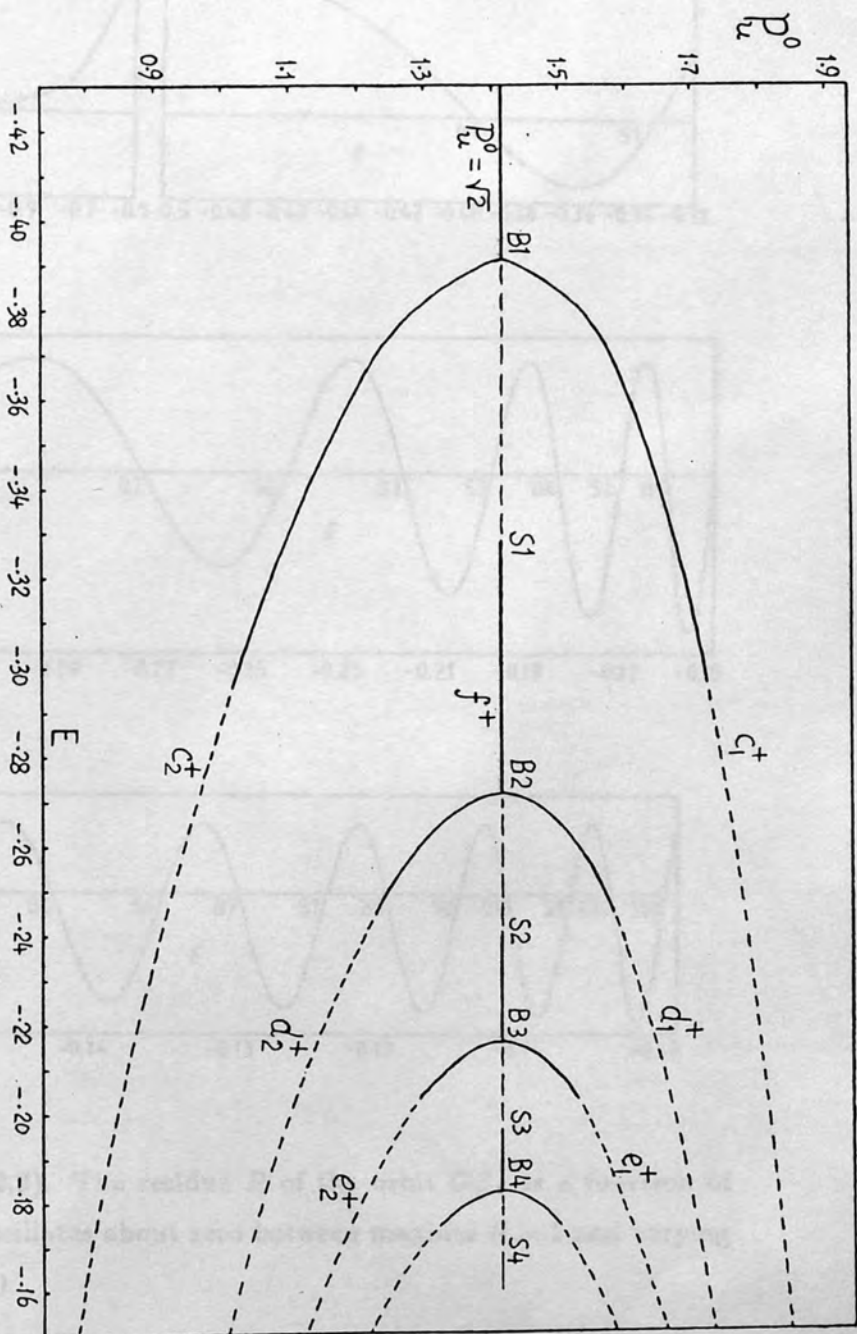


Figure (10.4.2.1). The p_u -component of the fixed points as functions of E . The orbit OZ ($p_u^0 = \sqrt{2}$) bifurcates at $B1, B2, B3, \dots$ into pairs of periodic orbits and becomes unstable at these points. At intermediate points $S1, S2, S3, \dots$ OZ regains its stability. The full curves denote stability and the broken curves denote instability. (—) elliptic points, (- - -) ordinary hyperbolic points.

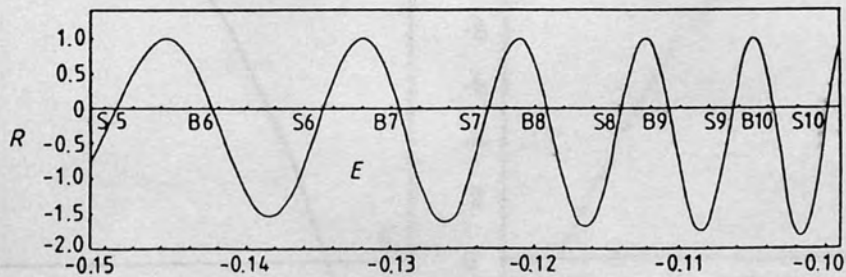
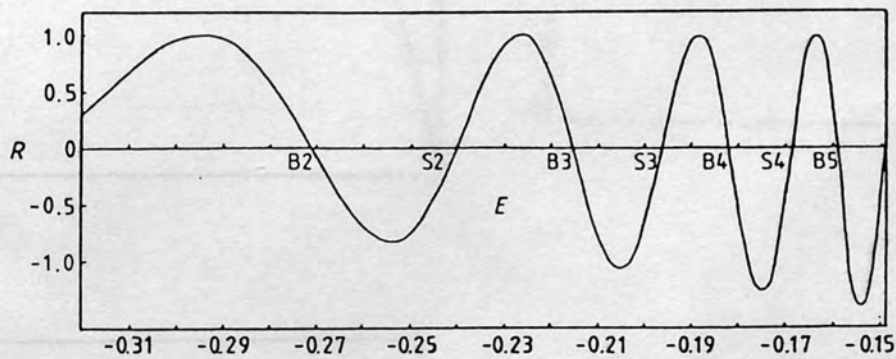
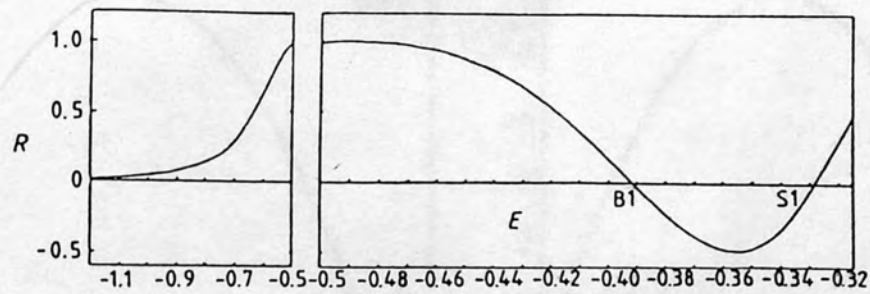


Figure (10.4.2.2). The residue R of the orbit OZ , as a function of the energy, oscillates about zero between maxima $R = 1$ and varying minima $R < 0$.

Figure (10.4.2.3). The residues for the bifurcations of the orbit OZ (a) CH1, (b) CH2, (c) CH3 and (d) CH4.

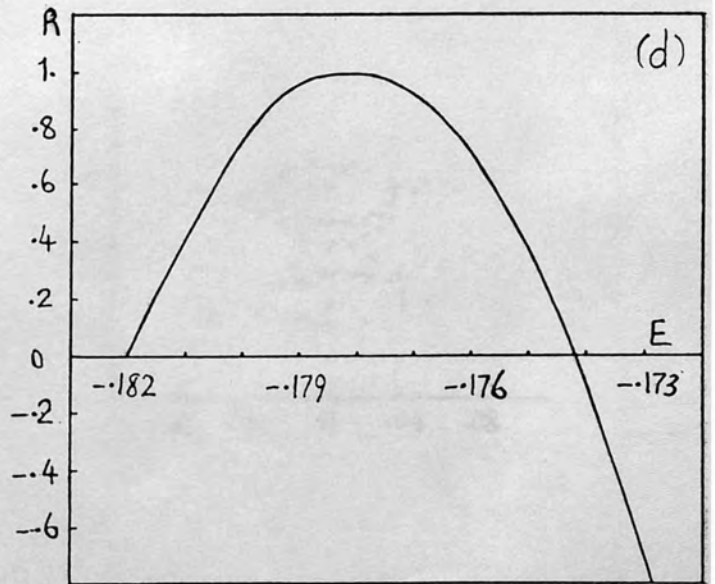
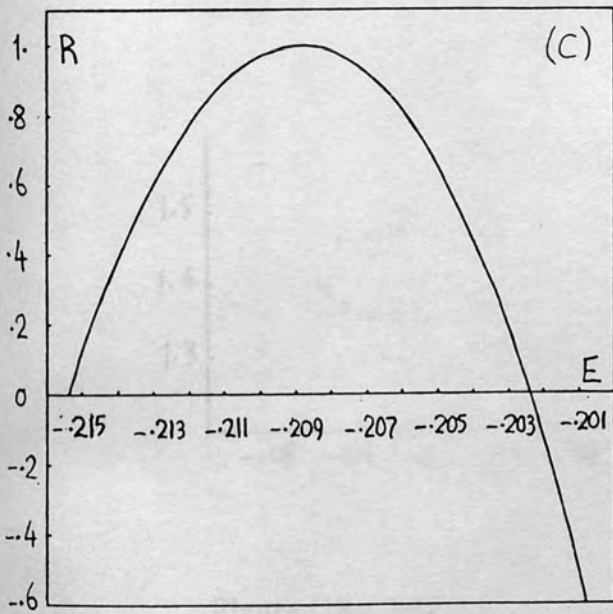
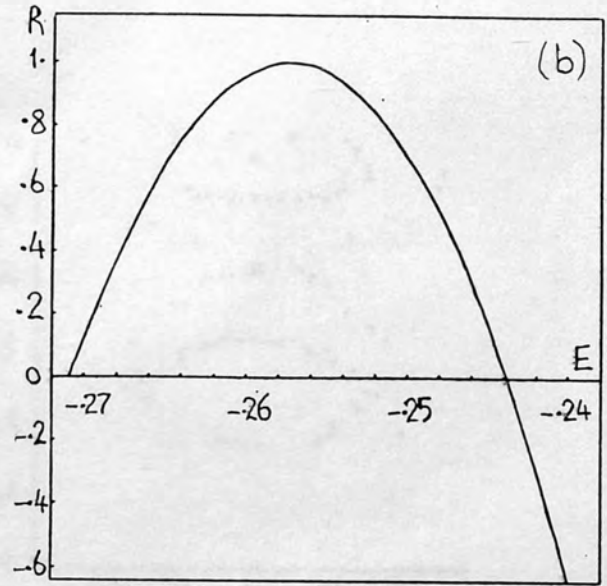
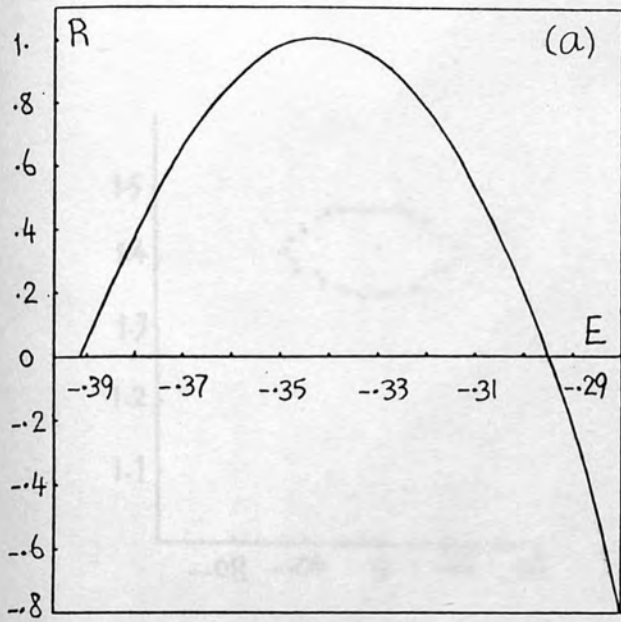


Figure (10.4.2.3). The residues for the bifurcated orbits: of subclasses (a) CII1, (b) CII2, (c) CII3 and (d) CII4.

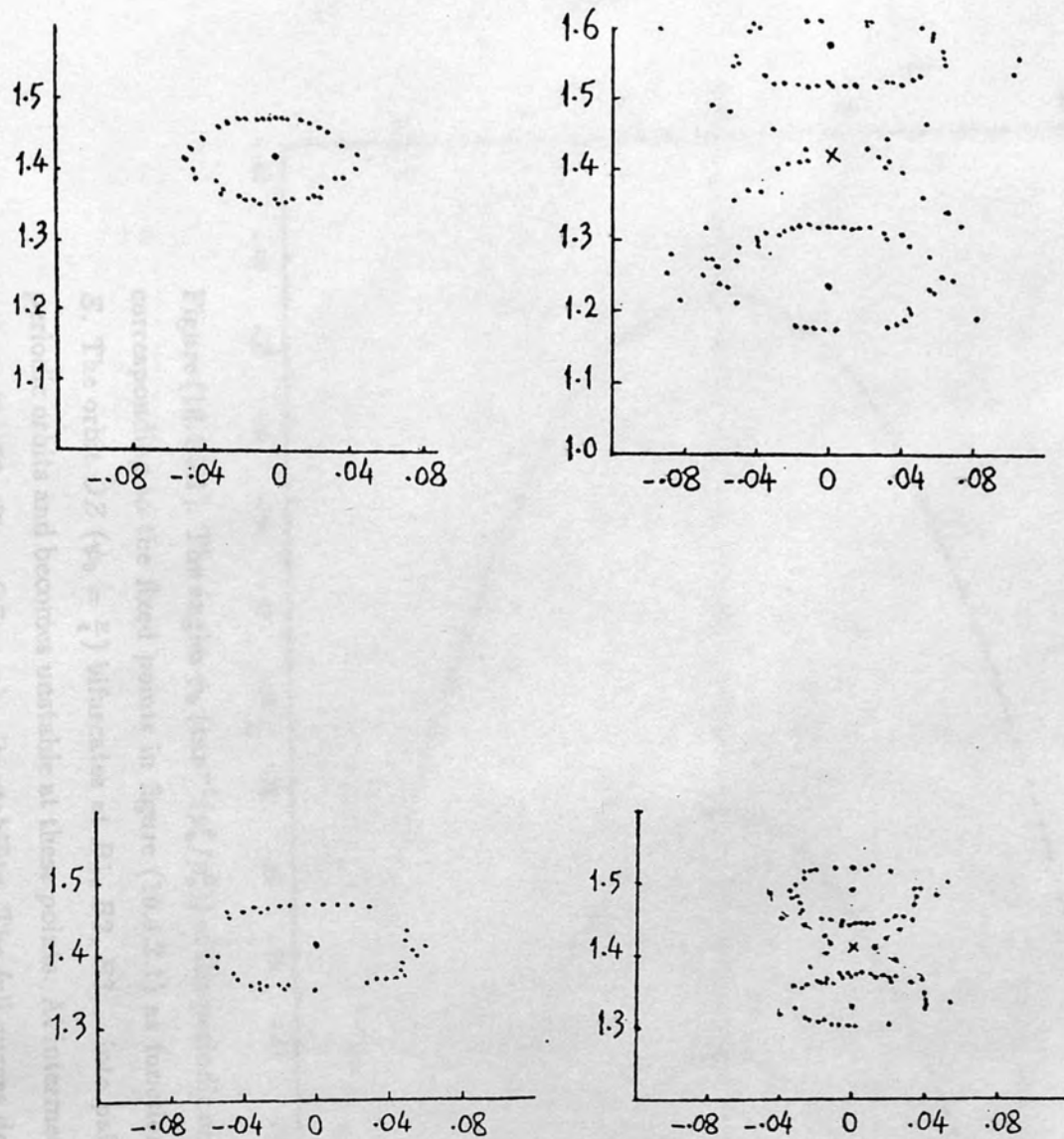


Figure (10.4.2.4).

- (a) Two surfaces of section before and after the bifurcation at $B1$ (figure (10.4.2.1)). An elliptic point changes to an ordinary hyperbolic point and two other elliptic points are created.
- (b) Like (a) but at the point $B2$ (figure (10.4.2.1)).

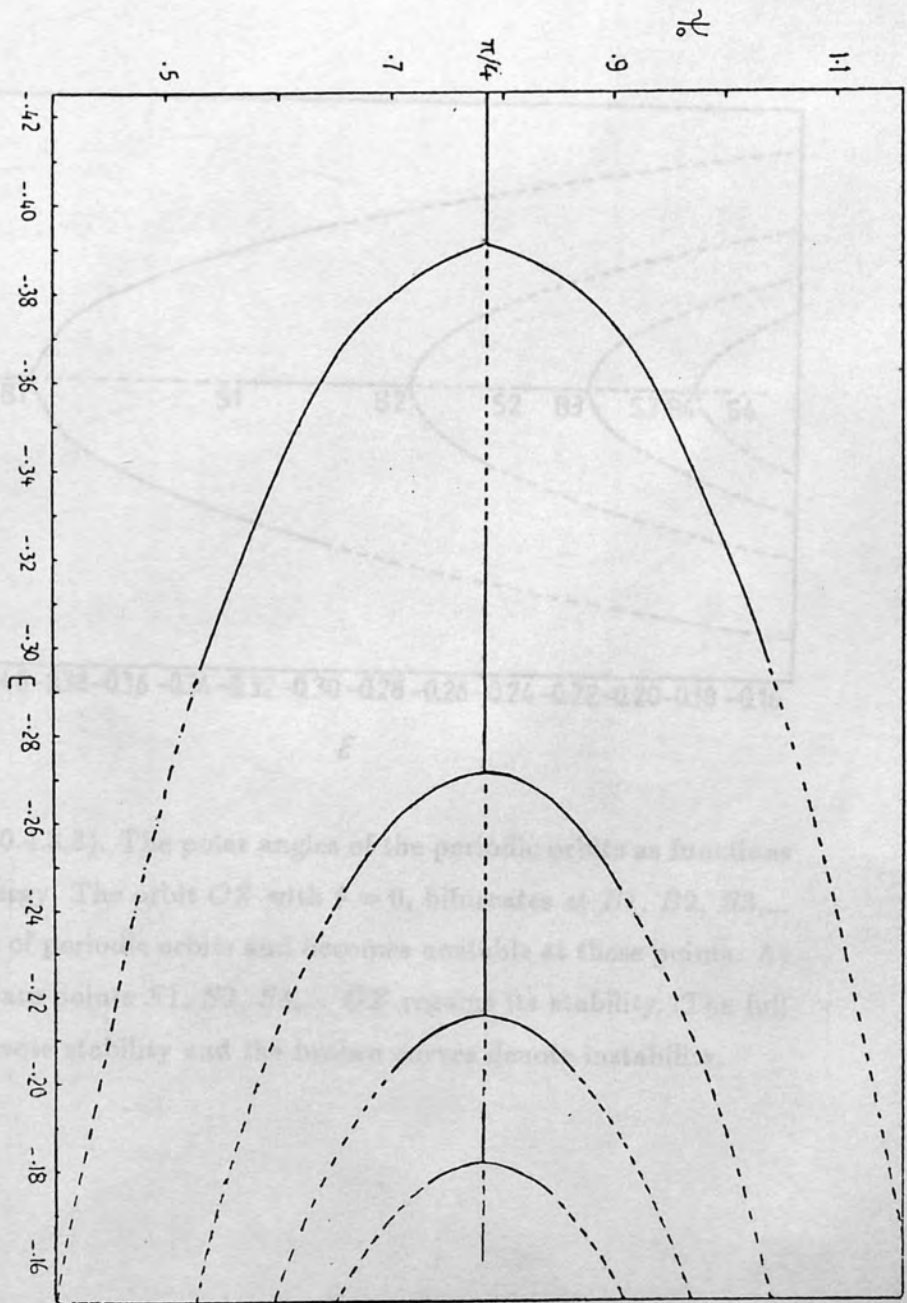


Figure (10.4.3.1). The angles ψ_0 ($\tan^{-1}(p_u^0/p_v^0)$) of the periodic orbits, corresponding to the fixed points in figure (10.4.2.1) as functions of ϵ . The orbit OZ ($\psi_0 = \frac{\pi}{4}$) bifurcates at B_1, B_2, B_3, \dots into pairs of periodic orbits and becomes unstable at these points. At intermediate points S_1, S_2, S_3, \dots OZ regains its stability. The full curves denote stability and the broken curves denote instability.

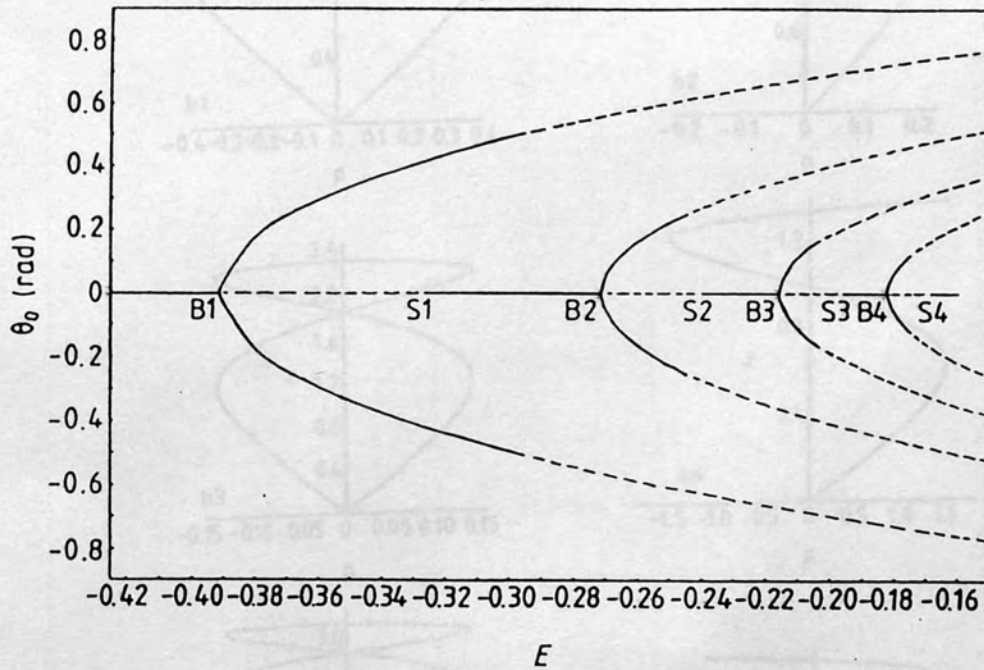


Figure (10.4.3.3). The polar angles of the periodic orbits as functions of the energy. The orbit OZ with $\theta = 0$, bifurcates at $B1, B2, B3, \dots$ into pairs of periodic orbits and becomes unstable at these points. At intermediate points $S1, S2, S3, \dots$ OZ regains its stability. The full curves denote stability and the broken curves denote instability.

Table(10.4.3.1). The zeros of the residue R of the periodic orbit QZ denoted by $B_1, S_1, B_2, S_2, \dots$ are the boundary points of the stable-unstable sequence of intervals over the range of energy until QZ escapes. The energy spacings at these points are given.

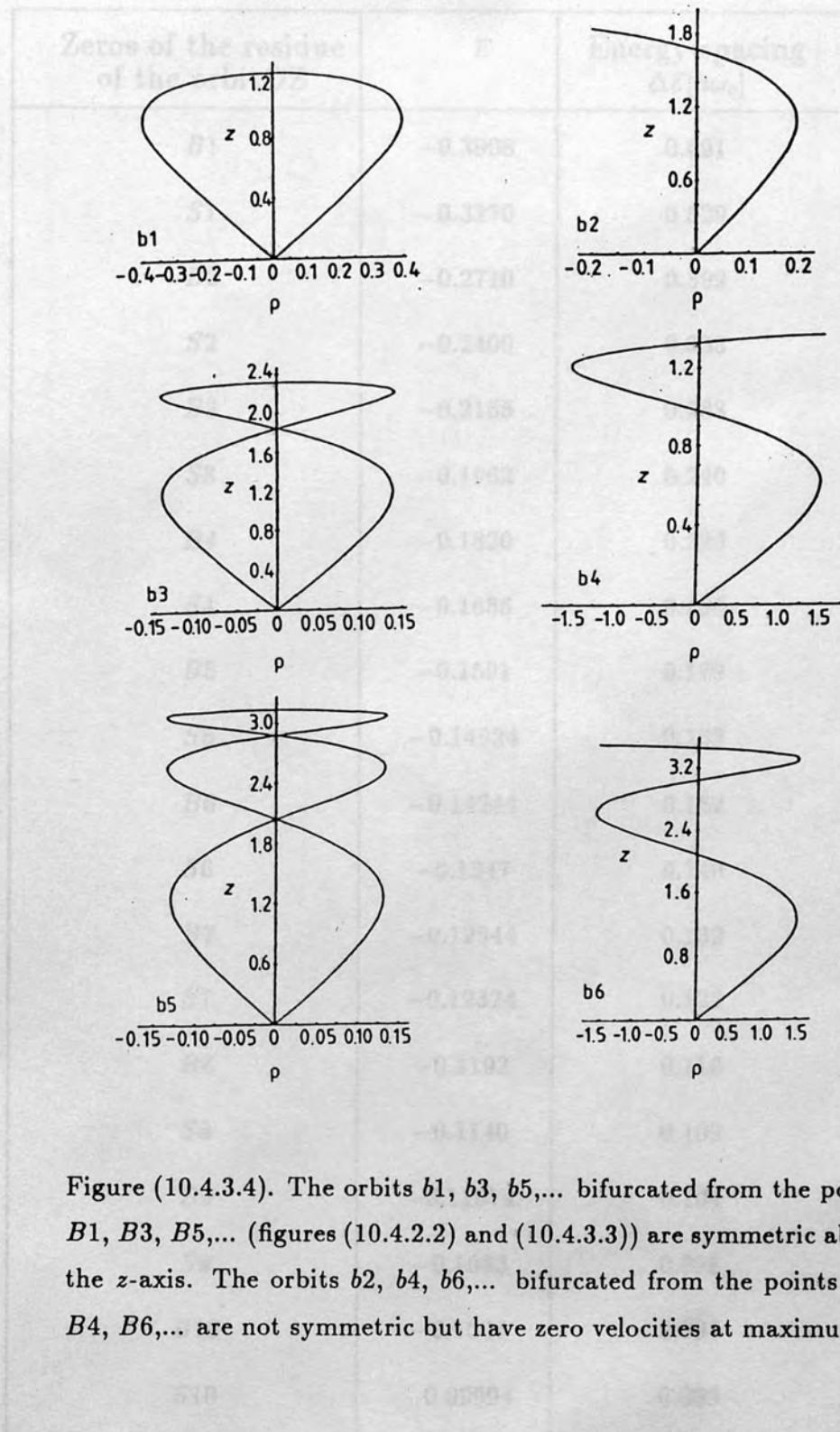


Figure (10.4.3.4). The orbits b_1, b_3, b_5, \dots bifurcated from the points B_1, B_3, B_5, \dots (figures (10.4.2.2) and (10.4.3.3)) are symmetric about the z -axis. The orbits b_2, b_4, b_6, \dots bifurcated from the points B_2, B_4, B_6, \dots are not symmetric but have zero velocities at maximum z .

Table(10.4.3.1). The zeros of the residue R of the periodic orbit OZ denoted by $B_1, S_1, B_2, S_2, \dots$ are the boundary points of the stable-unstable sequence of intervals over the range of energy until OZ escapes. The energy spacings at these points are given.

Zeros of the residue of the orbit OZ	E	Energy spacing $\Delta\mathcal{E}[\hbar\omega_c]$
B_1	-0.3908	0.691
S_1	-0.3270	0.529
B_2	-0.2710	0.399
S_2	-0.2400	0.333
B_3	-0.2155	0.283
S_3	-0.1962	0.240
B_4	-0.1820	0.220
S_4	-0.1686	0.196
B_5	-0.1591	0.179
S_5	-0.14924	0.163
B_6	-0.14244	0.152
S_6	-0.1347	0.140
B_7	-0.12944	0.132
S_7	-0.12324	0.122
B_8	-0.1192	0.116
S_8	-0.1140	0.109
B_9	-0.11074	0.104
S_9	-0.1063	0.098
B_{10}	-0.1036	0.094
S_{10}	-0.09994	0.089

Table (10.4.3.2) Intervals of energy over which the bifurcated pairs of orbits created at B_1, B_2, B_3, B_4 are stable.

Type of orbit	Interval of energy
B_1	(-0.3908, -0.295)
B_2	(-0.271, -0.2438)
B_3	(-0.2155, -0.2024)
B_4	(-0.182, -0.1742)

CHAPTER (11)

Quantization of periodic orbits and comparison with experiments.

(11.1) Semiclassical quantization.

The quantum spectral treatment poses great difficulties even in the case of integrable systems. An explicit solution (exact spectrum) can be obtained through exact quantization when the system belongs to the very special class of separable systems. By chaotic and integrable quantum systems we mean that they are irregular or integrable in the classical limit.

Einstein suggested that a quantization rule given by the invariant line integrals of the form

$$J = \frac{1}{2\pi} \oint \sum p_r dq_r = n\hbar, \quad (11.1.1)$$

along closed curves in coordinate space which need not be classical trajectories should be used instead of the quantization rule

$$I_i = \oint p_i dq_i = n\hbar, \quad i = 1, 2, \dots, n \quad (11.1.2)$$

which holds only if the motion is linear (Percival 1977).

Keller (1958) developed a theory and derived "corrected Bohr-Sommerfeld quantum conditions for separable and nonseparable systems". The method can be outlined as follows: For a time independent Hamiltonian ($H = E$), if an approximate solution to the Schrodinger equation, in the limit $\hbar \rightarrow 0$, of the form

$$\Psi = \sum_k A_k(q_r, t, \hbar) \exp[i\hbar^{-1} S_k(q_r, t, \hbar)], \quad (11.1.3)$$

is sought, S_k is then the classical action function of the coordinates

$$S_k(q_r, t, \hbar) = S_k(0) + \int_0^t \sum_{r=1}^n p_r dq_r - Et, \quad (11.1.4)$$

and A_k is a normalization factor that nearly everywhere varies slowly by comparison with S_k/\hbar . The function S_k in (11.1.4) is given at any point of the trajectory in terms of its value $S_k(0)$ at some fixed point on the trajectory. The boundary conditions on the action function provide the so-called EBK-quantization rule

$$\oint \sum p_r dq_r = h(n + \frac{\alpha}{4}). \quad (11.1.5)$$

where α denotes the total number of dimensions "lost" by the caustics which the curve passes plus the number of p_r which change sign at the $v = 0$ caustics through which the curve passes. α depends on whether the curve traverses the caustic in the direction of increasing or decreasing S .

The rule (11.1.5) gives the corrected quantum conditions for separable or nonseparable systems (Keller (1958)).

In 1917, also, Einstein pointed out that semiclassical quantum mechanics must be very different for integrable and non-integrable systems (Berry 1978). These remarks were revitalised by Percival (1973) who put them into explicit suggestions in the light of new developments in classical mechanics, such as the KAM theorem. His suggestion was that, in the semiclassical limit, an irregular spectrum arises from regions of phase space occupied by irregular trajectories while a regular spectrum is formed by regions of phase space filled with KAM tori: the energy levels in an n -dimensional integrable system may be labelled by n quantum numbers

$$\mathbf{m} \equiv (m_1, m_2, \dots, m_n). \quad (11.1.6)$$

Then the m 'th bound state is associated with a particular torus \mathbf{J}_m . Its energy E_m is given by the Hamiltonian, expressed in action variables

$$E_m = H(\mathbf{J}_m), \quad (11.1.7)$$

with action constants \mathbf{J}_m given by quantum conditions of the Bohr-Sommerfield-Wilson type:

$$\mathbf{J}_m = \mathbf{m} + \frac{\alpha}{4} \hbar. \quad (11.1.8)$$

Here $\alpha \equiv (\alpha_1, \alpha_2, \dots, \alpha_n)$, with α_i indicating the number of places on the irreducible circuit, γ_i , where the torus is normal to the configuration space, is called Maslov's index (Berry 1978). For example in 2-dimensional problems one of the α 's is 0 and the other is 2. Thus the Maslov's index is a correction to be added to the Einstein's quantization rule.

However, there is no quantization condition for irregular systems that is as explicit as (11.1.8). According to Percival (1973), in contrast to the regular spectrum, there is no unambiguous assignment of a vector quantum number to a state Ψ_0 : The discrete bound state quantal spectrum must tend to a continuous classical limit. The energy difference

$$E(\Psi) - E(\Psi_0) = \hbar\omega, \quad (11.1.9)$$

for fixed stationary Ψ_0 and varying Ψ form a discrete distribution which tends to the continuous distribution in $\hbar\omega$. The distribution of levels of the irregular spectrum could take on the appearance of a random distribution.

Whether the system is regular or irregular, periodic orbits are only a set of zero measure in phase space. This may give a misleading im-

pression of their role as being unimportant regarding the spectra contribution. However, the role of periodic orbits in describing the irregular spectrum has been discussed (with reference to the anisotropic Kepler problem) by Gutzwiller (1971) who calculated a single closed orbit and discussed its effect on the spectrum. Gutzwiller (1978) has also shown the importance of classically periodic orbits as contributors to the irregular spectrum in the semiclassical limit and concluded that the spectrum can be spanned by them. He used the Feynman path integrals (ordinary and phase space integrals) which are known to present an intimate link between classical and quantum mechanics. The conclusion was that in the semiclassical limit, only the closed periodic classical paths contribute to the response

$$d(E) = \sum \delta(E - E_i), \quad (11.1.10)$$

where the right handside of (11.1.10) is the sum of the Dirac delta spikes $\delta(E - E_i)$.

Since the work by Percival (1973), various collected material has shown that, for parameter-dependent Hamiltonians, irregular spectra (corresponding to irregular motions) tend to be more continuous rather than discrete as small changes occur in the parameter. Rather than using a quantization condition for individual energy levels, Zaslavskii (1981) gave grounds for better understanding of the response formula (11.1.10) as a distribution of energy levels rather than a quantization condition. If $P(s)$ is defined to be the probability density that two neighbouring levels are separated by s (normalized to the mean separation of levels), we have

- (i) For integrable systems, a generally acceptable result that $P(s) = e^{-s}$ indicates the possible existence of level crossings and the levels are clustered.

- (ii) For irregular systems, there is an agreement that $P(s) \propto s^\nu$. While Berry (1981) suggests that $\nu = 1$, Zaslavskii argues that $\nu = \text{constant} \times K^{-1}$, where K is the Kolmogorov K -entropy of the corresponding classical system in the energy shell around the levels considered, and the exponent ν itself is a measure of the instability of the classical trajectories. Then as $s \rightarrow 0$, no clustering occurs and the spectra are random.

Berry (1977) discusses how the wave function Ψ for a semiclassical regular state differs from the form of Ψ for an irregular state. For example, in two dimensional problems, the local average probability density for regular states rises to large values on caustics at the boundaries of the classical motion in coordinate space, and Ψ exhibits strong anisotropic interference oscillations. For irregular states the local average probability density remains constant on 'anticaustics' at the boundary of the classically allowed region, and Ψ appears to be a Gaussian random function exhibiting more moderate interference oscillations which, for ergodic classical motion, are statistically isotropic. This is demonstrated numerically by McDonald and Kaufman (1979), who carried out a pioneering numerical study of the distribution of eigenvalues and the nodal structure of eigenfunctions for the stadium problem (i.e. two parallel lines with semi-circular ends).

For ranges of energy E for which the motion is dominantly irregular, the energy spectra are generally accepted to be of a statistical nature. So, it seems quite reasonable that the energy levels in those ranges are effectively in terms of the density of states $d(E)$.

Berry (1981) discusses the problem of Sinai's billiard (i.e. free mo-

tion of a particle in a plane amongst reflecting discs of radius R centered on points of the unit square lattice). For $R > 0$, the system is a classically ergodic one. He uses the "Korringa-Kohn-Rostoker" determinant (Berry 1981) which gives (as $\hbar \rightarrow 0$) $d(E)$ as the sum of a steady contribution $\bar{d}(E)$ (the average density of states) and an oscillatory contribution $d_{osc}(E)$

$$d(E) = \bar{d}(E) + d_{osc}(E), \quad (11.1.11)$$

with both terms in the sum determined classically:

- i- The first, $\bar{d}(E)$, does not depend on the regular or irregular nature of the classical orbits, but, for large principle quantum numbers, depends only on the extent of the energy shell in the phase space

$$\bar{d}(E) = \frac{1}{h^2} \int d\mathbf{q} \int d\mathbf{p} \delta[E - H(\mathbf{q}, \mathbf{p})] \quad (11.1.2)$$

so that the density is proportional to the size of the energy surface.

- ii- Each closed orbit contributes to $d_{osc}(E)$

$$d_{osc} = \sum a_k(E) \exp\left[\frac{i S_k(E)}{\hbar}\right], \quad (11.1.13)$$

where $S_k(E)$ is the action of the k th orbit at energy E . The contributions of the closed orbits to $d_{osc}(E)$ depends on \hbar : non-isolated closed orbits (non-hitting discs) contribute terms with $\mathcal{O}(\hbar^{-\frac{3}{2}})$, while isolated closed orbits (bouncing between discs) contribute terms with $\mathcal{O}(\hbar^{-1})$. In general, the amplitudes $a_k(E)$ depends on whether the orbits are stable or unstable. So (11.1.13) is a complicated sum. The number of states, N , below energy E is given by

$$N = \int d(E) dE. \quad (11.1.14)$$

(11.2) Quantization of orbits in the quadratic Zeeman problem.

All the periodic orbits described in chapter (9) are located in classically chaotic regions. The stability of them and, in turn, of near by bundles of trajectories are investigated in chapter (10). The connection between such bundles of trajectories, in these regions of phase space, and quantum eigenstates is of fundamental interest.

We discuss this question in some detail and we obtain spacings through semi-classical quantization. This, we believe, should be the most relevant observable quantum mechanically. In the irregular region most of the trajectories wander over large regions of phase space as $t \rightarrow \infty$. It is well known that such chaotic regions of the phase space contain many strictly periodic orbits which are unstable (Arnold and Avez, 1968). In fact, two nearby trajectories separate exponentially in time (see section (10.2)).

$$\Delta r = e^{\lambda t} \Delta r_0 \quad (11.2.1)$$

However, λ is different for different classes of trajectories and hence there can exist bundles of trajectories which are slowly diverging compared to the period of an orbit. There can also exist small regions of phase space, surrounding periodic orbits, which are stable. Either of the above cases should give rise to features in the quantum spectrum. As we see above there is no real consensus on the role of periodic orbits in the quantum spectrum. Some authors believe that periodic orbits induce fluctuations in an otherwise random background density of states when the classical motion is chaotic (Berry, 1981). However, it has been shown recently by (Heller, 1984) that unstable periodic orbits, for a free particle moving in a *stadium* are extremely relevant in the quantum spectrum. He showed that a quantum eigenfunction was *scarred* by a periodic orbit in that its

density was strangely peaked about the trajectory. These orbits were a class of periodic orbits with small exponential separation rates and short periods (i.e. the values of λ were small compared to the periods of the orbits). We show that the unstable periodic planar orbit associated with the quasi-Landau resonances is giving the correct energy spacing between these resonances. A semi-classical quantization is achieved for some of the short period orbits we found (in chapter(9)). The linear stability of these orbits was studied in detail in sections (10.4.1) and (10.4.2).

Edmonds and Pullen (1980) used the correspondence relation (in the case $m = 0$)

$$\Delta\mathcal{E} = \hbar\omega_{cl}, \quad (11.2.2)$$

where ω_{cl} is the classical angular frequency $2\pi t^{-1}(0)$, and $t(0)$ is the period of return near the origin. They showed that near $E = 0$, the quantity $\Delta\mathcal{E}$ was approximately $1.5\hbar\omega_c$ in agreement with the semi-classical (JWKB) result of Edmonds (1970). Although (11.2.2) is known to give, for one-dimensional systems, the spacing between eigenvalues in the quantum mechanical spectrum so long as ω_{cl} does not vary significantly over the range $\hbar\omega_{cl}$, Pullen (1980) proposed that it may be applicable to two-dimensional motions. It is worth noting that for values of L comparable with 0.01, those values which we are interested in, the initial conditions for planar motions hardly change. In particular, for $L = 0$ the corresponding fixed point is always $(0,0)$ and is independent of E .

As in the one-dimensional case we shall, mainly, be concerned with orbits whose frequencies vary slowly with the energy. As we see in figure (11.2.1), this is satisfied for all the orbits which are emitted at the origin of the ρz -coordinates (i.e. class CII) except for the two

orbits CIIz (see figure (11.2.1)). Figure (11.2.2) shows the energy separations (as determined by (11.2.2)) of some of the orbits of the class CI as functions of E . Quantization of the orbit CIs (figure (9.1.2)), only, will be considered from among other members of that class.

Several authors (Edmonds 1970, Starace 1973, O'Connell, 1974 and Rau, 1979) have shown that the $z = 0$ planar orbits may be quantized semi-classically, and yield a clear explanation of the quasi-Landau spectrum. We extend this treatment to all our planar orbits, by evaluating

$$J_n = \oint p_\rho d\rho + \epsilon_z \quad (11.2.3)$$

where the coordinate ρ and the conjugate momentum p_ρ in (11.2.3) are unscaled values which are related to their dimensionless counterparts by scaling factors ℓ and $\frac{1}{2}m_e\omega_c\ell$ respectively (see the units used in chapter (5)) and $\epsilon_z = \oint p_z dz$ is found to be a small quantity which can be neglected. The integration in (11.2.3) is taken over the period of time in which the $u - p_u$ closed curve is traced once. For some values of the energy \mathcal{E}_n we find

$$J_n = h(n_\rho + \alpha_\rho), \quad (11.2.4)$$

where h is Planck's constant, n_ρ is a positive integer and α_ρ a constant. n_ρ can be roughly estimated by plotting $f(E) = \frac{J_n}{h} - \alpha_\rho$ versus E and determining the values of E at which $f(E)$ takes an integer value n_ρ .

The Maslov's constant generally depends on the action function (Percival 1977) and in turn on E and B . This constant is equal to $1/2$ in the Coulomb limit and $1/4$ in the Landau limit (Gay 1985). Setting $\alpha_\rho = 0$ will make small shifts for the energy levels which slightly vary

over the range of E . Since we consider fairly large quantum numbers this shift will only cause a minute effect to the differences $\Delta\mathcal{E}(n_\rho+1, n_\rho)$ in which we are primarily interested (McDowell 1985).

Our first example is for $B = 60 \text{ kG}$, $m = 0$, chosen because of the existence of experimental measurements. Table (11.2.1) shows the values of $\Delta\mathcal{E}(n_\rho + 1, n_\rho)$ obtained from (11.2.3) and from (11.2.2) for the planar orbits (Co). We notice the close agreement of the two approaches over a wide range of energies.

For the orbit CIIz (see section 9.2), we use the rule

$$\oint p_z dz + \epsilon_\rho = h(n_z + \alpha_z), \quad (11.2.5)$$

where, as above, z is the unscaled coordinate, p_z is its conjugate momentum and $\epsilon_\rho = \oint p_\rho d\rho$ is a small quantity which can be neglected. Again we put $\alpha_z = 0$. Table (11.2.2) shows the results for this orbit for the same values of m and B . Again (11.2.5) and (11.2.2) agree well. It is worth noting that the motion along the z -axis (i.e. the motions of the orbits in the subclass CIIz) are purely Coulombic, as the diamagnetic force is zero for arbitrary B (this can be seen in table (11.2.2) where the relation $\Delta\mathcal{E}(n_z + 1, n_z)n_z^3 = \text{constant}$ is verified).

We next consider the CIs orbits of section (9.1) (Figure (9.1.2)). Using the EBK-quantization rule (Keller 1958)

$$\oint \mathbf{p} \cdot d\mathbf{q} = h(n + \alpha), \quad (11.2.6)$$

where again we put $\alpha = 0$, since we are primarily interested in the differences $\Delta\mathcal{E}(n+1, n)$. The spacings agree with those obtained from measuring the classical frequency of the orbits (equation (11.2.2)). We also evaluated the components of the integral in equation (11.2.6)

along ρ and z

$$\oint p_i dq_i = n_i h, \quad i = \rho, z \quad (11.2.7)$$

where

$$n = n_\rho + n_z;$$

n_ρ and n_z are in general non-integral but may give a rough value of the numbers of nodes in ρ and z . Table (11.2.3) indicates that the resonances have a large number of nodes in ρ as $E \rightarrow 0$. This may have important implications for quantum calculations.

Our second example, again chosen because of the existence of experimental measurements, is for $B = 42 \text{ kG}$ and $m = 0, -1, -2$.

In table (11.2.4), we give results for $m = 0$ for the planar orbits (Co), the orbits CIIz and the orbits CIs which are described in chapter (9). For $m = -1$ (table (11.2.5)) we found no example of the CIIz orbits, and similarly in the case of table(11.2.6) for $m = -2$.

For the planar orbits Co the successive values of \mathcal{E}_{n_ρ} at which (11.2.4) holds (for successive n_ρ) satisfy

$$\Delta\mathcal{E}(n_\rho + 1, n_\rho) = \beta \hbar \omega_c, \quad (11.2.8)$$

where β is given in tables 11.2.1, 11.2.4, 11.2.5 and 11.2.6 for $B = 60 = kG$, $m = 0$ and $B = 42 \text{ kG}$, $m = 0, -1, -2$ respectively.

Near the critical energy where we have four-loop orbits we get

$$\Delta\mathcal{E}(32, 31) = 1.92 \hbar \omega_c \quad (\text{at } B = 60 \text{ kG}, m = 0)$$

$$\Delta\mathcal{E}(36, 35) = 1.91 \hbar \omega_c \quad (\text{at } B = 42 \text{ kG}, m = 0)$$

$$\Delta\mathcal{E}(35, 34) = 1.91 \hbar \omega_c \quad (\text{at } B = 42 \text{ kG}, m = -1)$$

$$\Delta\mathcal{E}(34, 33) = 1.91 \hbar \omega_c \quad (\text{at } B = 42 \text{ kG}, m = -2)$$

Near the ionization threshold where we have three-loop orbits we get

$$\Delta\mathcal{E}(40, 39) = 1.50 \hbar\omega_c \quad (\text{at } B = 60 \text{ kG}, m = 0)$$

$$\Delta\mathcal{E}(45, 44) = 1.49 \hbar\omega_c \quad (\text{at } B = 42 \text{ kG}, m = 0)$$

$$\Delta\mathcal{E}(44, 43) = 1.49 \hbar\omega_c \quad (\text{at } B = 42 \text{ kG}, m = -1)$$

$$\Delta\mathcal{E}(43, 42) = 1.49 \hbar\omega_c \quad (\text{at } B = 42 \text{ kG}, m = -2)$$

That is, roughly speaking we get $\beta \simeq 2$ near the critical energy and $\beta = 1.5$ near the ionization threshold.

Next, we consider the orbits that pass through the origin (the three orbits CII1, CII2, CII3) shown in figures (9.2.2), (9.2.3) and (9.2.4), as their corresponding wave functions will have amplitudes in the vicinity of the low lying states of hydrogen and hence should be seen in photo-absorption spectra. The most relevant aspect of each of these orbits should be the energy spacing between the resonances. We have calculated the phase integral (11.2.6) for each orbit at different energies to obtain the spacings. The spacings agree very well with those obtained from measuring the classical frequency of the orbits.

We also evaluated the components of the integral (11.2.6) along ρ and z (i.e. equations (11.2.7)), where again n_ρ and n_z are in general non-integral but we give in table (11.2.7) the values of the nearest integer. The spacings, values of n_ρ and n_z near $E = 0$ for the three orbits are given in table (11.2.7) and interestingly indicate that these resonances may have a large number of nodes in ρ . This may be significant in the quantum mechanical calculations.

(11.3) Comparison with Experiments.

Recently Holle *et al* (1986) have measured the absorption spectrum of atomic hydrogen in a constant magnetic field. They have results at 60 kG for $m = 0$ and at 42 kG for $m = 0, -1, -2$. So we compare the semiclassical frequencies we obtain with their spectra in figures (11.3.1)-(11.3.4).

For both 42 kG and 60 kG we find that the quasi-Landau spectrum for planar orbits ($z = 0$) is in good agreement with the most intense lines of the observed spectrum, allowing for a drift of about 1 cm^{-1} on 120 cm^{-1} in the 42 kG example. We code these lines \times in the figures (11.3.1)-(11.3.4). The lines arising from the orbits CIIz are coded + in close coincidence with the lowest lying lines of each manifold, apart from a shift of approximately 1 cm^{-1} in the 42 kG example, attributable to our choice of $\alpha = 0$. We also show the spacings due to the non-planar orbit CIs of section (9.1) (see figure (9.1.2)). The energy lines are coded \circ in figures (11.3.1)-(11.3.4). The matching with the experimental members of the manifolds, by allowing a constant shift of about 8 cm^{-1} upwards for the whole series of lines, gives a satisfactory agreement. This shift is attributable to our choice of $\alpha = 0$.

For the non-planar orbit passing through the origin and shown in figure(9.2.2), the spacing near $E = 0$ is calculated. We obtain very good agreement with the interval of $0.64 \hbar \omega_c$ found in the experiment of Holle *et al* (1986).

The other spacings that we predicted (see table (11.2.7)) for the non-planar orbits have now been seen experimentally (Main *et al* 1986).

Figure captions : (11.3.1)-(11.3.4)

Figure (11.3.1). The calculated energy lines, compared with the experimental spectra obtained by Holle *et al* (1986) for $B = 60 \text{ kG}$, $m = 0$.

- i- The series coded "x" is due to quantization (by (11.2.4)) of the planar motion ($z = 0$).
- ii- The series coded "+" is due to quantization (by (11.2.5)) of the orbit OZ .
- ii- The series coded "o" is due to EBK-quantization (eq. (11.2.6)) of the orbit CIs (shown in figure (9.1.2)).

Figure (11.3.2). As figure (11.3.1), but for $B = 42 \text{ kG}$, $m = 0$.

Figure (11.3.3). As figure (11.3.1), excluding the "+" series, for $B = 42 \text{ kG}$, $m = -1$.

Figure (11.3.4). As figure (11.3.3), but for $B = 42 \text{ kG}$, $m = -2$.

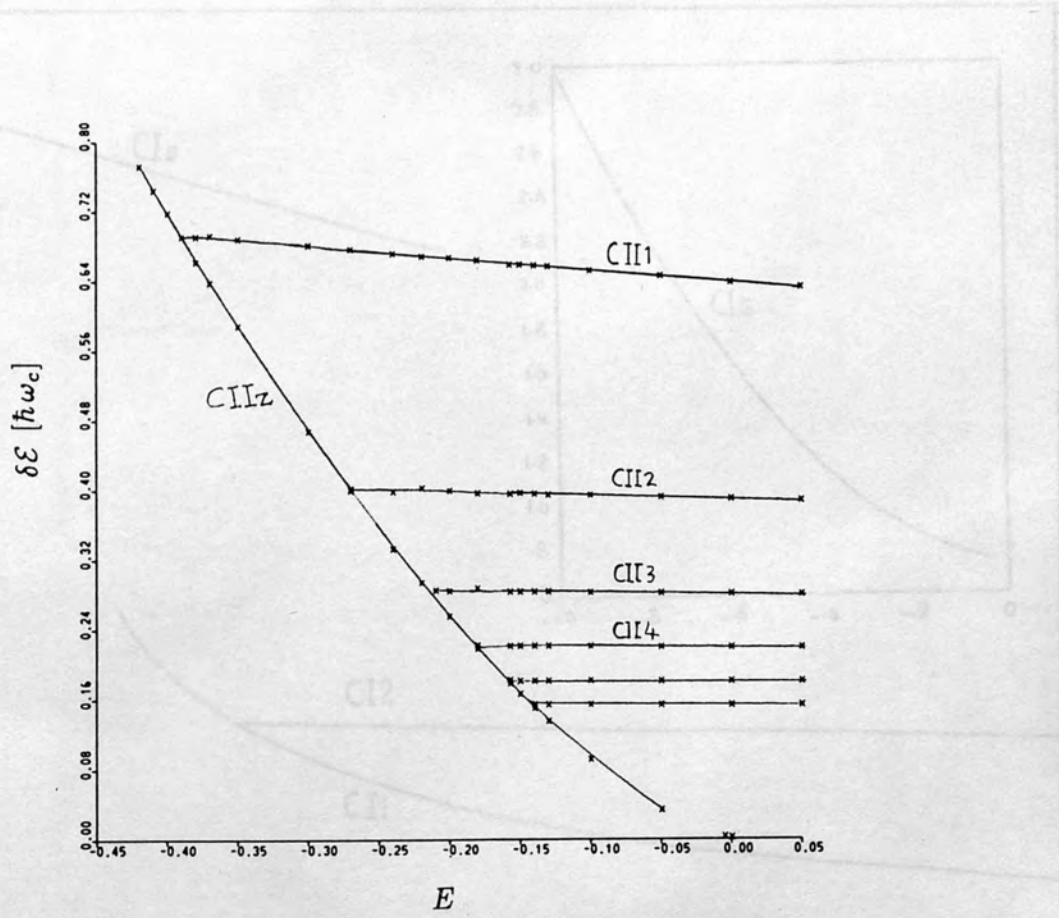


Figure (11.2.1). The energy separations, determined by eq. (11.2.2), of some periodic orbits of the class CII as functions of the energy parameter E .

Figure (11.2.2). The energy separations, determined by eq. (11.2.2) of some periodic orbits of the class CII as functions of E . The small segment shown in the figure, above the E -axis, belongs to period doubled orbits.

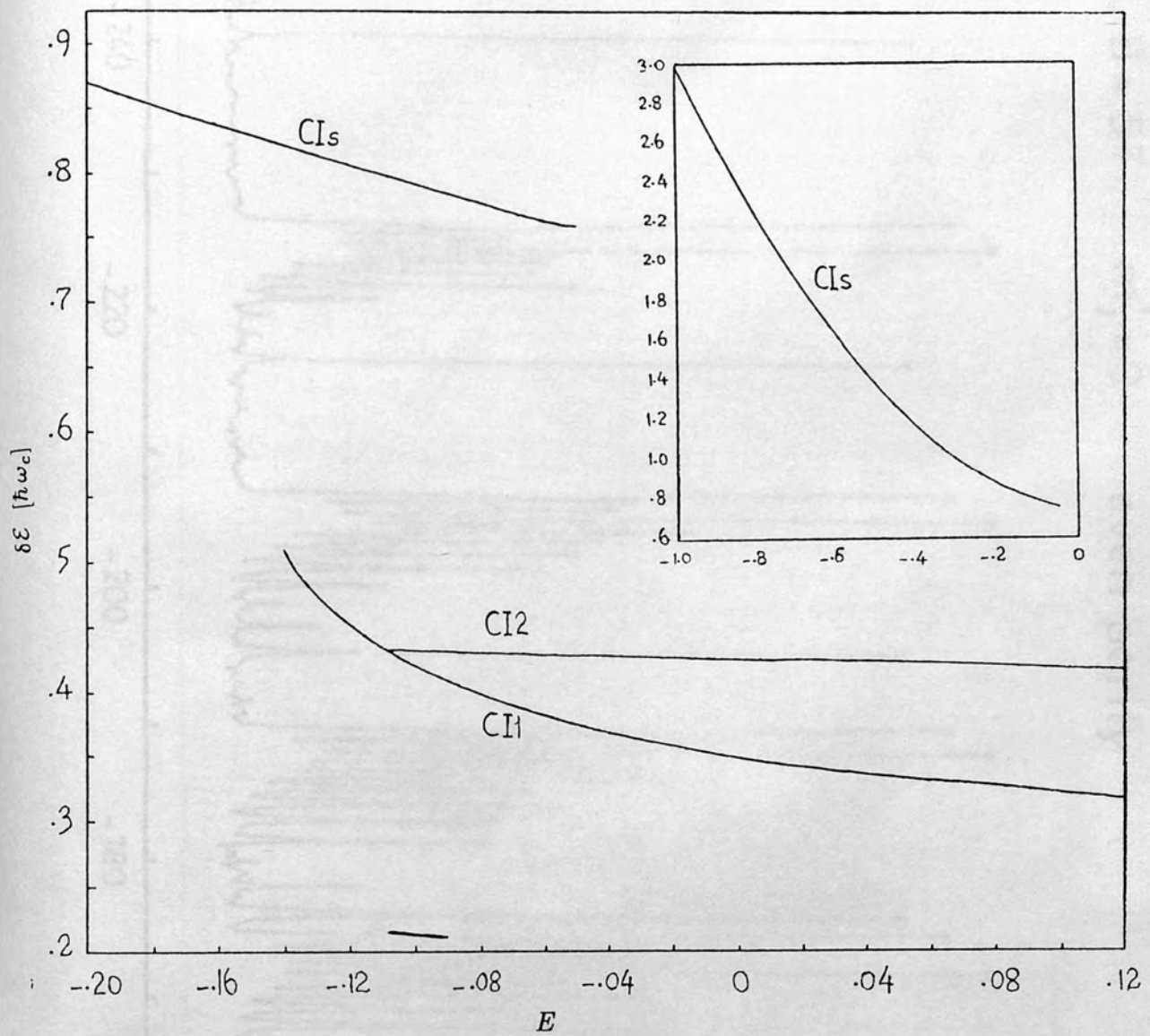
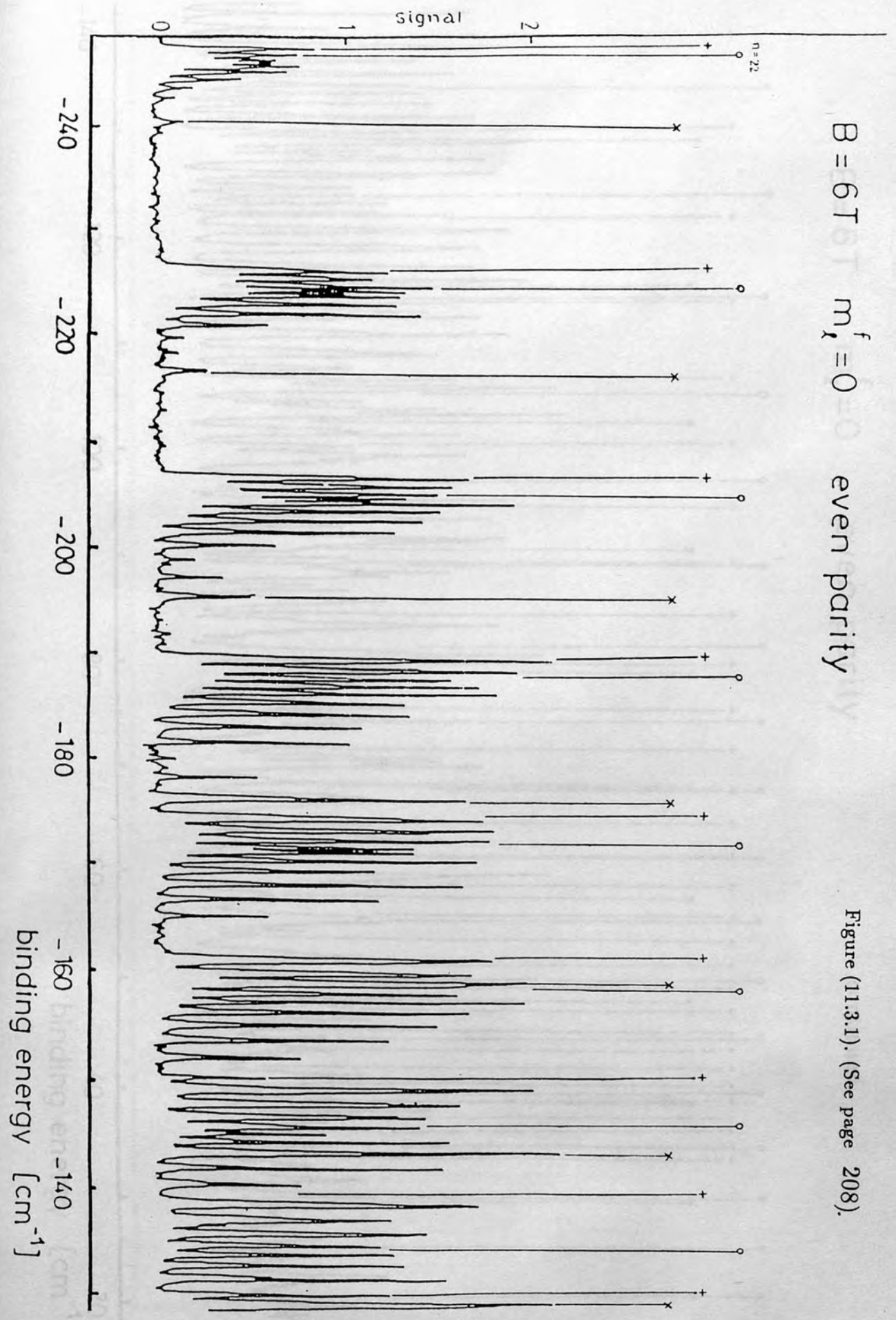


Figure (11.2.2). The energy separations, determined by eq. (11.2.2) of some periodic orbits of the class CI as functions of E . The small segment shown in the figure, above the E -axis, belongs to period doubled orbits.

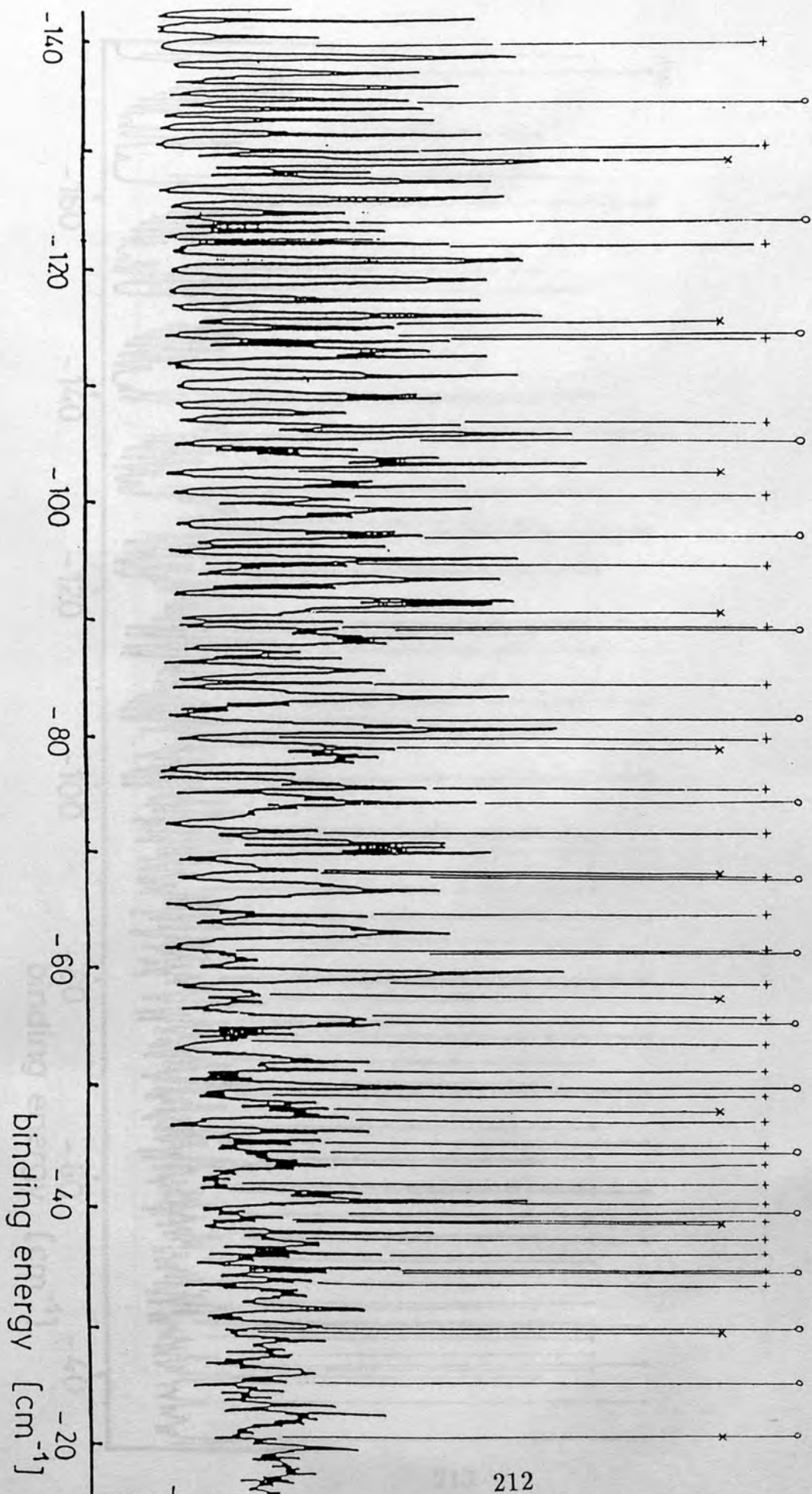
$B = 6T$ $m_l^f = 0$ even parity

Figure (11.3.1). (See page 208).



$B = 6\text{ T}$ $m_l^f = 0$ even parity

continued.



$B = 4.2 \text{ T}$

even parity

$m_l = 0$

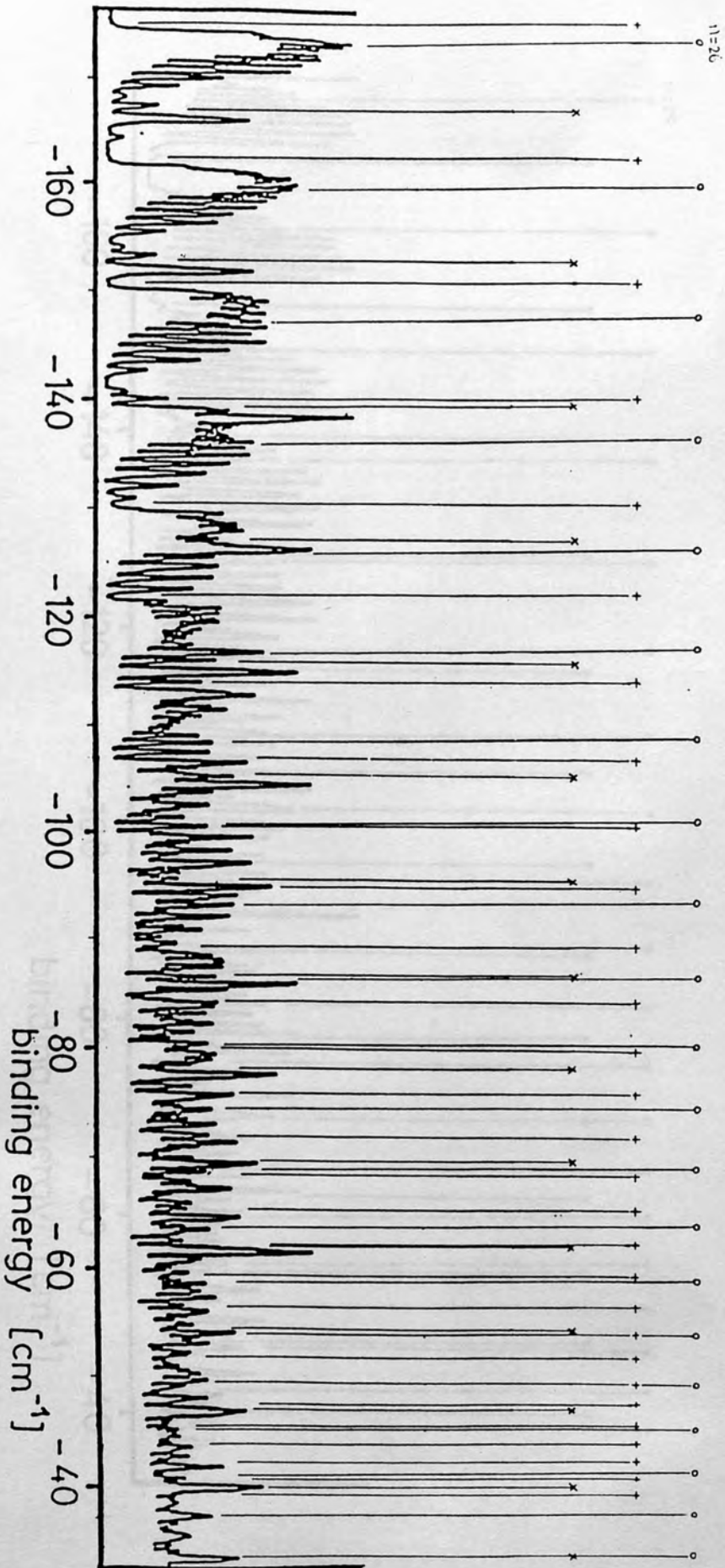


Figure (11.3.2). (See page 208).

$B = 4.2 \text{ T}$

even parity

$m_l = -1$

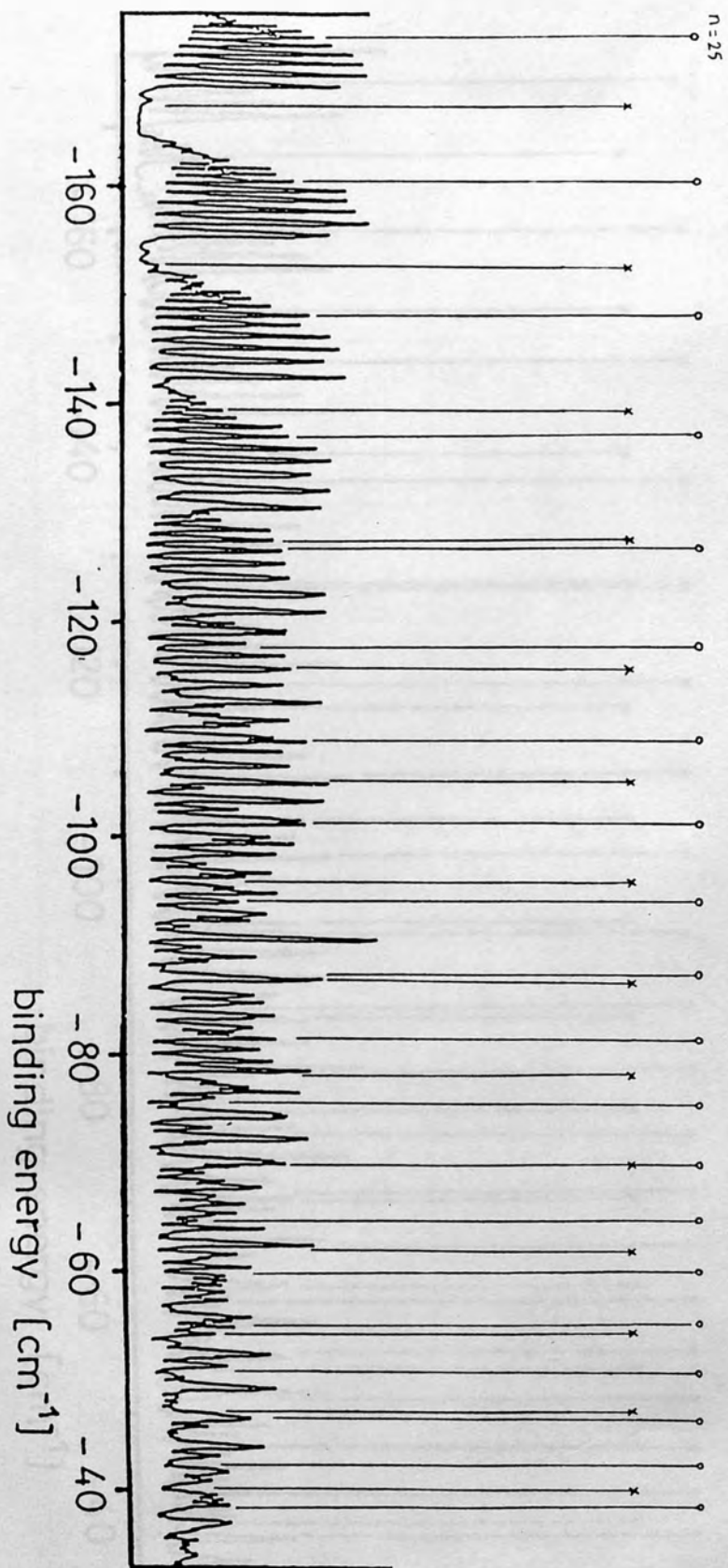


Figure (11.3.3). (See page 208).

$B = 4.2 \text{ T}$

even parity

$m_l = -2$

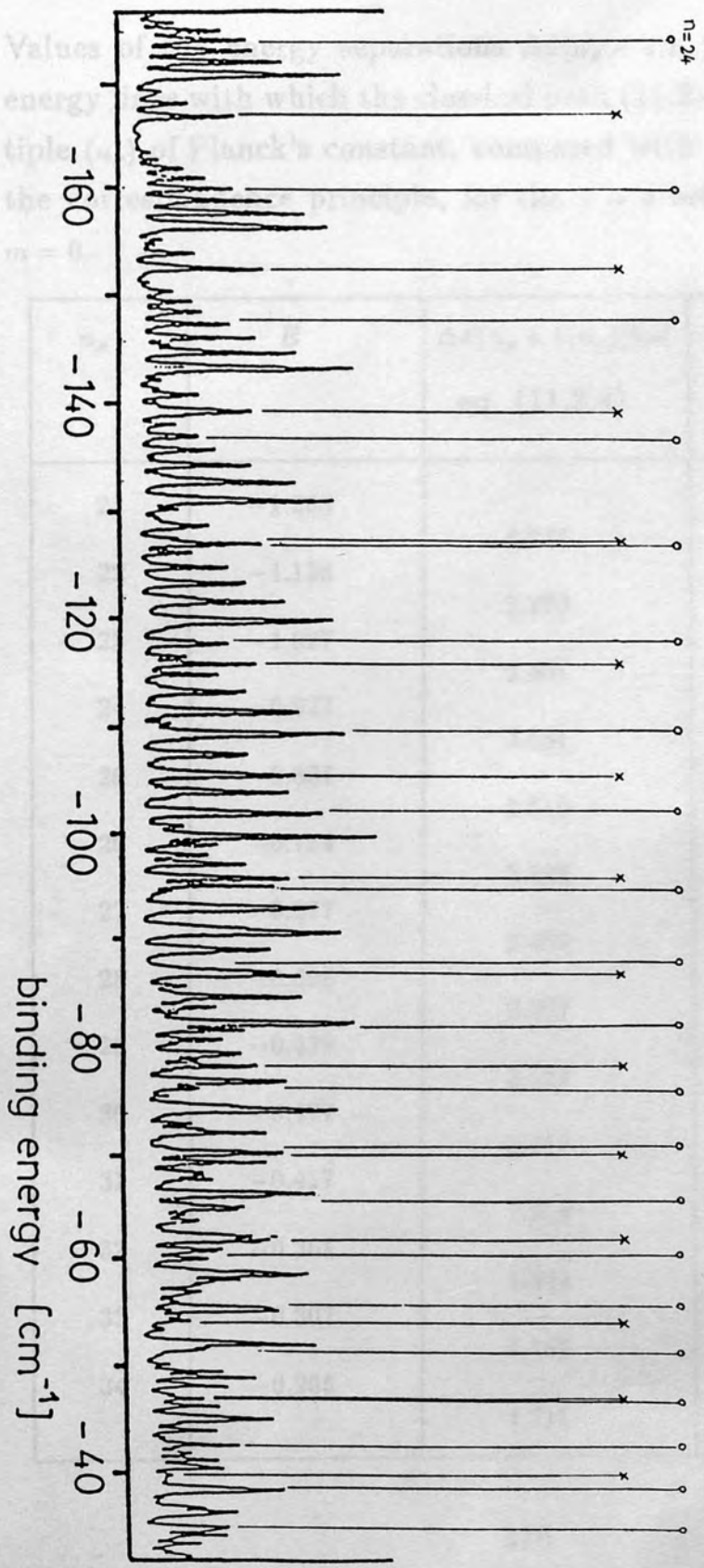


Figure (11.3.4). (See page 208).

Table (11.2.1)

Values of the energy separations $\Delta\mathcal{E}(n_\rho + 1, n_\rho)$ determined by the energy lines with which the classical path (11.2.4) is an integral multiple (n_ρ) of Planck's constant, compared with those obtained from the correspondence principle, for the $z = 0$ orbits, $B = 60$ kG and $m = 0$.

n_ρ	E	$\Delta\mathcal{E}(n_\rho + 1, n_\rho)[\hbar\omega]$ eq. (11.2.4)	$\Delta\mathcal{E}(n_\rho + 1, n_\rho)[\hbar\omega]$ eq. (11.2.2)
21	-1.263	4.254	4.250
22	-1.138	3.770	3.782
23	-1.027	3.401	3.398
24	-0.927	3.061	3.082
25	-0.837	2.819	2.819
26	-0.754	2.602	2.599
27	-0.677	2.407	2.416
28	-0.606	2.267	2.261
29	-0.539	2.127	2.130
30	-0.477	2.017	2.018
31	-0.417	1.919	1.923
32	-0.361	1.842	1.842
33	-0.307	1.766	1.771
34	-0.255	1.711	1.709

Table (11.2.1), continued.

As Table (11.2.1), but for the ω values $\omega = 0.01, 0.02, \dots, 0.1$.

n_ρ	E	$\Delta\mathcal{E}(n_\rho + 1, n_\rho)[\hbar\omega]$ eq. (11.2.4)	$\Delta\mathcal{E}(n_\rho + 1, n_\rho)[\hbar\omega]$ eq. (11.2.2)
35	-0.204	1.656	1.656
36	-0.155	1.609	1.608
37	-0.108	1.567	1.567
38	-0.062	1.533	1.530
39	-0.017	1.499	1.497
40	0.027	1.460	1.467
41	0.070	1.443	1.441
42	0.113	1.414	1.417
43	0.155	1.397	1.395
44	0.196	1.376	1.375
45	0.236	1.354	1.357
46	0.276	1.342	1.341
47	0.316	1.325	1.326
48	0.355		

Table (11.2.2)

As Table (11.2.1), but for the *OZ* orbit, $B = 60 \text{ kG}$ and $m = 0$.

n_z	E	$\Delta\mathcal{E}(n_z + 1, n_z)[\hbar\omega]$ eq. (11.2.5)	$\Delta\mathcal{E}(n_z + 1, n_z)[\hbar\omega]$ eq. (11.2.2)
21	-1.308	3.940	3.954
22	-1.192	3.443	3.449
23	-1.090	3.023	3.026
24	-1.001	2.666	2.670
25	-0.923	2.365	2.367
26	-0.853	2.110	2.109
27	-0.791	1.885	1.886
28	-0.735	1.694	1.694
29	-0.686	1.524	1.528
30	-0.641	1.384	1.382
31	-0.600	1.252	1.254
32	-0.563	1.142	1.142
33	-0.529	1.040	1.043
34	-0.499	0.955	0.955

Table (11.2.2), continued.

n_z	E	$\Delta\mathcal{E}(n_z + 1, n_z)[\hbar\omega]$ eq. (11.2.5)	$\Delta\mathcal{E}(n_z + 1, n_z)[\hbar\omega]$ eq. (11.2.2)
35	-0.471	0.875	0.876
36	-0.445	0.802	0.806
37	-0.421	0.743	0.744
38	-0.399	0.688	0.687
39	-0.379	0.637	0.636
40	-0.360	0.590	0.590
41	-0.343	0.548	0.548
42	-0.327	0.514	0.510
43	-0.312	0.475	0.476
44	-0.298	0.442	0.445
45	-0.285	0.416	0.416
46	-0.273	0.391	0.390
47	-0.261	0.3651	0.366
48	-0.250	0.344	0.343
49	-0.240	0.323	0.323
50	-0.231	0.301	0.304

Table (11.2.2), continued.

Values of the energy separations $\Delta\mathcal{E}(n_z, n_z+1)$ determined by the energy spacing from the EBK quantization for the new classical orbits (in figure 11.2.2) $E = \text{orbits}$

n_z	E	$\Delta\mathcal{E}(n_z + 1, n_z)[\hbar\omega]$ eq. (11.2.5)	$\Delta\mathcal{E}(n_z + 1, n_z)[\hbar\omega]$ eq. (11.2.2)
51	-0.222	0.289	0.287
52	-0.213	0.272	0.271
53	-0.205	0.255	0.256
54	-0.198	0.242	0.242
55	-0.191	0.229	0.229
56	-0.184	0.217	0.217
57	-0.178		

Table (11.2.3)

Values of the energy separations $\Delta\mathcal{E}(n, n+1)$ determined by the energy lines arising from the EBK-quantization, for the non-planar orbits CIs (figure (9.1.2)), $B = 60 \text{ kG}$, $m = 0$.

n	n_ρ	n_z	$\Delta\mathcal{E}(n+1, n)[\hbar\omega]$ EBK-quantization
22	10.46	11.54	4.025
23	10.98	12.02	3.481
24	11.50	12.50	3.016
25	12.02	12.98	2.826
26	12.58	13.42	2.479
27	13.15	13.85	2.242
28	13.74	14.26	2.038
29	14.35	14.65	1.868
30	15.00	15.00	1.749
31	15.68	15.32	1.613
32	16.39	15.61	1.464
33	17.12	15.88	1.379
34	17.90	16.10	1.318
35	18.72	16.28	1.230

Table (11.2.3), continued.

n	n_ρ	n_z	$\Delta\mathcal{E}(n+1, n)[\hbar\omega]$ EBK-quantization
36	19.57	16.43	1.189
37	20.48	16.52	1.104
38	21.39	16.61	1.046
39	22.32	16.68	1.019
40	23.29	16.71	0.992
41	24.29	16.71	0.934
42	25.29	16.71	0.914
43	26.33	16.67	0.887
44	27.37	16.63	0.859
45	28.42	16.58	0.822
46	29.47	16.53	

Table (11.2.4)

Values of $\Delta\mathcal{E}(n+1, n)$ for $B = 42$ kG, $m = 0$. For the $z = 0$ orbits (I) and the OZ orbits (II), the values are determined by the energy lines for which the classical paths (11.2.4) and (11.2.5) are, respectively, integral multiples n_ρ and n_z of Planck's constant, for the non-planar orbits (figure (9.1.2)) (III), by the EBK-quantization.

Table (11.2.4) (I)

n_ρ	E	$\Delta\mathcal{E}(n_\rho + 1, n_\rho)[\hbar\omega]$ eq.(11.2.4)
23	-1.342	4.552
24	-1.223	4.246
25	-1.112	3.596
26	-1.018	3.404
27	-0.929	3.098
28	-0.848	2.831
29	-0.774	2.678
30	-0.704	2.486
31	-0.639	2.333
32	-0.578	2.219
33	-0.520	2.104
34	-0.465	1.989

Table (11.2.4) (I), continued.

n_ρ	E	$\Delta\mathcal{E}(n_\rho + 1, n_\rho)[\hbar\omega]$ eq.(11.2.4)
35	-0.413	1.913
36	-0.363	1.874
37	-0.314	1.760
38	-0.268	1.721
39	-0.223	1.683
40	-0.179	1.645
41	-0.136	1.607
42	-0.094	1.530
43	-0.054	1.530
44	-0.014	1.530
45	0.025	1.492
46	0.064	1.454
47	0.102	1.415
48	0.139	

Table (11.2.4) (II)

n_z	E	$\Delta\mathcal{E}(n_z + 1, n_z)[\hbar\omega]$ eq.(11.2.5)
23	-1.383	4.322
24	-1.270	3.825
25	-1.170	3.366
26	-1.082	3.022
27	-1.003	2.678
28	-0.933	2.410
29	-0.870	2.180
30	-0.813	1.989
31	-0.761	1.798
32	-0.714	1.626
33	-0.672	1.473
34	-0.633	1.377
35	-0.597	1.262
36	-0.564	1.148
37	-0.534	1.052
38	-0.507	0.975
39	-0.481	

Table (11.2.4) (III).

Table (11.2.4) (II), continued.

n_x	n_y	n_z	E	$\Delta\mathcal{E}(n_x + 1, n_z)[\hbar\omega]$ EBK-quantization
20	n_z	2.40	E	$\Delta\mathcal{E}(n_z + 1, n_z)[\hbar\omega]$
27		2.83		eq.(11.2.5)
28		3.45		0.918
40		-0.457		0.822
39		4.01		0.803
41		-0.436		0.727
30		4.58		0.689
42		-0.415		0.631
31		5.16		0.593
43		-0.396		0.555
32		5.75		0.524
44		-0.378		0.490
33		6.35		0.459
45		-0.361		0.421
34		6.96		0.421
46		-0.346		0.383
35		7.58		0.363
47		-0.331		
36		8.22		
48		-0.317		
37		8.88		
49		-0.305		
38		9.56		
50		-0.293		
39		10.26		
51		-0.282		
40		10.98		
52		-0.271		
41		11.72		
53		-0.261		
42		12.48		
54		-0.251		
43		13.26		
44		14.07		
45		14.90		
46		15.75		
47		16.63		
48		17.54		
49		18.48		
50		19.45		
51		20.46		
52		21.50		
53		22.58		
54		23.70		

Table (11.2.4) (III).

n	n_ρ	n_z	$\Delta\mathcal{E}(n+1, n)[\hbar\omega]$ EBK-quantization
26	12.40	13.60	3.519
27	12.93	14.07	3.118
28	13.46	14.54	2.869
29	14.01	14.99	2.582
30	14.58	15.42	2.333
31	15.16	15.84	2.161
32	15.76	16.24	1.959
33	16.39	16.61	1.867
34	17.04	16.96	1.702
35	17.73	17.27	1.568
36	18.43	17.57	1.492
37	19.17	17.83	1.415
38	19.95	18.05	1.327
39	20.74	18.26	1.236
40	21.56	18.44	1.224
41	22.45	18.55	1.128
42	23.33	18.67	1.109
43	24.26	18.74	1.063
44	25.21	18.79	1.021

Table (11.2.4) (III), continued.

n	n_ρ	n_z	$\Delta\mathcal{E}(n+1, n)[\hbar\omega]$ EBK-quantization
45	26.19	18.81	0.975
46	27.17	18.83	0.956
47	28.19	18.81	0.918
48	29.21	18.79	0.880
49	30.23	18.77	

Table (11.2.5)

Values of $\Delta\mathcal{E}(n+1, n)$ for $B = 42\text{ kG}$, $m = -1$. For the $z = 0$ orbits (I), the values are determined by the energy lines for which the classical path (11.2.4) is an integral multiple (n_ρ) of Planck's constant, for the non-planar orbits (figure (9.1.2)) (II), by the EBK-quantization.

Table (11.2.5) (I)

n_ρ	E	$\Delta\mathcal{E}(n_\rho + 1, n_\rho)[\hbar\omega]$ eq.(11.2.4)
22	-1.343	4.628
23	-1.222	4.093
24	-1.115	3.710
25	-1.018	3.388
26	-0.930	3.106
27	-0.849	2.869
28	-0.774	2.678
29	-0.704	2.486
30	-0.639	2.333
31	-0.578	2.219
32	-0.520	2.104
33	-0.465	1.989

Table (11.2.5) (I), continued.

n_ρ	E	$\Delta\mathcal{E}(n_\rho + 1, n_\rho)[\hbar\omega]$ eq.(11.2.4)
34	-0.413	1.913
35	-0.363	1.836
36	-0.315	1.798
37	-0.268	1.721
38	-0.223	1.683
39	-0.179	1.645
40	-0.136	1.568
41	-0.095	1.568
42	-0.054	1.530
43	-0.014	1.492
44	0.025	1.492
45	0.064	1.454
46	0.102	1.415
47	0.139	

Table (11.2.5) (II).

n	n_ρ	n_z	$\Delta\mathcal{E}(n+1, n) [\hbar\omega]$ <i>EBK-quantization</i>
25	11.42	13.58	3.519
26	11.95	14.05	3.118
27	12.48	14.52	2.869
28	13.03	14.97	2.582
29	13.59	15.41	2.333
30	14.17	15.83	2.161
31	14.78	16.22	1.958
32	15.41	16.59	1.867
33	16.06	16.94	1.702
34	16.74	17.26	1.568
35	17.44	17.56	1.492
36	18.18	17.82	1.415
37	18.96	18.04	1.327
38	19.76	18.24	1.236
39	20.57	18.43	1.224
40	21.46	18.54	1.128
41	22.33	18.67	1.109
42	23.26	18.74	1.063
43	24.22	18.78	1.021

Table (11.2.5) (II), continued.

n	n_ρ	n_z	$\frac{\Delta\mathcal{E}(n+1, n) [\hbar\omega]}{EBK\text{-quantization}}$
44	25.20	18.80	0.975
45	26.18	18.82	0.956
46	27.20	18.80	0.899
47	28.21	18.79	

Table (11.2.6)

As Table ^(11.2.5), but for $B = 42$ kG, $m = -2$.

Table (11.2.6) (I)

n_p	E	$\Delta\mathcal{E}(n_p + 1, n_p) [\hbar\omega]$ eq.(11.2.4)
21	-1.343	4.590
22	-1.223	4.131
23	-1.115	3.710
24	-1.018	3.366
25	-0.930	3.098
26	-0.849	2.869
27	-0.774	2.639
28	-0.705	2.486
29	-0.640	2.372
30	-0.578	2.219
31	-0.520	2.066
32	-0.466	2.027
33	-0.413	1.913
34	-0.363	1.836
35	-0.315	

Table (11.2.6) (I), continued.

n_ρ	E	$\Delta\mathcal{E}(n_\rho + 1, n_\rho) [\hbar\omega]$ eq.(11.2.4)
36	-0.268	1.798
37	-0.223	1.721
38	-0.179	1.683
39	-0.137	1.607
40	-0.095	1.607
41	-0.054	1.568
42	-0.014	1.530
43	0.025	1.492
44	0.063	1.454

Table (11.2.6) (II).

n	n_ρ	n_z	$\frac{\Delta\mathcal{E}(n+1, n) [\hbar\omega]}{EBK\text{-quantization}}$
24	10.48	13.52	3.557
25	11.01	13.99	3.137
26	11.54	14.46	2.869
27	12.09	14.91	2.525
28	12.64	15.36	2.333
29	13.22	15.78	2.161
30	13.81	16.19	1.958
31	14.45	16.55	1.867
32	15.10	16.90	1.702
33	15.78	17.22	1.568
34	16.48	17.52	1.492
35	17.21	17.79	1.415
36	17.99	18.01	1.320
37	18.78	18.22	1.266
38	19.61	18.39	1.201
39	20.48	18.52	1.148
40	21.37	18.63	1.090
41	22.29	18.71	1.063

Table (11.2.6) (II), continued.

n	n_ρ	n_z	$\Delta\mathcal{E}(n+1, n) [\hbar\omega]$ <i>EBK-quantization</i>
42	23.24	18.76	1.021
43	24.22	18.78	0.975
44	25.20	18.80	0.956
45	26.22	18.78	0.918
46	27.24	18.76	0.910
47	28.27	18.73	

Table (11.2.7)

The energy spacings arising from the orbits shown in figures (9.2.2), (9.2.3), (9.2.4) near $E = 0$, and the corresponding values of n_ρ and n_z obtained from eq. (11.2.7).

Orbit	Energy spacing in units of $\hbar\omega$	n_ρ	n_z
1	0.641	39	20
2	0.388	37	33
3	0.270	37	41

CHAPTER (12)

Conclusions

Whereas Edmonds and Pullen (1980) considered a macroscopic treatment, via surfaces of section for the quadratic Zeeman problem in the particular case $L = 0$, our treatment of the problem is valid for $|L| \geq 0$. Moreover, we considered a serious microscopic investigation by studying the stability of periodic orbits.

- 1- We have used two different regularization of the equations of motion through two transformations, one is canonical but the other is not. Hence we were able to carry out numerical solutions to the equations of motion. The transformation that was used by Edmonds and Pullen (1980) to remove the singularities (for $L = 0$) proves to be suitable only for giving clearer surfaces of section in the transformed phase space. For $L \neq 0$ this latter transformation does not remove the singularities but is nonetheless still canonical.
- 2- A description of the planar orbits (in the xy -plane) is given. These orbits are found to consist of loops which precess round the nucleus as E changes. An integral number of loops is obtained at discrete intervals of E . The number of loops decreases as E increases. The stability of the planar orbits is studied and *they are* found to lose stability at $E = -0.127$ (unscaled units).
- 3- We locate the non-planar periodic orbits in the chaotic regime. Two classes of these orbits exist:

- a- The first class, CI, contains orbits which do not pass through the origin.
 - b- The second class, CII, contains orbits with initial conditions at the origin ($\rho = z = 0$).
- 4- The stability of both classes of orbits is studied by calculating the linearisation at the fixed points corresponding to the orbits (Al-Laithy and Farmer 1987).
- a- For the class CI there is a nongeneric fixed point bifurcation in addition to the generic period doubling type.
 - b- For the class CII the nongeneric fixed point bifurcation is found to be a dominant feature: one orbit of this class (denoted OZ) oscillates between stability and instability. At each energy value at which OZ becomes unstable the orbit bifurcates to produce a new *stable* pair of periodic orbits of the same period. These orbits lose stability with increasing E and the values at which they become unstable are given. This process repeats, generating a sequence of alternate stability and instability over decreasing intervals of E until the escape energy is reached. The peculiarity of such behaviour lies in the fact that the different generations of the orbits of this class are born of the *same* parent orbit OZ . The alteration between stability and instability of the orbit OZ is substantiated, again, by parametric resonance analysis of this particular motion.
- 5- We have discussed the quantum analogues of some of these orbits and calculated their energy spacings. The semiclassical quanti-

ization of the periodic classical orbits provides a good account of some features of the observed spectra. These features are

It is convenient to define

i. The spectral series associated with the quasi-Landau resonances appear to be associated with the planar orbits.

ii. The lowest lying members of each manifold appear to be associated with the motion along the z -axis which is purely Coulombic.

iii. A third member of each manifold is due to a non-planar periodic orbit of class CII. Near the ionization limit the energy spacing due to this orbit is $\frac{3}{4} \hbar \omega_c$.

Then equations (6.7) can be written in the following

iv. The energy spacing $0.64 \hbar \omega_c$ near the ionization limit, which has been found recently in the experiments of Holle *et al* 1986, is due to a non-planar orbit of the class CII (Al-Laithy *et al*, 1986).

v. Other new predicted spacings arising from other orbits of the class CII have been seen in high resolution experiments on atoms in external fields (Main *et al* 1986).

Although we have not examined the problem of relative intensities, perhaps a more detailed analysis of the periodic orbits, even within the region of classical chaos, might yield a good general description of the main features of the observed spectrum.

Appendix

It is convenient to define

$$y_1 = 2r^{\frac{1}{2}}p_r, \quad y_2 = 2r^{-\frac{1}{2}}p_\theta,$$

$$y_3 = 2r^{-\frac{1}{2}}p_\phi, \quad y_4 = 2r^{-\frac{1}{2}}p_\sigma,$$

$$C = \cos \frac{\theta}{2}, \quad S = \sin \frac{\theta}{2},$$

$$C_\pm = \cos \frac{\sigma \pm \phi}{2}, \quad S_\pm = \sin \frac{\sigma \pm \phi}{2}.$$

Then equations (6.2.6.a-d) can be written in the following abbreviated form :

$$(P_1C_+ + P_2S_+)C + (P_3C_- + P_4S_-)S = y_1 \quad (A1)$$

$$-(P_1C_+ + P_2S_+)S + (P_3C_- + P_4S_-)C = y_2 \quad (A2)$$

$$(-P_1S_+ + P_2C_+)C + (P_3S_- - P_4C_-)S = y_3 \quad (A3)$$

$$(-P_1S_+ + P_2C_+)C - (P_3S_- - P_4C_-)S = y_4. \quad (A4)$$

Solving equations A1, A2, A3, A4 for P_1 , P_2 , P_3 and P_4 we get :

$$P_1 = (y_1C - y_2S)C_+ - (y_3 + y_4) \frac{S_+}{2C}$$

$$P_2 = (y_1C - y_2S)S_+ + (y_3 + y_4) \frac{C_+}{2C}$$

It is known that

$$P_3 = (y_1 S + y_2 C)C_- + (y_3 - y_4) \frac{S_-}{2S}$$

$$P_4 = (y_1 S + y_2 C)S_- - (y_3 - y_4) \frac{C_-}{2S}$$

Then

Substituting

$$\sum_{i=1}^4 P_i^2 = y_1^2 + y_2^2 + \frac{1}{\sin^2 \theta} (y_3^2 + y_4^2) - \frac{2 \cos \theta}{\sin^2 \theta} y_3 y_4$$

or (3) we get

$$\sum_{i=1}^4 P_i^2 = 4r \left[p_r^2 + \frac{p_\theta^2}{r^2} + \frac{p_\phi^2}{r^2 \sin^2 \theta} \right] + \frac{4p_\sigma}{r \sin^2 \theta} (p_\sigma - 2p_\phi \cos \theta).$$

Setting

$$p_\sigma = 0, \quad (A5)$$

we get

$$\sum_{i=1}^4 P_i^2 = 4r \left[p_r^2 + \frac{p_\theta^2}{r^2} + \frac{p_\phi^2}{r^2 \sin^2 \theta} \right]. \quad (A6)$$

From equations (6.2.3) we get

$$\begin{aligned} C_+ &= \frac{Q_1}{r^{\frac{1}{2}} C}, & C_- &= \frac{Q_3}{r^{\frac{1}{2}} S}, \\ S_+ &= \frac{Q_2}{r^{\frac{1}{2}} C}, & S_- &= \frac{Q_4}{r^{\frac{1}{2}} S}. \end{aligned} \quad (A7)$$

Substituting from A7 into equations (6.2.6.a-d)) we get

$$P_r = \frac{1}{2r} \sum_{i=1}^4 P_i Q_i, \quad (A8)$$

$$P_\theta = -\frac{r}{2\rho} (P_1 Q_1 + P_2 Q_2 - P_3 Q_3 - P_4 Q_4) + \frac{z}{2\rho} \sum_{i=1}^4 P_i Q_i \quad (A9)$$

$$P_\phi = \frac{1}{2} (-P_1 Q_2 + P_2 Q_1 + P_3 Q_4 - P_4 Q_3) \quad (A10)$$

$$P_\sigma = \frac{1}{2} (-P_1 Q_2 + P_2 Q_1 - P_3 Q_4 + P_4 Q_3). \quad (A11)$$

References

It is known that

$$p_\rho = \frac{z}{r^2} p_\theta + \frac{\rho}{r} p_r \quad (A12)$$

$$p_z = \frac{z}{r} p_r - \frac{\rho}{r^2} p_\theta. \quad (A13)$$

Substituting from equations (6.2.4), (A8), and (A9) into (A12) and (A13) we get

$$p_\rho = \frac{1}{2\rho} \sum_{i=1}^4 P_i Q_i - \frac{z}{2\rho r} (P_1 Q_1 + P_2 Q_2 - P_3 Q_3 - P_4 Q_4), \quad (A14)$$

$$p_z = \frac{1}{2r} (P_1 Q_1 + P_2 Q_2 - P_3 Q_3 - P_4 Q_4). \quad (A15)$$

References

- Al-Laithy, M.A. Farmer, C.M. and McDowell, M.R.C., 1985, *Phys. Letts. A*, **108A**, 3,144.
- Al-Laithy, M.A. O'Mahony, P.F. and Taylor, K.T. 1986, *J. Phys. B: At. Mol. Phys.* **19** L773-777.
- Al-Laithy, M.A. and Farmer, C.M. 1987, *J. Phys. B: At. Mol. Phys.* **20** L747-L752.
- Arnold, V.I. 1963, *Russian Math. Surveys*, **18** 5 9-36.
- Arnold, V.I. and Avez, A. 1968, *Ergodic Problems of Classical Mechanics* (New York; Benjamin).
- Arnold, V.I. 1978, *Mathematical Methods of Classical Mechanics* (Springer-Verlag).
- Berry, V.I. 1978, *Regular and Irregular Motion*, from *Topics in Non-linear Dynamics*, Ed. Jorna S., Am. Ins. Phys. Conf. Proc., **46**, 16-120.
- Berry, M.V. 1981, *Ann. Phys. N.Y.* **131** 163-216.
- Berry, M.V. 1983, *Chaotic Behaviour of Deterministic Systems*, Edited by Gerard Looss *et al* (North-Holland).
- Berry, M.V. 1987, Private communication.
- Birkhoff, G.D. 1927, *Dynamical Systems*, vol. IX, Am. Math. Soc. (Providence, R.I.).
- Carnegie, A. 1984, *PhD Thesis*, Queen Mary College, London University.
- Chirikov, B.V. 1979, *Phys. Reports* **52** 265.
- Clark, C.W. and Taylor, K.T. 1980, *J. Phys. B: At. Mol. Phys. B.* **13** L737.
- Clark, C.W. and Taylor, K.T. 1981, *Nature* Vol. **292**, 437.
- Cohen, R. Lodenquai, L. and Ruderman, M. 1970, *Phys. Rev. Letters*, **25** 467.

- Cornish, F.H.J. 1984, *J. Phys. A.* **17** 323.
- Cvitanovice, P. 1984, *Universality in Chaos*, (Adam Hilger).
- Delande, D. Chardonnet, C. Biraben, F. and Gay, J.C. 1982 CNRS Colloquim **43** C297.
- Delos, J.B. Knudson, S.K. and Noid, D. 1984, *Phys. Rev. A* **30** 1208.
- Edmonds, A.R. 1970, *J. Phys. (Paris) Colloq.* C4, **31** 71.
- Edmonds, A.R. 1973, *J. Phys. B: At. Mol. Phys.* **6** 1603.
- Edmonds, A.R. and Pullen, R.A. Imperial College, London Preprints ICTP/79-80 Nos. 28,29,30.
- Einstein, A. 1917, *Verh. Deutsch. Phys. Ges.* bf 19 82-92.
- Faraday : see Sommerfield, A. 1964, *Lectures in Theoretical Physics* (Academic Press).
- Gajewski, R. 1970, *Physica* 47, 575.
- Gantmacher, F. 1970, *Lectures in Analytical Mechanics* (Moscow: Mir Publishers).
- Garstang, R.H. 1977, *Rep. Prog. Phys.* **40** 105-154.
- Garton, W.R.S. and Tomkins, F.S. 1969, *Astrophys. J.* **158** 839-45.
- Gasiorowicz, S. 1974, *Quantum Physics* (Wiley).
- Gay, J.C. Delande, D. and Biraben, J. 1980, *J. Phys. B: At. Mol. Phys.* **13** L729.
- Gay, J.C. 1984, *High-Magnetic-Field Atomic Spectroscopy*, Part C Edited by Beyer, H.I. and Klein Poppen, H. (Plenum).
- Gay, J.C. 1985, *New Trends in Atomic Diamagnetism*, from *Photophysics and Photochemistry in the Vacuum Ultraviolet*, Eds. McGlynn *et al* (D. Reidel).

- Gill, P.E. and Miller, G.F. 1972, *Comp. Journal* **15** 80-83.
- Goldstein, H. 1980, *Classical Mechanics* (Addison-Wesley).
- Greene, J.M. 1968, *J. Math. Phys.* **9** No. 5, 760.
- Greene, J.M. 1979(a), from *Non-linear Dynamics and Beam-Beam interaction*, Ed. M. Month **57** 257 (N.Y. : Am. Inst. Phys.).
- Greene, J.M. 1979(b), *J. Math. Phys.* **20** No.6, 1183.
- Greene, J.M. MacKay, R.S. Vivaldi, F. Feigenbaum, M.J. 1981, *Physica* **3D**, 468-486.
- Gutzwiller, M.C. 1971, *J. Math. Phys.* **12** No. 3 343.
- Gutzwiller, M.C. 1978, in *Path Integrals*, ed. Papadopoulos, G.J. and Devreese, J.T. (Plenum).
- Hall, G. and Watt, J.M. (eds.), 1976, *Modern Numerical Methods for Ordinary Differential Equations* (Oxford: Clarendon Press).
- Heller, E.J. 1984, *Phys. Rev. Lett.* **53** 1515.
- Henon, M. and Heiles, C. 1964, *Astron. J.* **69** 73.
- Henrici, P. 1962, *Discrete Variable Methods in Ordinary Differential Equations* (Wiley).
- Hochstadt, H. 1971, *The functions of Mathematical Physics*, (Wiley-Interscience).
- Holle, A. Wiebusch, G. Main, J. Hager, B. Rottke, H. and Welge, K.H. 1986, *Phys. Rev. Lett.* **56** 2595.
- Jackson, J.D. 1975, *Classical Electrodynamics* (New York: Wiley).
- Jenkins, F.A. and Segre, E. 1939, *Phys. Rev.* **55** 52.
- Keller, J. 1958, *Annals of Physics* **4** 180.
- Kolmogorov, A.N. 1954, *Dokl. Akad. Nauk. SSSR* **98** 527-530.
- Landau, L.D. and Lifshitz, E.M. 1976, *Mechanics* (Pergamon Press).

- Landau, L.D. and Lifshitz, E.M. 1977, *Quantum Mechanics, Course of Theoretical Physics* Vol. 3 (Oxford: Pergamon).
- Lande: see Bransden, B.H. and Joachain, C.J. 1983, *Physics of Atoms and Molecules* (Longman).
- Lichtenberg, A.J. and Lieberman, M.A. 1983, *Regular and Stochastic Motion* (Springer-Verlag).
- Lorentz, H.A. 1906, K. Akad. Wet. Amestrdam Proc. 8, 591.
- MacKay, R.S. 1982a, *PhD Thesis*, Faculty of Princeton University.
- MacKay, R.S. 1982b, *Islands of stability beyond period doubling*, Physica 3D.
- MacKay, R.S. 1985, *Introduction to the Dynamics of Area-Preserving Maps* for the *Proceedings of the US Particle Accelerator School* SLAC, 1985, Ed. M. Month.
- Main, J. Wiebusch, G. Holle, A. and Welge, K.H. 1986, Phys. Rev. Lett. Vol. 57, No.22, 2789-2792.
- McDonald, S.W. and Kaufman, A.N. 1979, Phys. Rev. Lett. 42 1189-1191.
- McDowell, M.R.C. 1985, Private communication.
- Moser, J. 1962, Nachr. Akad. Wiss. Gottingen, Math. Phys. Klasse, Nr 1 1-20.
- Moser, J. 1966, Ann. CCuola Normale Sup. Pisa Ser. III 20 499.
- Moser, J. 1973, *Stable and Random Motions in Dynamical Systems*, (Princeton University Press).
- Nemytskii, V. and Stepanove, V.V. 1960, *Qualitative theory of Differential Equations* (Princeton).
- O'Connel, R.F. 1974, Astrophys. J. 187, 275-6.

- Percival, I.C. 1973, J. Phys. B: At. Mol. Phys. **6** L229.
- Percival, I.C. 1977, Adv. Chem. Phys. **36** 1-61.
- Percival, I.C. and Richards, D. 1982, *Introduction to Dynamics* (Cambridge University Press).
- Percival, I.C. 1988, Roy. Soc. meeting (February 1988).
- Poincare, H. 1892, *Les Methodes nouvelles de la mecanique celeste* (Paris; Gauthier-Villars).
- Rau, A.R.P. 1979, J. Phys. B: Atmol. Phys. **12** No. 6 L193.
- Richards, D. 1984, Private communication.
- Rimmer, R. 1978, J. Diff. Eqns. **29**, 329.
- Rimmer, R. 1979, *Generic bifurcations from fixed points of involutory area-preserving maps*, Memoirs of AMS **41** (1983) no. 272.
- Robnik, M. 1981, J. Phys. A. **14** 3195.
- Robnik, M. 1982, Journal de Physique, colloque C₂, supplement au n° 11, Tome 43.
- Shilov, G.E. 1974, *Elementary Functional Analysis* (MIT Press).
- Solov'ev, E.A. 1982, JETP Lett. Vol. 34, No. 5, 265.
- Starace, A.F. 1973, J. Phys. B: At. Mol. Phys. **6** 585.
- Synge, J.L. 1960, *Handbuch Der Physik*, Edited by Flugge, S. (Springer-Verlag).
- Szebehely, V.G. 1967, *Theory of Orbits* (New York: Academic Press).
- Uhlenbeck and Goudsmit, 1925, *Naturwissenschaften* **13** 953.
- Whiteman, K.J. 1977, Rep. Prog. Phys. **40** 1033-1069.
- Whittaker, E.J. 1964, *A Treatise on Analytical Dynamics of Particles and Rigid Bodies*, (Cambridge University Press).
- Zaslavskii, G.M. and Chirikov, B.V. 1972, Sov. Phys. USP. **14** 549.
- Zaslavskii, G.M. 1981, Phys. Rep. **80** 158-250.
- Zeeman, P. 1909, Phys. Z **10** 217.